



UNIVERSITÀ  
DEGLI STUDI  
DI PADOVA

PADOVA UNIVERSITY

Department of Earth Sciences

PhD SCHOOL IN EARTH SCIENCES

CICLE XXIV

**THE VAJONT ROCKSLIDE: NEW TECHNIQUES AND  
TRADITIONAL METHODS TO RE-EVALUATE THE  
CATASTROPHIC EVENT**

**School Director :** Prof. Gilberto Artioli

**Supervisor :** Prof. Rinaldo Genevois

**Dottorando :** Laura Superchi

*A Mia Madre*

# ABSTRACT

---

The Vajont landslide is one of the largest catastrophic slope failures of the past century. About 270 million m<sup>3</sup> of limestones, mudstones and marls slid into the Vajont Reservoir on October 9, 1963, producing a displacement wave that overtopped the dam and killed over 2000 people in the valley below. Although the landslide has been extensively studied over the past several decades, its morphologic and structural controls, mechanisms, and dynamics are not completely understood yet. The first step in carrying out the research was the implementation of a bibliographic and geographic electronic geo-databases, including all existing bibliographic records. Published and unpublished documents, theses, technical reports and maps were collected and indexed and they are available for the scientific community.

Afterwards, new techniques and technologies which were not available yet in the 60's, were applied to this thesis in order to investigate more in detail the morpho-structural and geomechanical features and to better understand the different role that they played in the 1963 event, thus providing a more rigorous and less empirically based forecasting approach to the study of large catastrophic landslides.

In particular, the applied remote sensing techniques (DEM analyses, LIDAR technologies, photogrammetric analyses) allowed to characterize in detail the structure of inaccessible areas of the failure surface and, along with the geological and geomechanical field investigations, to clarify relevant aspects concerning the geological-structural setting of the northern slope of Mount Toc.

The geomechanical survey in 89 stations was performed in order to reach an accurate knowledge and in-depth evaluation of the characteristics of the rock masses outcropping on the Vajont area, both inside and outside the landslide.

The obtained results permitted the identification of the most significant parameters that influenced the rockslide triggering and displacement, so helping in the comprehension of both the phenomenon and the structural control on its development and collapse.

The implementation of laboratory tests Uniaxial and Triaxial on rock samples completed the geomechanical characterization of the rock-masses.

The amount of the collected data were used to characterize the rock mass quality, through the following different classifications: Rock Quality Designation (RQD) Rock Mass Rating System (RMR) and Slope Mass Rating (SMR).

In order to complete the knowledge of the deep geological structure of the rock masses two seismic reflection profiles were carried out. The results of their preliminary interpolation are still in progress.

The accurate and detailed results achieved through the implementation of the above mentioned techniques, combined with field investigations, laboratory tests and ongoing geophysical surveys allowed to obtain a reliable 3D geological model.

This 3D model firstly allowed to define the sliding surface depth and geometry more precisely than ever and, secondly, to evaluate the landslide kinematics. These aspects represent the essential starting point for the future 3D modeling elaborations.

# RIASSUNTO

---

La frana del Vajont è uno dei maggiori eventi catastrofici che si sono verificati in Italia nel secolo scorso.

Il 9 ottobre 1963, circa 270 milioni di m<sup>3</sup> di roccia, in prevalenza calcareo marnosa, si staccarono dal monte Toc e precipitarono nel bacino del Vajont producendo un'onda che risalì il pendio opposto per diverse centinaia di metri, trascinò la diga e scaricò la sua enorme energia nella valle sottostante causando la morte di più di 2000 persone.

Molti gli studi e gli approfondimenti portati avanti, da più parti, nei decenni successivi all'evento franoso ma, a tutt'oggi, i meccanismi e le dinamiche della frana non sono stati ancora completamente chiariti.

Il presente progetto di ricerca ha previsto, come primo step, la creazione di un GIS-database in continuo aggiornamento, contenente tutte le informazioni, edite ed inedite che è stato possibile reperire sulla frana del Vajont (articoli, report, rapporti scientifici, tesi, carte geologiche e topografiche)

Successivamente, sono state utilizzate nel presente lavoro nuove tecniche non disponibili negli anni '60 al fine di analizzare, in dettaglio, le caratteristiche morfo-strutturali e comprendere meglio il differente ruolo che hanno rivestito nell'evento del 1963.

In particolare, le tecniche remote sensing utilizzate (analisi DEM, tecnologie Lidar e analisi fotogrammetriche) hanno consentito di caratterizzare in dettaglio le caratteristiche strutturali di aree poco accessibili sulla superficie di scivolamento e, congiuntamente alle indagini di campagna, di chiarire gli aspetti rilevanti circa l'assetto geologico del versante Nord del Monte Toc.

Sono state, inoltre condotte indagini geomeccaniche su 89 stazioni di misura, al fine di ottenere un'accurata conoscenza e una approfondita valutazione delle caratteristiche degli ammassi rocciosi affioranti fuori e dentro l'area della frana.

I risultati ottenuti hanno permesso di identificare i parametri più significativi che hanno influenzato l'innesco e l'evoluzione della frana favorendo così la comprensione del fenomeno in termini di sviluppo e collasso.

La caratterizzazione geomeccanica degli ammassi rocciosi è stata completata mediante l'esecuzione di test di laboratorio (prove uniassiali e triassiali) sui campioni di roccia.

La consistente quantità di dati ottenuti è stata utilizzata per caratterizzare gli ammassi rocciosi attraverso differenti classificazioni standard tra cui RQD (Rock Quality Designation), (RMR) Rock Mass Rating System e SMR (Slope Mass Rating).

Tutti i dati acquisiti hanno dato la possibilità di creare per la prima volta, un modello geologico 3D della frana, che ha permesso di analizzare dettagliatamente la cinematica della frana medesima e di definire la geometria e la profondità della superficie di scivolamento.

Al fine di investigare la struttura geologica del versante Nord del Monte Toc, sono stati realizzati due profili sismici i cui risultati sono attualmente in corso di elaborazione.

In sintesi, gli accurati e dettagliati risultati raggiunti mediante l'utilizzo di nuove tecniche e di tradizionali indagini di campagna completate dai test di laboratorio ha permesso di ottenere un quadro completo delle caratteristiche geologiche, morfo-strutturali e geomeccaniche, che costituiscono la base fondamentale per l'elaborazione futura per l'analisi di stabilità attraverso elaborazioni numeriche in 3D.

# INDEX

---

<b>INTRODUCTION</b>	1
<b>CHAPTER 1. STATE OF THE ART</b>	
1.1 Geographic framework	5
1.2 Literature review	7
<b>CHAPTER 2. GEOLOGICAL FRAMEWORK</b>	
2.1 Regional Geo-structural setting	10
2.2 Stratigraphy of the Vajont valley	13
2.3 Structural setting	17
2.4 Description of the rockslide	21
2.5 Geological and geomorphological aspects	23
2.6 Hydrogeology	27
<b>CHAPTER 3. MORPHO-STRUCTURAL ANALYSIS</b>	
3.1 Structural analysis of folding deformation on the sliding surface	33
3.2 Morpho-structural setting assessment through remote sensing techniques	34
3.2.1 COLTOP 3D analysis for folding structures	37
3.2.2 Structural analysis of folds through field investigation	41
3.3 Interpretation of folds planes	50
3.4 Discussion	50
<b>CHAPTER 4. GEOMECHANICAL CHARACTERIZATION</b>	
4.1 Geomechanical survey of the Vajont study area	53
4.2 Discontinuity analysis	55
4.3 Joints characterization: geometrical and mechanical joints properties	57
4.3.1 Intersection and termination	58
4.3.2 Discontinuity orientation and discontinuity sets	59
4.3.2.1 <i>Joint sets of the Vajont area</i>	60
4.3.3 Application of remote sensing techniques to discontinuity analysis	72
4.3.3.1 <i>COLTOP 3D</i>	72
4.3.3.2 <i>Photogrammetry analysis</i>	76
4.3.4 Discontinuity spacing	85
4.3.5 $J_v$ (volumetric joint count) and $V_b$ (block volum)	88
4.3.6 Discontinuity roughness-JRC (Joint Roughness Coefficient)	90
4.3.7 Joint Compressive Strenght (JCS)	94
4.4 Intact rock measurement-Point Load test	101
4.5 Rock mass classification systems	104
4.5.1 GSI system	104
4.5.2 Rock mass classification. RQD, RMRb, SMR	110

4.5.2.1 <i>RQD</i>	110
4.5.2.2 <i>RMR</i>	111
4.5.2.3 <i>SMR</i>	118
<b>CHAPTER 5. LABORATORY TEST</b>	
5.1 Introduction	121
5.2 Experimental apparatus	122
5.3 Samples	122
5.4 Uniaxial compressive test	124
5.4.1 Test procedures	124
5.4.2 Results	126
5.4.2.1 <i>Fracture characterization</i>	132
5.5 Triaxial compressive test	133
5.5.1 Set up of triaxial tests	135
5.5.2 Results	136
5.5.2.1 <i>Estimation of material constants</i>	141
5.5.2.2 <i>Fracture characterization</i>	144
<b>CHAPTER 6. VAJONT 3D GEOLOGICAL MODEL RECONSTRUCTION- GOCAD SOFTWARE</b>	
6.1 Introduction	147
6.2 Input data to GOCAD 3D modeling	148
6.3 3D surface reconstruction	149
6.4 3D modeling of the Vajon surfaces	150
6.5 Kinematics blocks evaluation	152
6.6 Results	154
<b>CONCLUSIONS</b>	157
<b>REFERENCES</b>	161
<b>APPENDIX A</b>	167



# INTRODUCTION

---

The frequency of giant rockslides is relatively high in sedimentary rock areas, especially in the Northern and Southern European Alps (Poschinger, 2002). Italy's Vajont rockslide is one of the best known and most tragic examples of a natural disaster induced by human activity. It is commonly considered as a reference event both for the geological risk evaluation, as well as for rock mechanics studies, as its study laid the basis of modern Engineering Geology. Although the Vajont rockslide is not the largest rockslide in the Alpine region, it can be considered as a reference case study at a worldwide scale due to its kinematics as well as the influence of reservoirs on the stability of mountain slopes affected by the presence of paleo-landslide. It is common knowledge that on 9 October 1963, a catastrophic landslide occurred on the northern slope of Mount Toc (Vajont valley, Northern Italy). A rock mass of approximately 270 million m<sup>3</sup> collapsed into the reservoir at velocities up to 30 m/sec generating a wave that breached the dam and swept into the Piave valley below, causing the death of approximately 2000 people. The flood destroyed the villages of Pirago, Villanova, Rivalta and Faé and most of the town of Longarone. Over US\$16 million was paid in respect of civil lawsuits brought in respect of personal injury and death. The US\$100 million dam and reservoir were abandoned. The landslide deposit filled the lower half of the Vajont Reservoir in a matter of 30 to 40 seconds. The event produced seismic shocks that were recorded throughout Europe. Remarkably the dam remained intact and unbroken by the flood, with only minor damage at the crest. The landslide is one of the most studied in the world, not only because of its catastrophic consequences, but also because of its unexpected behaviour. The catastrophic failure was preceded by a phase of accelerating creep lasting two to three years clearly related to the reservoir water levels. The appearance of an M-shaped tension crack on the southern slope of Mount Toc, one meter wide and two and a half kilometres long, foretold the oncoming failure. Despite this evidence, technicians and experts of the time hypothesized the presence of a very large and slow moving landslide that could be controlled by reservoir operations (Müller, 1964; Müller, 1968; Müller, 1987). At that time, the limited development of the investigation techniques and the absence of geotechnical risk protocols for the construction of hydroelectric projects in mountainous topography left the engineers and geologists involved unaware of both the seriousness of the situation and the need to engage in adequate countermeasures.

The Vajont's history represents a dramatic example of the paucity of knowledge of relevant geological aspects as well as the inadequacy of the investigations carried out between 1961 and 1963. It is indeed a sequence of misconceived technical operations and natural events, but the catastrophic landslide also represents an event for which the presence and the role of the complex combination of geological *s.l.* factors involved did not lead to an unambiguous and complete explanation of the phenomenon. The Vajont landslide history has taught the scientific community the importance of a thorough knowledge of the complex mechanisms that regulate the behaviour of large rock slope instabilities.

The literature about the Vajont landslide is more copious than for any other landslide ever occurred worldwide. Indeed, several interpretations of the event have been attempted in these last 49 years refer to understanding the slope deformation process up to the final movement, but a comprehensive and convincing explanation of both the triggering and dynamics of the phenomenon remains elusive.

Just the vast amount of works and data on the landslide suggested the need to have a catalogue that would contain the numerous data of the landslide. The first step of this work has been the creation of a bibliographic and geographic electronic geo-databases, including all existing bibliographic records (published documents, theses, unpublished technical reports and maps) and data collected on the Vajont landslide. It is an open-access database implemented in GIS system which may be continuously up-dated as new documents on Vajont are published. The bibliography on Vajont (Superchi et al., 2010) shows that most of the studies for re-evaluating the failure mechanisms were conducted in the last decade, this is due to the exceptional increment of new tools for publishing and sharing scientific papers, but it can be also referred to the increment in new knowledge, methods and techniques for rock mass analyses.

A re-evaluation of extensive literature pointed out that some of the main factors concerning the Vajont landslide have been clarified, such as the presence of thick clay-rich layers along the failure surface (Hendron and Patton, 1985) and whether the 1963 slide was a new slide or resulted from the reactivation of a prehistoric slide (Semenza and Ghirotti, 2000; Semenza, 2010), however many contradictory statements and conclusions are still present.

Large amounts of works on Vajont are as a matter of fact based on very few available papers or reports dealing with the geological conditions of the slope before and after 1963; unfortunately, many others contain blunders that testify a superficial reading of the reference

works or any field survey. Actually, many papers on Vajont just use and re-elaborate data from previous ones, but probably new insights can come through new field observation and investigation. A focal point pertinent to many hypotheses formulated in most of the published works in order to explain both triggering or kinematics or slope stability conditions is represented by the choice and adoption of a reliable geological model of the northern slope of Mount Toc.

Hendron and Patton (1985) clearly demonstrate how the three-dimensional shape of the sliding surface has been a significant effect on the behaviour of the slide and, thus the potential bias of two-dimensional profiles justifies both as the bi-dimensional stability analyses have always provided limited results and they remark the importance of a three-dimensional characterisation of the failure surface. Many years after the 3D back-analysis of Hendron and Patton (1985), it is probably time to re-consider the problem using numerical modelling able to take into account this aspect.

Following this way, it's probably time to face again with a reevaluation of the failure mechanism of the Vajont landslide and new researches on some not yet well known features of the area are possible. Is therefore no doubt that a priority aspect to be considered in any kind of approach to the Vajont, whether hydrogeological, or geomorphological and numerical modelling, is the highly three-dimensional character of the geological structures of the northern slope of Mount Toc. The knowledge of the geometry and shape of the sliding plane, geometry and shape of minor structures, such as folds, cascades structures and steps present on it, together with the rock mass characterization of all the lithological units involved in the movement, represent the starting point for any subsequent analyses and interpretation of the landslide.

New techniques and technologies not available in the 60's are here applied to investigate more in detail the mentioned features and to better understand their role in the 1963 event.

The increasing availability and precision of remote sensing techniques (DEM analyses, LIDAR technologies, photogrammetric analyses) integrated by field data surveys provide an accurate knowledge and in-depth evaluation of structural and geomechanical setting of the area. The geomechanical characterization of the Vajont rock sequence has been integrated by laboratory tests. The position of the sliding surface has been reconstructed starting from analyses carried out on original pre-1963 borehole cores.

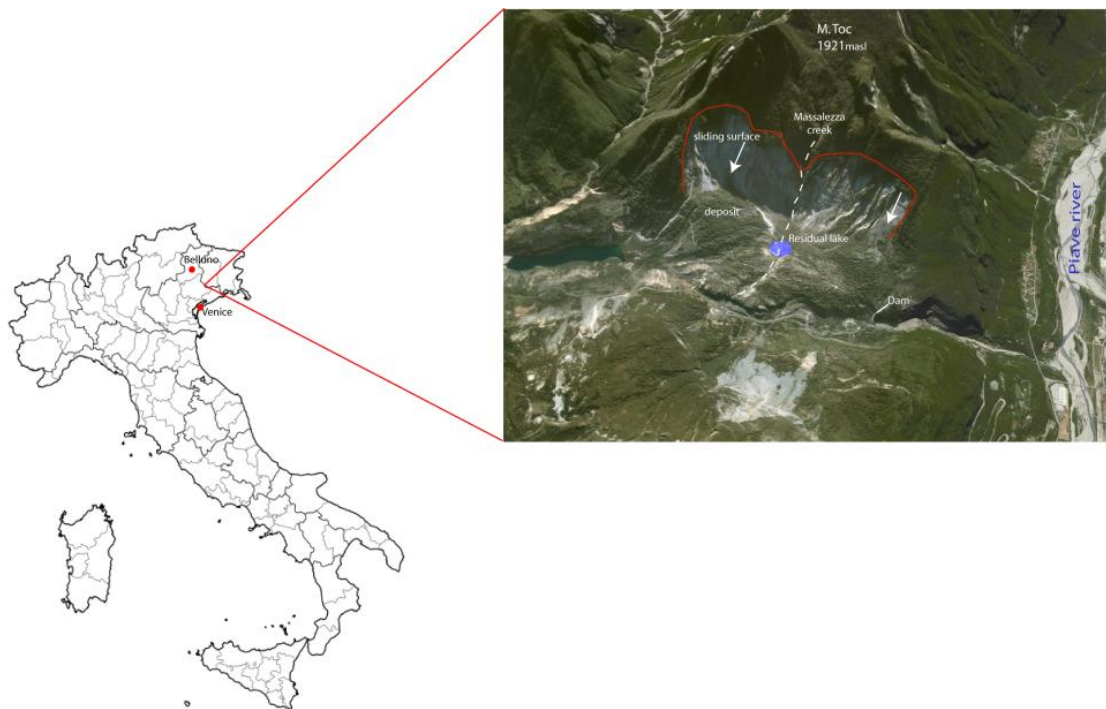
The present work proposes the first 3D geological model reconstruction of the landslide area pre- and post-landslide including the position and geometry of the sliding surface.

The accurate and detailed results achieved of the above mentioned techniques, combined with field investigations, laboratory tests and on-going geophysical surveys allowed to obtain a reliable 3D grid-based geological-technical model, which can be directly imported into numerical codes such as F.E.M, which may represent the fundamental starting point for future 3D slope stability numerical modelling of the Vajont landslide.

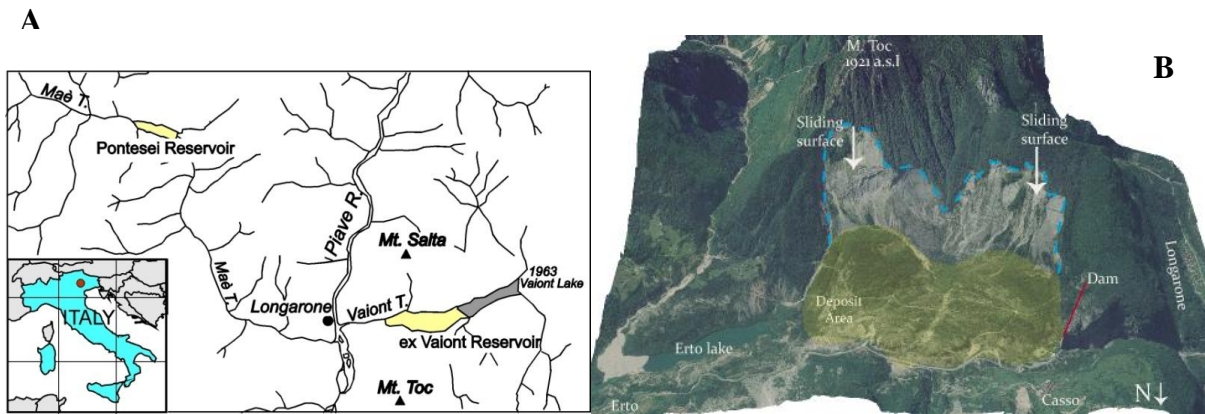
# CHAPTER 1

## 1.1 Geographic Framework

The Vajont landslide is located in the south-eastern area of the Dolomite region of the Italian Alps, about 100 km north of Venice, at the border between Veneto and Friuli-Venezia Giulia (Fig. 1.1). The rockslide is located at the confluence between the Vajont and the Piave River valley E-W and N-S trending respectively (Fig. 1.2A). It developed along the northern slopes of Mount Toc where the Vajont River had cut a canyon more than 300 m deep, just above its confluence with the Piave River. The landslide extends for almost 2.8 Km<sup>2</sup>, representing the deposit area of 1.6 Km<sup>2</sup> and the outcropping sliding surface of 1.2 Km<sup>2</sup> (Fig. 1.2B).

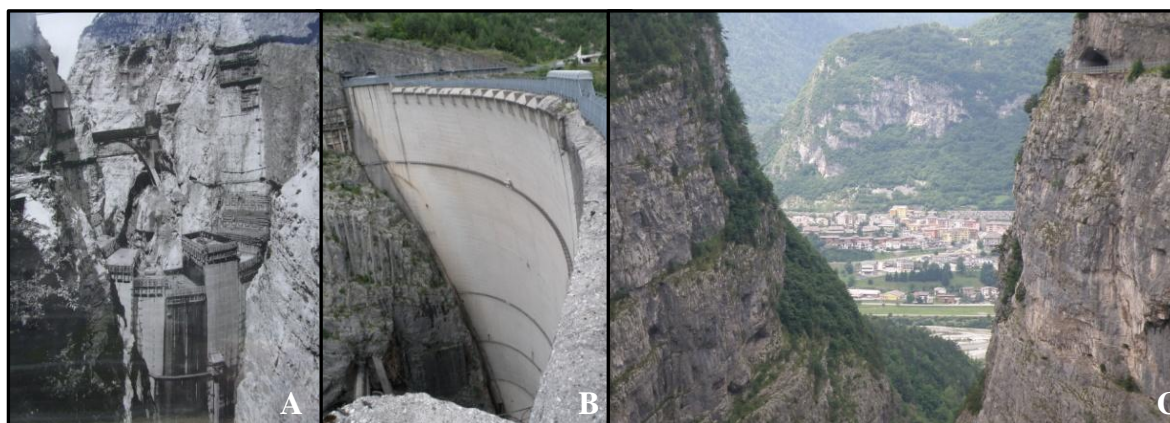


**Figure 1.1** – Location of the Vajont landslide.



**Figure 1.2** – A) Location of the Vajont reservoir (from Ghirotti et al.,2006). B) Details of the Vajont Rockslide.

By the end of the 1920s, the “Società Adriatica di Elettricità” (“SADE”) started a series of preliminary investigations with a view to using some valleys between Friuli-Venezia Giulia and the Veneto for hydroelectrical purposes. The Vajont valley was regarded as a suitable place since, among other things, it was considered deep enough to allow the filling of an artificial lake of estimated volume of 50 million m<sup>3</sup>. The Vajont dam was modified during construction to reach a maximum elevation of 721.60 m a.s.l, instead of the planned 677 m. The dam was built between 1957 and 1960 by the engineer Carlo Semenza. The doubly-curved arch dam, which rises 265.5m above the valley, was then the world’s tallest (Fig. 1.3). The planned full reservoir capacity was 169 million m<sup>3</sup>. The floor abutments were founded on the steep flanks of a deep canyon cut into limestone of the Malm and Dogger ages.



**Figure 1.3** - A) The Dam construction in 1959; B) Portion of the Vajont dam today; C) The narrow gorge of the Vajont valley as seen from the dam. Longarone in the background.

In February 1960, experimental filling of the reservoir began. The lake level reached 590m and along the northern wall of the slope two slide movements were verified. During the filling operation, a one-meter wide and two-and-half-kilometer long M-shaped tension crack opened

on the southern slope of Mount Toc. This is large-scale evidence of the presence of a large landslide and its re-activation as demonstrated in Giudici and Semenza's report (1960). At the end of October 1960, the movement of the perimetral crack reached and exceeded the velocity of 3 cm/day and, when the filling reached 650m a.s.l (November 4, 1960), a landslide of about 700,000m<sup>3</sup> slid into the reservoir producing a two-meter high wave. On February 1961, Prof. Leopold Müller reported the results of his investigation concerning the Vajont landslide, among other things, confirming Giudici and Semenza's finding that there had been a broad and deep landslide. Giudici and Semenza had calculated its mass at around 200 million cubic meters, with a front of almost two kilometres. In the following years, various on-site inspections by Professor Müller, Semenza and Giudici implemented different strategies to manage the emergency. Müller (1961) proposed to induce the progressive, slow mobilization of the entire mass by alternating slow filling and drawing down of the reservoir.

At same time, a very large by-pass gallery was excavated (in October 1961) into the right bank (Mount Salta) in order to ensure the preservation of the reservoir's functionality should the landslide divide the artificial lake. However, during October 1963 (which was during the third filling phase), the slide velocity exceeded the warning thresholds fixed by the technical commission and a rapid drawdown of the reservoir level was initiated. The drawdown action triggered the sudden rapid mobilization of the entire landslide mass and caused the Vajont catastrophe.

## **1.2 Literature Review**

Many published studies have considered the Vajont landslide over the last 48 years. However, several important aspects regarding failure mechanism and rockslide characteristics have not been exhaustively explained. The preliminary studies considered only some of the generic geological aspects of the Vajont area (Boyer, 1913, Dal Piaz, 1928). The first detailed geological studies were carried out in 1959-60 by F. Giudici and E. Semenza. They elaborated a technical and geological report, ordered by Müller, with a clear and detailed discussion of the geology, in which the hypothesis of the existence of a very old landslide on the left bank of the Vajont reservoir area was also made. Indeed, during their field investigations, they found a highly fractured zone named "mylonite" *auct* corresponding to cataclasite in the

update classification (Sibson, 1977) extending about 1.5 km along the left side of the valley corresponding to the sliding plane of the prehistoric landslide. The other studies conducted before 9 October 1963 (that is, the date of the catastrophe) were based on geoseismic investigations performed upstream of the Vajont dam by Caloi and Spadea in 1960, and by a formulation of a detailed report about the nature of the rockslide, its influence on the dam and about the effect of the lake level on the slope. After 1963, many papers were published in the international literature that can be subdivided into the following categories:

- Publications based on interpretations of the slide and focused on geological and geomorphological aspects (Carloni and Mazzanti, 1964a, 1964b; Frattini et al., 1964; Kiersch, 1964; 1965; Müller, 1964; 1968; 1987a, 1987b; Selli and Trevisan, 1964; Selli et al., 1964; Rossi and Semenza, 1965; Semenza, 1965; 2010; Broili, 1967; Martinis, 1979; Hendron and Patton, 1985; Riva et al., 1990; Semenza and Melidoro, 1992; Mantovani and Vita-Finzi, 2003; Semenza and Ghirotti, 1998; 2000).
- Investigations focused on the conditions underlying the landslide's development and triggering, providing detailed engineering geological descriptions, such as the geotechnical properties of the mass involved (particularly the important role of the clay interbed) and the rheological behavior of the failure mass, and considering different approaches of stability analysis, in order to explain the role of various factors that led to the movements (Ciabatti, 1964; Kiersch, 1964; Jäeger, 1965 a, b; 1972; Caloi, 1966; Mencl, 1966; Skempton, 1966; Kenney, 1967; Nonveiller, 1967; 1987; Lo et al., 1971; Habib, 1975; Chowdhury, 1978; Trollope, 1980; Corbyn, 1982; Voight and Faust, 1982, 1992; Hendron and Patton, 1985; Belloni and Stefani, 1987; Hutchinson, 1987; Leonards, 1987; Voight, 1988; 1989; Ghirotti, 1992; Sitar and Mac Laughlin, 1997; Tika and Hutchinson, 1999; Erismann and Abele, 2001; Vardoulakis, 2002; Crosta and Agliardi, 2003; Helmstetter et al., 2004; Kilburn and Petley, 2003; Sornette *et al.*, 2003; Sitar *et al.*, 2005; Rose and Hungr, 2007; Veveakis *et al.*, 2007; Alonso *et al.*, 2010; Alonso and Pinyol, 2010; Ferri *et al.* 2010; Mufundirwa *et al.*, 2010; Pinyol and Alonso, 2010).
- Publications related to the landslide-generated impulsive wave including, Panizzo *et al.*, 2005; Roubtsova and Kahawita, 2006; Pastor *et al.*, 2009; and Bosa and Petti, 2011; Ward and Day, 2011. A comprehensive review of research on the Vajont landslide has been published by Genevois and Ghirotti, (2005).



Published and unpublished reports on the Vajont landslide were collected in an electronic bibliographic database. A study relevant to the database structure and its details was published by Superchi et al. (2010) and included herein as Appendix A. For reasons of copyright, the database itself could not be reproduced in the present work.

# CHAPTER 2

## GEOLOGICAL FRAMEWORK

### 2.1 Regional Geo-structural setting

The study area is located in the Eastern-Southern Alps that, including the Dolomite region, are separated from the Orogenic wedge of the Alps *s.s* by an important fault system known as the Insubric (or Periadriatic) lineament (Fig. 2.1), which forms the northern geological limit of the region (Bosellini, 1992). The Eastern-Southern Alpine belt is affected by an intense south-vergent thrusting opposite to the tectonic polarity of the Alpine Orogenic wedge verging to the north (Castellarin, 2000). This portion of the Eastern Southern Alps is characterized by several south verging thrusts related to the different deformation phases that led to the Alpine chain development.

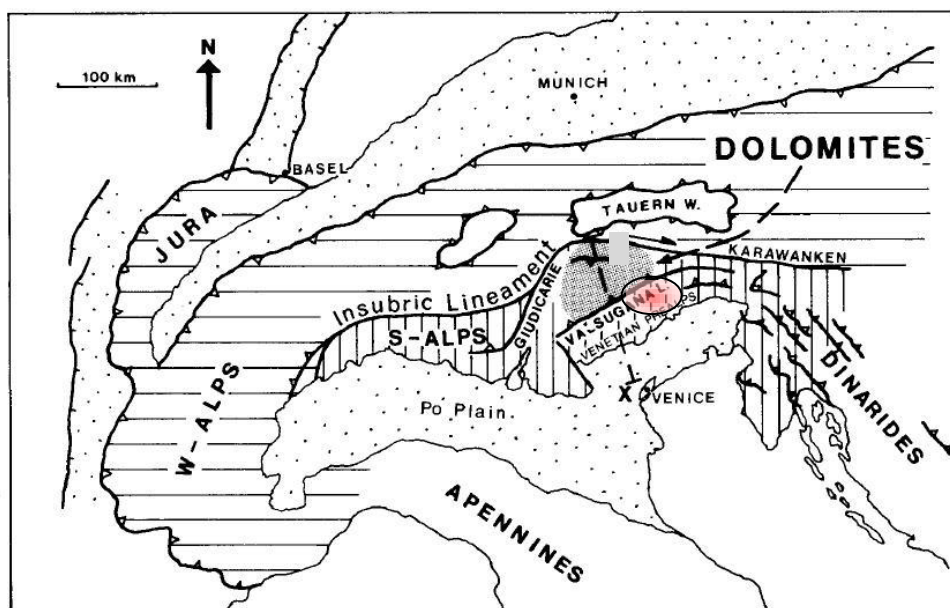


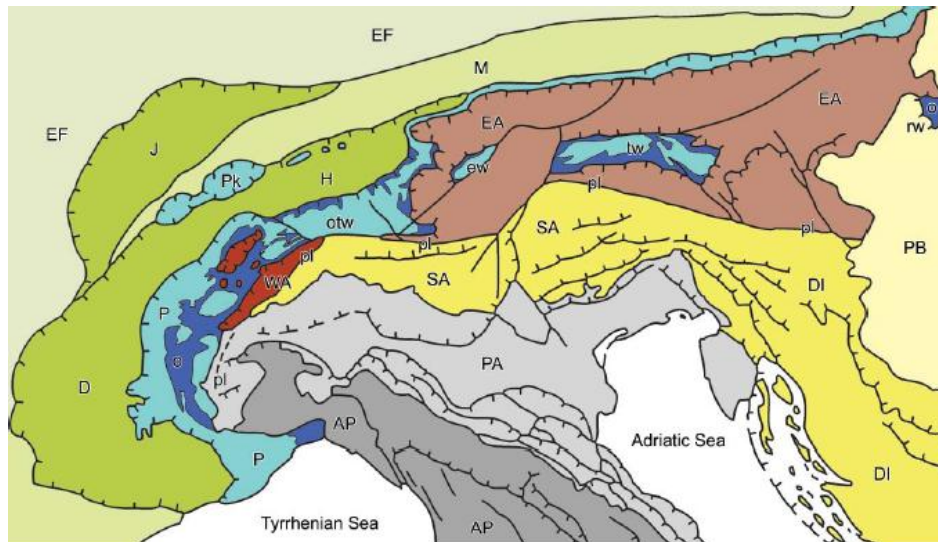
Figure 2.1 - Location of the study area in Alpine context. (Modified from Doglioni, 1987).

The early continental rifting evolution in the present Southern Alps results from the extensional tectonics and magmatic activities which occurred during the Lower Permian and Middle Triassic times (Dal Piaz, 1993; Selli, 1998). Indeed, in this period the Southalpine

domain was flooded and characterized by more a carbonate platform extending in the area of interest to the Cretaceous (internal Penninic) or Eocene (Briançonnais) synorogenic deposits, and basin systems (Dal Piaz et al., 2003). The whole region underwent a rifting phase, which developed from the Norian to the early Middle Jurassic, leading to the opening of the Piedmont-Ligurian Ocean, when the Austroalpine and Southalpine domains became the subsiding passive continental margin of Adria. (Dal piaz et al., 2003) Fig. 2.2

The Alpine belt is the result of the complex collision between African (Apulia or Adria) and European plates that developed during the following three main phases:

- The **Eo-Alpine** phase (Cretaceous-Paleocene) is the pre-collisional phase during which the Piedmont-Ligurian Ocean closed and subduction occurred.
- The **Meso-Alpine** phase (Eocene-Oligocene) is the post-occasional magmatism phase during which the collision between the European and African plates began. Indeed, the subduction complex was exhumed to shallower structural levels and overprinted by a Barrovian metamorphism of Late Eocene-Early Oligocene age. (Dal Piaz et al., 2003). A compressive event involved the eastern sector of the Southern Alps and several NW-SE thrusts verging towards the SW. This deformation is considered to be the front of the Dinaridism, which began to deform in the Late Cretaceous until at least the early Oligocene (Doglioni, 1987). This led to a NW-SE shortening of the Southern Alps, of about 10-15 Km (Castellarin, 2000).
- The **Neo-Alpine** phase (the Miocene - to the present) during which an opposite-vergent thrust-and-fold has taken place (South-vergent) moving against the rear of the wedge, and ultimately forming the Venetian Southern Alps (Castellarin, 2000).



**Figure 2.2** - Tectonic map of the Alps: (1) Europe-vergent collisional belt: i) Western (WA) and Eastern (EA) Austroalpine; ii) Penninic domain: continental and ophiolitic (o) nappes in western Alpine arc (P) and tectonic windows (otw: Ossola-Ticino, ew: Engadine, tw: Tauern, rw: Rechnitz); Prealpine klippen (Pk); iii) Helvetic-Dauphinois (H-D) domain; iv) Molasse foredeep (M); v) Jura belt (J). (2) Southern Alps (SA), bounded to the north by the Periadriatic lineament (pl). Pannonian basin (PB), European (EF) and Po Valley-Adriatic (PA) forelands, Dinaric (DI) and Apenninic (AP) thrust-and-fold belts. (Dal Piaz et al., 2003).

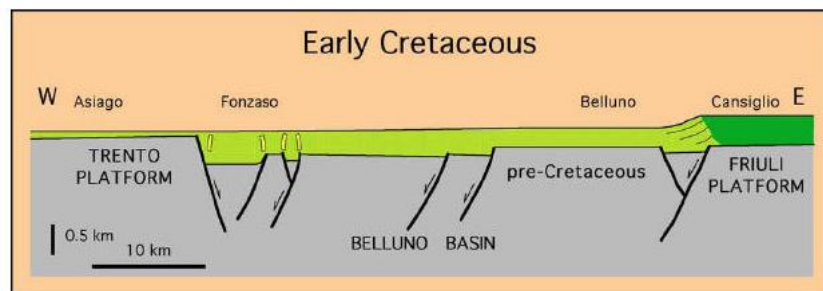
The EO-MESO Alpine events left no structural evidence in the Venetian Southern Alps. They are evidenced only by the drastic, Upper Cretaceous change in the marine sedimentation which is characterized by strong siliciclastic input of Flysch deposits in the basin areas. This kind of sedimentation is present also in the Dolomites. (Castellarin et al., 2004). Thus, the Eastern Southern Alps show predominantly Cenozoic compressive structures. Some of them are of neo-formation and some others are derived from the reworking of the Mesozoic extensional systems.

## 2.2 Stratigraphy of the Vajont valley

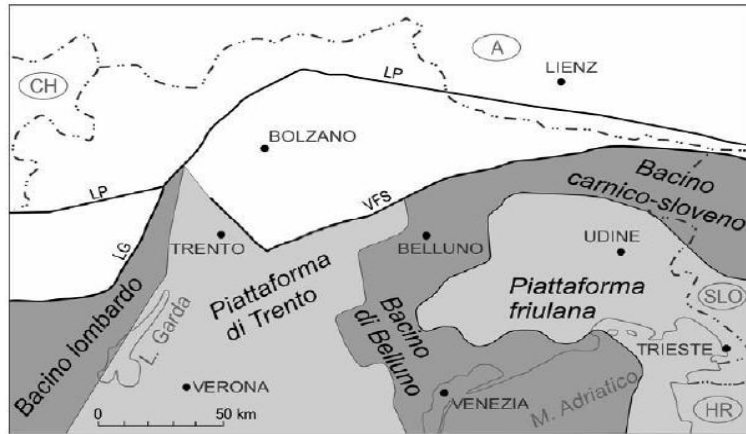
The stratigraphic sequence outcropping in the Vajont and adjoining valleys (Zemola and Tuora on the right and Messazzo on the left), covers the upper Trias (Dolomia principale) to Eocene (Flysh). It is constituted by the following units: Dolomia Principale, Soverzene formation, Igne formation, Vajont limestone, Fonzaso and Socchèr formations, Scaglia Rossa, Erto Marls and Eocenic flysh.

This stratigraphic sequence, predominantly formed by carbonatic rocks with chert intercalation, is typical of a basin area. Indeed, during Lias, the subsidence of the Triassic platform formed two main paleogeographic domains: the Friuli platform, and the Belluno basin or Trough. (Fig. 2.3 and 2.4). The Belluno Trough is a basin located on the northwestern corner of the Apulian Plate continental margin, and the Vajont landslide area is located within that basin. It acquired a geographic identity in the Early Liassic time, during the breakup of a widespread Upper Triassic carbonate shelf. It was a starved basin accumulating euxinic mudstone and bounded by two shallow-water carbonate banks, the Trento and Friuli Platforms (Bosellini et al.,1981).

The main differences between the formations in the Vajont valley reflect quantitative and qualitative changes related to the platform production.



**Figure 2.3** - Interpreted W-E Early Cretaceous cross section from the Asiago plateau to the Cansiglio plateau, showing the coeval tensional tectonics, which produced differential subsidence in the area (modified from Doglioni and Carminati, 2002).



**Figure 2.4** - Early and Middle Jurassic paleogeography of the Venetian Alps (modified from Bosellini et al, 1981; Cati et al, 1987).

- 1 DOLOMIA PRINCIPALE (Upper Triassic time): It constitutes the oldest outcrops in the Vajont area and consists of massive, dolomitic gray limestone, 1000m thick, presenting in some places clay intercalations
- 2 SOVERZENE FORMATION (Lower Jurassic)  
It formed by a continuous succession, 600m thick, of well-stratified, grey and brown micrites, alternated to centimetrical levels of grey and yellow marls. Black chert in nodules and beds is also present. This formation derives from the accumulation of carbonatic muds on the bottom of the Belluno basin (Masetti, 1986)
- 3 IGNE FORMATION (Upper Lias to Upper Cretaceous): The depositional environment of the Igne Formation, 150m thick, represents the continuation to the upper side of the basin sedimentation which developed in the whole Belluno area Fig.2.4. It is characterized by a lithologic heterogeneity due to the alternation of grey marl and limestones. In some places, the Igne formation reaches an arenaceous aspect because of the presence of fine-grained silts. At the unit base, black marls rich in organic materials can be seen.
- 4 VAJONT LIMESTONE (Dogger): It is composed of very compact oolitic and crystalline limestones of rigid formation, which are poorly stratified in intensely fractured thick layers. In the Vajont valley, the formation is about 300m thick and reaches 370m at elevation. The oolitic deposits are considered to have resulted from turbiditic streams that had moved west in the Belluno basin area. The Vajont dam lies upon this formation. However, the Dogger formation is at the base of the slide zone and was not involved in the 1963 movement.
- 5 FONZASO FORMATION: (Malm-Middle Cretaceous)  
The Malm consists of gray cherty limestones with black chert, usually nodular, from 10 to 40 metres thick. In particular, in the lowest part of the formation, the study area includes thin-bedded micritic limestones and calcarenites. The lower and middle Cretaceous portion is composed of limestones or marly limestones, containing cherts, with thin, soft calcareous marly or clayey-marley interbeds (sometimes about 10 cm thick). The color is prevalently red in the upper part, greenish in the middle and light gray at the base. The formation is of intensely fractured thin strata and it is easily deformed (Semenza, 1965).  
The upper part of the Fonzaso formation is characterized by a series of clay-levels interbedded of around 1-2 cm to 3m thick. The above-mentioned clay levels are one of the main parameters used in analyzing the slope failure mechanism of the Vajont

landslide (Hendron & Patton, 1985), and indeed, it is in this formation that the sliding surface of the landslide was located.

6 ROSSO AMMONITICO: (Kimmerdgian-Titonian)

Nodular reddish and grey micrites with Ammonites, massif or in layers of more than 1m of thickness that are different only in colour from the classic facies outcropping in the Veneto area (Masetti, 1986). The formation's thickness varies from 2m to 10m.

7 SOCCHÈR FORMATION: (Middle-Upper Cretaceous)

The lower part of the Socchèr formation is composed of an extremely compact conglomerate with pinkish or gray cement around 1m thick (Semenza, 1965). In the sequence, it is followed by compact beds of grey limestones and calcareous marls alternated with chert layers. The upper part of the Socchèr formation includes another layer of red marl calcareous limestone with calcite vein and red-black chert nodules. The thickness of this layer is around 3-4m. The main characteristic of this last layer is the presence of several green clay interbed levels 1-2 cm thick (Martinis, 1978). The formation is about 150m thick.

8 SCAGLIA ROSSA FORMATION (Upper Cretaceous)

The "Scaglia Rossa" formation consists of gray reddish marly-limestones. These marls are generally red except for a gray intercalation. The rock is fine-grained and shows a different fracturing degree. Its total thickness is approximately 300m (Semenza et al., 1986)

9 ERTO MARLS (Upper Paleocene)

This unit represents the transition between the Scaglia Rossa and Flysh and is composed of marls and grey marly limestones, intensely bioturbated, containing rare, thin layers of calcarenites and litharenites. The formation is 100 to 150m thick (Masetti, 1986).

10 FLYSH

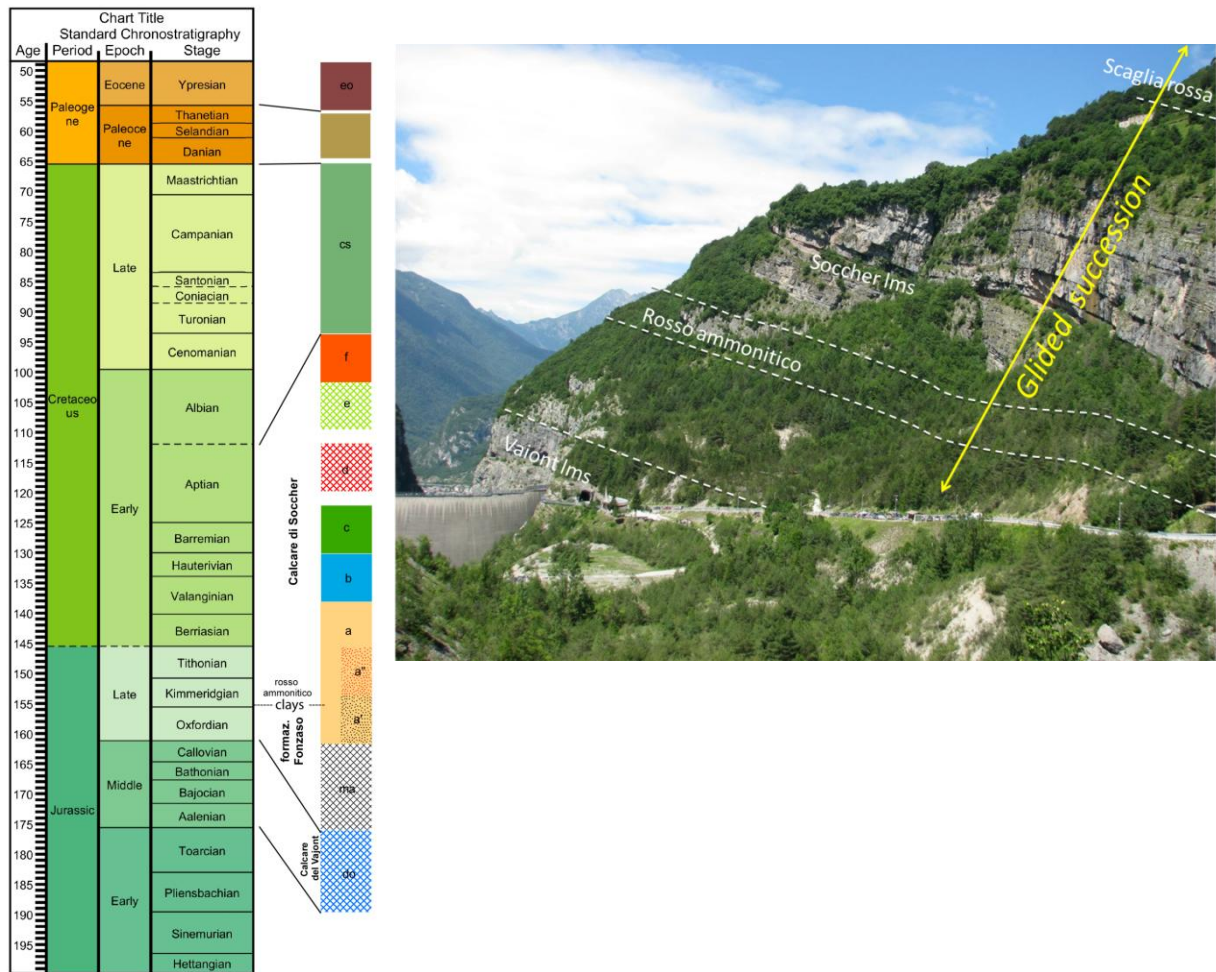
It is composed of gray or greenish marls with sandstone intercalations approximately 200m thick (Semenza et al., 1986).

The whole stratigraphic sequence outcrops on the right slope of the Vajont valley, in the opposite side of Mount Toc (Fig. 2.5).

The materials involved in the 1963 landslide include the Fonzaso formation, and in particular the lower and middle Cretaceous stratigraphic sequences that assumed an important role in the 1963 movement because of their typical plasticity. The Socchèr



formation constitutes the upper portion involved in the movement and it is still currently recognizable in several zones of the deposit area.



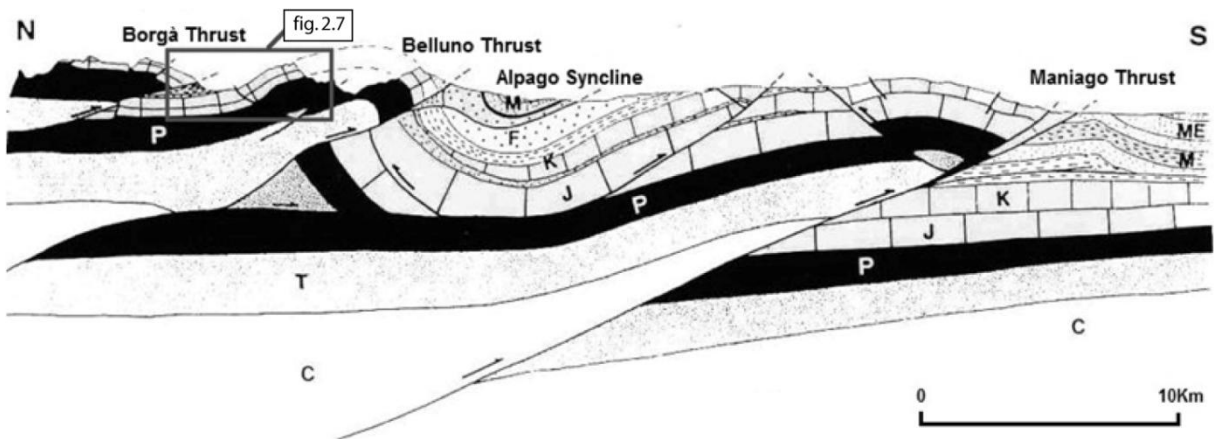
**Figure 2.5** - Stratigraphic sequence of the formations outcropping in the right flank of the Vajont valley, and detail of glided formations (photo by Zampieri, 2011).

### 2.3 Structural setting

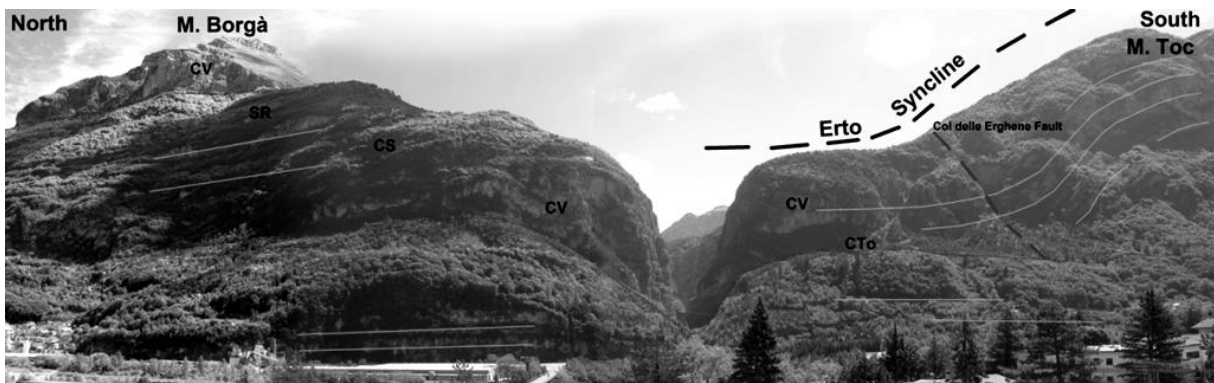
The Vajont area is characterized by a very complex structural setting, mainly due to the Alpine Orogenesis, and in particular, due to the South Alpine thrust belt that developed in the Oligocene-Miocene (Doglioni and Bosellini, 1987). The southern slope of the Vajont valley, from where the landslide developed, reflects Jurassic sequences entirely (Fig. 2.6 and 2.7).

The valley is dominated by a series of E-W folds, one of which (the Erto Syncline) marks the 1963 landslide area and represents the most evident structure. It plunges upstream to the east and can be clearly seen from the Piave valley (Fig. 2.7). A very narrow gorge along the east-

west axis of the asymmetric Erto syncline, incised from the Vajont Stream, can be recognized (Fig. 2.7). The southern flank of the Syncline dips with  $30^{\circ}$  to  $40^{\circ}$  to the North and forms the 1963 slope failure surface, whereas the northern flank dips with  $20^{\circ}$  to  $30^{\circ}$  to the East. The shape of the plane is “chair like” (Giudici & Semenza, 1960), with the lightly bended upper portion dipping rather steeply towards the valley and with the ‘seat’ flattening into a more horizontal structure (Fig. 2.6).



**Figure 2.6** - Legend: C, undifferentiated crystalline basement; T, Late Permian and Early-Middle Triassic formations; P, Late Triassic Dolomia Principale; J, undifferentiated Jurassic: platform facies (Calcari Grigi) in the southern part of the section, gradually passing northward to basinal facies (Soverzene Formation, Igne Formation, Vajont Limestone, Fonzaso Formation, Ammonitico Rosso); K, Cretaceous, platform facies (Calcare del Monte Cavallo, brick pattern) gradually passing northward to slope deposits and basinal facies (Calcare di Soccher, Biancone); S, Scaglia Rossa, Late Cretaceous - Paleocene; F, Eocene Flysch; M, Late Oligocene - Early-Middle Miocene Molasse; ME, Messinian conglomerates. (Modified from Doglioni and Carminati, 2008).

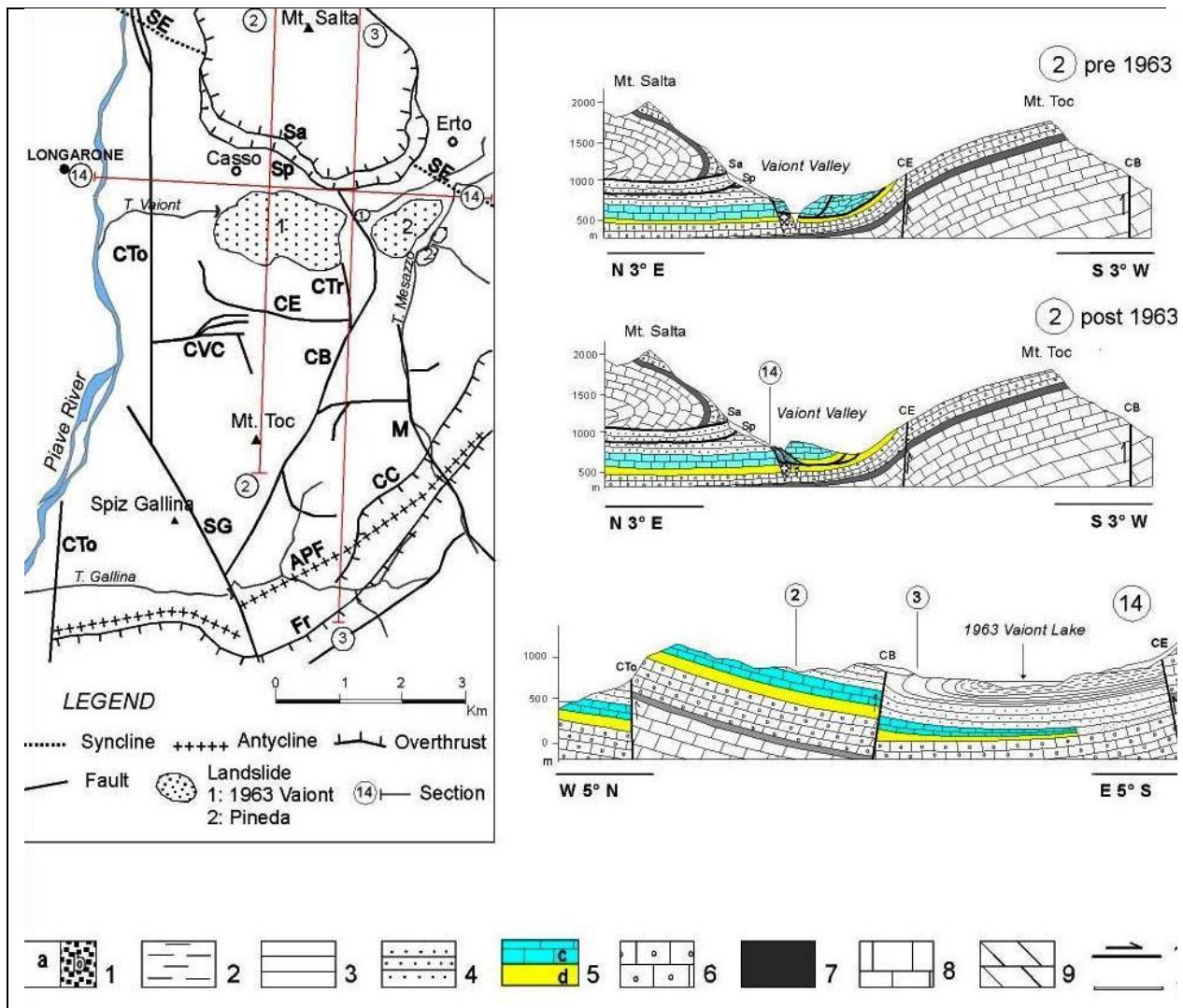


**Figure 2.7** - Structural setting of the eastern slope of the Piave valley. Labels of symbols. CTc: Col delle Tosatte Fault; CE: Col delle Erghene Fault. CV: Vajont limestone Fm.; CS: Socchèr limestone; SR: Scaglia Rossa.

A series of thrusts developed along the syncline flanks. A portion of the M.Borgà thrust is represented by Monte Salta (Fig. 2.8). It makes contact with the Jurassic formation of the “Scaglia Rossa”. The folded and fractured limestone strata at the hanging wall of the M. Borgà thrust gave rise to some rockfalls which affected the southern slope of Mount Salta. These phenomena occurred because Mount Salta is carved within the front of the hanging wall anticline of the Mount Borgà thrust. The Erto Syncline is characterized by several important longitudinal, trasversal or oblique dislocations (Riva et al., 1991) cutting the syncline flank and defining the Vajont landslide boundaries. The landslide area is laterally bordered by a system of southward, converging subvertical faults, partly inherited from extensional Mesozoic deformations: the Croda Bianca and Col Tramontin Lines.

The latter represents the eastern boundary of the 1963 landslide. The western boundary is not, however, intersected by important trasversal dislocation apart from the terminal side of the E-W trending normal fault, Col delle Erghene. This shows a N-S strike in correspondence to the southwestern limit (Fig. 2.8).

Col delle Tosatte line (Cto) represents the eastern border of Longarone graben (Riva et al., 1990, Doglioni & Carminati, 2008), clearly visible from the Piave valley (Fig. 2.7).



**Figure 2. 8-** Tectonic map and geological sections of the western part of the Vajont Valley. Labels symbols in the tectonic map. CB: Croda Bianca Fault; CE: Col delle Erghene Fault; CTr: Col Tramontin Fault; Sa M. Salta overthrust; CVC: Costa Vasei-Calta Faults; Cto: Col delle Tosatte Fault; SG: Spiz Gallina Fault; CC: Cima di Camp Fault; FR: Val Ferron Fault; M: Val Mesazzo Fault; APF: Pelf- Frugna Antycline; SE: Erto syncline. Legend of the geological sections. 1- a Quaternary; b stratified alluvial gravels; 2- Flysh Fm. (Eocene); 3- Marne di Erto (Paleocene); 4- Scaglia Rossa Fm. (Upper Cretaceous-Lower Paleocene); 5- Cretaceous-Jurassic Fms. (Socchèr )Fm. *Sensu lato* and coeval); c Socchèr Fm. s:s, d Ammonitico Rosso and Fonzaso Fms.; 6- Vajont limestone (Dogger); 7- Igne Fm. (Upper liassic); 8- Soverzene Fm (Lower and Middle Liassic); 9- Dolomia Principale (Upper Triassic); 10- Faults and overthrusts; 11- Failure surface of 1963 rockslide. (Modified from Riva et al.,1990 and from Semenza and Ghirotti, 2000).

As mentioned in paragraph 2.2, the Vajont landslide involved Jurassic and Cretaceous rocks (limestones and marls), which slid along the chair-shaped southern flank of the Erto syncline, partly corresponding to a pre-existing slip surface as already recognized before 1963 (Semenza, 1965).

Some approximately east-west folds were observed in the area by Semenza. The most evident were the Toc Syncline, clearly visible on the north-western wall of “ Punta del Toc”, also subdivided by a minor faulted anticline. The “Main” anticline, faulted along the whole

southern side and a syncline in the Pozza plain area, are both easily observed in the Massalezza valley (Semenza, 1965).

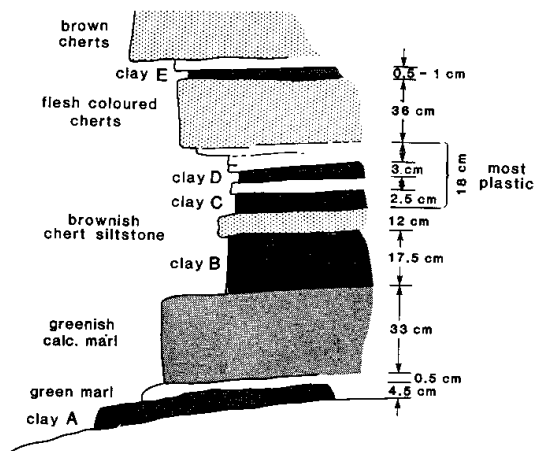
## **2.5 Description of the rockslide**

On October 9, 1963 about 270 million m<sup>3</sup> of limestone, mudstone and marl slid from the southern slope of Mount Toc into the Vajont Reservoir, producing a displacement wave that breached the dam (265 m), swept into the populated Piave Valley below and ultimately resulted in the deaths of over 2000 people. The slide moved a 250 m-thick mass of rocks, some 300 to 400 m horizontally, collapsed at velocities of up to 30 m/s before running up and stopping against the opposite side of the Vajont Valley wall (Semenza, 1965). The Jurassic and Cretaceous rocks (limestones and marls mainly of the Socchér Formation) that were involved in the movement showed varying degrees of fracturing; they slid down along the “chair-like” bedding planes, causing the outcropping of the Fonzaso Formation (Genevois and Ghirotti, 2005). The failure was indicated to be principally confined within the 0.5–18 cm thick, clay-rich layers, which were observed to be continuous over large areas of the failure surface (Hendron and Patton, 1985) (Figure 2. 9). Clays can be seen on the sliding surface, and they also form the matrix of the lower portions of the slide mass (Hendron and Patton, 1985). However, the role of the clay layers involved in the 1963 movement is not clear: researchers have expressed a number of different opinions on the matter in the decades since the slide: Selli & Trevisan (1964), Muller (1964) and Broili (1967), following several investigations and analyses both of the nature of the rocks and the interbed material, have come to the conclusion that the stratigraphic sequence contained a limited percentage of clay minerals [montmorillonite and in part probably illite, amounting to on average 16% of the total (Broili 1967)], and not exceeding 25-30% of the total and therefore considered as marls rather than clays.

The new slide displaced an old slide mass that was isolated on the north side of the valley during the 1963 event. The old slide material moved about 100 to 100 m above its original position before slumping backwards 30 to 40 m to the south (Hendron & Patton, 1985).

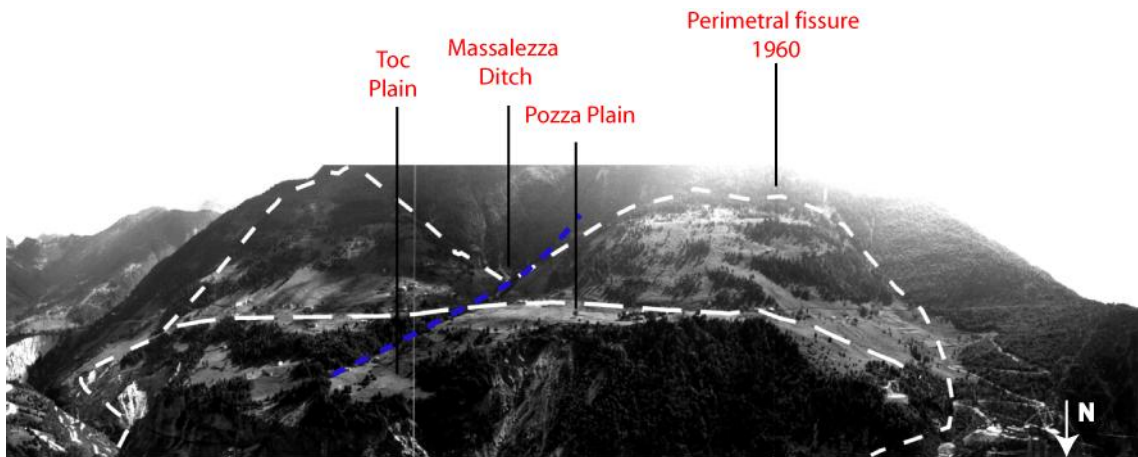
The wave, triggered by the rock mass slid into the reservoir, eroded trees and soil on the north side of the Vajont Valley up to a maximum elevation of 935 m (235 m above the reservoir level). The wave swept across the dam, reaching over 140 m above its crest (435 m above the downstream base of the dam), and moved down the Vajont Gorge.

Actually the most important and evident morphological effect of the landslide is the disappearance of the Valley (deep 300m) which is now replaced by a Mount constituting the deposit of the slide, 400m above the Vajont Gorge.



**Figure 2. 9**– Sketch of outcrop of lower Cretaceous Formation with clay interbeds, varying from 0.5 to 17.5 cm thick, west of Casso. This outcrop lies in the same stratigraphic position of the strata located at the base of the 1963 Vajont landslide. (from Hendron & Patton, 1985).

The southern slope of Mount Toc prior to the slide was characterized by central north-south trending dry valley of the Massalezza, a tributary to the Vajont River (Figure 2.10) and there was a prominent bluff at 777 m elevation called the Punta del Toc. A prominent bench at about 840 to 850 m elevation was present part-way up the western side of the slide. This plain was called the Pian della Pozza, or Pozza, and contained several enclosed depressions (Fig. 2.12-2.13) and constituted one of the main pieces of evidence of the earlier period slope movements.



**Figure 2.10** - The northern slope of Mount Toc in 1959 from Casso. The dashed line delimits the boundary of 9 October 1963 landslide. The lower dotted white line indicates the first Semenza's hypothesis regarding the boundary of the ancient landslide (Semenza, 1965 modified).

## 2.6 Geological and Geomorphological Aspects

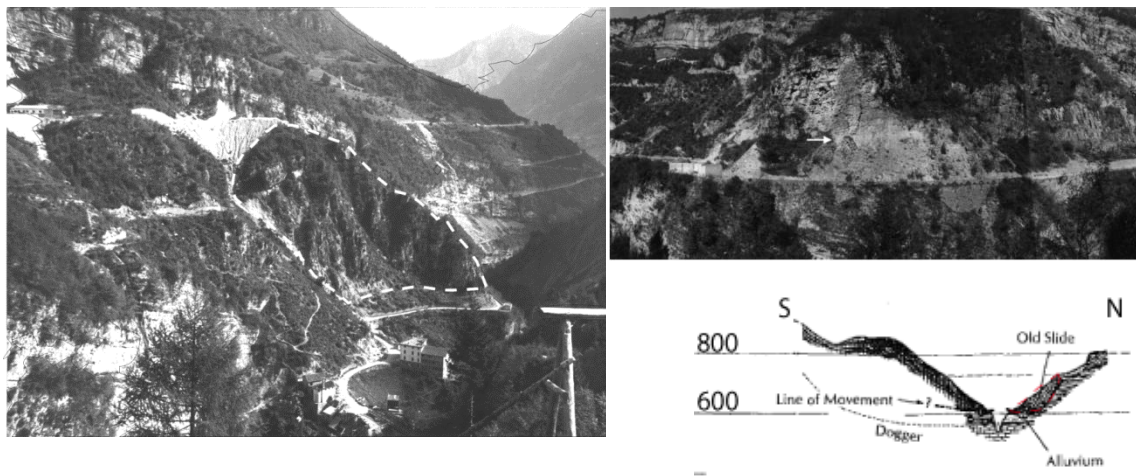
The Vajont landslide was a reactivation of an old slide (Giudici & Semenza, 1960, Hendron & Patton, 1985). It is not known when the older slide occurred, but it is generally thought that it occurred during the post-glacial period, and thus earlier than the Vajont valley's period of recorded history.

The first hypothesis regarding the existence of a large paleo-landslide on the northern slope of Mount Toc was put forward, as mentioned above, by Giudici and Semenza (1960). It was based essentially on the geomorphologic evidence gathered between 1959-1960 through various, accurate field investigations. The main geomorphologic markers were:

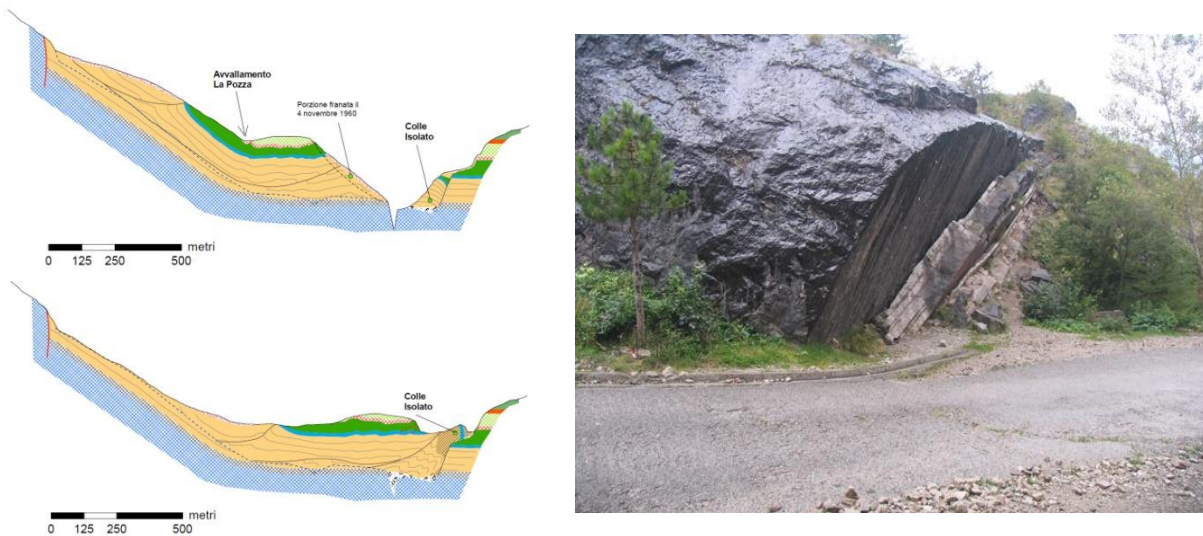
- ✚ The presence of a small and elongated depression of about 2Km<sup>2</sup> on the western side of the slope, the Pozza plain (Figure 2.10). This depression was characterized by a trench and very steep wall near the Massalezza ditch.
- ✚ The Toc plain (Figure 2.10) constituted a sub-horizontal strata crossed by vertical fractures trending east-west. Its northwestern area also came into contact with the east-west trending fold system. The anomalous altitude of the strata was recognized between the “back” and the “seat” of the chair-structure, the latter characterized by an abrupt dip variation in the slope mainly in its eastern sector.
- ✚ The discovery of a small preserved part of the ancient landslide on the northern slope of the valley, (Fig. 2.11) was clearly distinguishable from the regular *in situ* rock mass, as it showed vertical fracturing totally absent in the surrounding rock mass.

Moreover, this mass was nonconforming with respect to the *in situ* Socchèr formation. It was consequently called "Colle Isolato" (Isolated Hill). Colle Isolato was a fractured rock resting on stratified alluvial gravels deposited by the old postglacial Vajont River resulting from the postglacial landslide deposit. It was composed of a thin horizontal band of white cataclasite (arrow), and separated from *in situ* rocks by sub-horizontal layers of the overlying ancient landslide.

As a consequence of the Vajont landslide, the "Colle Isolato" was pushed uphill about 50 m on the right side of the valley (Genevois & Ghirotti, 2005). (Figure 2. 12).



**Figure 2. 11** - View of Colle Isolato outlined with dashed line, first mapped by Giudici and Semenza in 1965. A thin horizontal band of white cataclasite (arrow) separates *in situ* rock from subhorizontal layers of the overlying ancient landslide (Semenza & Ghirotti, 2000, Hendron & Patton, 1985. Modified).



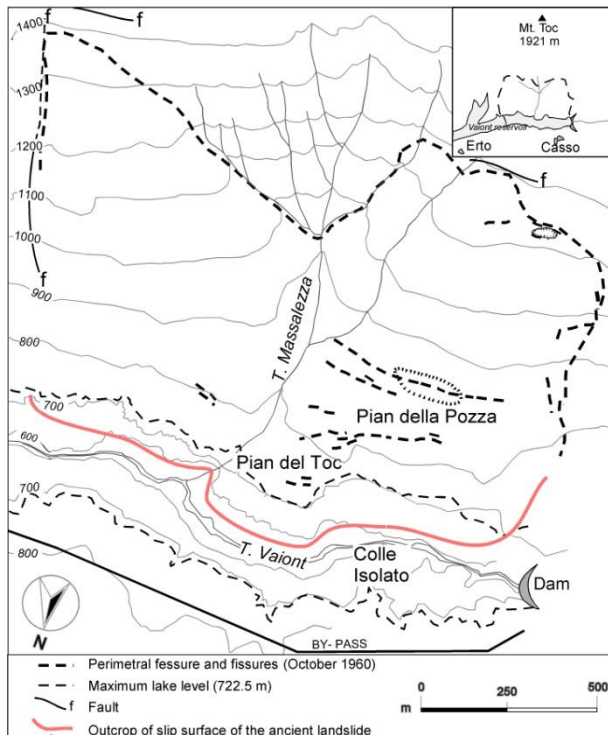
**Figure 2. 12** - Evolution of Isolated Hill, pre and post the 1963 landslide (Rossi and Semenza, 1965, modified).



- ✚ The discovery of the previously-mentioned mylonite<sup>1</sup> belt extending about 1.5 km along the left side of the valley was confirmed also by field investigations carried out in 1960. The belt outcropped at the foot of the cliffs below Punta del Toc near their eastern extremity. It separated the ancient landslide from the *in situ* bedrocks and corresponded to the sliding plane of the prehistoric landslide discovered by Giudici & Semenza (1960). Cataclasite and tectonic breccia layers were also observed in the Pian della Pozza area at an altitude of approximately 850 m asl (Figure 2.13) and on the western branch of the Massalezza Stream (Semenza & Ghirotti, 2000).

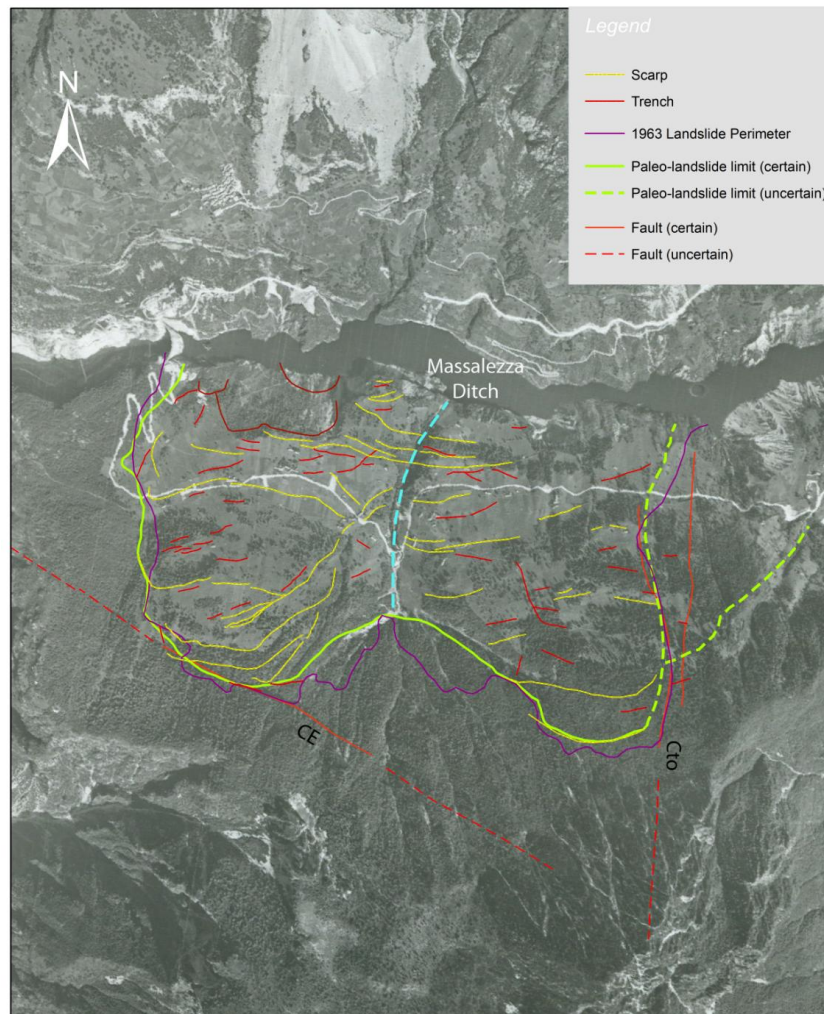
The existence of the highly fractured mylonite belt on top of the *in situ* rock was confirmed by the several boreholes drilled after 1963 by the companies Sorinco (between 1964 and 1966) and Rodio (between 1964 and 1965). Indeed, eleven out of eighteen boreholes drilled by Sorinco reached the bedrock oolitic limestones. It was noted that some layers of the cataclastic and mylonitic rocks, a few meters thick, were encountered immediately before the *in situ* rocks. This was considered to confirm that the movement zone had developed in correspondence to the above-mentioned belt (Broili, 1967). The cataclastic layers were also found in some of Rodio's boreholes as shown in Martini's work (1978).

- ✚ The perimetral crack (Fig. 2.1) which first appeared in 1960 clearly marked the upper limit of the future slide, as well as the general trend of the outcropping portion of the presumed slip surface (Giudici & Semenza (1960), Broili, (1967) and Hendron & Patton (1985)).



**Figure 2.13** - 1) Map of the 1963 pre-landslide area. 2) The Pian della Pozza depression in 1959. It was incorrectly indicated to be a doline, but here a trench of 30 to 40 centimetres' depth, excavated in April 1960, revealed the presence of thin sub-horizontal layers of highly fractured cherty Cretaceous limestone. 3) The perimetral crack opened in 1960 (photograph by Semenza, August 1959) (Ghirotti, 2005, 2006 modified).

The major geomorphological and structural features diffusely discussed by Semenza (1965), Hendron & Patton (1985), and by Guerricchio & Melidoro (1986) are represented in the map of the Fig. 2.14 . These analyses confirmed the presence of the depression areas and defined the eastern and western limit of the Vajont landslide by the abrupt change in morphology and lineaments. Furthermore, the Northern slope of Mount Toc displayed different landform including trench systems and scarps, crossing both the western and eastern areas of the slope suggesting that these areas were marked by previous slides (Semenza, 1965) (Fig.2.14). Another very interesting geomorphologic feature was the discovery of an important karstic area in a basin above the slide on the west of the Mount Toc peak as well as other small sinkholes in the surface of the Dogger beyond the western and southern limits of the slide.



**Figure 2. 14 -** Morphological analysis of the Vajont area delineated from 1960 Airphotos. Cto: "Col Tramontin" fault; CE: "Col delle Erghene" fault.

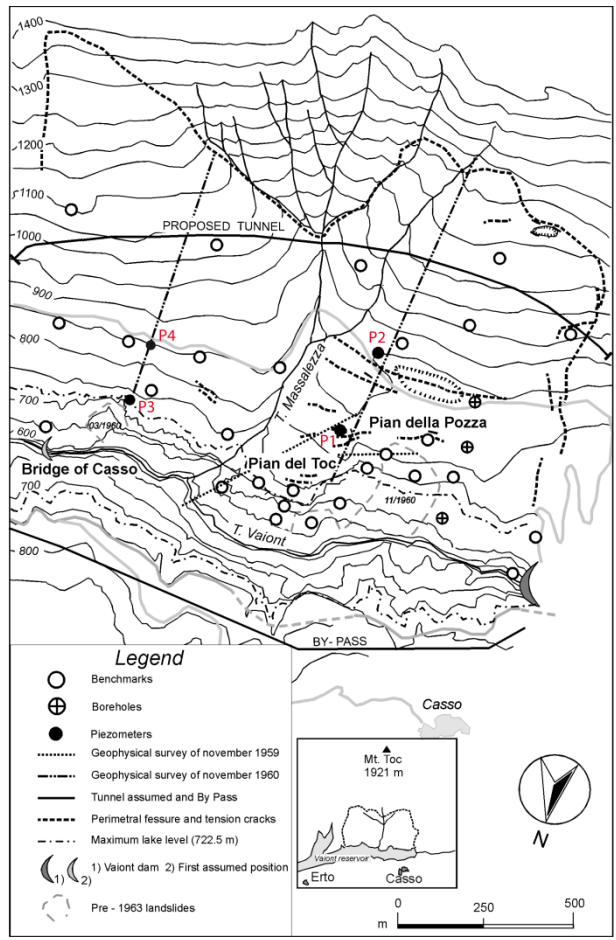
## 2.7 Hydrogeology

The hydrogeological aspect of the southern slope of the Vajont valley is important to understanding and analysing better the effect of water impact pressures on joints due to the sudden collapse of the rock mass into the reservoir. The aspect and fracturing rock mass condition may indicate that pressure pulses propagated into various joints. Indeed, it can cause, on the one hand, the failure of the rock and, on the other hand, lead to a progressive deterioration of the integrity of the rock mass itself. Despite a half-century of scientific research concerning the Vajont landslide, the correlations between the water table levels and rainfall remain uncertain.

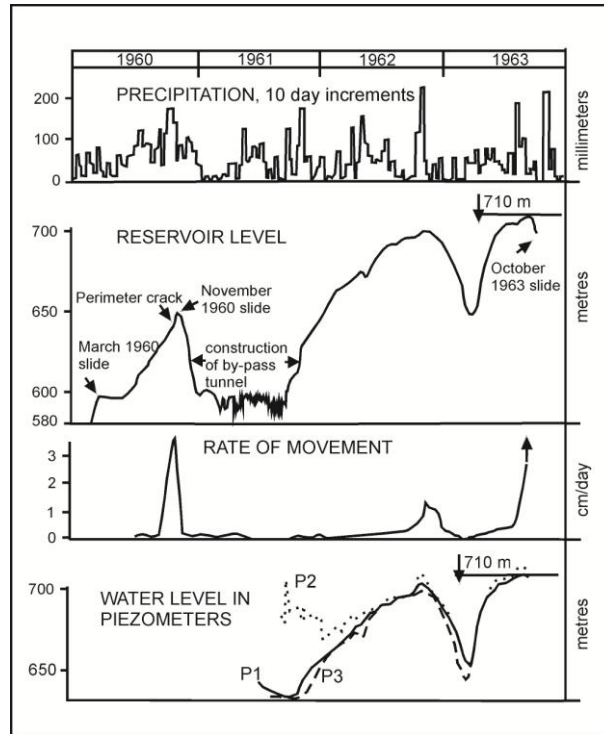
The area around Mount Toc is characterized by a reduced presence of surface water and by some springs, most of which demonstrate fairly small-discharges. This situation likely reflects

a karstic groundwater circulation. This hypothesis follows direct observation of dolines in the area above the Vajont landslide, where the main part of the meteoric waters infiltrates without causing a significant, visible surface flow. The presence of karstic phenomena, as well as the minimal or otherwise absent surface hydrography are well reported in the literature. Hendron and Patton in 1985 provided the first detailed study about the hydrogeology of the Vajont landslide. This was an important step in determining the distribution of the water pressures acting along the sliding surface. This study, was carried out by means of measurements recorded in the three functioning piezometers installed in 1961 (Figure 2.15).

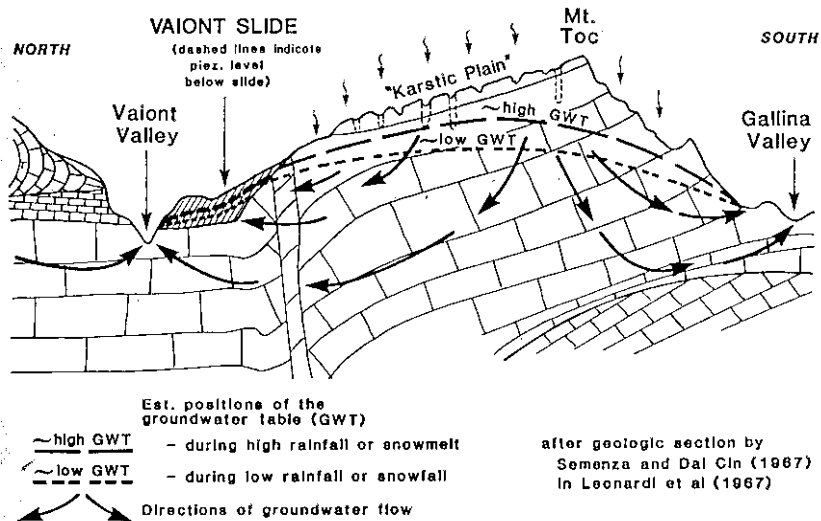
P1 and P3 showed readings of the variation of the lake level while the third (P2), recorded much higher values until the middle of 1962 and did not follow the lake variation (Fig.2.16). This anomaly was interpreted as the result of the pressure of a confined aquifer, which fed P2 directly. The lower aquifer located in the slightly fractured Vajont limestone and characterized by karstic phenomena mainly developed around various bedding planes of the upper part of Mount Toc (Figure 2.17). This confined aquifer was fed mainly by precipitation. The permeability values and the shape of the two aquifers, as well as their recharge régime and refill times, were subject to many changes and consequently their piezometric levels were also different. In particular, following a spring thaw or prolonged rainfall, the water level in the lower aquifer could have gradually reached much higher values than in the upper aquifer and thus caused neutral pressures which would have diminished the shear resistance along the failure surface, leading to instability of the mass (Ghirotti & Semenza, 2000).



**Figure 2.15** - The Vajont landslide area before 1963. Location of different investigations carried out between 1959 and 1961.(from Semenza and Ghirotti, 2000 modified).



**Figure 2.16** - Comparison of lake water levels, piezometer levels, rate of movement of landslide and precipitation, from 1960 to 1963 (Hendron and Patton, 1985).



**Figure 2.17** – Schematic section through vajont slide, showing estimated regional groundwater flow system (Hendron & Patton, 1985).

Actually, two springs were chosen to be monitored. Since July and September 2010 two data-loggers (Diver) were installed to measure hourly discharge, electrical conductivity and temperature of spring waters.

The chosen springs were Eganass since July and September 2010 two data-loggers (Diver) were installed to measure hourly discharge, electrical conductivity and temperature of spring waters. The chosen springs were Ega Nass, on the West of Mount Toc (Dogna, Longarone), and Le Spesse, on the opposite side of the Vaiont landslide (Le Spesse, Erto e Casso) (Fig.2.18). These data were compared with rainfall from two different weather stations (ARPAV, Servizio Idrografico Regione FVG), in order to have an idea of the spring behaviour after rainy events. A cross-correlation analysis was carried out to estimate linkage among rainfall and spring water discharge, conductivity and temperature. The first results show clear karst behaviour within the springs, with a very short recharge circuit, since the time delay from the rainy event to the increase of the spring discharge is very short. At the moment, the data available are insufficient for further commentary (at least one hydrological year of data would be necessary).

This groundwater level was one of the consequences of the water level in the impounding basin. Indeed, the general distribution of the water pressures was likely different from that which typically results from a regular filtration process along the slope because the effective filtration direction was – highly irregularly – almost perpendicular.

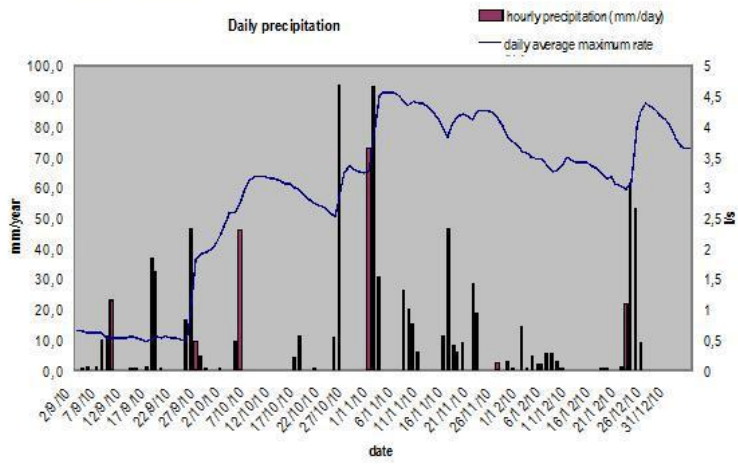
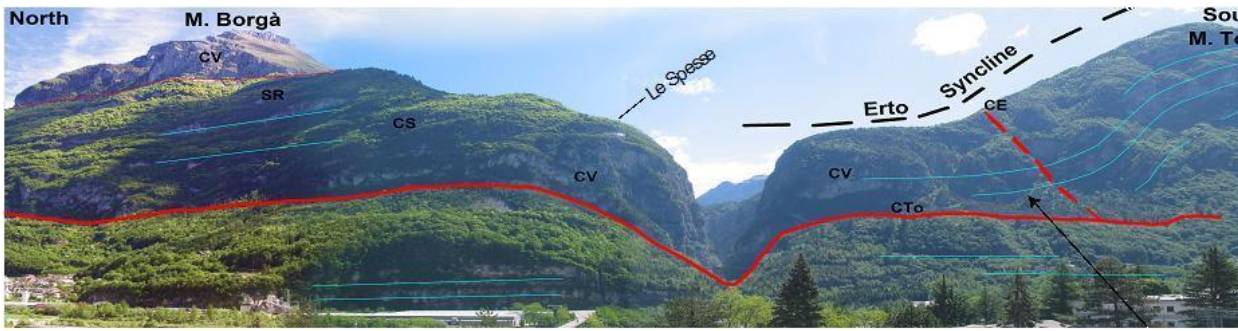


Figure 2.18 - Eganass spring water measurements.





# CHAPTER 3

## **2.4 Structural analysis of folding deformation on the sliding surface**

The main historical investigations regarding the geomorphological and structural aspects of the Vajont area, were carried out by Semenza (1965), Broili (1967), Selli & Trevisan (1964), Carloni & Mazzanti (1964), Hendron & Patton (1985). They described the main morpho-structural features of the landslide area but as they could not take advantage of the nowadays available techniques and methodologies, (as digital elevation model analysis, and photogrammetry survey) they did not reach a high accuracy level of knowledge on the landslide's dynamics, triggering and failure mechanisms.

Considering the state of art, in these paragraphs it is described the morpho-structural analysis performed on the Vajont study area, in order to identify the main morpho-structures features that could be played a relevant role in the kinematic of the 1963 event. The analysis was carried out through the application of: traditional geological field investigations and remote sensing techniques.

The remote sensing techniques used are:

- stereo air-photo interpretation pre 1963 event
- DEM analysis through COLTOP 3D software (Jaboyedoff et al., 2004)

### 2.4.1 Morpho-structural setting assessment through remote sensing techniques

The main advantages of these techniques in terms of morphological analysis, joint studies, block volume estimates and mapping, are:

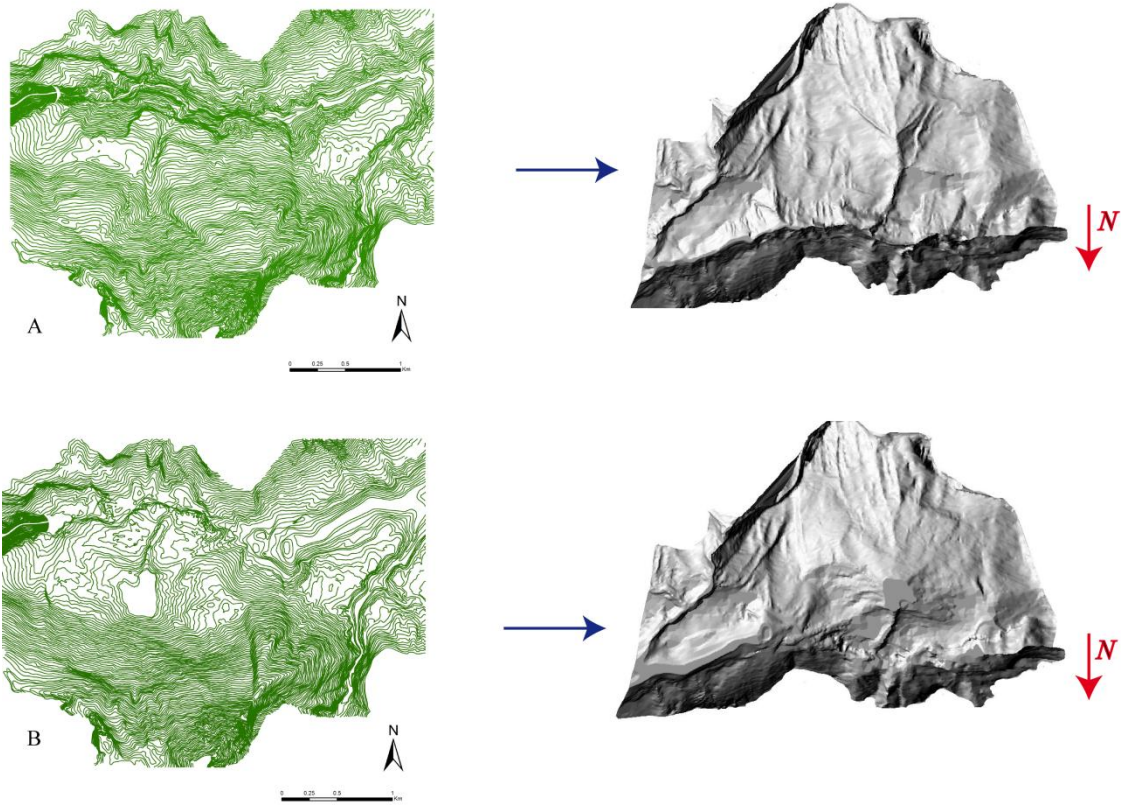
- Provide high resolution image data, to geological and morphological recognition and analysis.
- Map geological features (folds, faults, fractures, etc...)
- Monitoring of morphological changes
- Obtain quantitative measurements over large areas in particular, bed attitudes from topographic slopes evaluation.
- Detail methodologies to measure landslide displacements and strain field, based on the large amount of dense and accurate spatial information (Sturznegger & Stead, 2009).

The combination of both airborne and terrestrial methods, joined with traditional field investigations, allow to consider of a wide range of observation scales.

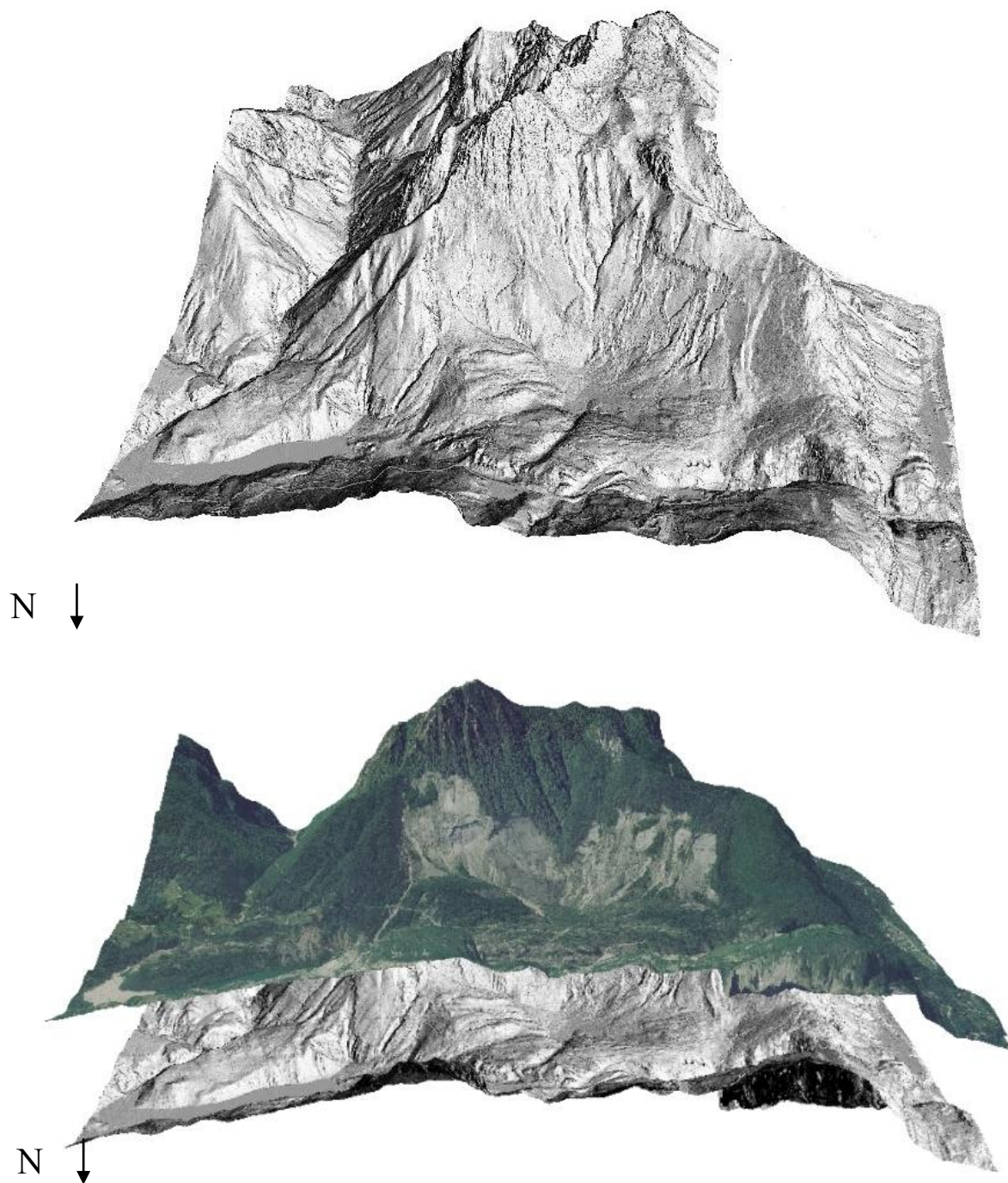
Therefore, the remote sensing approach should be considered as a preliminary technique to be implemented before carrying out field investigations. The digital elevation models (DEM) of the Vajont landslide analyzed, were obtained from:

- ✓ digitizing the contour lines of pre to post landslide topographic maps (nominal scale 1:5.000) Figure 3. 1 A-B, and from pre-landslide stereo-airphotos (nominal scale 1:30.000) gently provided from Land Technology & Services srl.
- ✓ Airborne laser scanning data, (gently provided from Friuli Venezia Giulia Region) to the classical natural neighbor interpolation method of the derived x,y,z, points. The latter has been chosen as reference for the post event analysis for its accuracy and better resolution, especially if compared with DEMs derived from digitizing contour lines(Figure 3. 2).

Furthermore, the ortophos of the study area, provided from Friuli Venezia Giulia Region, have been overlapped on the lidar DEM and analyzed in order to obtain an accurate match aiming at the identify all the relevant morpho-structural features of the area (Figure 3. 1).



**Figure 3. 1-** Dem construction digitizing from geologic maps contour lines. A) Pre 1963 event B) Post event.



**Figure 3. 2-** 3D hillshade lidar overview of the Northern slope of Mount Toc (A). Orthophotos overlapping allowed to define useful landmarks to pattern recognition in the field investigations.

### **2.4.2 Coltop 3D analysis for folding structures**

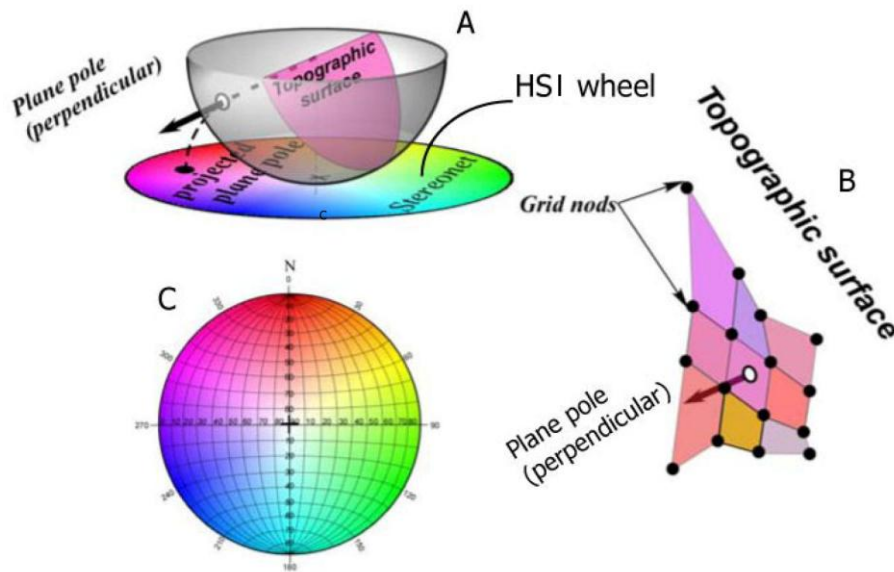
COLTOP3D was used as highly valid support for field data identification and for a general detailed understanding of the Vajont area structural setting as well as for a prompt identification of the morpho-structural factors influencing the rock mass movement.

This software, based on topographic analysis of DEM, was designed to identify and analyze structural features affecting topography (Jaboyedoff & Couture, 2003).

It allows visualization and the characterization of the structures through a specific- colouring of DEMs (Jaboyedoff et al., 2011). Using the orientation of each series of quadrilateral surface segments (cells), a point cloud data set can be represented by a 3D image, where each single point has a colour defined by its dip angle and dip direction and representing by mean Schmidt-Lambert projection in a lower-hemisphere. (Figure 3.3). The slope orientation is coded by the Intensity Hue-Saturation system (HSI). Then the colour representations are attributed to each DEM cell on the basis of its pole spatial orientation in the stereonet (Figure 3.3)

While GIS systems, usually requires a map for the dip of the slope and another one for the dip direction (respectively named “slope angle” and “slope aspect”) - Coltop 3D allows to represent both of them in only one map (Figure 3.3).

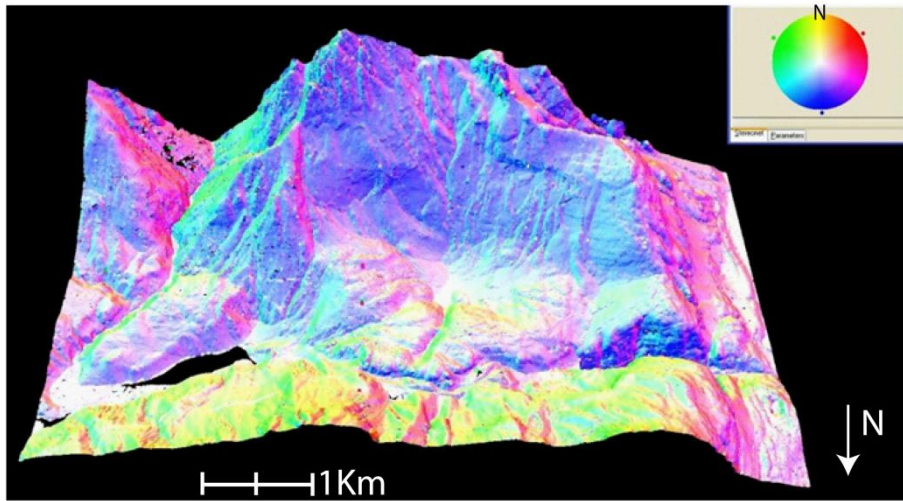
Then, the 3D surface reconstruction allowed firstly an easier automatic delineation of the faults and main morpho-structural characterization, and secondly it carried out a better structural representation.



**Figure 3.3-** (A) Color coding principle of the pole represented in a lower Schmidt-Lambert stereonet (B) Example of a colored DEM grid. Explanation of the vector computation is indicated at the center of one cell (from Jaboyedoff and Couture, 2003).

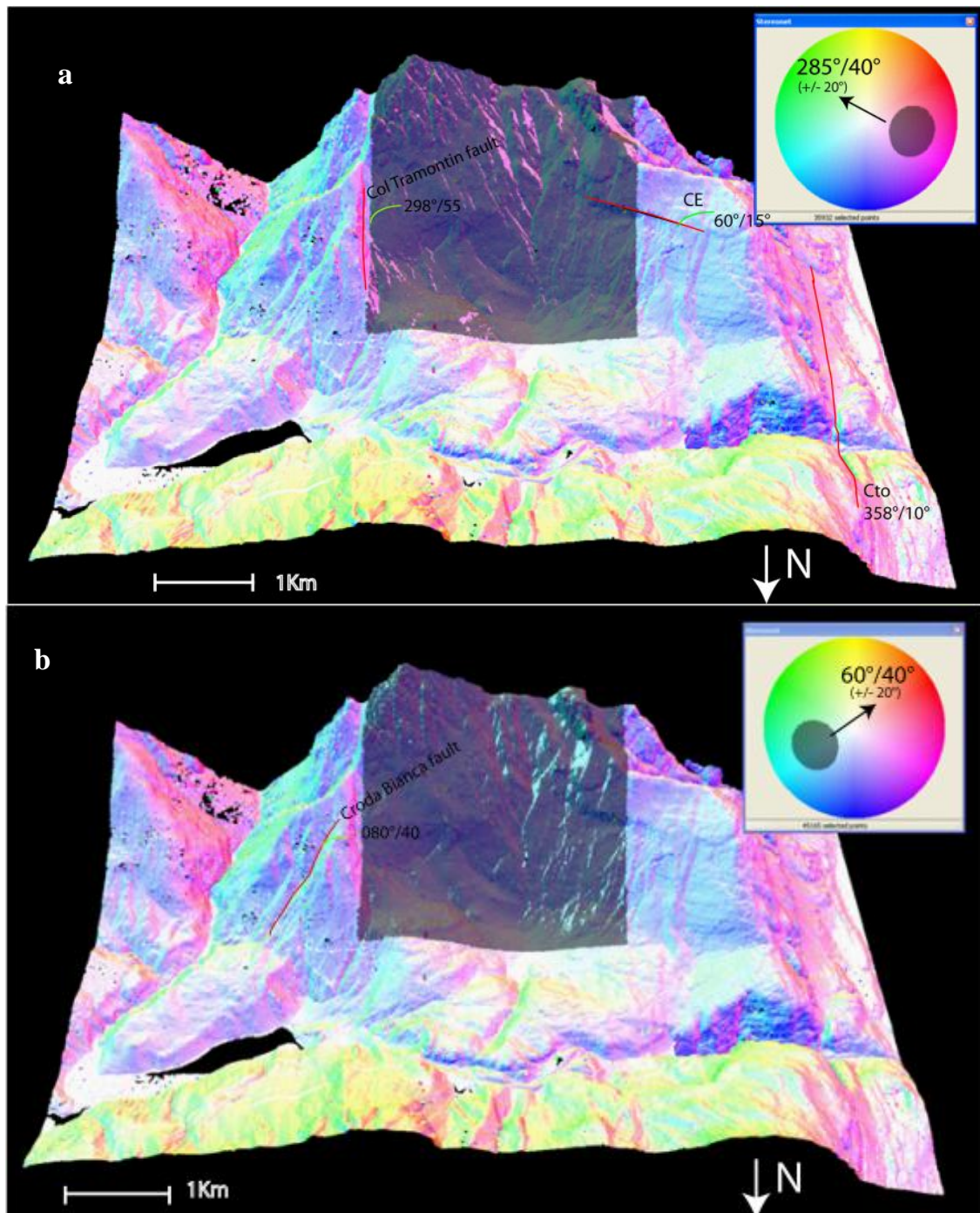
Indeed, as showed in Fig. 2.12a-b, the sliding surface is displayed with different colours, evidencing the eastern portion is mainly controlled by the orientation of the bedding planes dipping toward NW (pink colour) with an average dip direction of  $285^\circ$  and dip  $40^\circ$ , whereas the western portion is represented by bedding planes dipping toward NE (cyan colour) with an average dip direction of  $60^\circ$  and dip  $40^\circ$  (Fig. 2.12b). Furthermore, the strata orientations detected can be related to the main structural faults of the landslide area, in particular the bedding planes dipping towards NW is in agreement with the Col tramontin fault dipping  $298^\circ/55^\circ$ , whereas part of the Col delle Erghene fault results in line with the bedding planes dipping towards NE. These data were also plotted in a stereonet (Fig. 2.13).

These different orientation between the western and eastern sliding surface regions, converging towards Massalezza ditch, can lead one to believe that the geometry results is not related to only one deformation phase. Indeed, Coltop analysis clearly highlighted a wide N-S fold axis oriented and moderately dipping  $30^\circ$  towards N corresponding to the Massalezza ditch. This latter wide fold, Massalezza syncline, could be related to the dynaric deformation linked to dinarides forebelt evolution especially pronounced in the eastern southern Alps (Doglioni & Carminati, 2008) (paragraph 2.1). In order to verify the really existence of the dynaric deformation phase the sling surface and neighbor areas were investigated.

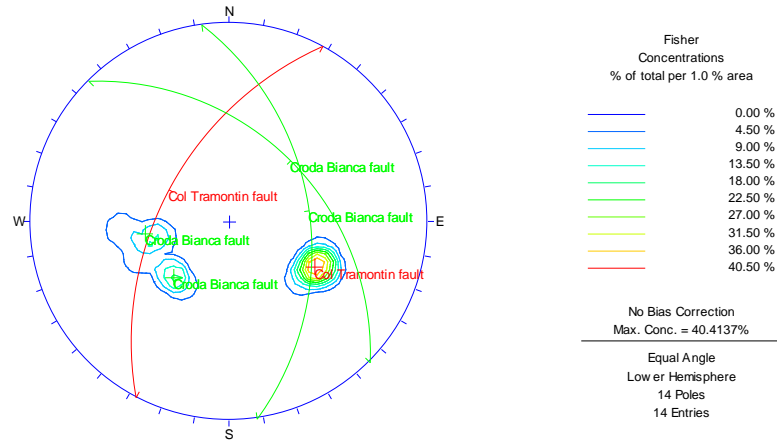


**Figure 3.4** - 3D DEM visualization of the Vajont landslide. Each cell DEM is represented by a colour corresponding to its dip and dip direction





**Figure 2.12** – Different sliding surface orientations and main faults of the Vajont area detected by COLTOP3D. The different orientation are represented by pink (a) and cyan (b) colour respectively and attested the sliding surface unflatness. The main faults system of the landslide area were identified: Cto: Col delle Tosatte line, CE: Col delle Erghene line, Col Tramontin and Croda Bianca faults.



**Figure 2.13** - Equal area stereoplot, lower hemisphere of poles to relevant faults of the Vajont landslide area.

### 2.4.3 Structural analysis of folds through field investigation

The structural features observed in the Vajont area are linked to its polyphasic intense tectonic evolution. A close inspection of the area and in particular of the sliding surface highlighted some deformation structures not in line with the mean Alpine tectonic orientation (E-W to ENE-WSW oriented). The detailed geological survey made possible to differentiate the sliding surface into three main structural domains:

The eastern domain which is characterized by a relatively smooth surface marked by a major large fold with a E-W axis and limbs dipping from 37° to 47° towards south(Fig. 2.14a,).

The western domain marked by mild folds N-S oriented (Fig. 2.14b,)

The middle domain which is the most complex zone of the three because it is characterized by the interference pattern between two fold systems: E-W to ENE-WSW and NNW-SSE to N-S oriented (Fig. 2.14c,)



**Figure 2.14** - Morpho-structural details of the sliding surface: A- western side B-eastern side, C-.morpho-structures on the Massalezza area.



**photo 2.1** – Details of the eastern side of the sliding surface

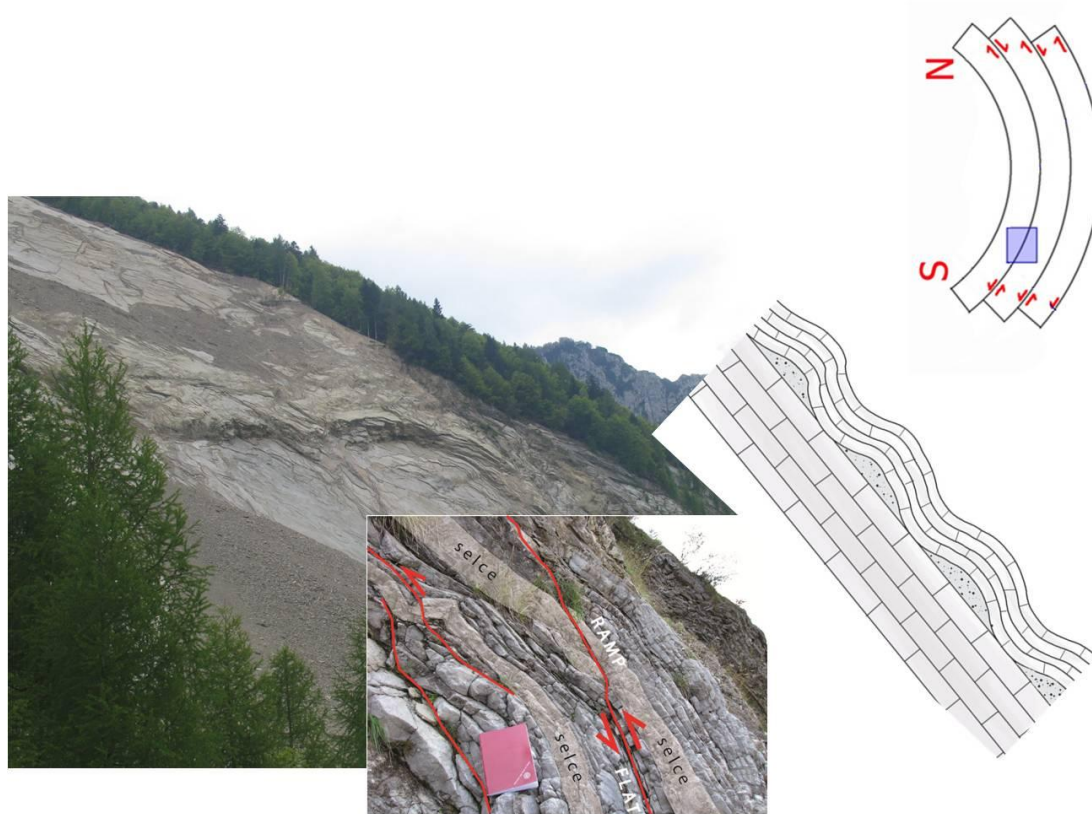


**photo 2.2** – Details of the western side of the sliding surface



**photo 2.3** – Details of the interference fold system in correspondence of the Massezza confluence.

Therefore, the shape of the sliding surface is the result of two deformative events. Indeed the E-W folds formation strictly related to the Erto syncline development. In particular, during the Neopalpine phase whereas the NNW-SSE oriented folds are associated to deform event while generated the Massalezza syncline. In the field investigation was observed that the local contraction of the bed pack of the Fonzaso formation, has been foliated by flexural slip mechanism. The flat and ramp geometry, produced by flexural slip mechanism were identified on the sliding surface (Fig. 2.15). The E-W (flat and ramp) folds south vergent cut north dipping strata. Therefore it possible exclude, for the E-W folds a gravitative genesis, but they are related to tectonic event indeed Erto syncline and consequently to Alpine deformation.



**Figure 2.15** – Bed pack of the Fonzaso formation deformed by flexural sleep mechanism, identify the E-W folds on the sliding surface.

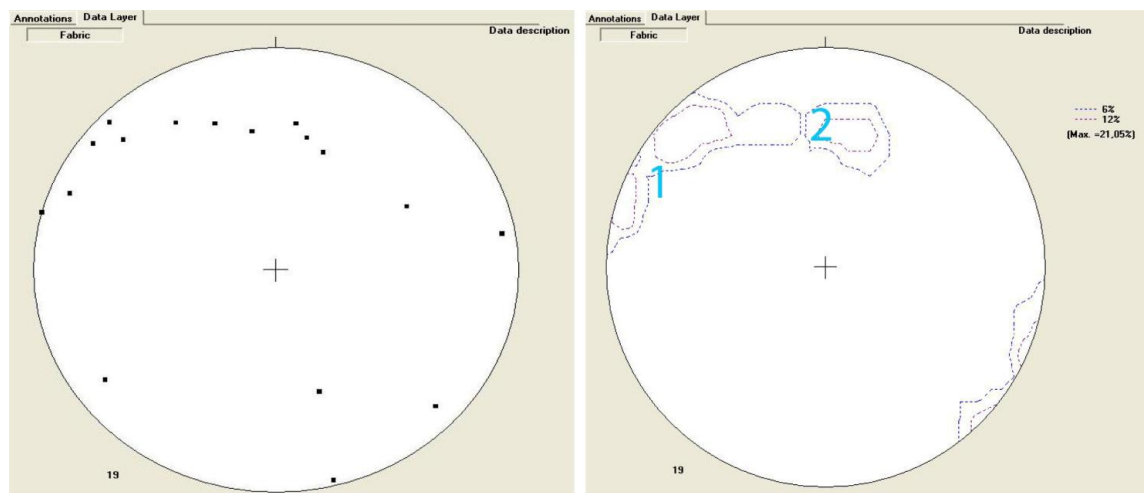
In order to better define the complex structures geometry derived from the interplay between two folds sets, folds axes and axial planes measuring, folds limbs in accessible areas of the sliding surface (see also Mr.Riccardo Ravagnan, 2011).

The data of the fold axis in are represented in the stereographic plots Fig. 2.16.

Although the collected data are not yet statistically representative, a relevant pole dispersion is evident.

This dispersion could be represent to the interference pattern between two different folds system: the first one E-W oriented and likely related to alpine compression and the second one N-S to N-NW oriented. The data projected in the stereoplot show a different density distribution.

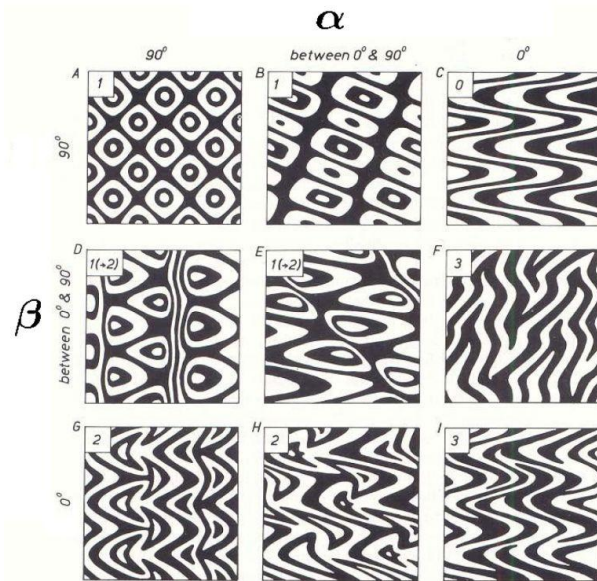
The first distribution (1) is composed by sub-horizontal fold axis, related to folds thrust could be associated to neo-alpine deformation phase. The second density distribution (2) indeed, shows N-S fold axis dipping almost  $35^\circ$  that could be related to dinaric deformation phase.



**Figure 2.16** - Folds axis representation. 1 and 2 could be identify two different folds system: 1 - shows fold axis W-NW oriented. 2- fold axis N-S oriented (Ravagnan, 2011).

With the aim of better understanding the interference patterns geometry, Ramsay models.(1967) were applied(Fig.2.16). Ramsay classified four major types of interference patterns, based on the angular relationships between the folds axes of two folds sets (Fig. 2.17)



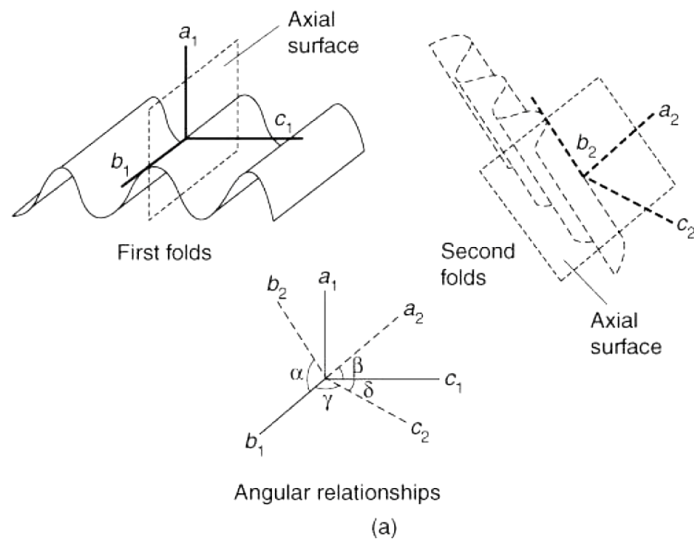


**Figure 2.17** – 2D Ramsay classification of interference geometry, Ramsay 1967

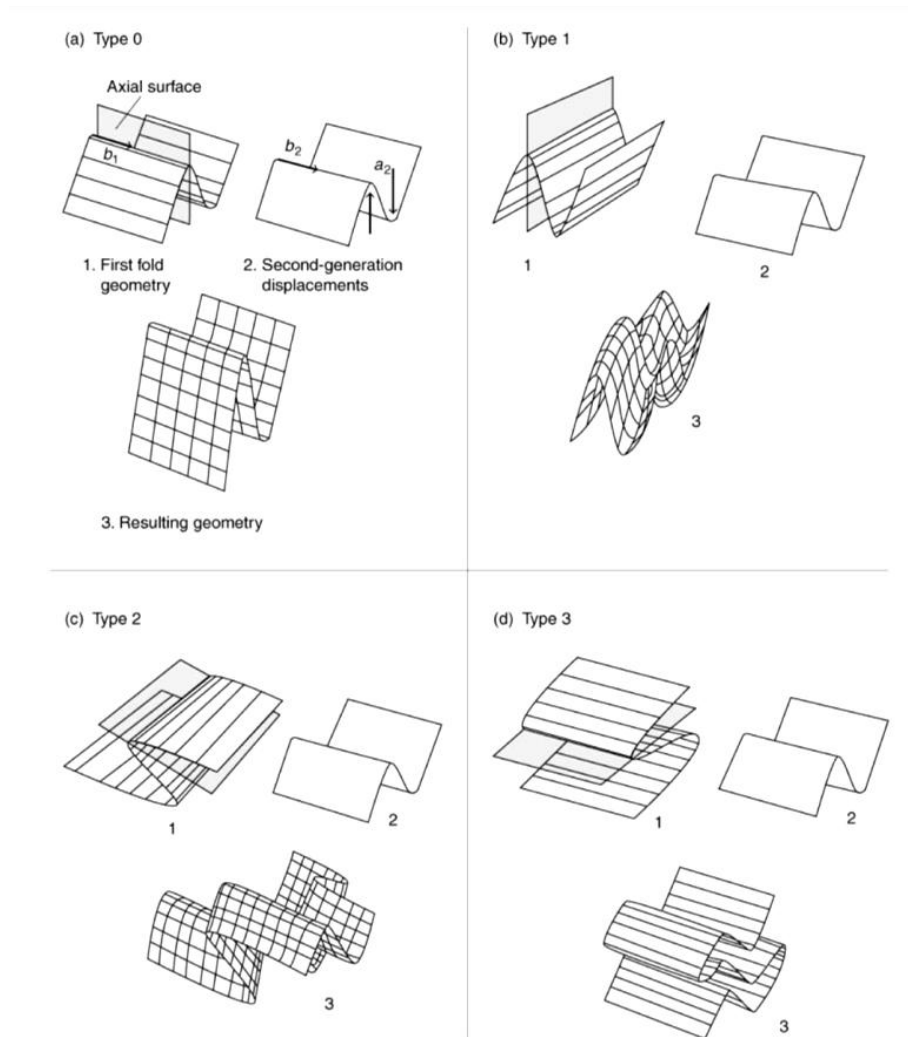
The major interference patterns are:

- Type 1: Dome-basin pattern
- Type 2: Dome-crescent-mushroom pattern
- Type 3: Convergent-divergent pattern
- Type 0: Redundant superposition (defined by two identical fold systems temporarily separated).

Thiessen and Means (1980) expanded the Ramsay classification adding two more angles between the folds orientation (Fig. 2.18). The interference pattern of the study area is well represented by 1 and 2 type of Ramsay classification and K type in relation to Thiessen and Means classification (Fig. 2.19).



**Figure 2.18** - Angular relation between different folds orientation (Thiessen & means, 1980)



**Figure 2.19** – The four principal types of three-dimensional fold interference pattern (Ramsay, 1967).

#### **2.4.4 Interpretation of the folds planes**

The interference between the E-W to ENE-WSW and NNW-SSE to N-S systems can be explained through two different interpretations.

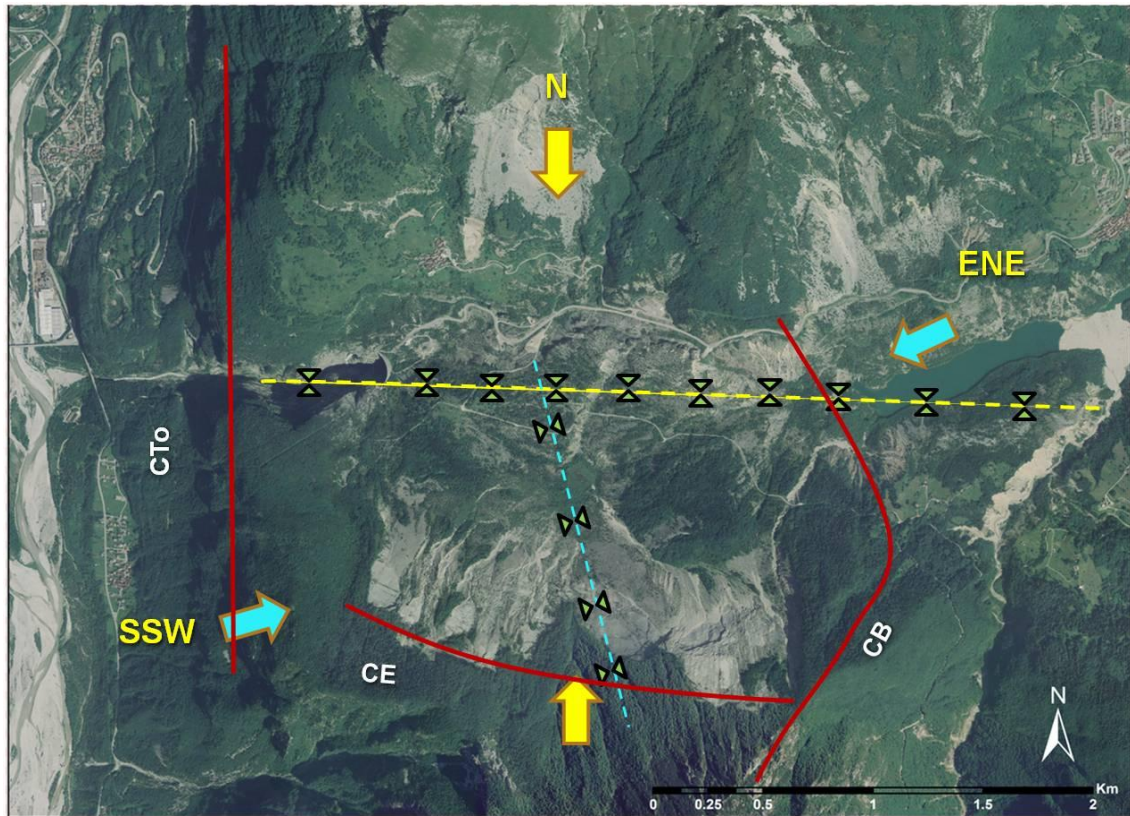
According to the first interpretation, the Vajont area is located in the eastern Southern Alps, where the dinaric Paleogene thrust belt is overprinted by the Neogene Southalpine thrust belt. The two thrust overlap produced an interference pattern in which the dinaric trend of WSW-vergent folds is overprinted by the southalpine trend SSE-vergent folds.

The second interpretation take in account the meso-scale structural setting of the area.

The sub-vertical roughly N-S faults: Col delle Tosatte (Cto) and Croda Bianca (CB), showing no parallel strike and southwards converging (Fig 2.20), could play a relevant role in folds planes interference. Indeed, during the Alpine compression, the E-W folds sets, included Erto syncline, have been laterally constrained by the two southward N convergent S faults could giving rise to the interference structures.

#### **2.4.5 Discussions**

Considering the accurate filed survey carried out in the study area (inside and outside the landslide), results that the largest number of interference pattern is found in the Massalezza area. As showed by the photos(2.3) the interference fold systems on the sliding surface are very clear. This can be due to the main interference pattern products: Erto (E-W) and Massalezza (N-S) synclines. Moreover, this clear evidence is a reason to believe that the interference pattern between the E-W to ENE-WSW and NNW-SSE to N-S systems is related to the Alpine fold system superimposed by the dynaric fold system. In addition,an important consideration is the role of the interference folds system played on the rockslide cinematic and more in general in controlling stability.



**Figure 2. 19** – Interpretation of the interference pattern of the vajont area. The yellow line represents the Erto syncline axis generated by southalpine compression. The cyan line identify the massalezza syncline axis produced by dinaric deformation.(first interpretation). Main dislocations affecting the Vajont area. Cto: Col delle Tosatte line. CE. Col delle Erghene line. CB Croda Bianca line.

# CHAPTER 4

## GEOMECHANICAL CHARACTERIZATION

This chapter describes any single aspect of the geomechanical survey carried out in relation to the Vajont landslide. The geomechanical characterization aimed to identifying the most significant parameters of rock masses, that influenced the rockslide triggering and displacement. To this purpose the field investigations were performed inside and outside the landslide. In order to gather detailed information of the rock mass condition, the traditional geomechanical fieldwork was integrated with different remote sensing techniques (some of these latter already mentioned in the previous chapter) and laboratory tests. The rock mass is composed by blocks and fragments separated by discontinuities (Palmstrom, 2001). The presence of discontinuities in a rock mass reduces its shear strength and homogeneity, and plays an important role in rock slope instability. The assessment of the discontinuity features within a rock mass volume, as: density, roughness, discontinuity pattern, etc. is an essential investigation to comprehend the mechanical behaviour of the rock masses involved in the movement. The geomechanical survey was performed according to the ISRM standards (*International Society for Rock Mechanics*), analyzing the rock mass components (joint and intact rock characteristics).

### 4.1 Geomechanical survey of the Vajont study area

In order to perform an accurate geomechanical survey, it is necessary to focus on the identification of the areas suited to be investigated as well as on their accessibility. Indeed, the survey required a detailed planning of the outcropping rock masses to be analyzed and an accurate methodological scheme, to describe the overall features of the suitable outcropping rock masses and their peculiar features. The geomechanical survey is performed with sub planar rock faces, sufficiently large in relation to the size and the spacing of the exposed discontinuities. At least 200 discontinuities should be measured in order to obtain representative samples (Priest, 1993). It has been considered that the rock surfaces' size should be approximately at least 4x2meters, in relation to the average features of discontinuities.. To characterize the geomechanical properties of the investigated area and in

particular of the material involved in the 1963 movement, 89 geomechanical stations were carried out. The geomechanical parameters, required by ISRM(1978), for each station were acquired and will be discussed in this chapter.

The geomechanical survey was achieved detecting:

- general lithological description
- analysis and characterization of discontinuities
- analysis and characterization of intact rock
- rock masses characterization

The geomechanical stations, as above mentioned, inside and outside the landslide, have been accurately chosen for the geomechanical characterization. The inaccessibility and dangerousness of some areas, overall in correspondence of the sliding surface, didn't allow to increase the number of geomechanical stations and, it made the investigations difficult. In order to obtain a homogeneous data distribution (in terms of discontinuity properties) and to improve the geomechanical characterization of the outcropping rock masses, remote sensing techniques were applied.

Field geomechanical measurements were performed along scan-lines (at least 3 m long) on the outcropping rock. Therefore, the attitudes and characteristics of approximately 3000 discontinuities were recorded on 89 stations, located on the following areas: the failure surface, the deposit area and outside the landslide. The collected geomechanical data were organized in tables in an *ad hoc* GIS Geo Data Base (see Superchi et al., 2010, appendix A) . The geomechanical stations have been identified by x,y coordinates detected by a GPS related to the Geodatabase (Tab 4. 1). The selected coordinate system is Gauss Boaga Monte Mario Italy2.

OBJECTID *	counter	ID_stop *	intersection_cm	Dip_dir	Dip	ending *	comments
6332	1	VJ001	7	305	90	a	<Null>
6333	2	VJ001	14	295	80	a	<Null>
6334	3	VJ001	18	295	80	a	<Null>
6335	4	VJ001	20	295	80	a	<Null>
6336	5	VJ001	33	300	80	a	<Null>
6337	6	VJ001	51	310	80	a	<Null>
6338	7	VJ001	59	310	90	a	<Null>
6339	8	VJ001	76	310	50	a	<Null>
6340	9	VJ001	97	310	80	a	<Null>
6341	10	VJ001	99	310	80	a	<Null>
6342	11	VJ001	101	210	90	a	<Null>
6343	12	VJ001	103	320	90	a	<Null>
6344	13	VJ001	105	310	80	a	<Null>
6345	14	VJ001	108	310	90	a	<Null>
6346	15	VJ001	113	310	90	a	<Null>
6347	16	VJ001	115	295	45	a	<Null>
6348	17	VJ001	136	310	90	a	<Null>
6349	18	VJ001	138	310	90	a	<Null>
6350	19	VJ001	140	310	90	a	<Null>
6351	20	VJ001	142	310	90	a	<Null>

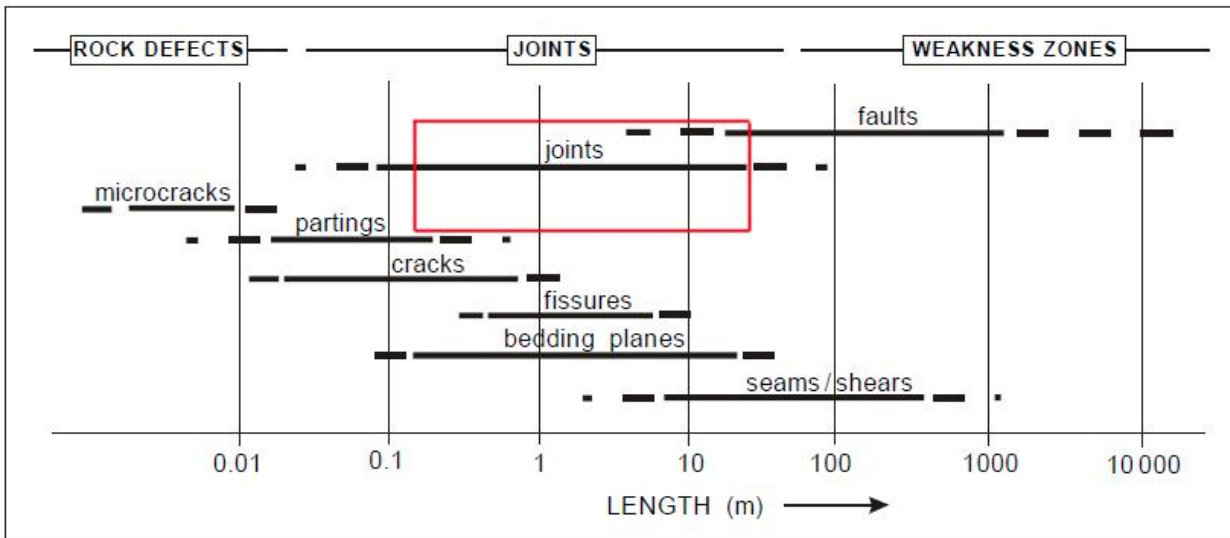
**Tab 4. 1** – An example of the geomechanical data collected in the Geo-database

## 4.2 Discontinuity Analysis

The term discontinuity is a general definition used to describe several type of fractures, including: joints, bedding planes and faults. The more fitting definition for this term in rock mechanics and engineering geology is “joint”, which is defined by ISRM (1975) as: " discontinuity plane of natural origin along which there has been no visible displacement." A joints' classification criterion, was elaborated by Palmström on the basis of their length. (Figure 4. 1).

The discontinuity analysis was performed at different scales of observation and from different points of view: geometrical and mechanical.

Conventional methods used to sample discontinuity parameters systematically, include scanlines and window (cell) mapping (Priest, 1993). (Figure 4. 2)

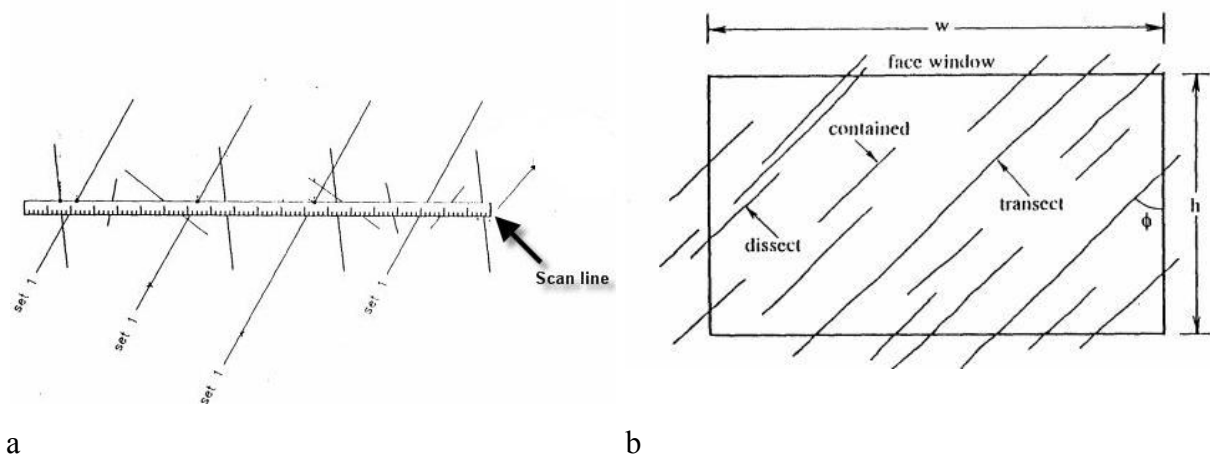


**Figure 4. 1** - The difference in size between the main types of discontinuities (rock defects, joints and weakness zones).The red box represents the range considered in this thesis. (Palmstrom, 2000 modified).

Two methods are suggested by the ISRM (1978) to determine the discontinuities

- Subjective criterion: according to which, only those discontinuities apparently playing an important role in relation to the mechanical features of the rock mass are detected.
- Objective criterion: according to which, all discontinuities intersecting the “scan-line” or included in a window are sampled.

The principle on which scanline mapping is based upon is the evaluation of the different parameters of discontinuities through the intersection between discontinuity and metrical tape measure. Similarly, in window mapping, the parameters of all discontinuities intersecting the window within are recorded.



**Figure 4. 2** – Different methods to detect the discontinuity sets of a rock mass. a:scanline; b: window (Priest, 1992 modified)



The objective criterion results in a statistical data elaboration. In order to achieve a significant result, the sampling of many discontinuities intersecting the scanline is required. The subjective approach requires indeed, a preliminary and subjective detection of the main joint sets characterizing the outcropping rock mass. The relative simplicity of the measurement process on the exposed faces and the statistical precision of these techniques make them ideally suited to determine discontinuity orientation and other large-scale geometrical properties of the rock structure. Discontinuity measurements may also be affected by orientation bias, depending on the exposed face orientation of outcropping rocks. Discontinuity parameters are naturally subject to variability. In order to minimize bias standardized survey techniques have been developed, which consider discontinuities' networks as ensembles (or sets) and allow application of basic statistical tools to characterize their parameters. Major joints forming the outcropping rock masses selected for sampling were detected with additional scanlines placed on different faces, with different orientations, in order to provide a three-dimensional joints system.

#### **4.3 Joints characterization: geometrical and mechanical joints properties**

The joints characterization is one of the most important phases in order to quantify the influence that discontinuities have on rock mass behaviour. On the basis of the above mentioned criteria, geometrical and mechanical properties of the joint surfaces, were analyzed. The joints' geometrical characterization is evaluated, as established by ISRM (1978), mainly through the measurement of the following parameters:

- Intersection and termination
- orientation
- spacing

Mechanical properties of rock masses are instead related to both the intact rock and discontinuities.

The Point load test is the parameter to be applied in order to determine the shear compressive strength of intact rocks

The frictional resistance along the joint results to be the major component of the strength.

The parameters allowing its evaluation in the field, are:

- Joint Roughness Coefficient (JRC)
- Schmidt rebound hammer test

The discontinuities' parameters, as well as the rest of the collected geomechanical and structural data, were organized in the GIS-database (Appendix A) The GIS systems improved the capability to manipulate, visualize and analyze multi-scale data which are spatially and temporally variable. Moreover, this technology helped the comprehension of the geomechanical and structural control on the slope deformations.

Moreover, this technology helped the comprehension of the geomechanical and structural control on the slope deformations.

#### 4.3.1 Intersection and termination

The intersection is the distance in metres (rounded to the nearest cm) between the scanline and its intersection point with the discontinuity. If the surface of fractures is irregular and not in contact with the tape, it will be necessary to project the plane on the tape so that the position of these fractures can be accurately recorded ( Figure 4. 3).



**Figure 4. 3** – Typical example of joints system (red segments) intersecting a scanline. The tape length is almost 3m.

The discontinuity termination is instead helpful for evaluating the nature of the termination of each semi- trace discontinuity.

The scheme recommended by ISRM (1978) is:

‘I’ Discontinuity trace ends on intact rock

‘A’ Discontinuity trace ends on another discontinuity

‘O’ Termination obscured or ends outside the considered outcropping

The intersection and termination measurements detected for the geomechanical stations were collected and organized in tables contained in the GIS-database (T ab 4. 2)

ID_stop	intersection_cm	Dip_dir	Dip	ending
VJ029	0	5	73	A
VJ029	12	290	85	A
VJ029	13	2	75	O
VJ029	29	103	60	O
VJ029	34	217	58	A
VJ029	47	61	75	O

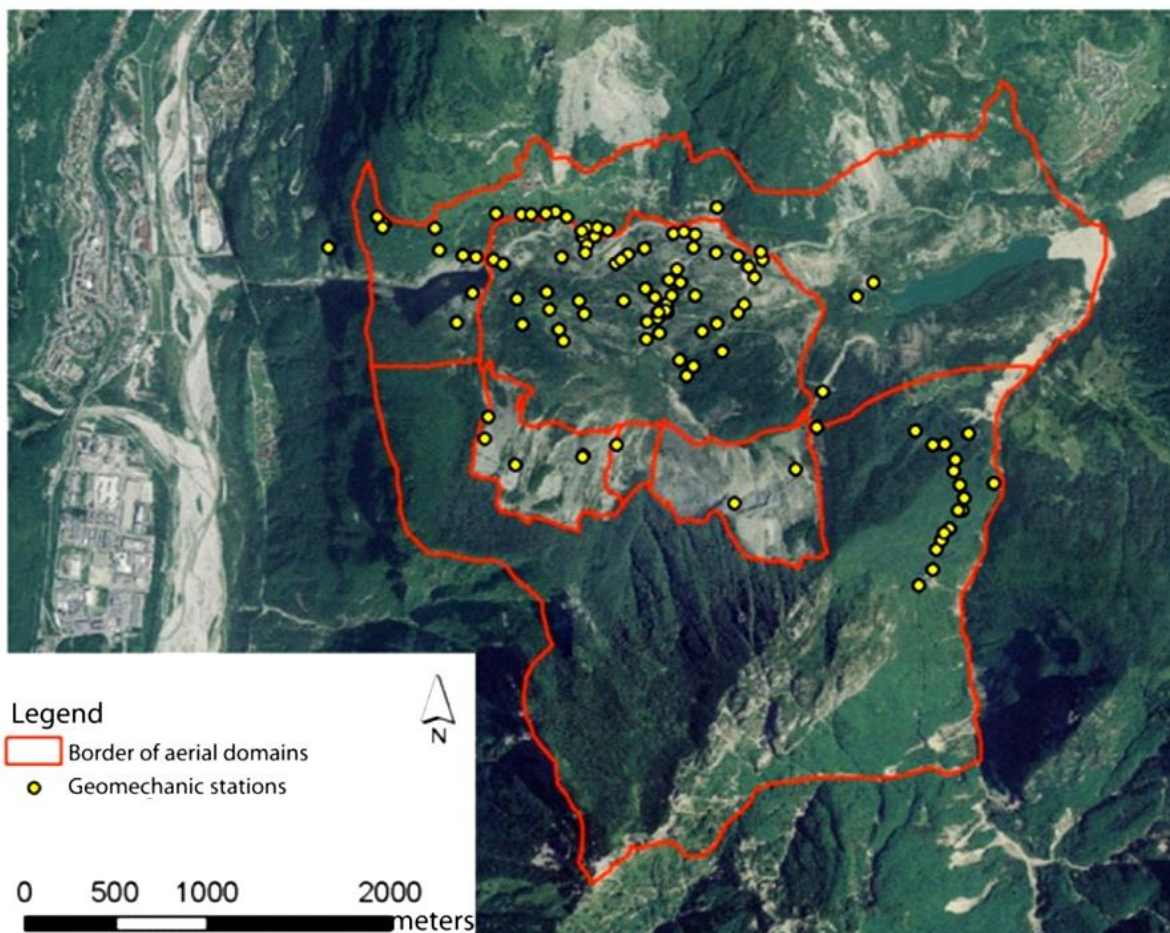
**Tab 4. 2** –Example of intersection and termination parameters recorded in tables for each geomechanical station. The “*intersection cm\_*” column shows the values, expressed in cm, of the intersection points between the joint and the tape and their relative orientations

#### 4.3.2 Discontinuity orientation and discontinuity sets

Discontinuity surveys are usually determined along a series of scan lines. A scanline is made up through a metric tape fixed along the outcropping exposure. The distance among the intersection points of discontinuities along the tape is systematically recorded. The information collected concern the geometrical characteristics of each discontinuity, as dip and dip direction. These data are carefully recorded using a compass clinometer. Orientation is the parameter to define a single fracture plane in space, using angular relationships, as for any geological planar surface. It is defined in terms of dip of the line of steepest declination and dip direction, measured clockwise from the true north. Moreover the discontinuity orientation contained in the rock masses represents the most important geometric parameter in order to identify the main joint sets affecting the investigated area. Moreover, they reflect the mass movement directions and the deformative phases connected to it (Ghirrotti, 1994). Indeed, discontinuity orientation is commonly used to delineate structural domains (Piteau, 1973). To this purpose, the discontinuity sets identified on the rock masses of the study area, with constant orientation, were gathered and plotted in a lower hemispherical stereographic projection.

### 4.3.2.1 Joint sets of the Vajont area

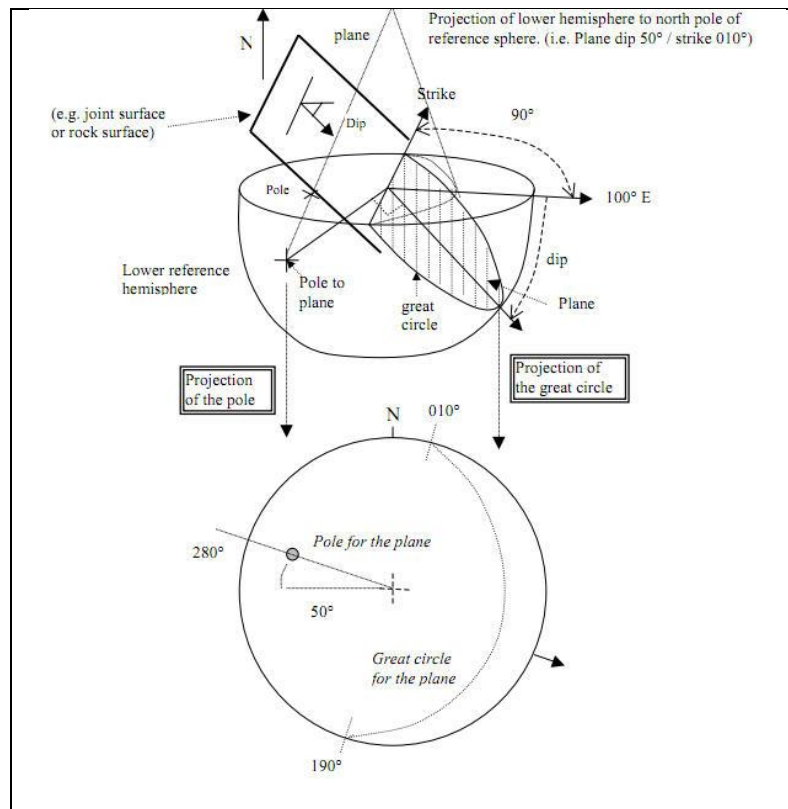
The study area, as discussed in the previous chapter, has been divided in five structural domains. The 89 scan lines (Figure 4. 4) analyzed fall within these domains with different proportions.



**Figure 4. 4** – Geomechanical stations performed in the Vajont area within the different domains: n. 48 in the deposit area; n.33 outside the landslide; n.8 on the sliding surface.

As some areas are inaccessible, the discontinuity orientation didn't provide a homogeneous data distribution. In order to achieve this aim, remote sensing techniques have been applied both to detect new discontinuity data and to compare then with the acquired field data.

The collected orientation data were analyzed through the stereographic projection techniques on the lower hemisphere. (Hoek and Bray, 1991). (Figure 4. 5).



**Figure 4. 5** - 2D stereographic projection of the discontinuity data

The identification of pole concentration and discontinuity patterns is assisted by the density contouring of the pole plots. The analysis was performed by Dips software of Rocscience and allowed to achieve a qualitative appraisal of discontinuities sets (Figure 4. 6).

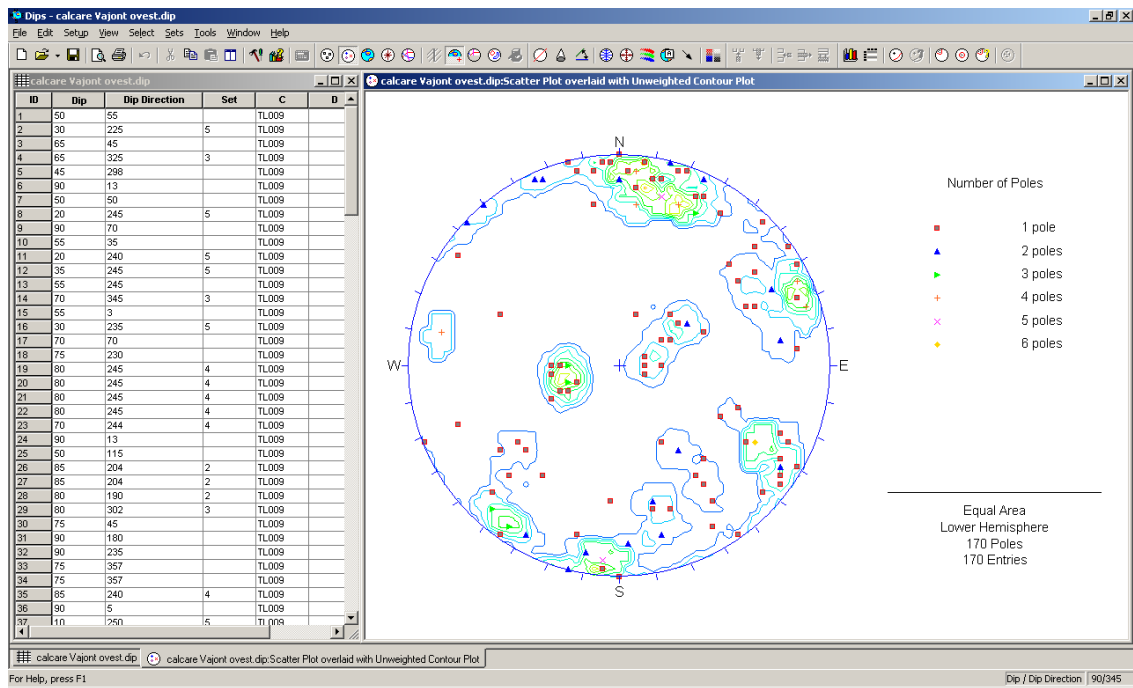


Figure 4. 6 – Discontinuities data orientation elaborated by DIPS software

In the study area, 9 discontinuity sets, have been recognized constituting all together the 89 geomechanical stations ( Figure 4. 7):

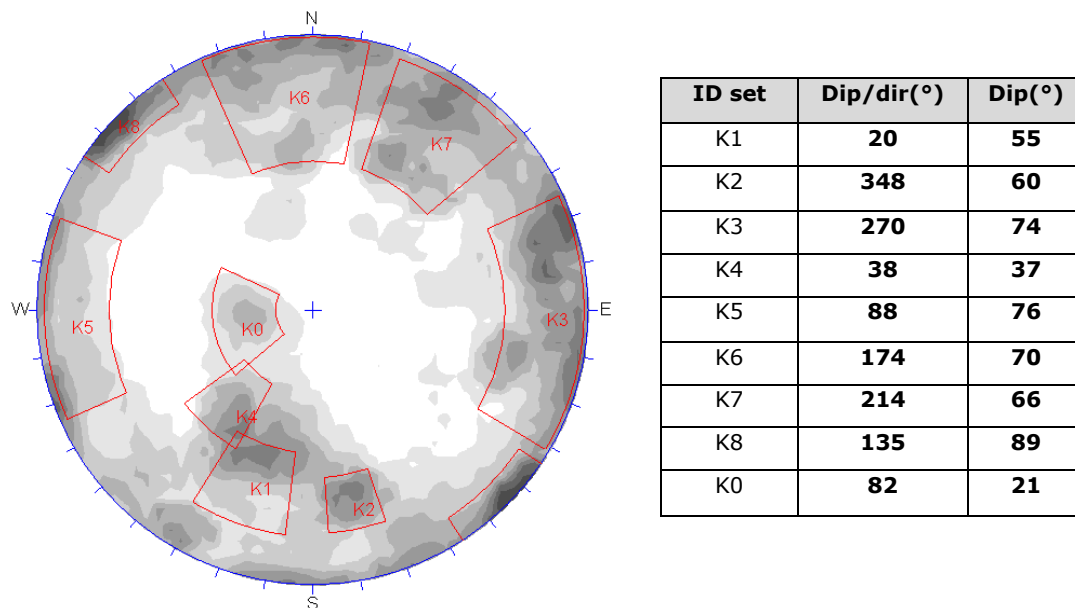


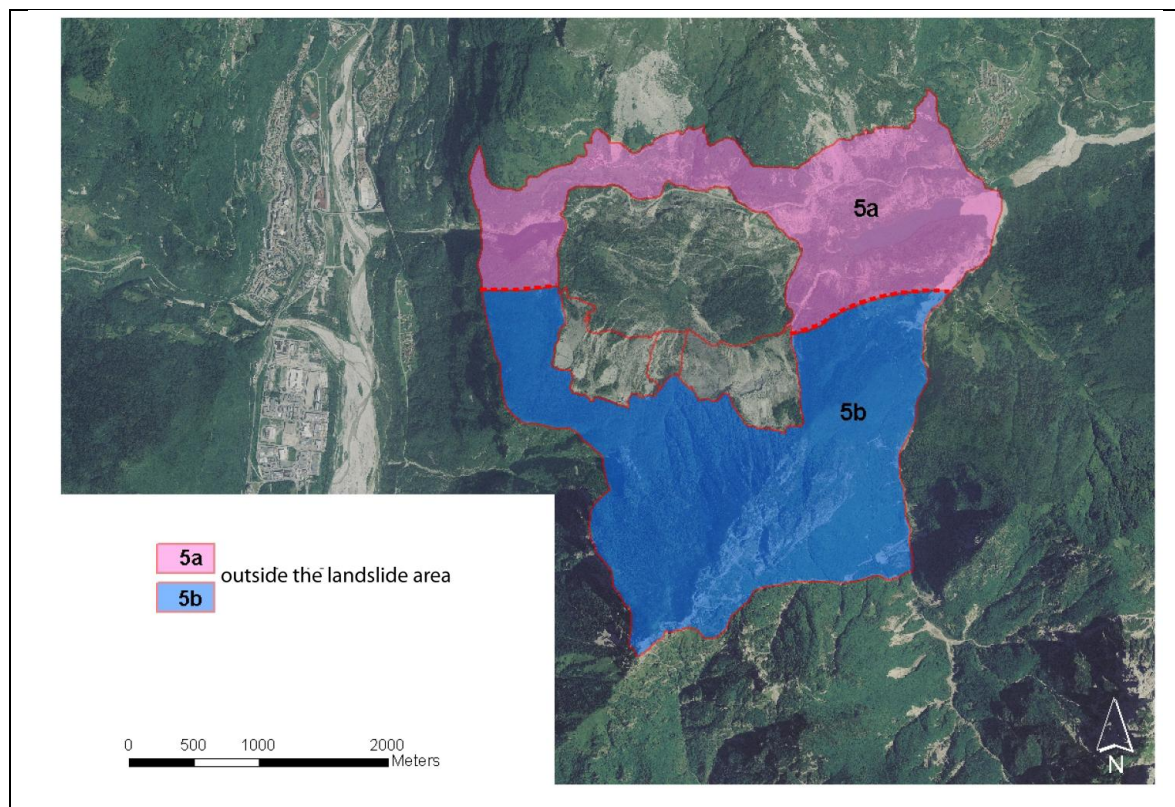
Figure 4. 7 - Stereoplot of all discontinuity sets of the investigated rock masses

Some of these discontinuities sets are easily connectable to meso-structures, identified during the geological structural survey, characterizing the area. Indeed K3 and K5 sets could be related to the NS oriented structures as Col Tramontin and Col delle Erghene faults. (discussed in the chapter 3) while the K0, K1, K2, K4 are related to the bedding plane of the sliding surface.

In order to investigate accurately the rock masses' condition for every area involved in the movement, the discontinuities' have been analyzed in relation to the domains.

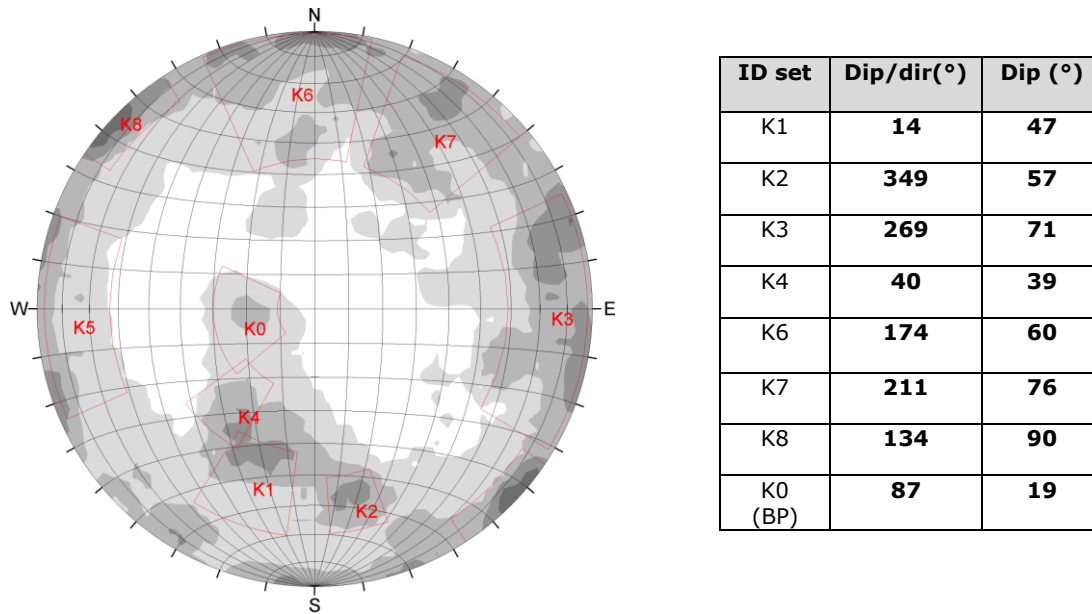
#### Joints sets outside the landslide

The area outside the landslide has been divided in two different domains because of its different structural features ( Figure 4. 8).



**Figure 4. 8** - Subdivision in domains of the area outside the landslide

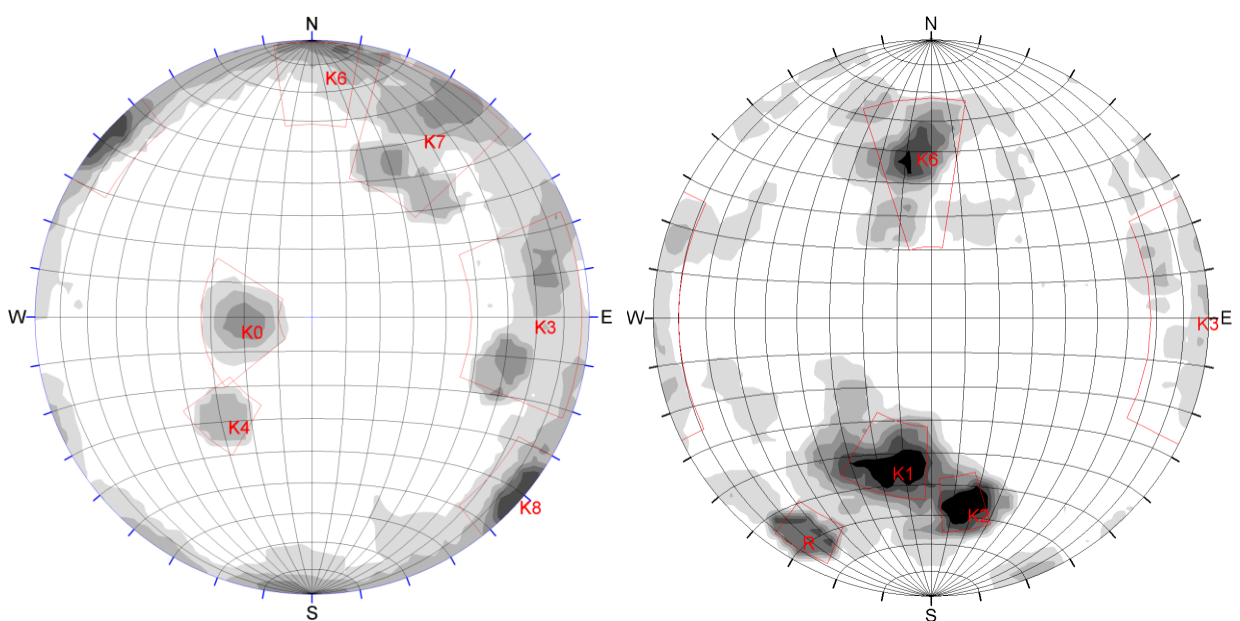
The 33 geomechanical stations fall within both the areas and the discontinuity difference in terms of orientations are reported in the stereplot of Figure 4. 9



**Figure 4. 9** – Isodensity contours representing the discontinuity sets of the area outside the Vajont landslide

Only eight sets of nine, characterizing the whole study area, have been recognized. K5 is not a representative set of this domain. The K1, K2, K4, K0, instead, belong to different joint sets, but considering the domains division they belong to the same bedding plane represented in the 5a and 5b domains respectively ( Figure 4. 10)

.The 5a domain is characterized by K0 and K4 while the domain 5b by K1 and K2.

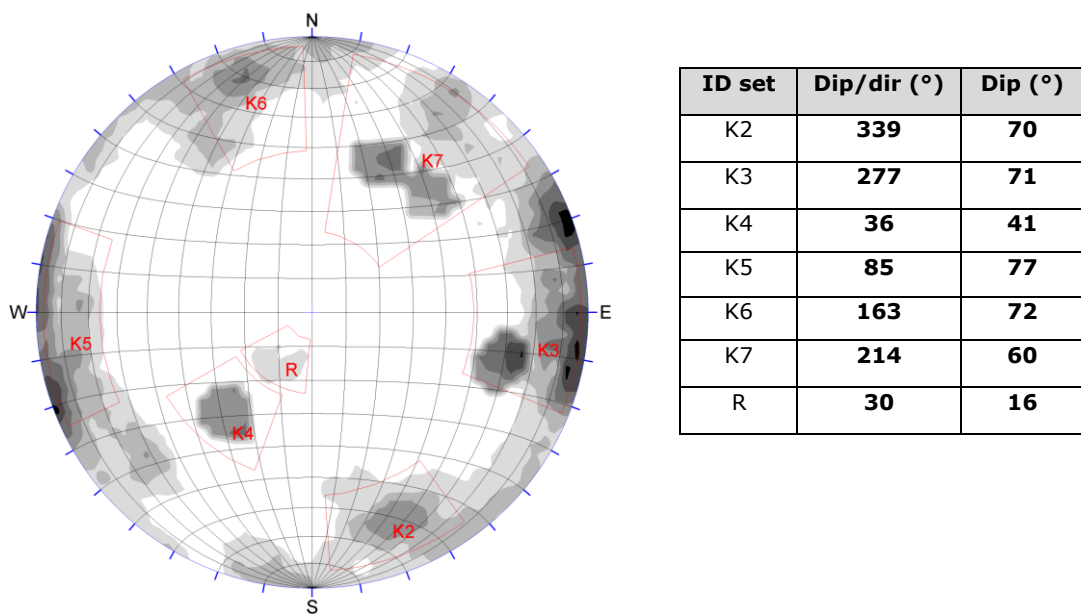


**Figure 4. 10** – Stereoplots of domains 5a (on the left) and 5b (on the right) data.



### Joint sets of the deposit area

In the deposit area almost all discontinuity sets were recognized but, , the dispersion of the values is very high due to the information following the landslide occurrence. In this area 48 scan lines have been examined; some of these highlighted the presence of different joint set, identified as R (random) set. It could be interpreted as the rotation of some discontinuity system during the 1963 movement related to the geometry of the sliding surface .. The most representative joint sets in the deposit area, as shown in the stereoplot, are K3, K5, K7 (Figure 4. 11). K5 and K7 could be not easily recognizable when they are almost vertical.

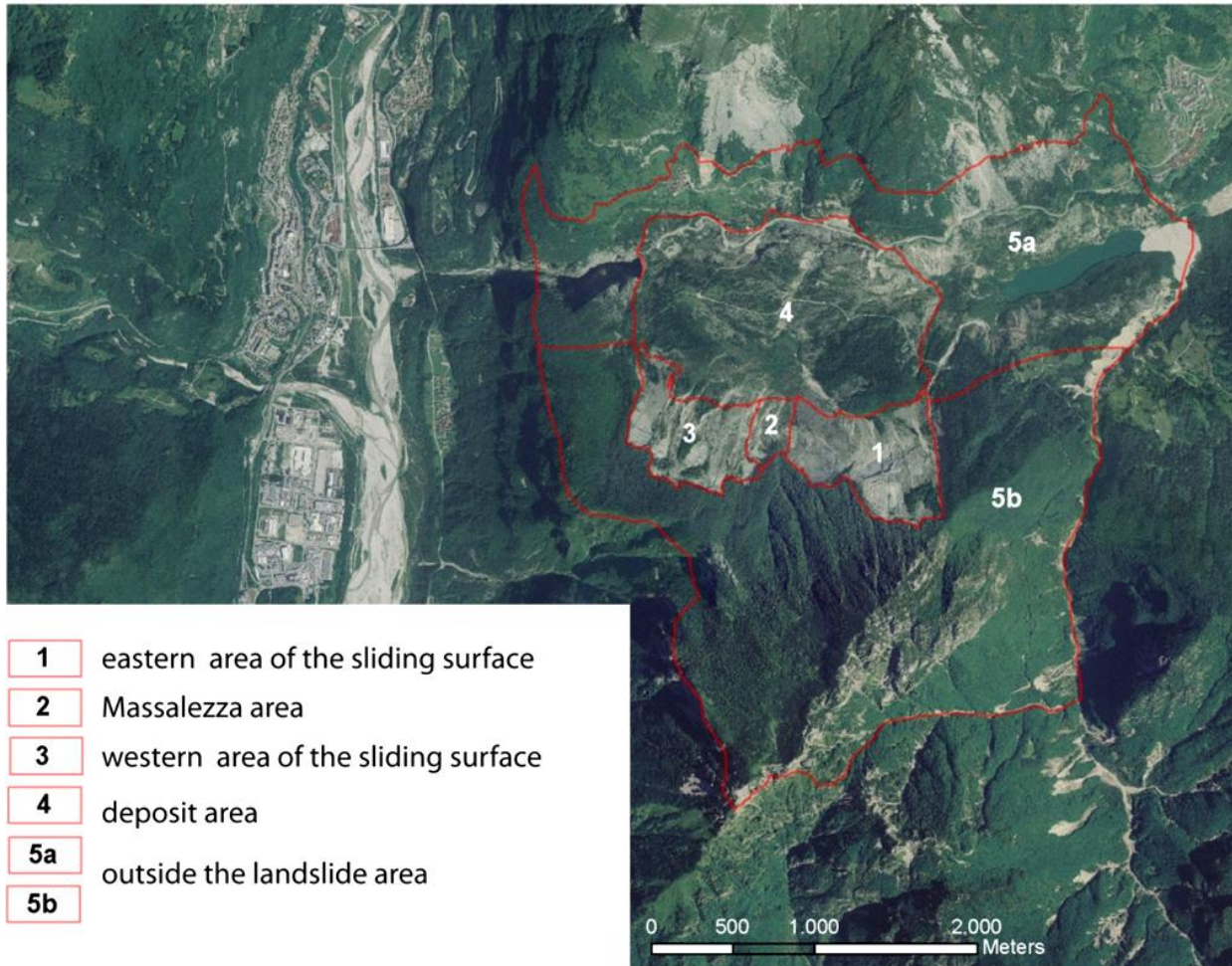


**Figure 4. 11** – Discontinuity sets detected in the deposit area

### Joint sets on the sliding surface

The sliding surface shows different discontinuity characteristics because of its peculiar shape and tectonic setting. According to the field structural analysis, the discontinuity sets have been analyzed for every sliding surface domain (Figure 4. 12).

Only eight scan lines were performed on the sliding surface, because of the inaccessibility and dangerousness of the sites.

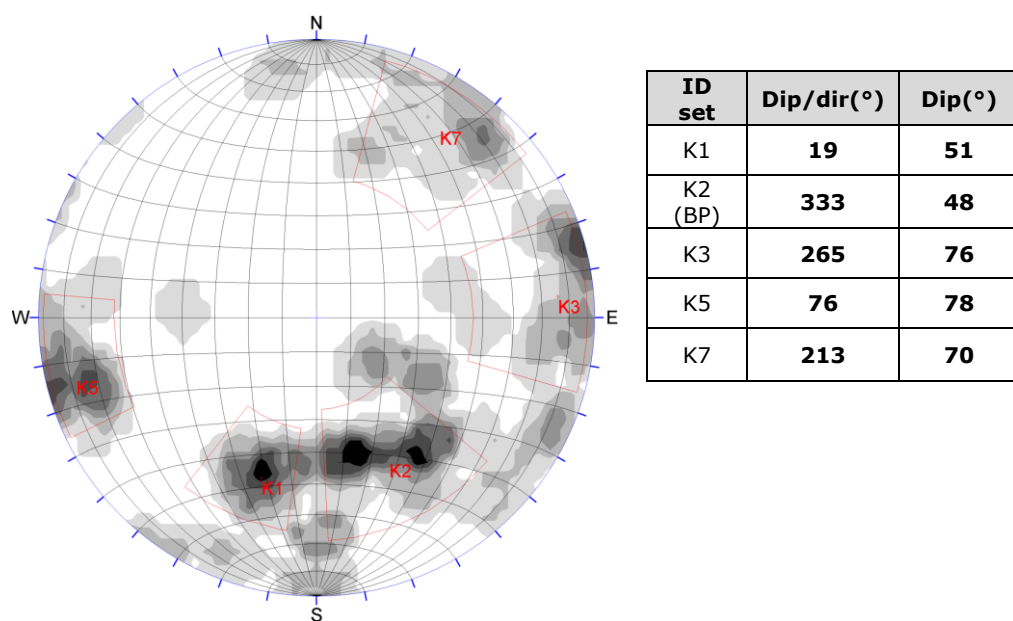


**Figure 4. 12** –Scheme of the domains subdivision of the Vajont study area.

In this area the sliding surface coincides with the bedding planes and the other observed systems correspond to the intersection of relative planes with the same sliding surface.

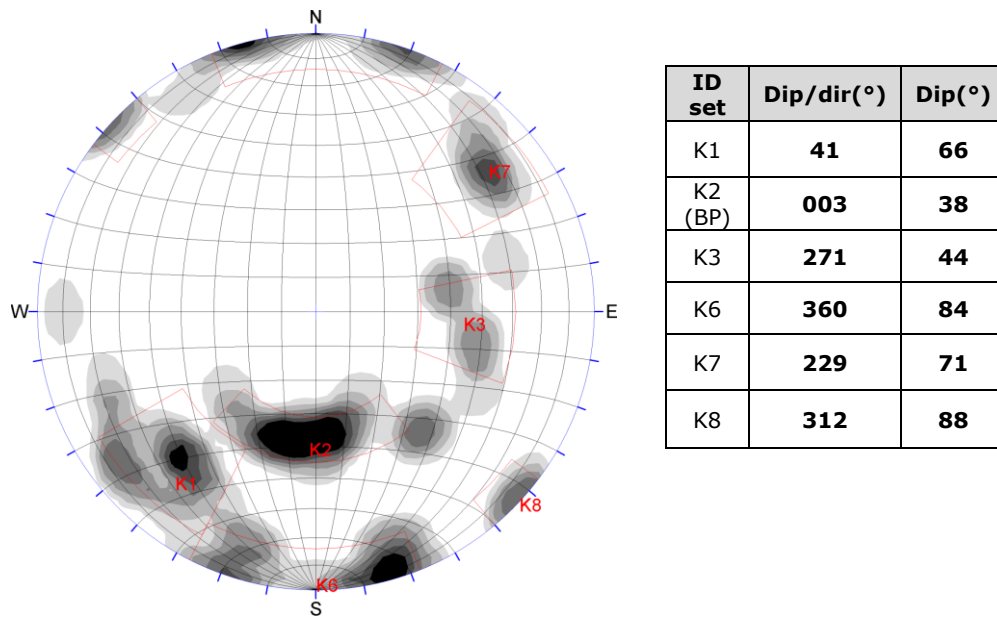
The eastern side of the sliding surface is characterized by K1 and K2 discontinuity sets corresponding to the bedding plane and this result is in agreement with the structural survey, that highlighted a general NW structures orientation.

K3 and K5, instead, show high values of dip angle (almost vertical strata). It is not easy to understand if there is only one vertical system NS oriented or many more.



**Figure 4. 13** – Stereoplot of the domain 1 corresponding to the eastern area of the sliding surface

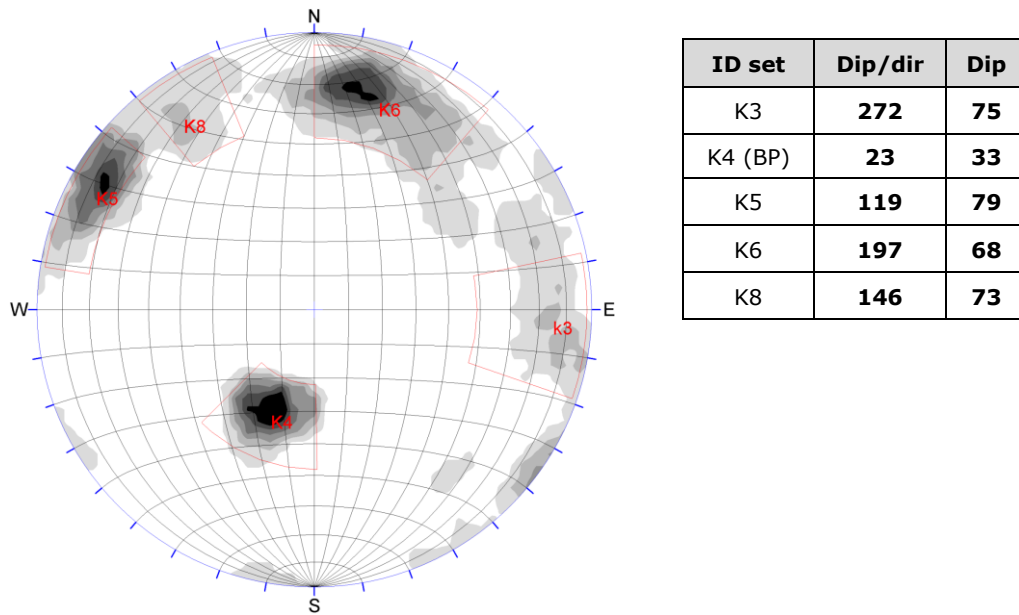
The bedding plane of the central area domain (n.2) is represented by the K2 joint set (Figure 4. 14 – Stereoplot of the Massalezza area- domain2). This area, as evaluated through the structural analysis, shows a relevant complexity due to the interference of two fold systems. Indeed, the discontinuity sets analysis are in agreement with the general setting obtained by the geological survey. The presence of the different vertical joint systems could be related to a southwards converging sub-vertical faults system, as resulted by the structural analysis.



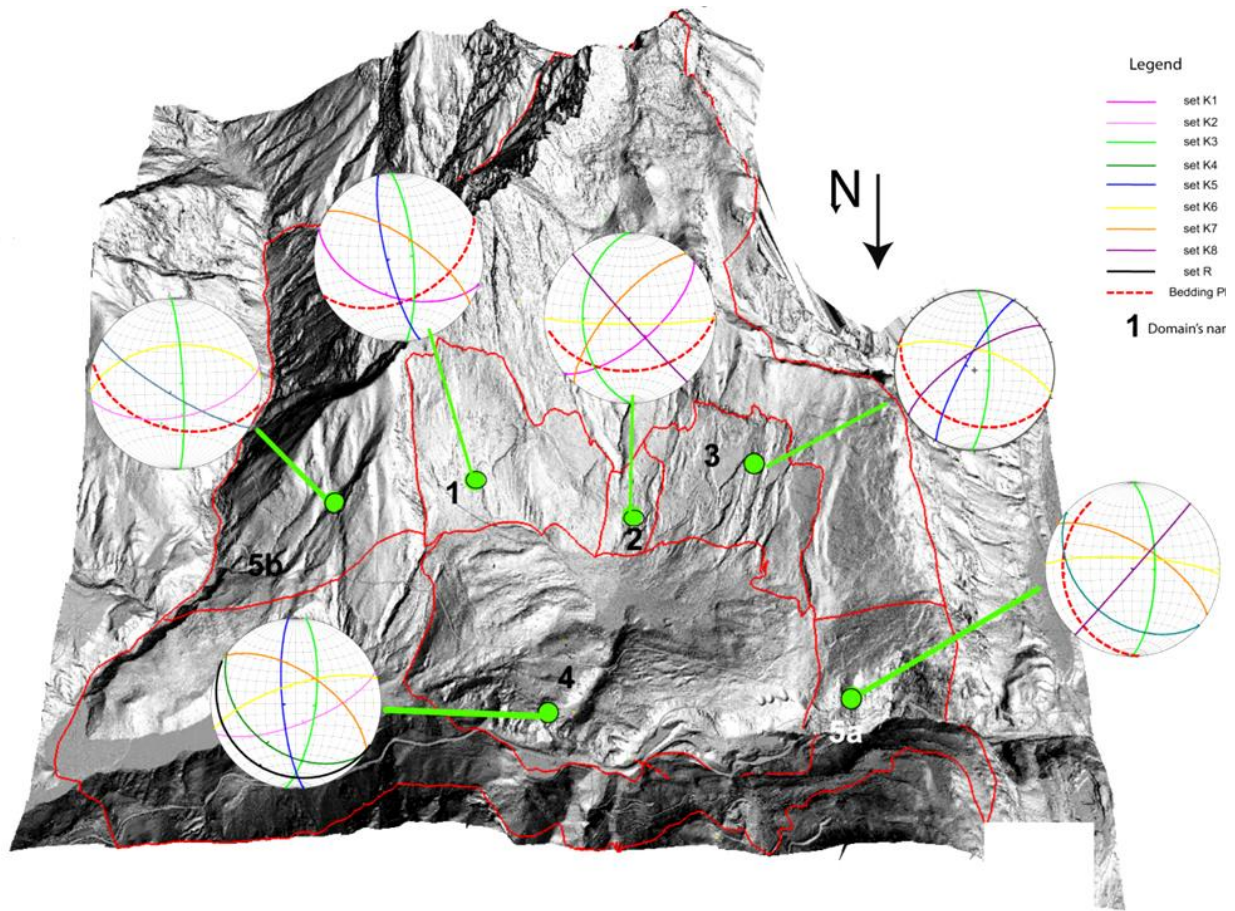
**Figure 4. 14** – Stereoplot of the Massalezza area- domain2

In the western portion of the sliding surface the bedding planes are identified by K4 system (Figure 4. 15). The Figure 4.16 and 4.17 show a summarizing pattern of the joint sets systems in area.

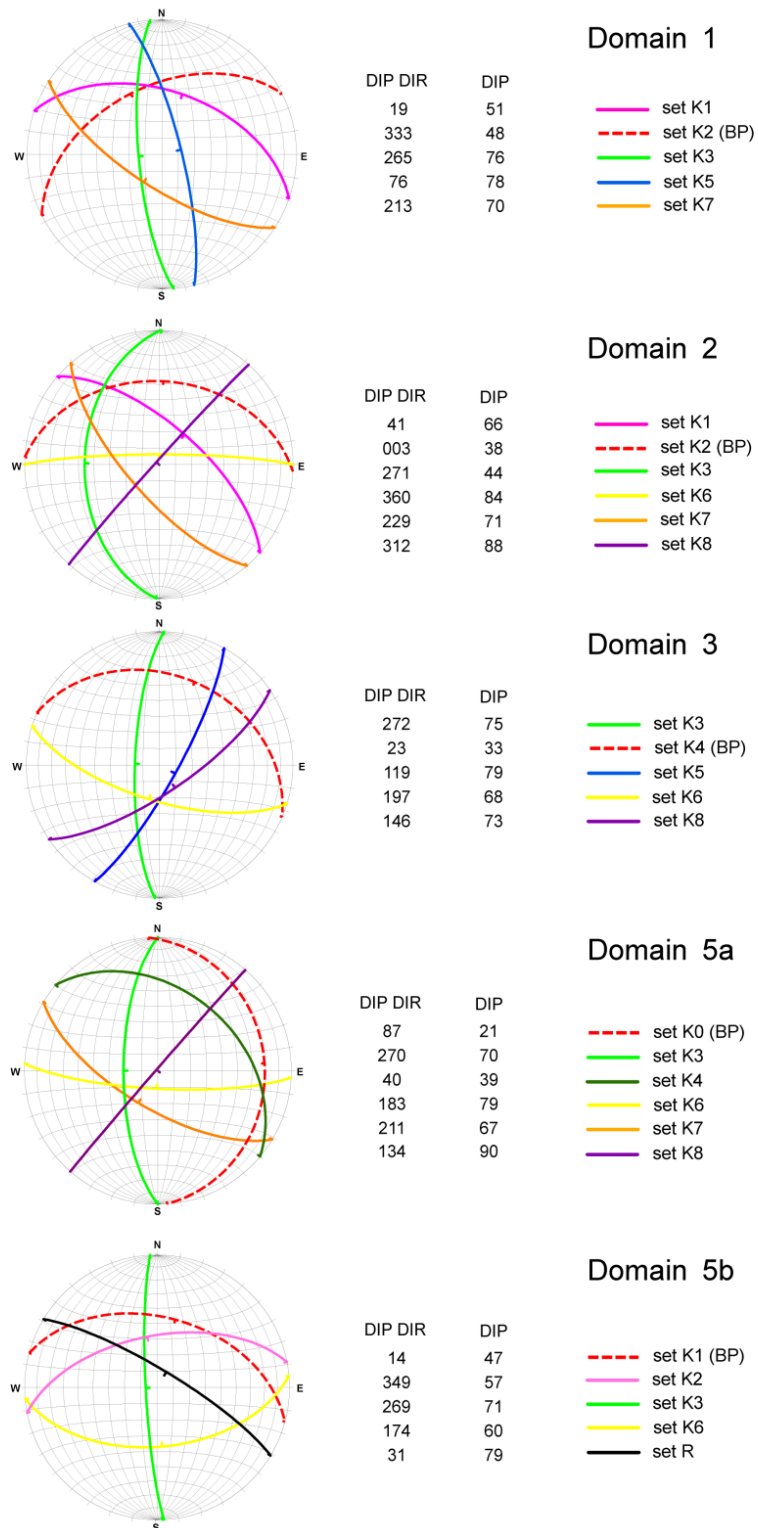
From an accurate analysis of the bedding plane in the 3 different domains, the non-planarity of the sliding surface and the convergence toward the Massalezza axis syncline is clearly shown.



**Figure 4. 15** – Stereonet of the western area of the sliding surface- domain3



**Figure 4.16** - Stereoplots of the main discontinuity sets for each domains



**Figure 4.17** – Discontinuity sets for each domain provided by field data

### **4.3.3. Application of remote sensing techniques to discontinuity analysis**

The increasing amount of terrestrial remote sensing applications is the result of technological advances, that made these techniques accessible to the researchers. The use of remote sensing techniques to characterize rock mass discontinuity parameters is a relatively recent technology, which considerably developed in the last decade. Indeed these methods are potentially valuable to measure discontinuity surface geometry at small and large scale. Discontinuity characteristics obtained in this way agreed with those values provided by manual traditional procedures. The potentiality of these techniques were demonstrated by Jaboyedoff et al., 2003, Ghirotti and Genevois 2007, Oppikofer et al., 2008, Sturzenegger 2007, Pedrazzini et al., 2011.

The methods applied in this study aimed at characterizing the rock mass discontinuity properties were the following:

- COLTOP 3D
- TERRESTRIAL PHOTOGRAMMETRY

The application of terrestrial laser scanning (TLS) was not useful because of the large distances to reach.

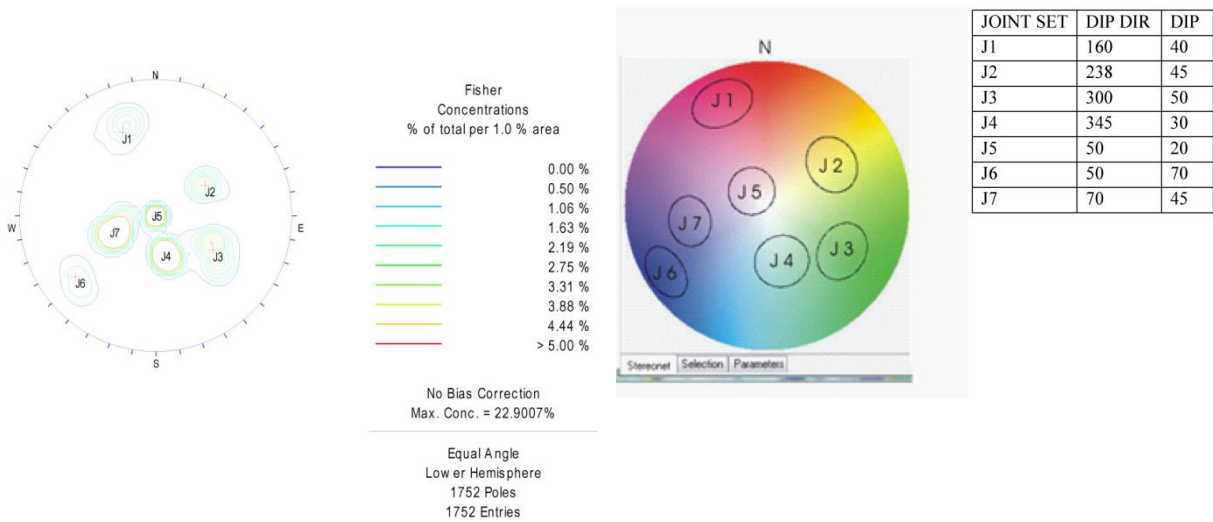
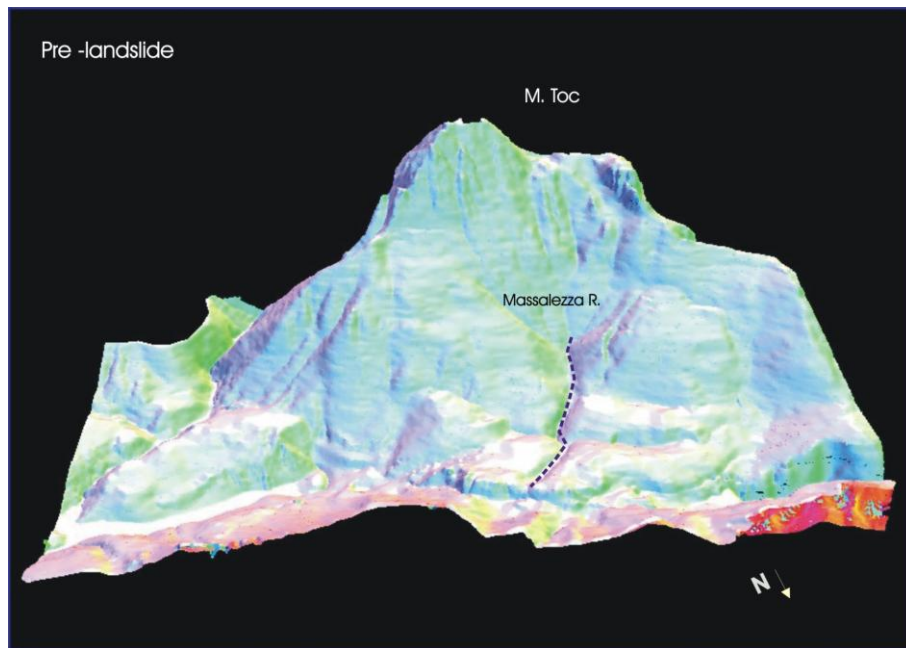
#### **4.3.3.1 COLTOP 3D**

COLTOP 3D is an important support for structural and geomechanical field survey. It allowed to increase the knowledge of the geomechanical and morpho-structural Vajont conditions pre and post landslide. Indeed, the COLTOP 3D application on grid data as well as on unstructured point cloud data provided a complete discontinuity analysis pre and post 1963 event. The discontinuity analysis was performed through the Digital Elevation Model (DEM) investigation of the Vajont topography area with a 3D shaded relief. The shaded relief showed the strata orientation by a Schmidt-Lambert projection, represented by one color for a given dip and dip direction, so that the colours difference will represent the different strata orientations.

The results of discontinuity analysis, displayed the discontinuity setting condition before the catastrophic event and seven joint sets result to characterize the area (Figure 4. 18).

The comparison between pre and post discontinuity sets allowed to better identify the pre-existing morpho-structure setting and the most important movement directions of the 1963 event.

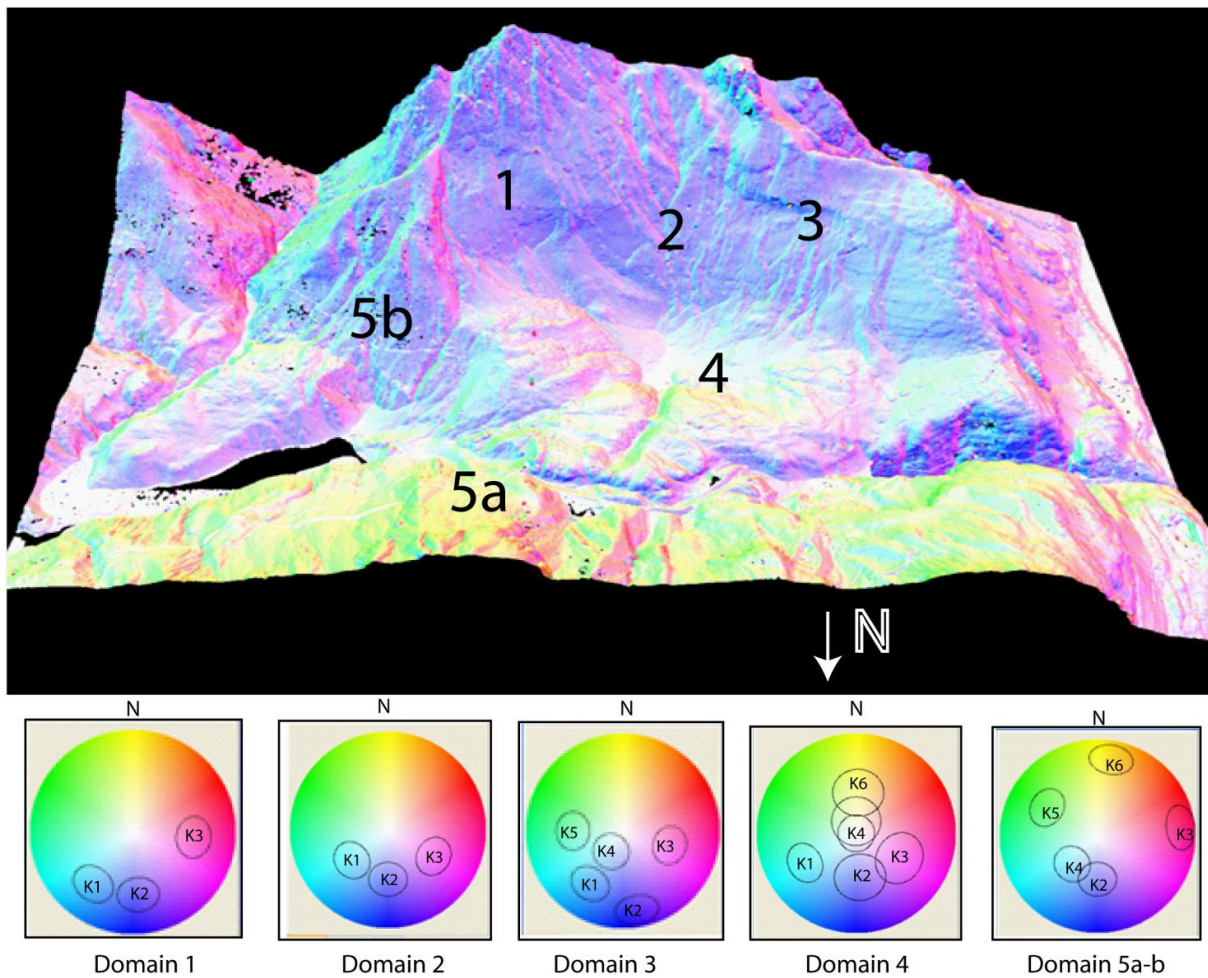




**Figure 4. 18** - COLTOP 3D analysis of the Vajont DEM pre 1963. Different colours show different strata orientations so indicating the morpho-structural features (faults and lineaments). Seven discontinuity sets were detected.

The discontinuity analysis post event, was performed using an airborne laser scanning digital elevation model provided by Friuli Venezia Giulia Region (Figure 4. 19).

The discontinuity analysis results for each domain allowed to identify six main discontinuity sets, some of which directly influenced the Vajont landslide morphology.



**Figure 4. 19** – Orientation-specific coloring of the airborne lidar DEM in COLTOP 3D. The strata orientations for each domain are displayed by unique colour given by the pole in a lower-hemisphere Schmidt stereonet in association with HIS wheel. Numerical data of different joint sets are reported in Tab 4. 3.

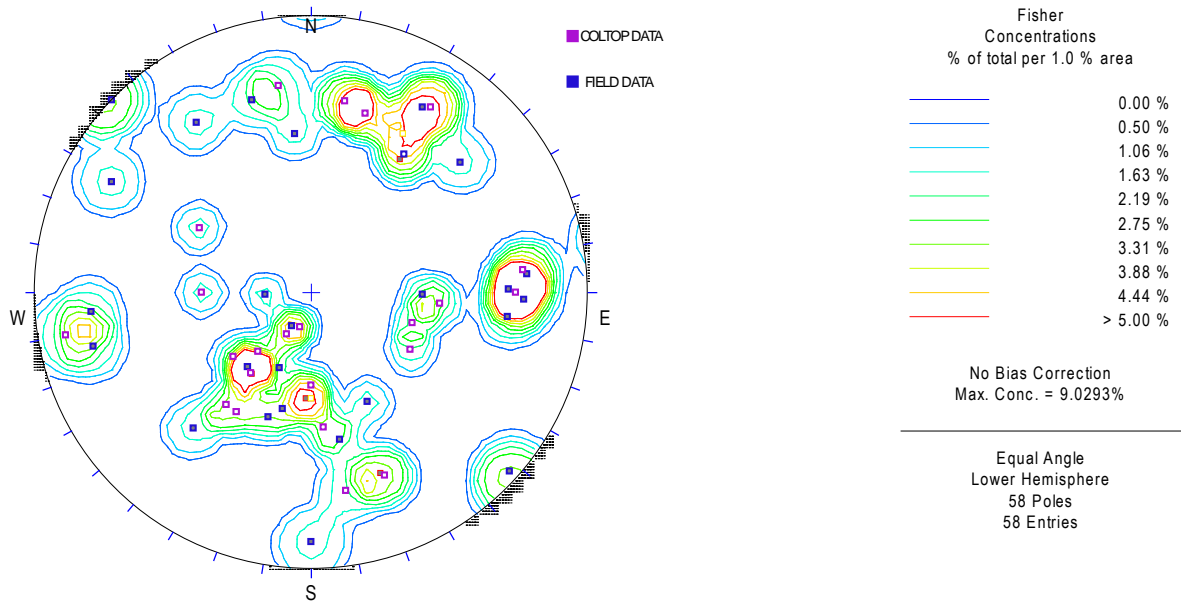
The results achieved were validated by a comparison with the field data (Tab 4. 3 and Figure 4.20). The lack of recognition of some discontinuity sets detected by COLTOP 3D is due to the functionality of remote sensing techniques: it cannot detect all of the visible surfaces, as in field survey. Thanks to the COLTOP3D analyses a homogeneous data distribution has been obtained. In synthesis the COLTOP 3D data allowed to recognize the geometrical features of the discontinuities in the exposed sliding surface, so completing the geomechanical measurements of the landslide area.

**Tab 4.3 – Discontinuity data comparison between field investigation and COLTOP3D**

domains	Bedding Plane	Joint set detected by COLTOP-3D	Dip directions (°)	Dip (°)
1	K2	K1	37	54
		K2	355	52
		K3	275	50
			213	77
2	K2	K1	50	40
		K2	0	42
		K3	300	45
3	K4	K1	32	54
		K2	350	72
		K3	287	42
		K4	30	20
		K5	90	43
			190	70
			197	68
4		K1	18	15
		K2	338	71
		K3	270	73
		K4	37	40
			80	84
			171	74
			214	62
5		K2	0	37
		K3	264	75
		K4	42	32
		K5	120	50
		K6	190	70
			210	67

domains	Bedding Plane	Joint set detected by Data Field (DIPS)	Dip directions (°)	Dip (°)
1	K2	K1	19	51
		K2	333	48
		K3	265	76
		K5	76	78
		K7	213	77
2	K2	K1	41	66
		K2	3	42
		K3	271	44
		K6	360	84
		K7	229	71
		K8	312	88
		K3	272	75
		K4	23	33
3	K4	K5	119	79
		K6	197	68
		K8	146	73
		R	30	16
		K2	339	70
		K3	277	71
4		K4	36	40
		K5	85	77
		K6	163	72
		K7	214	60
		K1	14	47
		K2	349	57
5		K3	269	71
		K4	40	39
		K6	174	60
		K7	211	76
		K8	134	90
			87	19



**Figure 4.20 – Comparison between field and Coltop discontinuity data detected.**

#### 4.3.3.2 PHOTOGRAMMETRY ANALYSIS

Digital photogrammetry is increasingly being used in studies of large rockslides, providing three-dimensional models of slope faces and failure surfaces and data on rock mass properties. Moreover this remote sensing technique allows an accurate assessment of the properties of large structures that may potentially affect slope stability.

Terrestrial remote sensing techniques are being increasingly used as a complement to traditional scanline and window mapping methods. Indeed they provide a more comprehensive information on rock cuts, allow surveying of inaccessible outcrops, and increase user safety.

The photogrammetric analysis was conducted thanks to the 2-year time long cooperation with the PhD student of the Simon Fraser University, Andrea Wolter. The photogrammetric analysis was used to provide detailed DEM of the rock slide failure surface and to add detailed structural and geomechanical information on inaccessible areas of the rock slide. The photogrammetry is used to provide a detailed DEM of the rock slide failure surface and to obtain information on movement directions, rear and lateral release structures.

The terrestrial photogrammetry analysis of the Vajont landslide is a main topic of A. Wolter's PhD program. To this purpose in this thesis it will be exposed the preliminary results together performed to complete the structural and geomechanical characterization. In order to obtain an accurate photogrammetric model and discontinuity information the study area was investigated

It was dividing in different windows.

The data results were compared with the field data successively collected. In order to map discontinuity dips and dip directions, the AdamTech programme 3DM Analyst was used. Photogrammetry on the Vaiont landslide was performed using a range of focal lengths ( $f = 20, 50, 100, 200, \text{ and } 400 \text{ mm}$ ) and provides the first measurements of structures on inaccessible parts of the failure surface. The camera used for capturing the digital images of the rock cuts is a Canon EOS 30D digital camera.

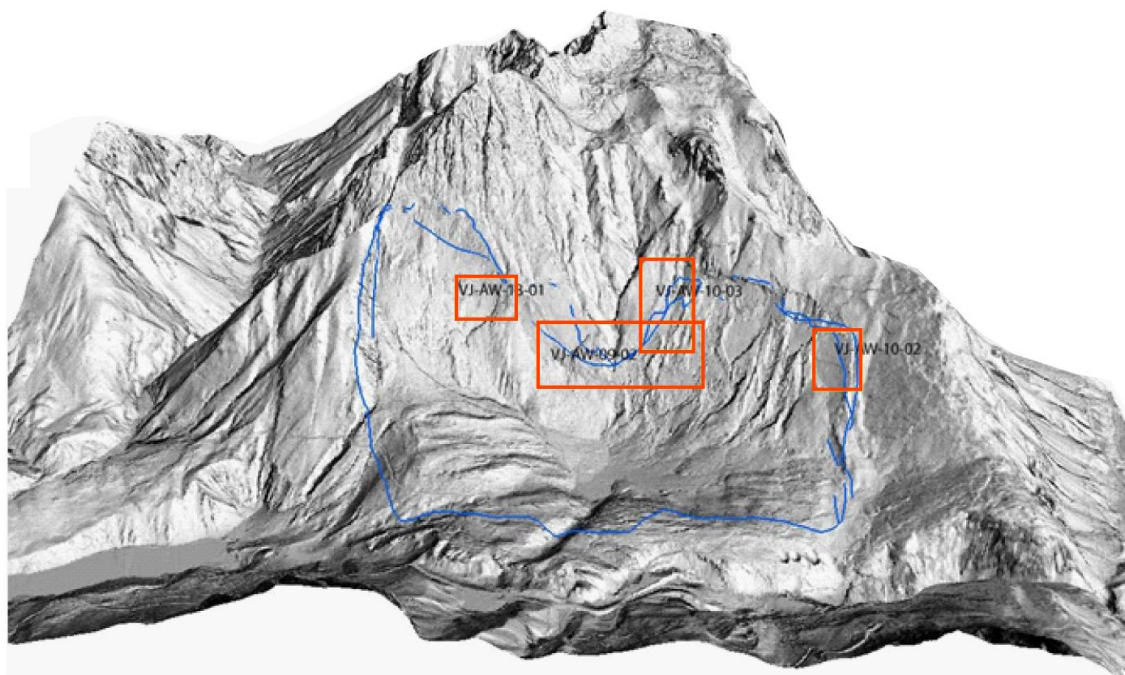
Calibration of the camera and lenses, construction of 3D models and discontinuity measurements were all achieved using the 3DM CalibCam and 3DM Analyst software (Adam Technology,2007).

In order to compare the photogrammetric and field data, some photogrammetric models that coincided with field stations were used in preliminary analyses.(Figure 4. 21 and Figure 4. 22).

These are labeled as: VJ-AW4, VJ AW10-02, VJ AW 10-03, VJ AW 09-02 and VJ AW 13-01 (Tab 4. 4)

**Tab 4. 4** – Photogrammetry windows model

ID	USED LENS
VJ-AW-4	20mm
VJ AW10-02	400mm
VJ AW 10-03	400mm
VJ AW 09-02	400mm
VJ AW 13-01	400mm

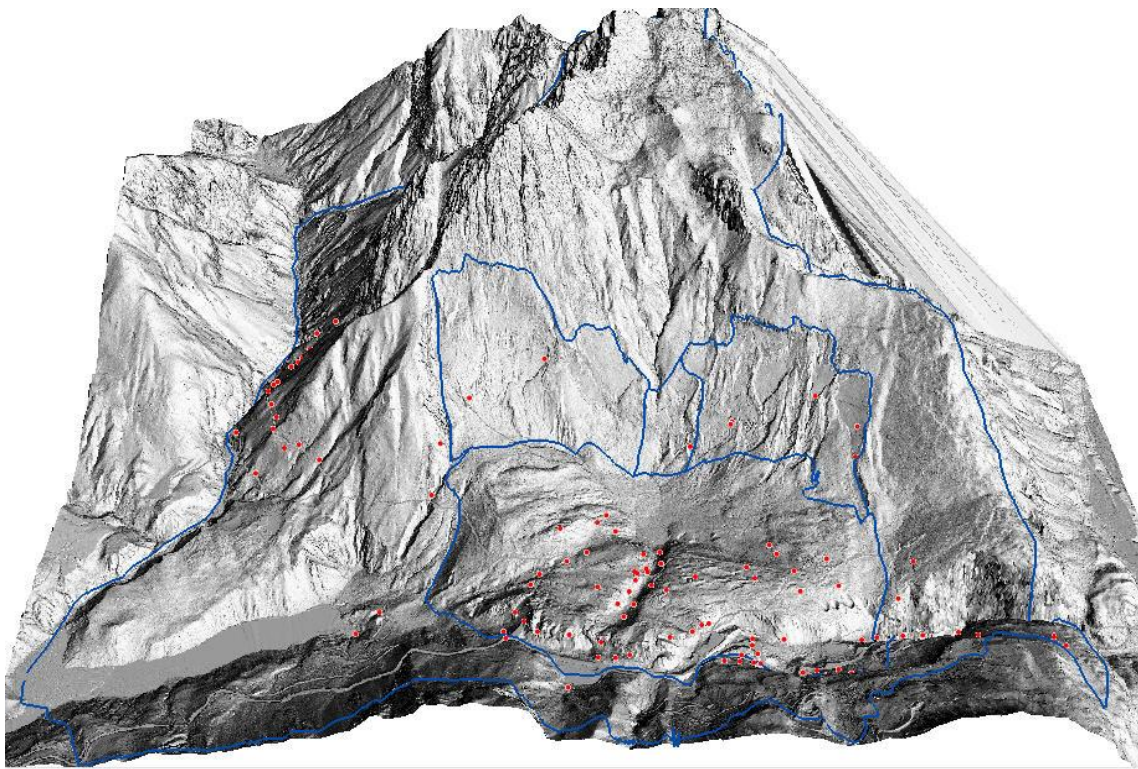


**Figure 4. 21** - Areas investigated by preliminary photogrammetric analysis

To obtain a first assessment of the main structural features detected by photogrammetry on the sliding surface and to evaluate their general distribution, a 20 mm focal length model, that includes the whole sliding surface, has been initially chosen. Next, four areas of the sliding surface captured with a 400mm lens were analyzed for getting more details.

The used programme considers the data of discontinuities outcropping in a circular one, with convenient tolerance, and assigns the mean values due to the resolution, orientation, and sampling bias, including the flatness of the sliding surface, discontinuities may be mapped with only one or two circular areas in ADAM Tech, and thus may not be representative of real field densities.

Hence, only one plane in the photogrammetric models may represent the only representation of a discontinuity set observed in the field. This is recognized as being statistically invalid but is described only for preliminary interpretative purpose. Polyworks IMAlign has been used for georeferencing.



**Figure 4. 22** – Geomechanical stations performed in the field investigation

The results for each window model are shown below and compared with the structural features detected by field data summarized in stereoplots (fig 4.16 and 4.17). In comparing the data, it has been considered a broader range of values due to the errors associated with orientation measurements, both in the field and in photogrammetric analyses

- Window VJ – AW4: (Figure 4. 23)

This window belongs mainly to the structural domains n. 1, 2, 3. 5 sets can be observed but 3 may be compared with the field data. Discontinuity sets 1 and 2 are clearly visible in domain 3 and may correspond to set K5 and K8 respectively (Figure 4.17). Set 3 can be associated with K6 present also outside in the domain 5b. The attitude of the bedding plane is more similar to the range of values in domain 3, than in the two others.

- VJ – AW - 10 – 02: (Figure 4. 24)

This window belongs entirely to the domain 3. The mean set (n.7) coincides with the bedding planes dip of domain n.3. Two different sets could be attributed to sets n.3 and n.8, even if they are represented in the stereoplots by a single point (remembering that each point is a mean of all the measurements read in the circle area. The n.3 set considered the discontinuities present on the landslide crown, while the n.8 set is quite anomalous and should not be considered.

- VJ – AW – 10 – 03: (Figure 4. 25)

Is located between domains 2 and 3. It includes the Massalezza area which is highly deformed, and thus was difficult to map. The attitude of the bedding planes in this area are closer to domain BP 2 values, whereas in domain 3 they are oriented more towards NE. It is interesting to observe the attitude of joint set 1 ( $40^{\circ}/309^{\circ}$ ) and 5 ( $38^{\circ}/066^{\circ}$ ) respectively, which could correspond to K3 and K1 of domain 2. Sets 3 ( $52^{\circ}/010^{\circ}$ ) and 4 ( $57^{\circ}/025^{\circ}$ ) detected by photogrammetry could correspond to joint set K6 of domain 3. Joint set 6 ( $60^{\circ}/146^{\circ}$ ) is visible in domain 3 and corresponds to K8. This photogrammetric window did not detect the set K5 observed in field survey in domain 3.

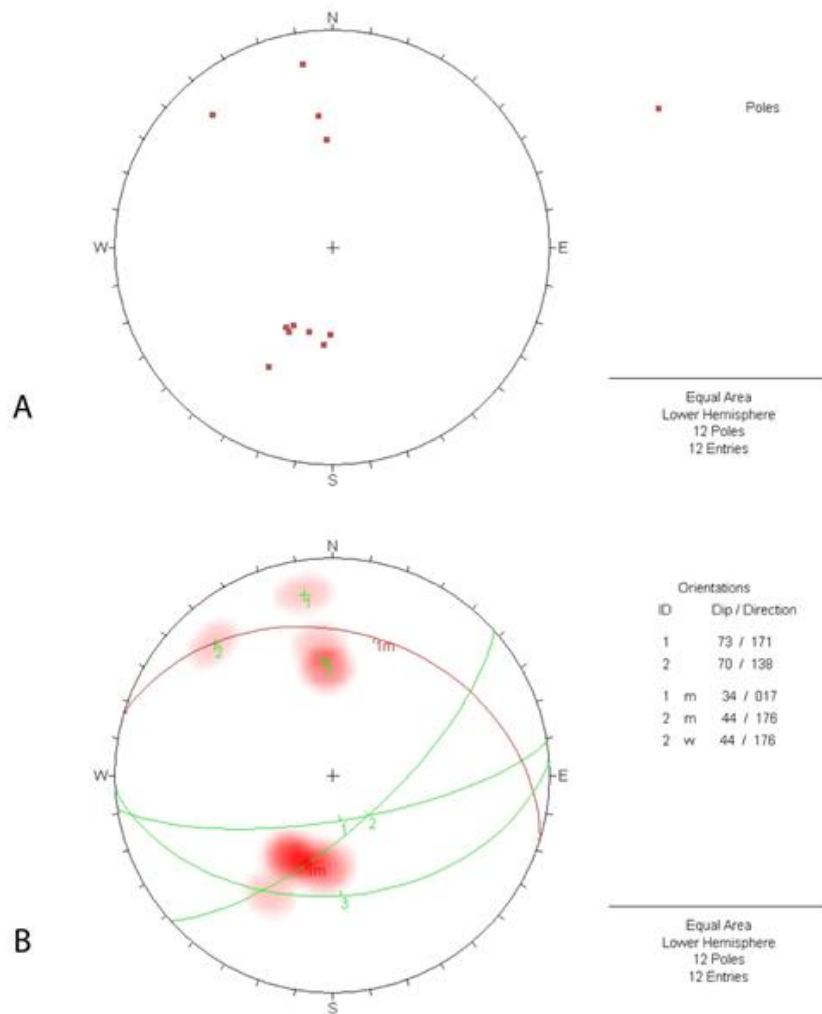
Window VJ – AW9: ( Figure 4. 26)

This window includes the Massalezza trench; thus the analysis shows more complex structural characteristics. The discontinuity sets detected in this window by photogrammetry are: This window includes the Massalezza trench; thus the analysis shows more complex structural characteristics. The discontinuity sets detected in this window by photogrammetry are:

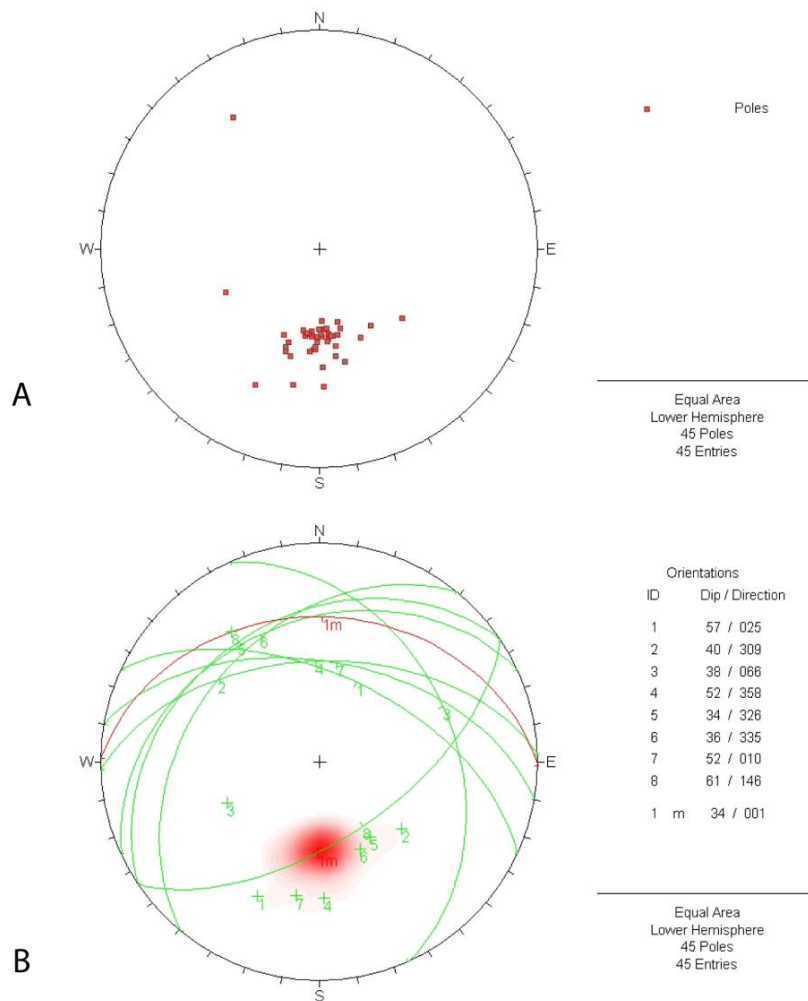
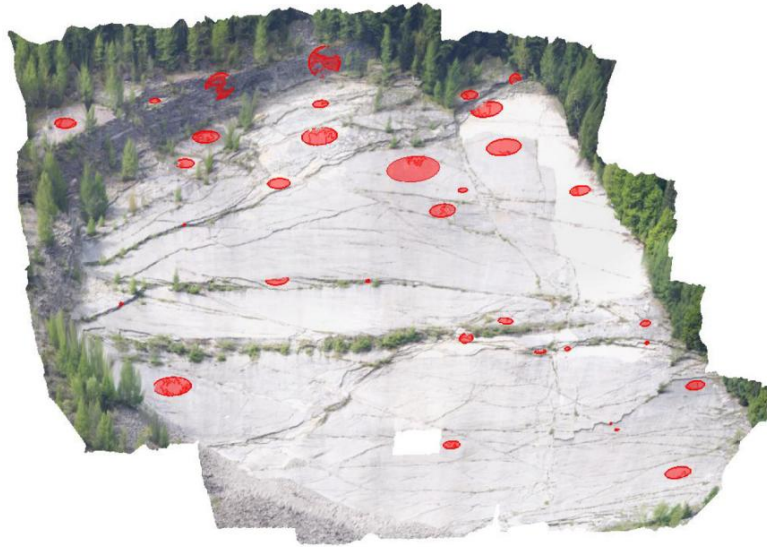
Dip°/Dip Dir°	Discontinuity set	Domains (cfr. 4.18)
76/131	K3	3-2
26/075	K2	5b
76/131	K8	3
52/334	K8	2

The 26°/075° discontinuity set is also found outside the landslide area and could represent pre-failure tectonic conditions. The photogrammetric analysis has revealed another discontinuity set (11°/136°) which is not identified in field data measurements.

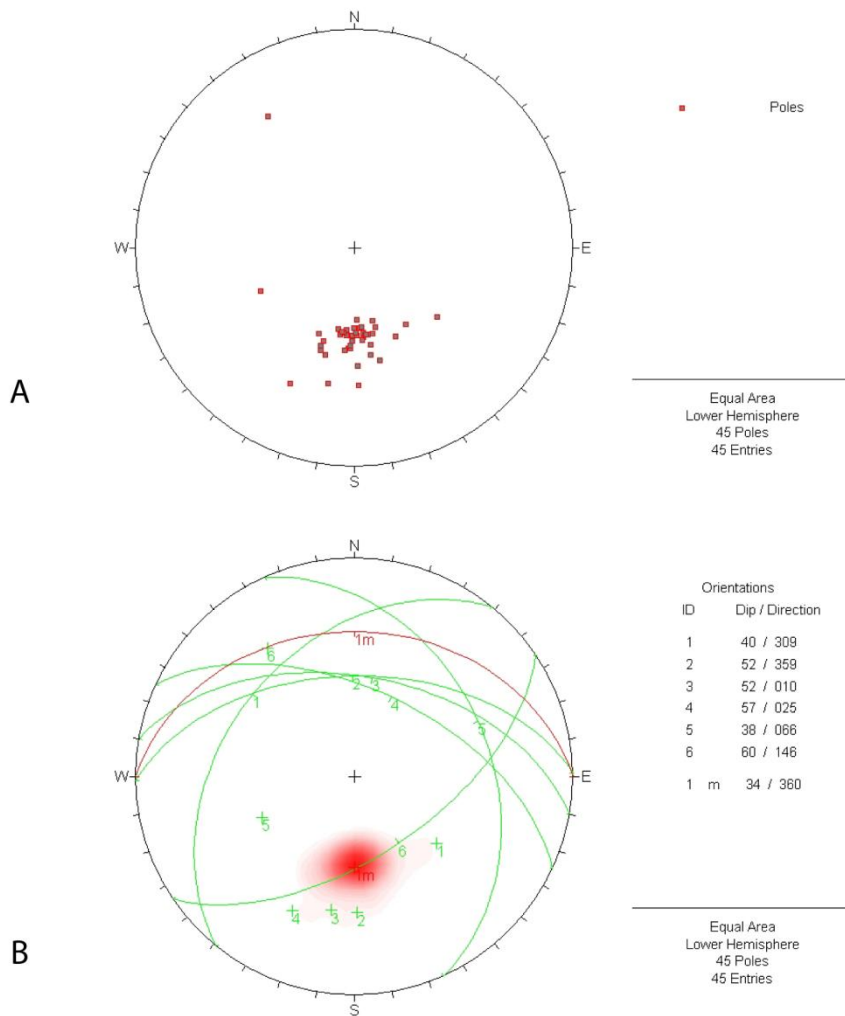
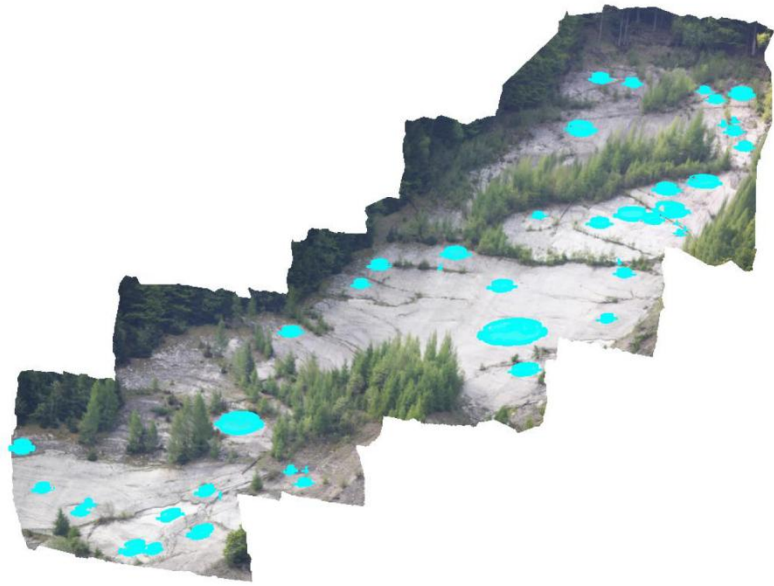




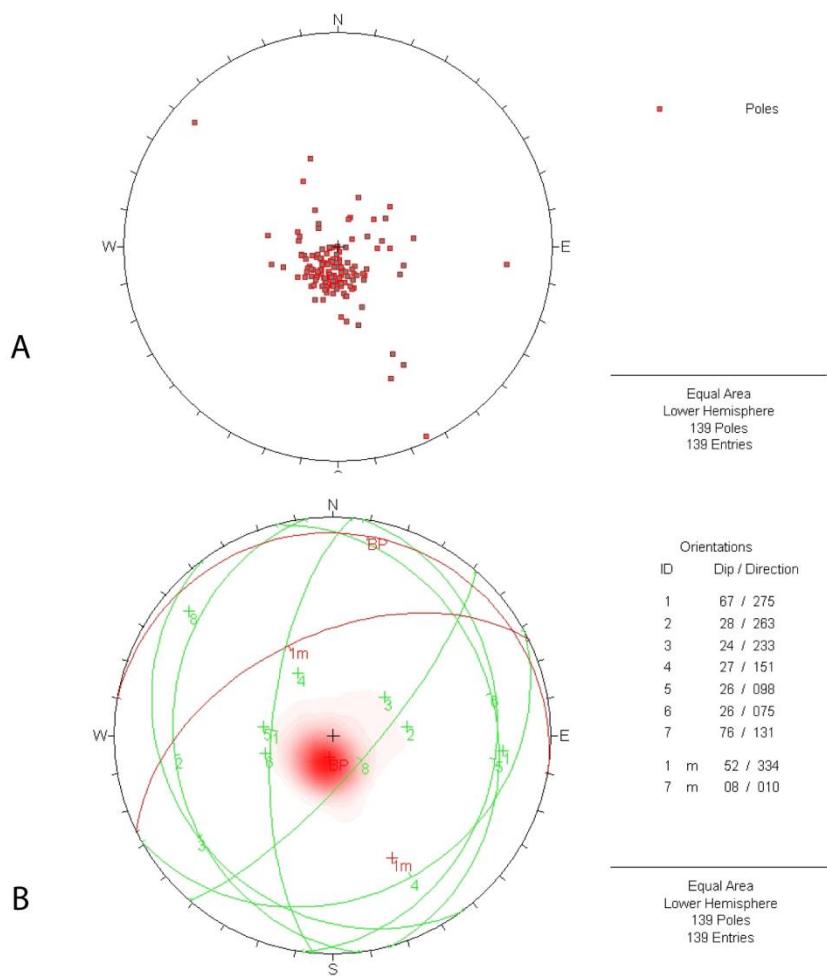
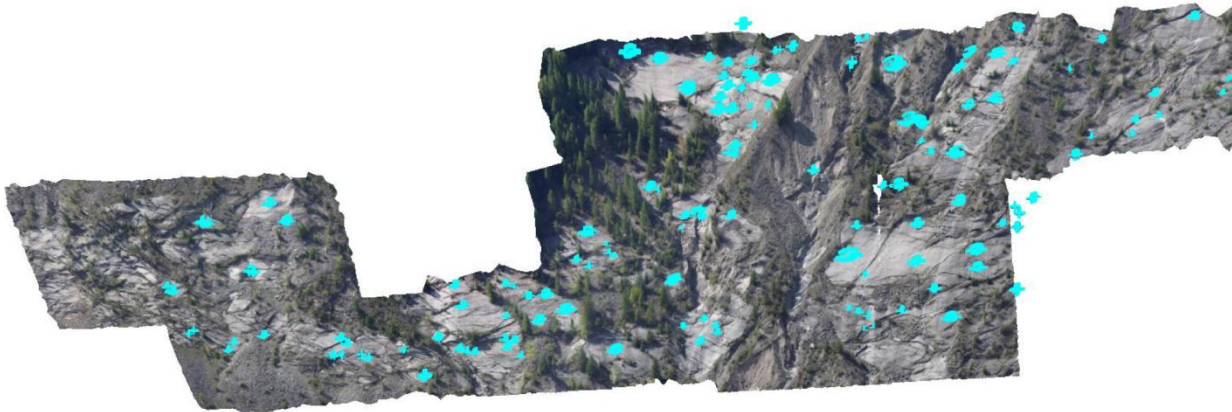
**Figure 4. 23** - Joint sets detected by photogrammetry analysis  $f=20\text{mm}$  for VJ-AW4 window. A : Point plot B: Plane plot



**Figure 4. 24** – Joint sets detected by photogrammetry analysis  $f = 400\text{mm}$  for VJ-AW 10-02 window. A : Point plot B: Plane plot.



**Figure 4. 25** - Joint sets detected by photogrammetry analysis  $f=400\text{mm}$  for VJ-AW 10-03 window. A : Point plot B: Plane plot

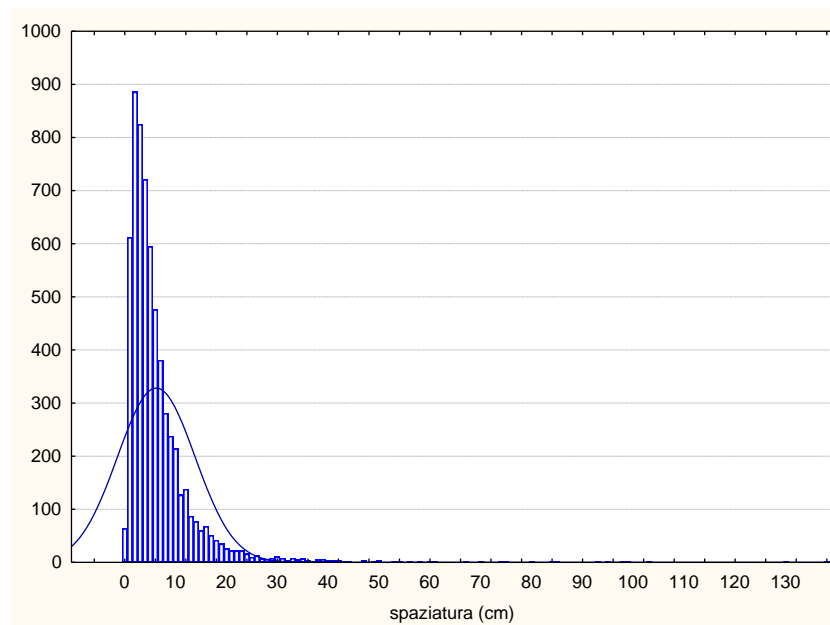


**Figure 4. 26** - Joint sets detected by photogrammetry analysis  $f=400\text{mm}$  for VJ-AW 09-02 window. A : Point plot B: Plane plot

#### 4.3.4 Discontinuity spacing

Discontinuity spacing is a basic measurement of the perpendicular distance between two adjacent discontinuity (Wines and Lilly, 2002). This is a relevant parameter in the rock mass characterization, as stability analysis strongly depends on the block size in a rock mass. In the present work the distribution of distances between two successive discontinuities has been considered representative of the fracturation grade of the rock mass.

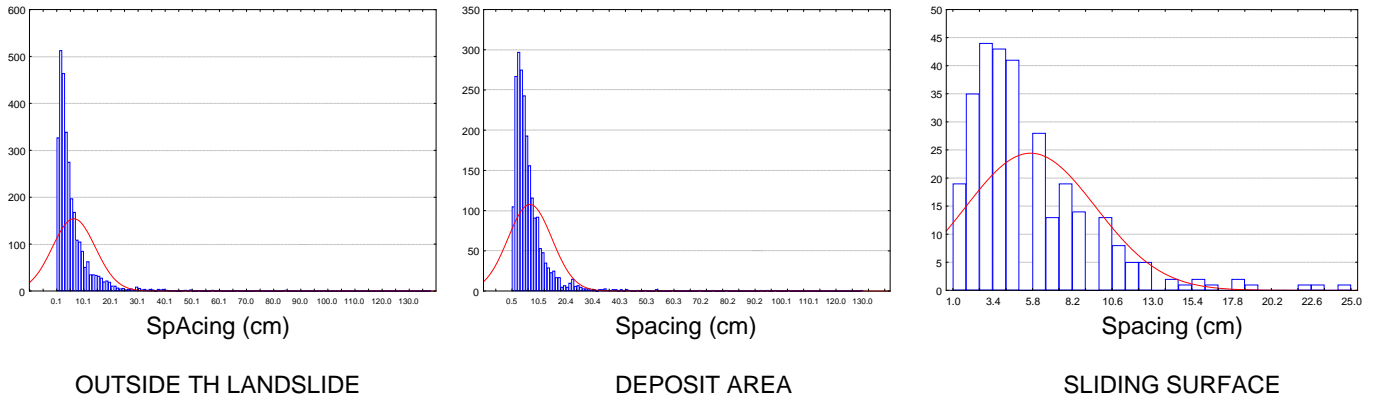
The general trend of the all spacing distribution is showed in the Figure 4. 27. It is well-rendered that the most frequent values range between 1 and 15 cm, the mean value is 6.6 cm with a standard deviation of 7.6cm.



**Figure 4. 27** – Spacing distribution histogram

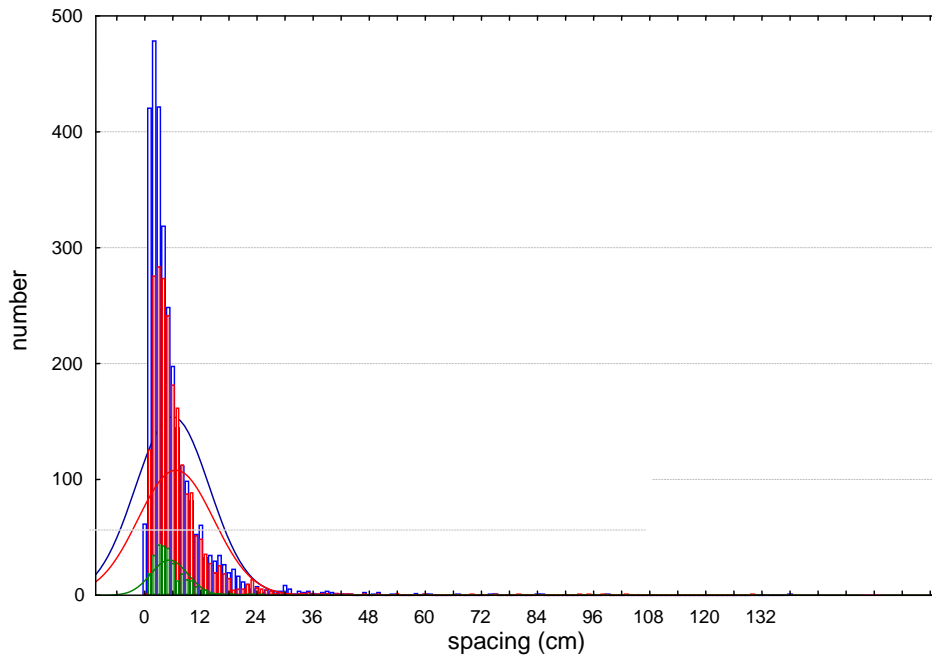
The next analysis has been performed considering the spacing distribution for each domain. The considered areas are: 1) detachment area 2) deposit area and 3) outside of the landslide area. The spacing distribution of the areas, (

Figure 4. 28) displayed a mean value of 6.34 cm, for the area outside the landslide; 5.6 cm for the detachment area (sliding surface); 7.1 cm for the deposit area.

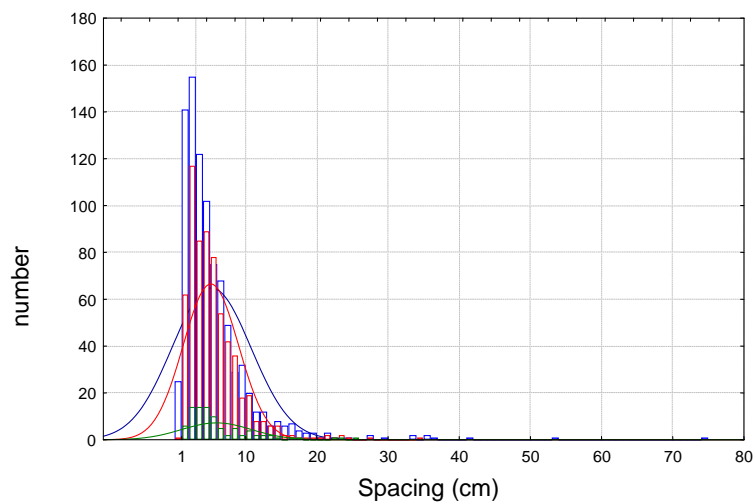


**Figure 4. 28** – Spacing distribution histograms of areas identified in the Vajont study area

The overlap of the histograms shows that the discontinuity spacing data of the three areas have the same distribution with similar mean value (Figure 4. 29). Furthermore, it was compared the spacing distribution of the bedding plane for each domains. Even this analysis, as displayed in the histogram (Figure 4. 30) did not evidence essential differences among the mean values of the spacing distribution. Indeed, the mean values are: 5.11 cm in the outside the landslide area, 5.16 cm and 5.7 cm in the deposit and sliding surface areas respectively.



**Figure 4. 29** – Comparison among the spacing distribution histograms of outside the area (blu), deposit area (red) and sliding surface (green)



BEDDING PLANES

**Figure 4. 30** – Comparison among spacing distribution of the bedding planes of the outside landslide area (blu), the deposit area (red) and the sliding surface (green)

### 4.3.5 Jv and V(b)

The volumetric joint count, Jv, (Palmstrom, 1982) is a parameter for the quantification of discontinuity frequency in the rock masses. It is strictly connected to spacing measurements and is expressed as:

$$\frac{1}{S_1} + \frac{1}{S_2} + \frac{1}{S_3} + \dots + \frac{1}{S_n} + \frac{Nr}{5}$$

Where  $1/S_n$  are the joint frequencies of n sets and  $Nr/5$  is a parameter accounting for  $Nr$  random joints.

The Vb for the Vajont rock masses were evaluated through field measurements. Indeed it is often much quicker - and also more accurate - to have the block volume directly measured in the field (Palmstrom, 2001). The Jv distribution was evaluated for domains and lithology. This allowed to deepen the knowledge of the Vajont rock masses discontinuity condition.

**Tab 4. 5** – Jv mean values for each lithology in the 5a and 5b (outside the landslide) domains. Symbols refer to different formation outcropping. (chapter 2 paragraph 2.2)

Domain 5a	Jv mean	Dev.Stand.	Domain 5b	Jv mean	Dev.Stand.
general	29,4	17,4	general	51,2	23,5
f	41,4	25,2	f	48,2	==
e	25,4	14,2	e	53,6	32,9
d	24,4	==	d	34,7	11,1
c	29,4	==	c	39,8	4,65
a''	42,5	25,4	a	66,5	==
a'	16,4	5,64	ma	==	==
ma	22,4	==	do	89,6	==
do	22,2	6,3			

As it can be inferred from the above results, the Jv values of the 5b domain are always higher than the corresponding ones of the 5a domain: this is due to the fault systems characterizing the 5b domain. The same analysis performed on the deposit area provided the following results:

**Tab 4. 6** – Jv mean values for each lithology in 4 domain

Domain 4	Jv mean	Dev.Stand.
general	34,5	15,8
f	54,5	18,4
e	36,9	20,9
d	21,6	16,6



c	25,17	12,75
a''	38,95	8,33

The rock mass of sliding surface (divided into 3 domains) is made up by one lithology represented in tab 4.7:

**Tab 4. 7** – Jv mean values for the sliding surface domains made up Fonzaso formation

Domain	Jv mean	Dev.Stand.
3	34,6	16,2
2	29,8	==
1	==	==

### Block Volume(Vb)

When the individual blocks can be observed in a surface, their volumes can be directly measured from relevant sizes by selecting several representative blocks and measuring their average dimensions. For small blocks or fragments having volumes of  $\text{dm}^3$  or less, this method of block volume measurement is often beneficial as it is much easier to estimate the block size instead of the several measurements required to include all the joints (Palmstrom, 2001). The block size is expressed as:

$$Vb = S_1 * S_2 * S_3 * (\sin \gamma_1 * \sin \gamma_2 * \sin \gamma_3) \quad (1)$$

Where :

$S_1, S_2, S_3$  are the spacings between the joint sets;

$\gamma_1 \gamma_2 \gamma_3$  are the angle between the joint sets.

The angle measurement was obtained through the Palmstrom's spreadsheet, in which Jv is the input and Vb is the output parameter.

The results obtained provided an overview of the block mean size distributed in each domain (Tab 4. 8). In the 5a, the mean size is  $4.8 \text{ dm}^3$ , while in the 5b is  $0.9 \text{ dm}^3$  as expected.

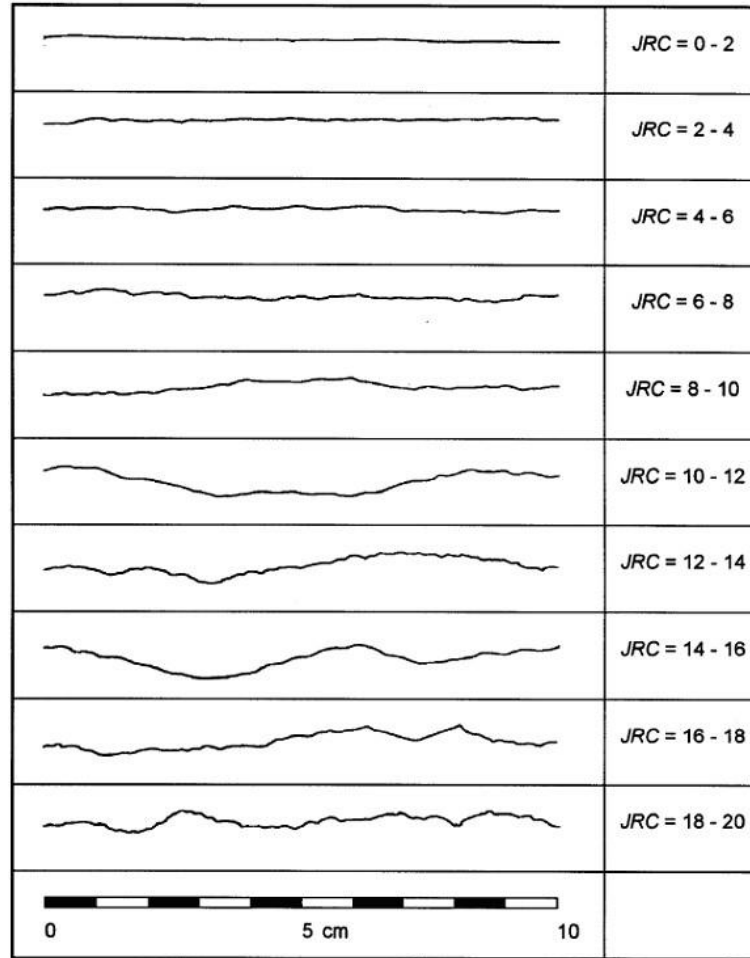
In the deposit area Vb is  $2.2 \text{ dm}^3$ . The rocks of sliding surface provided the following Vb values:  $3.0 \text{ dm}^3$  in domain 3 and  $1.4 \text{ dm}^3$  in domain 2. Domain 1 did not show any measurable block so consequently, it had not Vb value.

**Tab 4. 8** – Vb mean values distributed in each domain and lithology

<i>domain</i>	<i>lithology</i>	<i>Vb</i> <i>dm<sup>3</sup></i>		<i>domain</i>	<i>lithology</i>	<i>Vb</i> <i>dm<sup>3</sup></i>		<i>domain</i>	<i>lithology</i>	<i>Vb</i> <i>dm<sup>3</sup></i>
1	a'			5a	f	0,51	5b	f	0,32	
2	a'	1,49			e	2,17		e	0,23	
3	a'	0,87			d	2,48		d	0,86	
4	f	0,22			c	1,42		c	0,57	
	e	0,72			a''	0,47		a	0,12	
	d	3,57			a'	8,16		ma		
	c	2,28			ma	3,2		do	0,05	
	b			do	3,29					
a''	0,61									

#### 4.3.6 Discontinuity roughness -JRC (Joint Roughness Coefficient)

The roughness define the undulations and asperities on a natural joint surface and has a significant influence on its shear behavior. The description of the rock surface roughness is commonly quantified using the joint roughness coefficient (JRC). The traditional method of evaluating the JRC of a joint entails the comparison of discontinuity surface profile (ISRM, 1978) with a set of standard JRC profiles produced by Barton and Choubey (1977). The JRC value corresponds to the profile which most closely matches to the considered discontinuity surface.



**Figure 4. 31** - Roughness profiles and corresponding *JRC* values (Barton and Choubey, 1977).

Choubey (1977) incorporate the *JRC* into the discontinuity shear strength equation (2):

$$\tau = \sigma'_n \tan \left[ JRC \log_{10} \left( \frac{JCS}{\sigma_n} \right) + \phi_b \right] \quad (2)$$

where  $\sigma'_n$  is the effective normal stress, *JCS* is the wall compressive strength and  $\phi_b$  the basic friction angle. The basic friction angle ( $\phi_b$ ) could be identified through laboratory shear strength test or by bibliography.

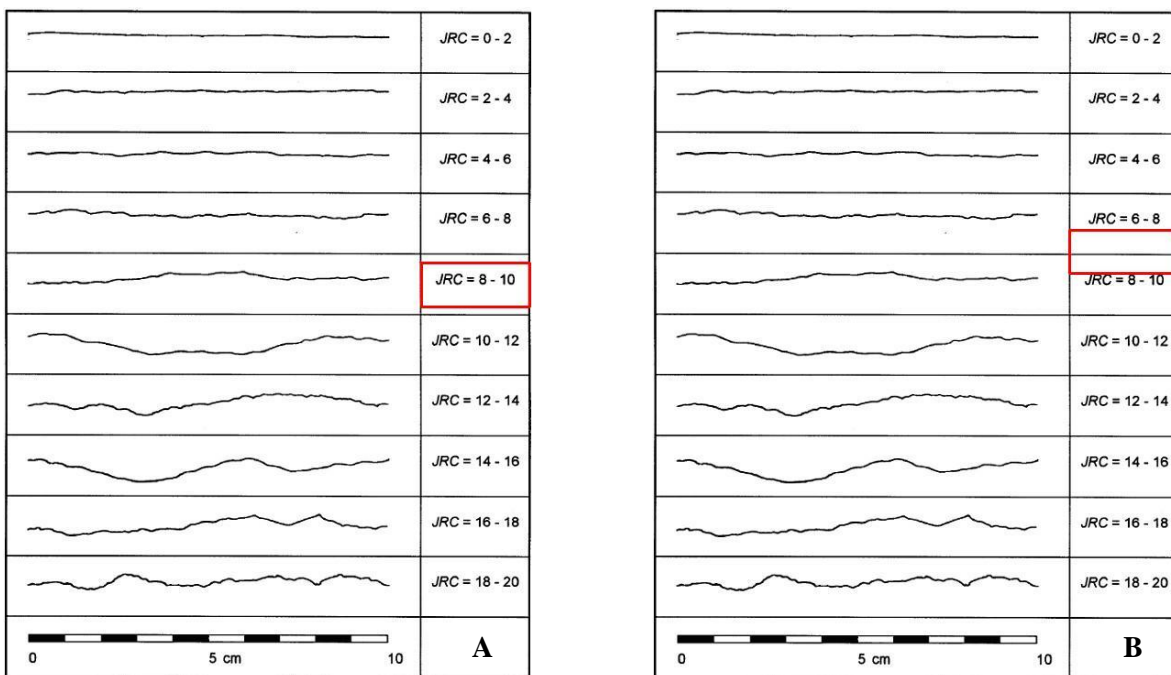
The roughness can be described at various observation scales. Curvature refers to surface irregularities with a wavelength greater than 100mm, while primary roughness, or waviness, represents surface irregularities with a wavelength smaller than 100mm. Secondary roughness, or unevenness, considers the scale of asperities and can be qualified as rough, smooth or slickensided.

Scale effect are more pronounced in the case of rough, undulating joint types, whereas they are virtually absent for planar joints. Moreover they are related to the changing stiffness of a rock mass as the block size or joint spacing increase or decrease (Bandis et al., 1981).

Recent works by Oppikoffer (2009), Wolter et al.(2011) has shown that discontinuity surface profiles of the secondary roughness can be easily obtained from laser scanning or digital photogrammetry 3D models.

The Joint Roughness coefficient (JRC) is probably the most commonly-used measure of the roughness of rock joint surfaces in current use, and forms an important part of the Barton-Bandis rock joint shear strength criterion (Beer et al., 2002).

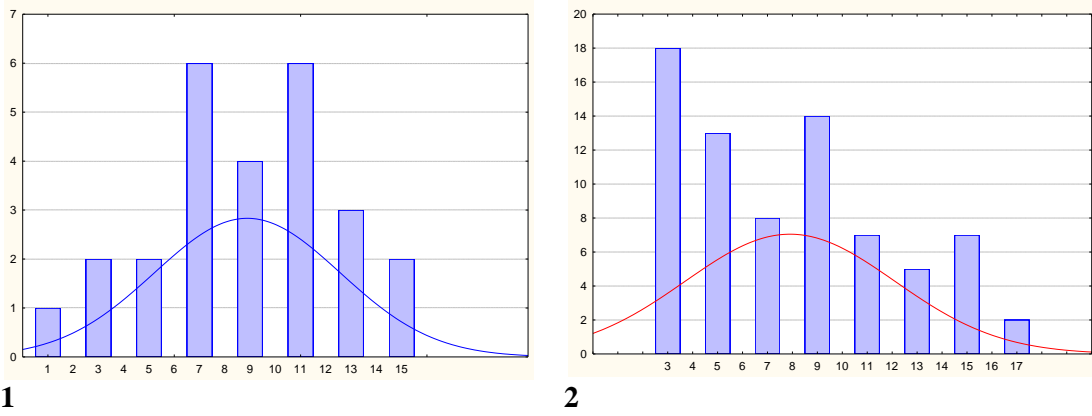
The JRC measurements have been performed on the discontinuity surfaces identified in the geomechanical stations crossed the scanlines. The JRC profile was executed along both the discontinuity surfaces' dip and dip strike (Figure 4.32).



**Figure 4.32** – Mean value (red box) of the JRC profiles detected along dip strike (A) and dip (B) of the study areas' discontinuity surface.

The values obtained along the dip of the discontinuity surface are higher than the corresponding ones of the dip direction, as showed in the histograms.

The JRC profiles have been obtained for each joint set belonging to different domains. The results were summarized in the table Tab 4. 9. It can be observed that the JRC values detected on the bedding planes are generally lower than all other discontinuity surfaces (Figure 4. 33) Therefore, the bedding plane could represent a preferential joint failure.



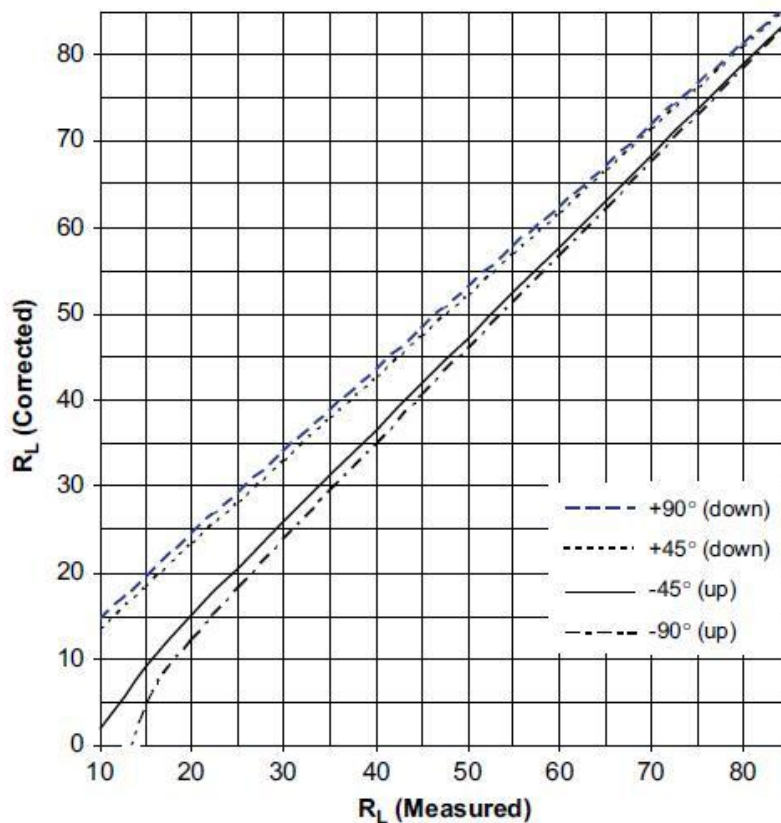
**Figure 4.33** – JRC mean values measured along the dip direction (1) and dip (2) of the discontinuity surfaces

**Tab 4.9** – JRC roughness values detected for each domain along the dip surface

domains	Bedding Plane	Joint set detected by Data Field (DIPS)	Dip directions	Dip
1	K2	K1	19	51
		K2	333	48
		K3	265	76
		K5	76	78
		K7	213	77
2	K2	K1	41	66
		K2	3	42
		K3	271	44
		K6	360	84
		K7	229	71
		K8	312	88
3	K4	K3	272	75
		K4	23	33
		K5	119	79
		K6	197	68
		K8	146	73
4		R	30	16
		K2	339	70
		K3	277	71
		K4	36	40
		K5	85	77
		K6	163	72
		K7	214	60
5		K1	14	47
		K2	349	57
		K3	269	71
		K4	40	39
		K6	174	60
		K7	211	76
		K8	134	90
		K0	87	19

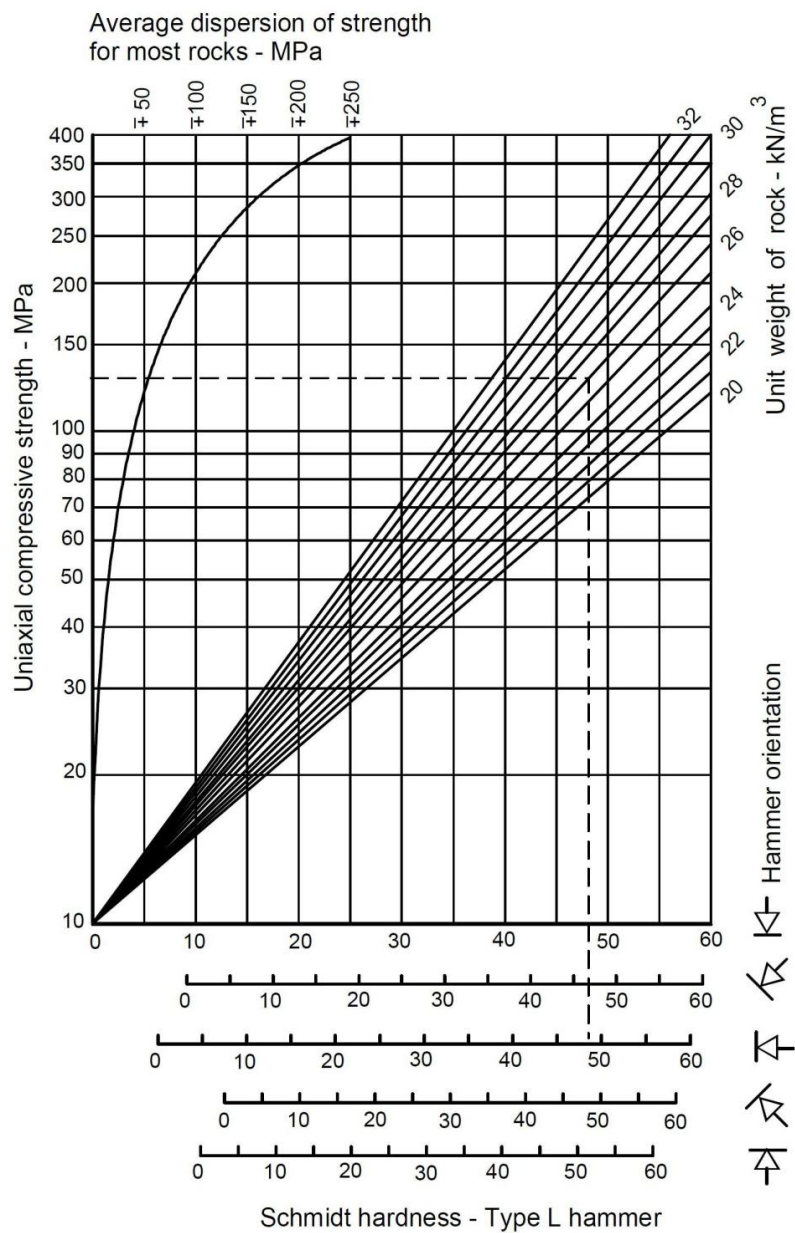
### 4.3.7 Joint Compressive Strenght (JCS)

The Joint wall Compressive Strenght is a fundamental parameter to identify the compressive shear strength of the discontinuity walls. It is determined by the Schmidt hammer, a useful tool to measure rock strength in field conditions. The use of the Schmidt rebound hammer for estimating joint wall compressive strength was proposed by Deere and Miller (1966). It measures the “rebound hardness” of the joint wall. The test mechanism is based on a spring-loaded mass that is released against a plunger when the hammer is pressed on the rock surface. The rebound distance of the plunger is read directly from a numerical scale. The Schmidt hammer allowed to measure rebound values on vertical, oblique and horizontal rock surface, but the surfaces irregularities influences the accuracy of the test. The specimens should be intact (free of visible cracks), petrographically uniform and representative of the rock mass domain being characterized (Aydin 2008).



**Figure 4. 34** - Normalization of rebound values obtained by L- N-type Schmidt hammer at selected angles (Positive and negative angles refer to the downward and upward positions of the SH, respectively. (Basu and Aydin, 2008)

It is necessary to obtain a sufficient large dataset of individual rebound values, which provide a significant numerical value of mean strength. The number of individual rebound is usually intuitive and arbitrary. A minimum number recommended by the earlier ISRM suggested method is 20 rebound values. In this thesis, minimum 40 rebound values from both intact and polished rock exposures has been obtained for each joint sets of the geomechanical station. The 10 lowest values resulting from natural surface (r) and polished (R) one are excluded. Therefore the remaining measures are used to the purpose of calculating uniaxial compressive strength. This one has been obtained both through the traditional abacus (Figure 4. 35) carrying out, on the basis of the rebound number (x), the shear strength (y).



**Figure 4. 35** – Traditional method to obtain the Uniaxial compressive strength from the Schmidt values rebound and different hammer orientations. The scale diagram is semi-logarithmic. (ISRM, 1978)

To the purpose of calculating the uniaxial compressive strength preliminary analysis was carried out through the ISRM diagram which allows the calculation of  $\sigma_c$  from the rebound values, based upon the inclination of the hammer and the density of the examined rock.

This method is quite elaborated. As second analysis certain empiric elaborations provided from various authors were used and compared in order to indentify the most suitable one for data interpolation:

- Miller (1965), whose  $\sigma_c$  value is linked to the rebound value and to the density of the rock through the relation:

$$\log \sigma_c = 0.00088\gamma r + 1.01 \quad 4)$$

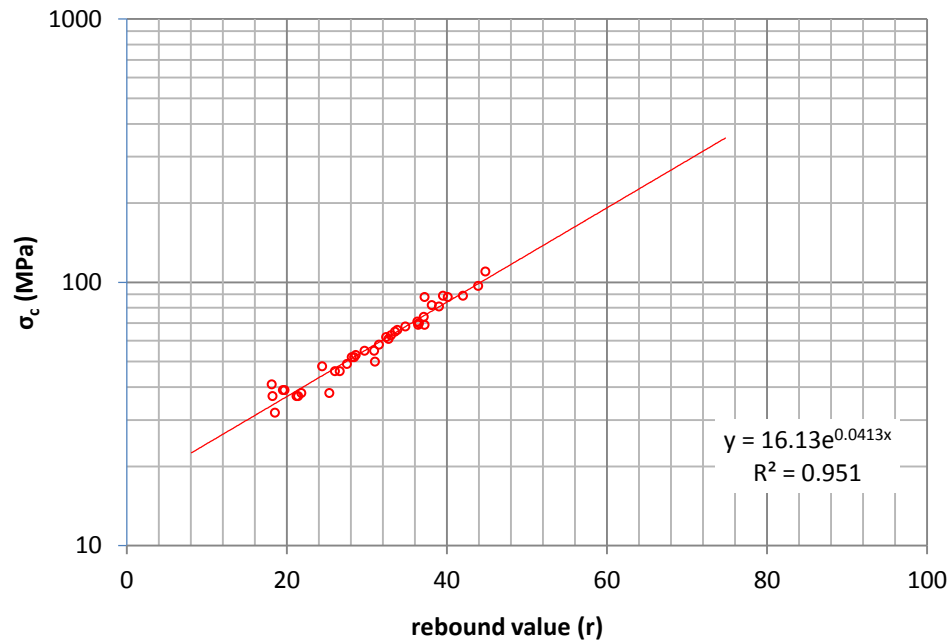
Where  $\gamma$  is expressed in  $\text{kN/m}^3$

- Irfan e Dearman (1978), who suggested a different relation, applicable to any litology

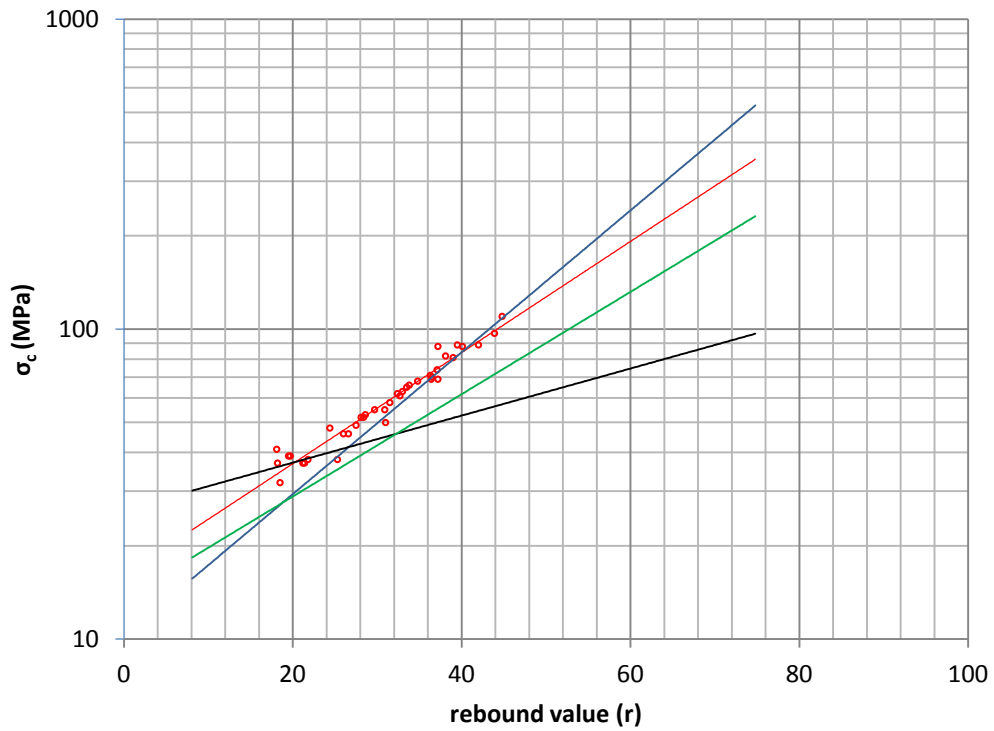
$$\sigma_c = 0.0775r + 21.03 \quad (5)$$

Calculating the  $\sigma_c$  values through the ( 3),( 4) (5) equations it was observed that the distribution of experimental data is closer to the trend proposed by Miller (1965), while Irfan and Dearman relation is the furthest from the experimental values (Fig. 4.36).





**Figure 4. 36** – Correlation between the rebound values obtained for the VJ1 geomechanic station’ joint sets and  $\sigma_c$  calculated through traditional diagram.



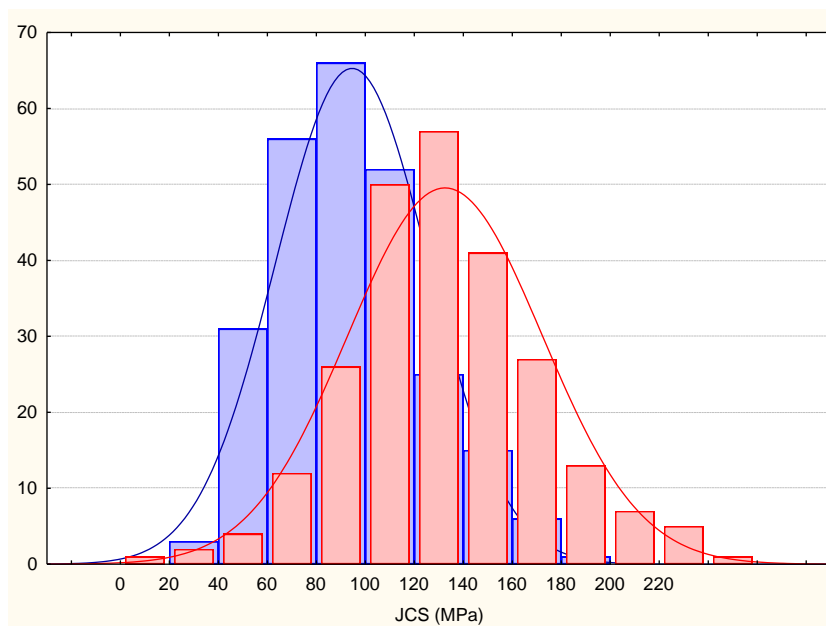
**Figure 4. 37** – Comparison between the  $\sigma_c$  values obtained by Deere and Muller abaqus (red circles) and than obtained from equations of: Miller (blu line), National Japanese Council (green line) and Irfan and Derman (black line). It can be noted as the Miller line better approximates experimental data..

The ISRM suggested a classification scheme related to the strength rock values:

$\sigma_c$ values (MPa)	DESCRIPTION	ISRM class
1-5	Very low	R1
5-25	low	R2
25-50	moderate	R3
50-100	medium	R4
100-250	high	R5
> 250	Very high	R6

The JCS analysis has been carried out in relation to the lithology more than of the domains, because this parameter is strictly connected to the rock properties. In the Figure 4. 38

were represented all the JCS values estimated both natural joint surface (r) and polished (R).



**Figure 4. 38** – Comparison between the rebound values on natural joint (blu) and polished joint (red) surface

It can be noted that the peak frequency and the mean values show a medium shear strength value for the natural joints and high values for the polished joints. The JCS on natural joint showed a mean value of 93.9 MPa and a standard deviation of 31.1 MPa; on the polished joint instead, the mean value is 131.7 MPa and standard deviation is 39.6 MPa. The same analysis on the bedding planes, highlights a similar trend: on the natural joint the mean value is 95 MPa and standard deviation of 34.8 MPa, instead the polished joint, is characterized by 128.3 MPa and 41.4 MPa mean value and standard deviation respectively. In the table Tab 4. 10 the JCS mean values and relative standard deviation have been illustrated for the different investigated lithology. The JCS values for each joint sets have been analyzed and represented in the Figure 4.39.

**Tab 4. 10** – JCS mean values lithology distribution for natural and polished joints

lithology		JCS (r) <i>MPa</i>	Standard deviation (r) <i>MPa</i>	JCS (R) <i>MPa</i>	Standard deviation (R) <i>MPa</i>
Soccher	f	91,2	25,8	113,4	29,3
	e	97,9	36,1	131,3	40,7
	d	93,5	23,8	138,6	35,7
	c	101,5	26,25	133,8	33,2
	a''	89,9	26,7	127,8	31,7
Fonzaso	a'	91,9	28,3	116	31
	ma	115,2	31,5	162,3	48,4
Vajont limestone		106,8	28,4	137,6	37,5

domains	Bedding Plane	Joint set detected by Data Field (DIPS)	Dip directions	Dip	JCS [MPa] giunto naturale
1	K2	K1	19	51	
		K2	333	48	
		K3	265	76	
		K5	76	78	
		K7	213	77	
2	K2	K1	41	66	
		K2	3	42	135,6
		K3	271	44	
		K6	360	84	51,8
		K7	229	71	109,5
3	K4	K8	312	88	
		K3	272	75	
		K4	23	33	143,3
		K5	119	79	
		K6	197	68	108,4
4		K8	146	73	
		R	30	16	
		K2	339	70	97,02
		K3	277	71	87,6
		K4	36	40	104,82
		K5	85	77	89,7
		K6	163	72	104,0
5		K7	214	60	112,0
		K1	14	47	
		K2	349	57	83,5
		K3	269	71	82,5
		K4	40	39	106,14
		K6	174	60	73,460
		K7	211	76	80,87
		K8	134	90	55,14
		K0	87	19	66,46

**Figure 4.39** – JCS values for each joint sets characterizing the study area

#### 4.4 Intact rock measurement- Point Load test

Point load testing is (Broch and Franklin 1972; ISRM 1985) used to determine rock strength index for intact rock samples.

Specimens in the form of rock cores, blocks, or irregular lumps with a test diameter from 30 to 85 mm can be tested by this method.

The apparatus for this test consists of a rigid frame, two point load platens, a hydraulically activated ram with pressure gauge and a device for measuring the distance between the loading points. The pressure gauge should be capable to read the failure pressure. Considering the irregular specimen geometries, the point load strength index is expressed by :

$$I_{s50} = I_s 0.138 \frac{P}{(D \times W)^{0.75}} \quad (5)$$

Where P = force required to break the specimen (kN), D = distance between the platen contact points, and W= equivalent core diameter (mm).

The results give a measure of the tensile strength of the rock. The relationship between UCS and the point load strength could be expressed as:

$$\sigma_c = K \times I_{s50} \quad (6)$$

Where K is the "conversion factor." Many authors suggested different values of K related to rock type investigated. Table 1 summarizes some K values proposed by different authors:

The K-value used and considered more suitable is 24 as suggested by standards ISRM (Tab 4. 11).

**Tab 4. 11** – Different K-values suggested by different authors.

author	K	Palmstrom I <sub>s</sub> (MPa)	K
Franklin (1972)	16	1,8 – 3,5	14
Brock & Franklin (1972)	24	3,5 – 6	16
ISRM (1985)	20 – 25	6 – 10	20
Gosh & Srivastava (1991)	16	> 10	25

The point load test has been performed on samples belonging to every lithology investigated. The tests were performed perpendicularly and parallel to rock stratification. The results were summarized in the table below.

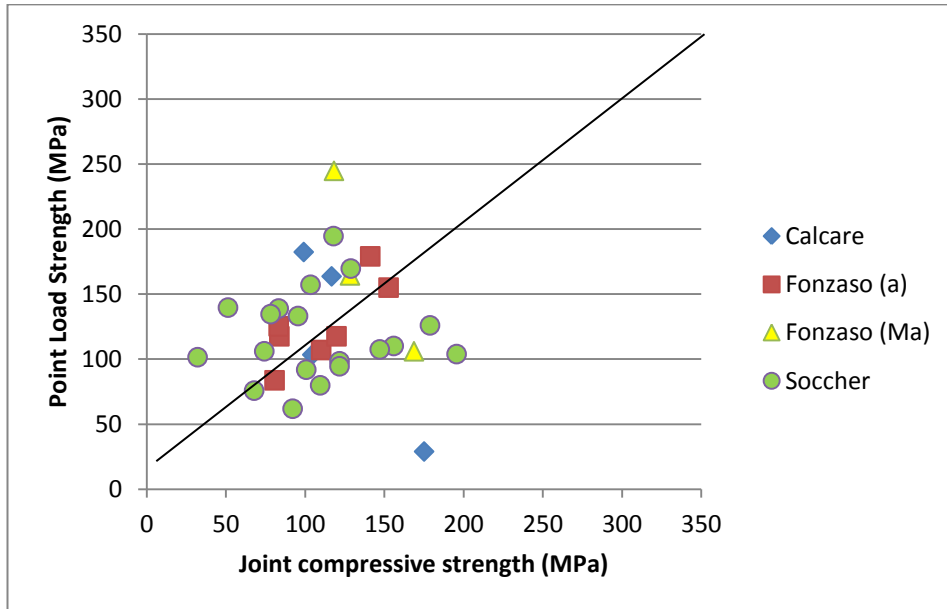
**Tab 4. 12** -  $Is_{50}$  and  $\sigma_c$  values obtained from Point Load test. The lithology abbreviation are referred to Semenza and Rossi (1965) legend.

lithology	Sample orientation /stratification P = parallel O = orthogonal	$Is_{50}$	Standard deviation	$\sigma_c$
		<i>MPa</i>		<i>MPa</i> ( <i>k=24</i> )
cs	O	3,2	1,3	76,8
	P	2,48	1,9	59,52
f	O	4,98	2,3	119,52
	P	5,82	-	139,68
e	O	4	1,2	96
	P	3,8	1,4	91,2
d	O	4,48	1,7	107,52
	P	7,2	3,6	172,8
c	O	4	1,6	96
	P	6,32	5,1	151,68
a''	P	4,05	-	97,2
	O	4,7	1,9	112,8
a'	P	5,35	0,7	128,4
	O	2,02	0,3	48,48
a	O	4,5	1,2	108
	P	5,37	0,4	128,88
ma	O	6,5	3,9	156
	P	6,8	1,9	163,2
do	P	3,22	2	77,3
	O	6,2	1,7	148,8

The obtained results of 103 tests did not show any particular trend because of the insufficient data. It could be interesting to observe a comparison between the Schmidt hammer and point load data, obtained on polished joint. Moreover the analysis has been focused on the bedding plane and perpendicularly to the specimen stratification .

The estimated values of compressive strength with point load were plotted against the values of compressive strength measured with schmidt hammer (Figure 4. 40). The results show For the Fonzaso formation (a) the data points fall closer to the line. This suggest an exact

correlation between the two methods in the estimation of compressive strength . Whereas, for Fonzaso (ma) and Vajont limestone the data result more scattered suggesting a weak correlation. The data points of the Soccher formation show the best correlation at low to medium strength values but become in considerable variability at higher strength.



**Figure 4. 40** - Correlation between Point Load Strength and Joint Compressive Strength

**Tab 4. 13** – Comparison between the uniaxial compressive strength obtained from Schmidt hammer and point load tests

lithology	JCS <i>MPa</i>	$\sigma_c$ from Point Load <i>MPa</i>
<b>cs</b>	83	76.8
<b>f</b>	113.4	119.5
<b>e</b>	131.3	96
<b>d</b>	138.6	107.5
<b>c</b>	133.8	96
<b>a''</b>	127.8	112.8
<b>a'</b>	116	48.5
<b>a</b>		108
<b>ma</b>	162.3	156
<b>do</b>	137.6	148.8

## 4.5 Rock mass classification systems

### 4.5.1 GSI system

Rock mass strength and deformability are controlled by both the intact rock properties, and geometric and mechanical discontinuity properties.

To characterize and evaluate the rock mass and the rock mass properties, many classification systems such as RQD, Rock Mass Rating, Q and Geological Strength Index have been developed. The geological strength index (GSI) (Hoek and Brown 1997) is the only classification system that is directly linked to engineering parameters such as Mohr-Coloumb, Hoek-Brown strength parameters (Cai et al., 2004). This system has been developed both for hard and weak rock masses. It provide an evaluation of the rock mass quality, in terms of interlocking of rock pieces and discontinuity surfaces, through a numerical value.

The GSI values are obtained from a chart in which descriptive geological terms and measurable field parameters such as joint spacing and joint roughness are linked ( Figure 4. 41). Block volume is estimated based on joint set orientation, spacing and persistence.

The main advantage of GSI is to evaluate very quickly the reduction in rock mass strength for different geological conditions through field observation.

$$\sigma_1 = \sigma_3 + \sigma_c * \left( m_i * \frac{\sigma_3}{\sigma_c} + 1 \right)^{\alpha_{0,5}} \quad (7)$$

Parameters  $m_i$ ,  $s$  and  $\alpha$  are rock material constants can be conducted using the Geological Strength Index (GSI). Moreover, the geological character of rock material, together with the visual assessment of the mass, is used as a direct input to the selection of parameters relevant for the prediction of rock-mass strength and deformability.

The GSI is directly used in the evaluation of the rock mass strength by the Hoek-Brown empirical failure criterion (Hoek et al.,2002):



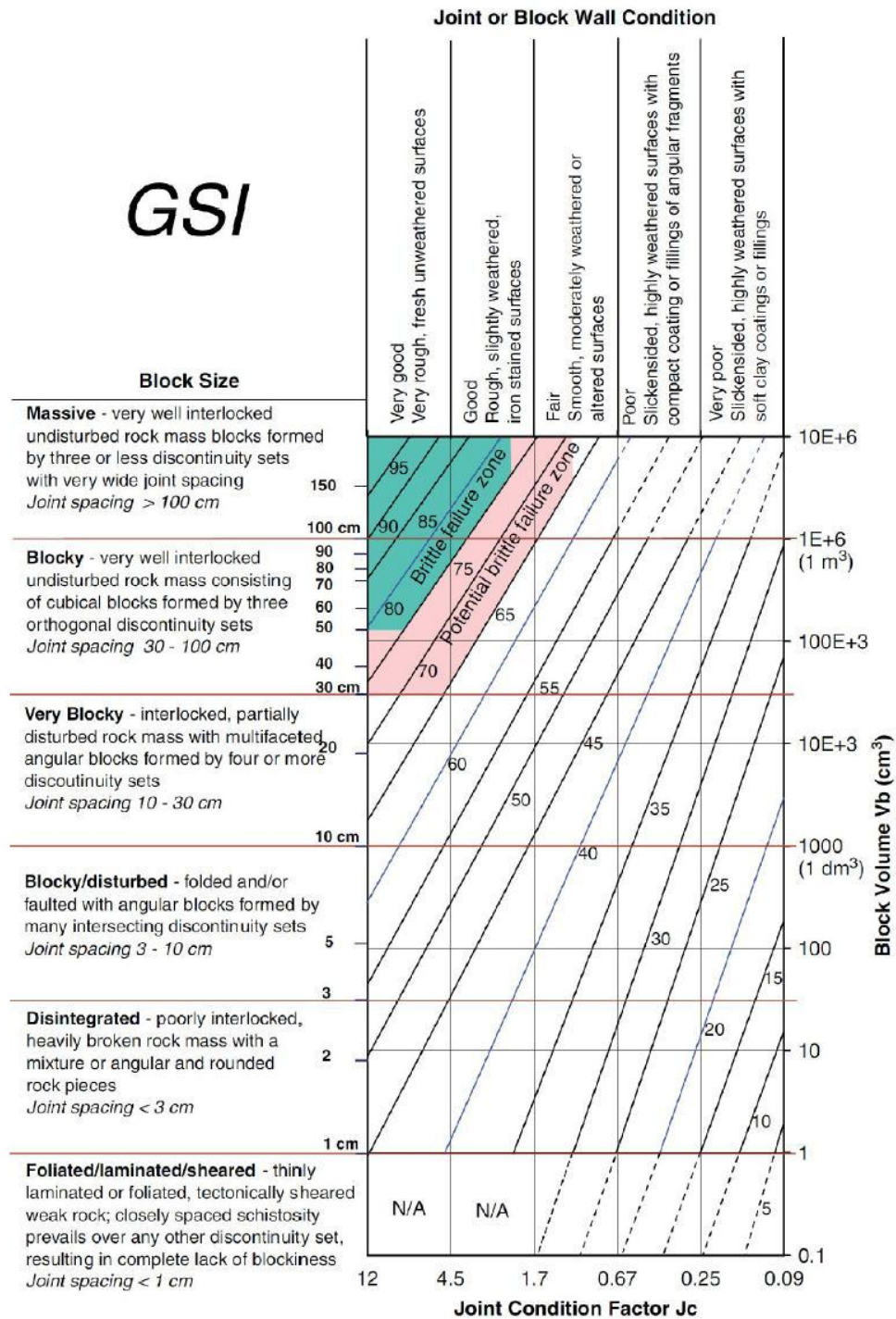


Figure 4. 41 - Quantification of the GSI chart (Cai et al., 2004).

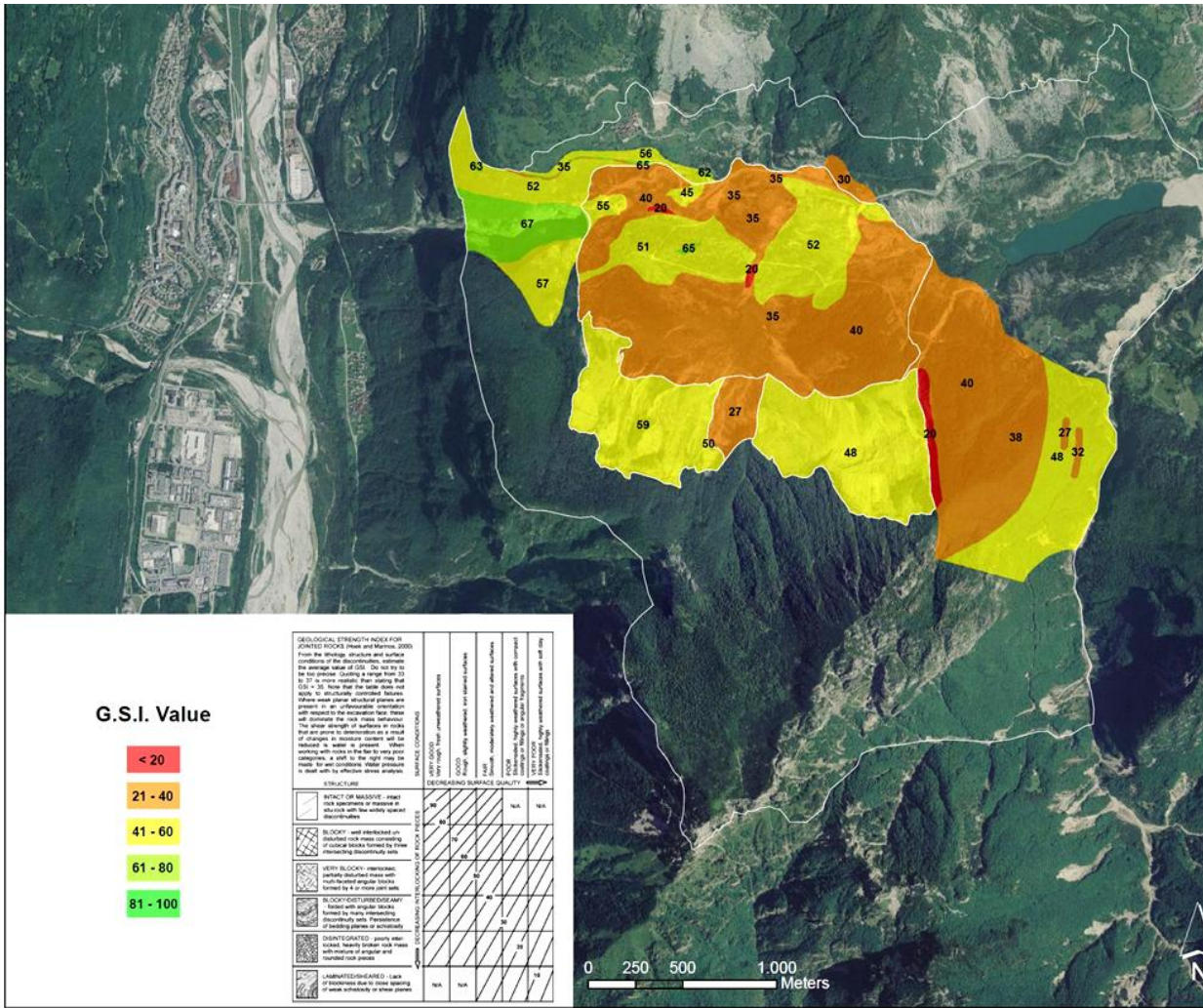


Figure 4.42 – GSI distribution for each structural domain.

The GSI evaluation for the Vajont study area has been performed in relation to the rock masses joint conditions for each structural domain (Figure 4.42).

The GSI distribution shows a range of values comprised between 25 in correspondence of the areas subjected to a more structural control (Massalezza area) and 70 outside the landslide in the Vajont limestone rock masses. The mean value is 48 and the distribution is also represented by the histogram (Figure 4.43).

The data distribution in the Figure 4.44 highlighted as in general, the parameter variability is more influenced by very blocky to blocky disturbed rock masses with good joint surface conditions (Figure 4.44).

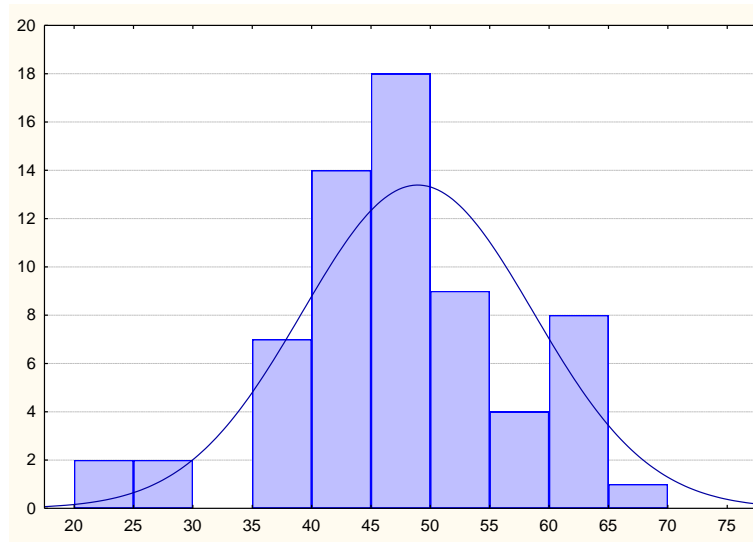


Figure 4. 43 – Distribution histogram of the study area GSI values

GSI

Pick GSI Value		SURFACE CONDITIONS				
Rock Type:	General	VERY GOOD	GOOD	FAIR	POOR	VERY POOR
GSI Selection:	5	DECREASING SURFACE QUALITY →				
STRUCTURE		DECREASING INTERLOCKING OF ROCK PIECES ↓				
	INTACT OR MASSIVE - intact rock specimens or massive in situ rock with few widely spaced discontinuities	90	80	70	N/A	N/A
	BLOCKY - well interlocked undisturbed rock mass consisting of cubical blocks formed by three intersecting discontinuity sets	70	60	50	40	30
	VERY BLOCKY- interlocked, partially disturbed mass with multi-faceted angular blocks formed by 4 or more joint sets	50	40	30	20	10
	BLOCKY/DISTURBED/SEAMY - folded with angular blocks formed by many intersecting discontinuity sets. Persistence of bedding planes or schistosity	N/A	N/A	N/A	N/A	10
	DISINTEGRATED - poorly interlocked, heavily broken rock mass with mixture of angular and rounded rock pieces	N/A	N/A	N/A	N/A	10
	LAMINATED/SHEARED - Lack of blockiness due to close spacing of weak schistosity or shear planes	N/A	N/A	N/A	N/A	10

A

Pick GSI Value		SURFACE CONDITIONS				
Rock Type:	General	VERY GOOD	GOOD	FAIR	POOR	VERY POOR
GSI Selection:	5	DECREASING SURFACE QUALITY →				
STRUCTURE		DECREASING INTERLOCKING OF ROCK PIECES ↓				
	INTACT OR MASSIVE - intact rock specimens or massive in situ rock with few widely spaced discontinuities	90	80	70	N/A	N/A
	BLOCKY - well interlocked undisturbed rock mass consisting of cubical blocks formed by three intersecting discontinuity sets	70	60	50	40	30
	VERY BLOCKY- interlocked, partially disturbed mass with multi-faceted angular blocks formed by 4 or more joint sets	50	40	30	20	10
	BLOCKY/DISTURBED/SEAMY - folded with angular blocks formed by many intersecting discontinuity sets. Persistence of bedding planes or schistosity	N/A	N/A	N/A	N/A	10
	DISINTEGRATED - poorly interlocked, heavily broken rock mass with mixture of angular and rounded rock pieces	N/A	N/A	N/A	N/A	10
	LAMINATED/SHEARED - Lack of blockiness due to close spacing of weak schistosity or shear planes	N/A	N/A	N/A	N/A	10

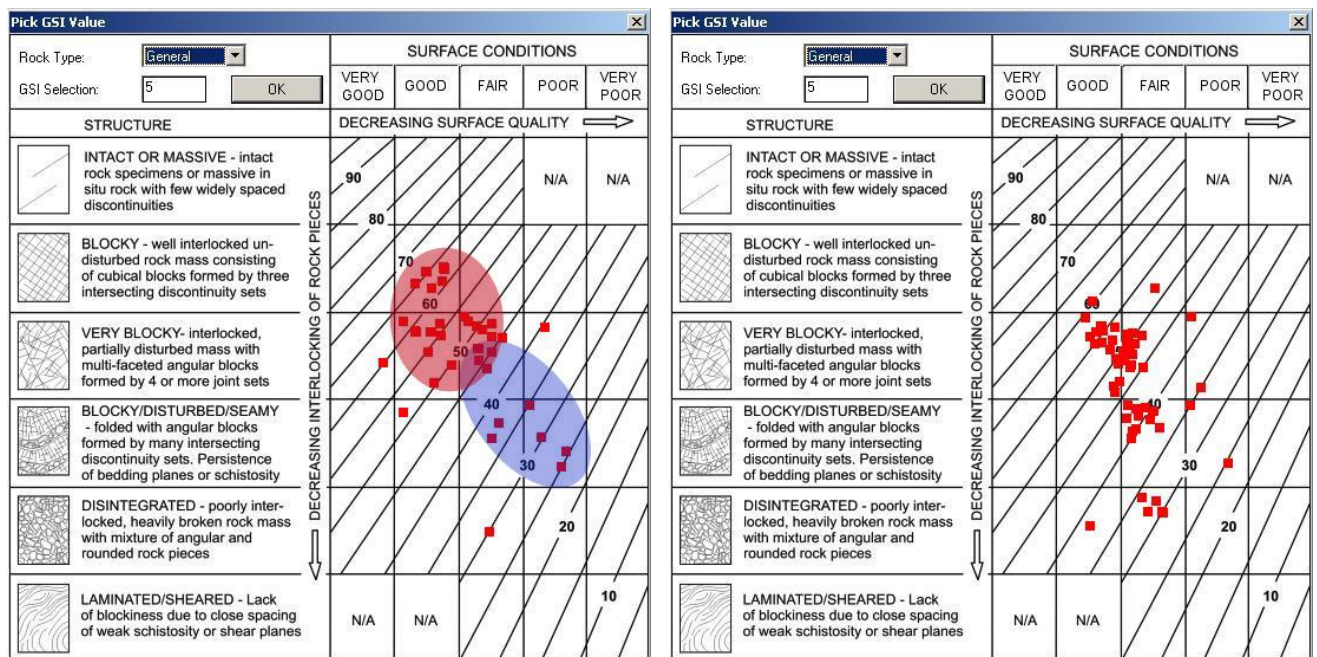
B

Figure 4. 44 – A-Range definition adopted for evaluating GSI distribution. B GSI distribution in the whole study area

In addition, it can be observed that the GSI distribution for each domain is very variable, in agreement with the different structural setting of the area.

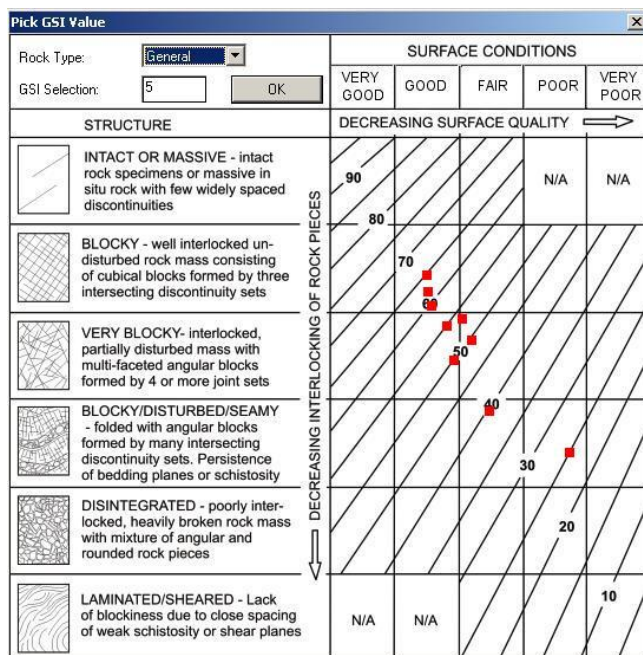
Indeed, the 5a and 5b areas outside the landslide ( Figure 4. 45 A-B)

analyzed showed a clear difference of GSI values distribution: the area 5a is characterized by horizontal strata not disturbed by relevant tectonic structures and represented by a red circle in the diagram; the 5b area falls within the northern flank of the Erto syncline, a disturbed structural setting (blue circle in the diagram). In the deposit area the GSI distribution showed a rock mass condition varying between the very blocky and blocky disturbed and fair-poor joint surface conditions. As regards the sliding surface the GSI chart revealed a fair values variability due to different morpho-structural condition characterizing the area (Figure 4. 45 C )



A

B



C

**Figure 4. 45** – GSI distribution in different domain of the study area: A GSI values distribution outside the landslide: 5a (red circle), 5b (blue circle). B GSI values distribution in the deposit area. C: GSI values distribution on the sliding surface.

## 4.5.2 Rock mass classification. RQD, RMRb, SRM

### 4.5.2.1.RQD

The amount of data collected were used to define the rock mass quality through different classification methods developed by Deer, Bieniawski and Romana. To determine the rock mass quality, these methods used different input parameters.

The rock quality designation (RQD) is a standard parameter in drill core logging (Deere, 1963). It is defined as the percentage of the intact core pieces longer than 100 mm to the total length of core. It provide a basis for making preliminary design decisions involving estimation of required depths of excavation for foundations of structures. The RQD values also can serve to identify rock outcropping quality and is expressed by:

$$RQD = \frac{\sum L_c}{L_t} * 100 \quad (8)$$

Where  $L_c$  is the sum of length of core pieces longer than 100mm and  $L_t$  is the total length of core.

The relation is solely validly applicable for  $J_v$  values lower than 35, as for values higher than this threshold it would provide negative RQD values. Given that the data collected in the area of study show  $J_v$  values higher than 35, the Priest and Hudson relation was applied. The RQD value can be calculated from outcrops through the  $J_v$  value evaluated in the field and through the joint density (Priest and Hudson, 1981) . In the first case the RQD is expressed by:

$$RQD = 115 - 3,3 * J_v \quad (9)$$

Where  $J_v$  is the fractures number per volume  $m^3$

In the second one:

$$RQD = (100e^{-N\lambda}) * (N\lambda + 1) \quad (10)$$

Where  $\lambda$  is the discontinuity frequency , N is the lenght of the line.

The results were reported and summarized in Tab 4. 18 and enclosed at the end of the chapter.

#### 4.5.2.2 RMR

The RMR classification, developed by Beniaowski in the 1976. RMR has become a standard for use in tunnels and many professionals apply it to describe any rock mass. ORR (1996) has given a good overview of the RMR use in slopes. ROMANA (1985, 1993, 1995) proposed new addenda to RMR concept, especially suited for slopes. The main feature of this classify method is to determine a numerical index that allows to identify the quality rock mass class. The rock mass is classified in five classes.

<b>RMR</b>	100-81	80-61	60-41	40-21	$\leq 20$
<b>Class</b>	I	II	III	IV	V
<b>description</b>	<b>Very good</b>	<b>good</b>	<b>Fair</b>	<b>Poor</b>	<b>Very poor</b>

The RMR<sub>b</sub> (Beniaowski) needs to evaluate of 5 coefficients (Tab. 4.14)

$$RMR_b = A1 + A2 + A3 + A4 + A5 \quad (11)$$

The RMR<sub>c</sub> (Romana) instead, is evaluated through the identification of 6 parameters:

$$RMR_c = A1 + A2 + A3 + A4 + A5 + A6 \quad (12)$$

The results of this classification have been summarized in the tables enclosed at the end of the chapter.

**Tab 4. 14** – Rock Mass rating system (after Beniaowski 1989)

Parameter	Range Values						
$\sigma_c$ (MPa)	>250	100-250	50-100	25-50	5-25	1-5	<1
Coefficient <b>A1</b>	<b>15</b>	<b>12</b>	<b>7</b>	<b>4</b>	<b>2</b>	<b>1</b>	<b>0</b>
RQD (%)	90-100	75-90	50-75	25-50	<25		
Coefficient <b>A2</b>	<b>20</b>	<b>17</b>	<b>13</b>	<b>8</b>	<b>3</b>		
Discontinuity spacing (cm)	>200	60-200	20-60	6-20	<6		
Coefficient <b>A3</b>	<b>20</b>	<b>15</b>	<b>10</b>	<b>8</b>	<b>5</b>		
Joint condition	<i>Very rough surfaces</i>  <i>Not continuous</i>  <i>No separation</i>  <i>Unweathered wall rock</i>	<i>Slightly rough surfaces</i>  <i>Separation &lt; 1 mm</i>  <i>Slightly weathered walls</i>	<i>Slightly rough surfaces</i>  <i>Separation &lt; 1 mm</i>  <i>Highly weathered walls</i>	<i>Slickensided surfaces</i>  <i>or Gouge &lt; 5 mm thick</i>  <i>or Separation 1-5 mm</i>  <i>Continuous</i>	<i>Soft gouge &gt;5 mm thick</i>  <i>or Separation &gt; 5 mm</i>  <i>Continuous</i>  <i>Rating 30 25 20 10 0</i>		
coefficient <b>A4</b>	<b>30</b>	<b>25</b>	<b>20</b>	<b>10</b>	<b>0</b>		
Rock condition	<i>Completely dry</i>	<i>Damp</i>	<i>Wet</i>	<i>Dripping</i>	<i>Flowing</i>		
coefficient <b>A5</b>	<b>15</b>	<b>10</b>	<b>7</b>	<b>4</b>	<b>0</b>		



**Tab 4. 15** - Values to dermine the coefficient A4 in the Beniaowski RMR classification

<b>Persistence</b>	<b>V1</b>	<b>Note</b>
< 1	6	
1 – 3	4	
3 – 10	2	
10 – 20	1	
> 20	0	
<b>Aperture</b>	<b>V2</b>	
none	6	
< 0,1	5	
0,1 – 1	4	
1 – 5	1	
> 5	0	
<b>Roughness</b>	<b>V3</b>	
Very rough	6	JRC 10 – 8
rough	5	JRC 8 – 6
Slightly rough	3	JRC 6 – 4
smooth	1	JRC 4- 2
slickensided	0	JRC 0
<b>wethering</b>	<b>V4</b>	
Unweathered	6	
Slightly wethered	5	
Moderately whetered	3	
Highly wethered	1	
Decomposed	0	

The parameters of  $c$ , and  $\phi$  have been calculated by

$$c = 5 * RMR_b \quad (13)$$

$$\phi = 0,5 * RMR_b + 5 \quad (14)$$

Furthermore the modulus of deformation (GPa) has been calculated (Beniaswki, 1978) . The static modulus of deformation is among the parameters that best represent the mechanical behaviour of a rock and a rock mass. Therefore it is a cornerstone of many geomechanical analyses. It is expressed by

$$E_d = 2 * RMR_b - 100 \quad (15)$$

This relation is valid only for RMR b values higher than 50. For values lower than 50 it is more appropriate the relation suggested by Serafim e Pereira in 1983

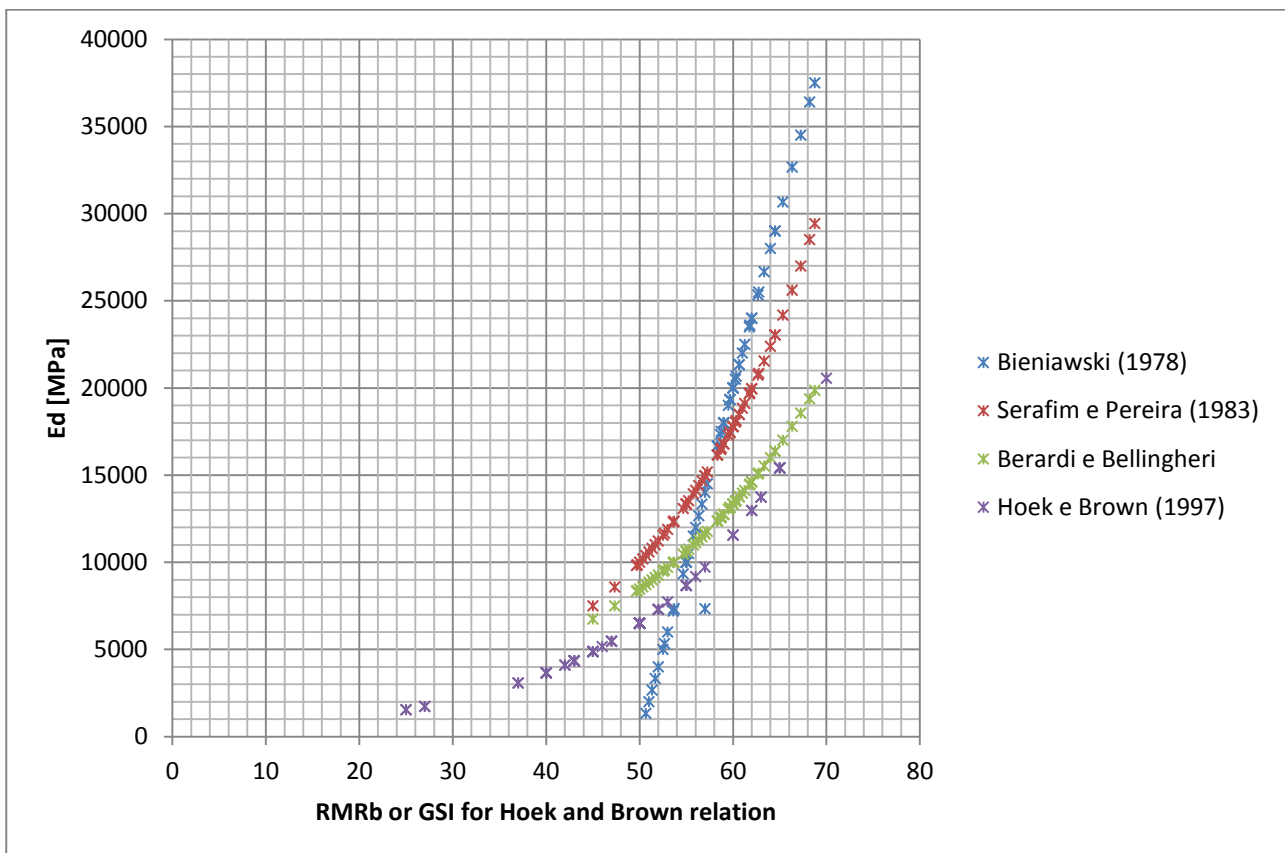
$$E_d = 10^{\left(\frac{RMR_b - 10}{40}\right)} \quad (16)$$

$$E_d = 0,87e^{0,0455 * RMR_b} \quad (17)$$

and Hoek and Brown (1997), in which a D factor related to rock mass disturbance compares.

$$E_d = \left(1 - \frac{D}{2}\right) * 10^{\left(\frac{GSI - 10}{40}\right)} \quad (18)$$

The figure 4.46 resumes the rock mass modulus of deformation measured through the different authors methods:



**Figure 4. 46** – Comparison among relations, suggested by different authors, to identify the rock mass modulus of ddeformation .

The results obtained in terms of cohesion, friction angle and modulus of deformability revealed that: the friction angle varies from 29° to 41° with a mean value of about 35,°. the cohesion shows values from 0.15 MPa to 0.33MPa, the rock mass parameters obtained are reported in the table 4.16.

**Tab 4. 16** – Rock mass parameter in relation to aerial domains and lithology formations

<i>domain</i>	<i>lithology</i>	$\Phi$	<i>c</i> <i>MPa</i>	<i>E (Mpa) Bieniawski</i>	<i>E (Mpa) Serafim Pereira</i>
1	a'	==	==	==	==
2	a'	32	0,15	7083	12277
3	a'	36	0,17	22500	18836
4	f	32	0,27	10666	13754
	e	34	0,28	20439	17538
	d	34	0,27	22665	17765
	c	33	0,25	14151	15572
	b	==	==	==	==
	a''	36	0,32	26666	21833
5a	f	33	0,16	10500	13528
	e	34	0,29	23422	16988
	d	33	0,28	10667	13335
	c	35	0,3	20667	17782
	a''	37	0,28	29222	23297
	a'	33	0,16	11500	13923
	ma	35	0,23	23833	20480
	do	38	0,18	31966	25922
5b	f	==	==	==	==
	e	37	0,32	28000	22387
	d	33	0,26	11200	14125
	c	36	0,17	22500	1883633
	a''	34	0,17	16666	16155
	ma	==	==	==	==
	do	35	0,18	2000	17782

### 4.5.2.3 SMR

The SMR (Slope Mass Rating) classification was introduced by ROMANA (1985) obtained from Bieniawski's Rock mass Rating by subtracting adjustment factors for the joint-slope relationships and method of excavation (Tab 4. 17). SRM introduces four adjusting factor which allow a simple estimation of RMR correction factors:

$$RM = RMR_b - |(F1 \cdot F2 \cdot F3)| + F4 \quad (19)$$

**Tab 4. 17 -** Values adjustment factors for different joint orientations

condition	very good	good	fair	poor	very poor
dip dir S- dip dir J	$30^\circ < \alpha < 330^\circ$	$20^\circ < \alpha \leq 30^\circ$ $330^\circ \leq \alpha < 340^\circ$	$10^\circ < \alpha \leq 20^\circ$ $340^\circ \leq \alpha < 350^\circ$	$5^\circ < \alpha \leq 10^\circ$ $350^\circ \leq \alpha < 355^\circ$	$0^\circ < \alpha \leq 5^\circ$ $355^\circ \leq \alpha < 360^\circ$
<i>Index F1</i>	<b>0.15</b>	<b>0.4</b>	<b>0.7</b>	<b>0.85</b>	<b>1</b>
Dip J	$\beta < 20^\circ$	$20^\circ < \beta < 30^\circ$	$30^\circ < \beta < 35^\circ$	$35^\circ < \beta < 45^\circ$	$\beta > 45^\circ$
<i>Index F2</i>	<b>0.15</b>	<b>0.4</b>	<b>0.7</b>	<b>0.85</b>	<b>1</b>
dip S-dip J	$\Delta < -10^\circ$	$-10^\circ < \Delta < 0^\circ$	$\Delta = 0^\circ$	$0^\circ < \Delta < 10^\circ$	$\Delta \geq 10^\circ$
<i>Index F3</i>	<b>0</b>	<b>6</b>	<b>25</b>	<b>50</b>	<b>60</b>
	Natural slope	Pre splitting	Smooth blasting	Reg. blasing	Blasting errato
<i>Index F4</i>	<b>15</b>	<b>10</b>	<b>8</b>	<b>0</b>	<b>-8</b>

The results obtained define the adjustment factors F1, F2 and F3. F4 has been considered 15. The table enclosed at the end of the chapter resumed the values obtained by the 3 rock mass classifications :RQD, RMRb and SMR

**Tab 4. 18** Comparison among different rock mass classifying systems

<i>domain</i>	<i>lithology</i>	<i>RQD</i> <i>mean</i>	<i>Rock mass</i> <i>quality</i>	<i>RMRb</i> <i>mean</i>	<i>Rock mass</i> <i>quality</i>	<i>SMR</i> <i>mean</i>	<i>Rock mass Quality</i>
1	a''	==	==	==	==	==	
2	a''	45	Poor	53,5	fair	68	Very good
3	a''	51	fair	61	good	64	Very good
4	f	50	fair	55,5	fair	68	Very good
	e	54	fair	60,2	fair	69	Very good
	d	56	fair	58,5	fair	68	Very good
	c	47	poor	52,4	fair	69	Very good
	b	==	==				
	a''	61	fair	63,5	good	79	Very good
5a	f	27	Poor	55	fair	69	Very good
	e	57,5	fair	61,6	fair	71	Very good
	d	==	==	==	==		
	c	53	fair	60	fair	68	Very good
	a''	68	fair	64,5	good	76	Very good
	a'	52	fair	56	fair	64	Very good
	ma	67	fair	62	good	73	Very good
	do	68	fair	66	good	72	Very good
5b	f	==	==	==	==		
	e	64	fair	64	good	49	fair
	d	53	fair	56	fair	59	fair
	c	28	poor	61	good	76	Very good
	a	34	fair	61,5	good	68	Very good
	ma	==	==				
	do	23	Very poor	60	good	68	Very good

**THE TABLE RESUMING THE GEOMECHANICAL RESULTS IS REPOTED IN  
THE FOLLOWING**

STOP	area	Lithology	N. Joint sets	Sets	mean attitude		spacing mean [cm]	JRC	JCS mean [Mpa] natural surface	JCS mean [Mpa] polished surface	IS <sub>50</sub>	Point Load [Mpa]	SRM	RMR <sub>b</sub>	φ	c (Mpa)	E (Mpa) Bieniawski	E (Mpa) Serafim Pereira	C (Kg/cm <sup>2</sup> )	Rock mass classification based on SMR	G.S.I. (analytical)	G.S.I. (subjective)
					Dip_dir	Dip																
VJ001	outside the landslide	e : Socchère formation	5	BP	60	15	5.0	3	178.8	184.6	5.3	126	71	62	36°	0.18	23600	19724	1.83	GOOD	57	47
					310	90	8.9		110.7	124.3												
					240	80		2	133.1	133.8												
					350	35	26.3		78.2	71.1												
					200	90	7.1	8	59.8	68.9												
VJ002	outside the landslide	a": Socchère formation	4	BP	90	20	10.0	4	141.1	148.7	7.5	179.04	79	66	38°	0.33	31000	25119	3.34	GOOD	61	62
					230	70	6.5	9	65.4	126.2												
					190	85	21.5	5	88.7	141.1												
					300	85	11.6	4	63.3	102.3												
VJ003	outside the landslide	a": Fonzaso formation	4	BP	30	30	6.5	2	59.77	82.84	4.90	117.6	72	64	37°	0.32	28000	22387	3.20	GOOD	59	40
					185	80	3.8	3	83.74	108.40												
					230	60	7.9	2	43.80	72.60												
					140	80	13.1	4	72.6	89.2												
VJ004	deposit area	e:Socchère formation	4	BP	180	25		6	103.4	125.6	6.55	157.2	64	63	36°	0.31	25500	21135	3.20	FAIR	58	52
					10	75		8	82.4	138.4												
					315	80	14.8	5	78.2	124.3												
					248	85	9.4	8	75.0	108.4												
VJ005	outside the landslide	e:Socchère formation	3	BP	32	50	6	6	63.3		3.2	75.84	44	64	37°	0.32	28000	22387	3.26	FAIR	59	50
					210	40	7.3	8	61.8													
					120	70	13.3	8	67.8													
VJ006	outside the landslide	cs: scaglia rossa	4	BP	30	40	7.3	6	43.3				43	65	37°	0.32	29000	23041	3.29	FAIR	60	50
					255	50	17	7	46.0													
					300	70	16.6	10	50.1													
					180	70	20.7	8	47.3													
VJ007	deposit area	e:Socchère formation	3	BP	150	30	5.6	7	58.2				55	60	35°	0.30	19333	17445	3.04	FAIR	59	40
					250	90	6.6	8	64.3													
					10	60	7	8														
VJ008	outside the landslide	cs: scaglia rossa	4	BP	30	30	10.6	3	94.0	119.8			78	66	38°	0.33	31500	25119	3.35	GOOD	61	45
					220	90	11.6	5	61.4	84.6												
					290	60	8.7	2	43.6	57.9												
					170	90	3.8	9	47.2	65.3												
VJ009	outside the landslide	do: Vajont limestone	5	BP	50	30	17.5	3	90.6	138.1	4.3	103.44	85	71	41°	0.20	42400	33497	2.07	VERY GOOD	66	50
					245	60	13.1	3	83.3	117.3												
					260	5	7.3	3	104.5	123.0												
					190	90	19.1	5	77.4	117.9												
					310	55	5.7	5	104.5	119.8												
VJ010	outside the landslide	do: Vajont limestone	4	BP	70	20	5.2	4	77.0	112.4	6.8	163.68	76	67	39°	0.19	34500	26993	1.97	GOOD	62	42
					110	90	17.5	3	116.7	147.1												
					275	75	9.4	3	100.7	138.1												
					215	80	6.8	4	82.9	107.8												
VJ011	outside the landslide	f: Socchère formation	4	BP	80	10	3.9	6	128.8	128.90	7.1	169.68	69	55	33°	0.16	10500	13529	1.66	GOOD	50	62
					220	90	5.3	4	102.84	138.90												
					130	90	3.4	5	122.36	143.30												
					190	85	3.2	6	119.18	135.24												

STOP	area	Lithology	N. Joint sets	Sets	mean attitude		spacing mean [cm]	JRC	JCS mean [Mpa] natural surface	JCS mean [Mpa] polished surface	I <sub>S50</sub>	Point Load [Mpa]	SRM	RMR <sub>b</sub>	φ	c (Mpa)	E (Mpa) Bieniawski	E (Mpa) Serafim Pereira	C (Kg/cm <sup>2</sup> )	Rock mass classification based on SMR	G.S.I. (analytical)	G.S.I. (subjective)
					Dip_dir	Dip																
VJ012	outside the landslide	a: Fonzaso formation			200	50	4.0	4			5.2	123.6										
					120	80	5.5	7														
					10	55	2.9	8														
VJ013	outside the landslide	do: Vajont limestone	4	BP	180	50	3.7	4	78.61	114.90	7.6	182.4	68	60	35°	0.18	20000	17783	1.78	GOOD	55	47
					150	90	4.0	2	99.11	132.40												
					75	75	2.0	6	95.52	84.60												
					25	60	4.5	3														
VJ014	outside the landslide	a":Fonzaso formation	3	BP	10	50	3.3	6	101.8	133.8	4.5	107.04	64	58	34°	0.17	16667	16156	1.74	GOOD	53	52
					190	30	3.2	7	91.6	113.7												
					120	75	3.2	5	110.1	133.8												
VJ015	outside the landslide	c: Socchèr formation	4	BP	20	50	2.3		98.07	144.80	3.8	91.92	76	61	36°	0.18	22500	18836	1.82	GOOD	56	45
					220	60	4.0		100.69	147.90												
					200	80	8.5		97.05	144.10												
					125	80	2.6		59.77	81.10												
VJ017	deposit area	c: Socchèr formation	3	BP	120	30	4.4		32.1		4.2	101.52	63	51	30°	0.15	1333	10391	1.55	GOOD	46	25
					310	70	6.4				3.0	72.96										
					270	90	5.18															
VJ018	deposit area	d: Socchèr formation	4	BP	130	30	2.43		51.3		5.0	120	61	50	30°	0.15		9857	1.52	GOOD	45	25
					320	80	5.67															
					230	90	4.31				5.8	139.68										
					350	80	3.96															
VJ019	deposit area	e:Socchèr formation	3	BP	340	90	4.7	6	88.7	109.5			76	62	36°	0.18	24000	19953	1.84	GOOD	57	60
					220	12	8.8	3	121.7	135.2	4.1	98.4										
					80	90	6.3	8	71.8	115.4	2.7	65.76										
VJ020	outside the landslide	ma: Fonzaso formation	4	BP	160	20	13.4	3	118.8	144.5	10.2	244.8	69	61	36°	0.18	22500	19110	1.82	GOOD	56	57
					255	70	3.7	5	109.2	125.2												
					184	90	8.6	7	117.0	155.9												
					30	20	9.4	3	150.2	182.6												
VJ021	deposit area	c: Socchèr formation	3	BP	200	30	7.1	7	92.1	135.2	2.6	61.92	75	60	35°	0.18	20667	17783	1.79	GOOD	55	50
					190	90	8.1	6	72.6	90.6												
					60	80	6.0	5	58.2	88.7												
VJ022	deposit area	c: Socchèr formation	4	BP	55	20	6.2	5	155.9	208.3	1.5	36.72	85	70	40°	0.20	40000	31623	2.04	VERY GOOD	65	45
					155	75	5.9	5	115.5	143.3	4.6	110.16										
					280	65	8.3	6	86.9	120.4												
					210	80	11.1	8	129.0	165.2												
VJ023	sliding surface	a":Fonzaso formation	3	BP	0	45	7.1		152.67	172.33	5.92	142.08	70	55	33°	0.16	10667	13335	1.67	GOOD	50	27
					340	90	7.3		99.64	119.18	6.46	155.04										
					45	80	5.7		110.71	148.70												
VJ024	outside the landslide	a":Fonzaso formation	3	BP	115	15	5.2	8	49.70	105.03	5.22	125.28	78	64	37°	0.19	28667	22387	1.89	GOOD	59	63
					240	80	11.2	9	83.30	166.97												
					340	90	31.3	7	71.12	125.63	4.95	118.8										
VJ025	outside the landslide	a': Fonzaso formation	4	BP	97	40	4.1	5	84.2	133.8	3.1	74.4	64	56	33°	0.16	11500	13924	1.68	GOOD	59	46
					0	75	4.9	5	119.8	153.5	4.9	117.6										
					275	70	6.6	7	99.6	133.8												
					225	75	13.2	8	84.2	118.6												

DOC. 2 (continued)



STOP	area	Lithology	N. Joint sets	Sets	mean attitude		spacing mean [cm]	JRC	JCS mean [Mpa] natural surface	JCS mean [Mpa] polished surface	IS <sub>50</sub>	Point Load [Mpa]	SRM	RMR <sub>b</sub>	φ	c (Mpa)	E (Mpa) Bieniawski	E (Mpa) Serafim Pereira	C (Kg/cm <sup>2</sup> )	Rock mass classification based on SMR	G.S.I. (analytical)	G.S.I. (subjective)
					Dip_dir	Dip																
VJ026	sliding surface	a': Fonzaso formation	4	BP	30	30	3.4	8	143.31	147.92			66	61	36°	0.18	22500	18836	1.82	GOOD	56	65
					200	65	8.3	10	108.40	147.14												
					160	90	7.7	8	70.37	125.63												
					220	65	6.6	7	66.76	102.30												
VJ027	sliding surface	a': Fonzaso formation	4	BP	360	35	4.7		118.6	112.5			66	52	31°	0.15	3500	11220	1.57	GOOD	47	50
					225	80	4.3		109.5	113.1												
					180	75	3.7		51.8	49.7												
					115	85	5.1		135.2	136.7												
VJ028	outside the landslide	ma: Fonzaso formation	3	BP	80	25	18.4	7	168.7	215.0	2.4	58.56	77	65	38°	0.19	30667	24173	1.92	GOOD	60	65
					310	80	11.2	4	144.1	218.4		0										
					215	85	7.9	5	150.3	227.8	4.4	106.08										
VJ029	outside the landslide	do: Vajont limestone	4	BP	14	76	5.5	4	135.2	193.5			54	60	35°	0.17	19000	17278	1.77	FAIR	55	70
					102	60	8.1	7	154.3	188.5												
					225	40	10.2	8	137.4	178.8												
					90	20	9.5	4	175.1	224.3	1.2	29.04										
VJ030	outside the landslide	cs: scaglia rossa	4	BP	90	15	8.0	2	141.1	207.2	4.5	107.04	73	60	35°	0.17	19333	17445	1.78	GOOD	65	63
					161	80	6.6	6	151.1	212.8												
					225	85	5.8	5	119.8	187.5												
MG002	outside the landslide	a":Socchèr formation	3	BP	6	38	7.5	3	80.7	95.5	3.5	83.76	72	65	38°	0.33	30000	23714	3.31	GOOD	60	43
					270	80	5.1	7	71.1	168.7												
					126	75	11.6	7	40.7	145.6												
MG003	outside the landslide	b: conglomerate Fonzaso formation	3	BP	44	32	7.5	4	74.2	105.1			75	65	38°	0.33	30000	23714	3.31	GOOD	60	43
					145	75	11.6	7	79.0	156.7												
					270	45	5	9	45.7	82.4												
MG004	outside the landslide	d: Socchèr formation	5	BP	28	50	3.8	3	102.8	178.0			64	56	33°	0.27	11200	14125	2.85	GOOD	51	27
					153	30	11.2	5	103.9	136.6												
					280	76	7.3	3	92.6	165.2												
					84	68	6.6	2	91.6	163.5												
					336	60	5.3	5	113.1	191.5												
MG007	outside the landslide	ma: Fonzaso formation	4	BP	74	21	3.6	2	64.68	89.70	4.75	114	70	59	34°	0.29	17000	16788	2.98	GOOD	54	55
					184	84	9.4	1	75.76	117.90	6.85	164.4										
					230	85	9.7	4	108.40	178.81												
					312	80	7.3	5	128.30	170.53												
MG008	outside the landslide	ma: Fonzaso formation	3	BP	120	45	6.2	5	60.1	108.4			71	64	36°	0.32	27333	22387	3.25	GOOD	59	53
					212	74	4.8	2	108.4	158.4												
					150	70	6.7	1	123.0	241.4												
MG009	Isolate hill	d: Socchèr formation	4		115	65	10.2	8	117.9	174.2			53	59	39°	0.29	17500	16788	3.00	FAIR	50	40
					2	48	10.1	9	89.7	158.4												
					314	40	11.9	10	68.9	100.7	4.7	113.76										
					65	68		9	85.1	128.3	8.1	194.64										

STOP	area	Lithology	N. Joint sets	Sets	mean attitude		spacing mean [cm]	JRC	JCS mean [Mpa] natural surface	JCS mean [Mpa] polished surface	IS <sub>50</sub>	Point Load [Mpa]	SRM	RMR <sub>b</sub>	φ	C (Mpa)	E (Mpa) Bieniawski	E (Mpa) Serafim Pereira	C (Kg/cm <sup>2</sup> )	Rock mass classification based on SMR	G.S.I. (analytical)	G.S.I. (subjective)
					Dip_dir	Dip																
MG011	colle isolato	c: Socchèr formation	3	BP	326	40	6.4	3	109.5	158.4	3.3	79.92	67	60	35°	0.30	20000	17783	3.06	GOOD	55	45
					76	60	7.4	3	103.9	115.5												
					208	72	8.1	5	74.2	139.6	3.1	75.12										
MG012	outside the landslide	e:Socchèr formation	3		86	12	8.1	3	57.6	106.1			76	62	36°	0.31	24667	19953	3.18	GOOD	57	52
					202	85	7.3	2	77.4	136.7												
					140	86	5.1	4	108.4	170.5												
MG015	outside the landslide	cs: scaglia rossa	3	BP	155	17	6.0	2	71.9	86.0			66	52	31°	0.26	3333	11007	2.63	GOOD	47	
					115	90	6.0	7	50.8	74.2												
					42	60	3.2	10	21.4	31.9												
MG016	deposit area	e:Socchèr formation	3	BP	241	24	2.6	6	65.4	89.7			59	49	30°	0.25		9441	2.50	DISCRETO	44	55
					62	76	4.7	7	79.0	125.6												
					334	80	4.7	10	42.9	61.4												
MG017	outside the landslide	e:Socchèr formation	3	BP	75	25	4.1	5	60.1	106.1			67	61	36°	0.31	22000	18836	3.11	GOOD	56	56
					150	78	5.5	8	77.4	131.0												
					200	70	10.8	9	99.6	131.0												
MG018	outside the landslide	d: Socchèr formation	3	BP	55	20	1.7		35.3	42.0			63	55	33°	0.28	10667	13335	2.82	FAIR	50	50
					190	70	5.7		71.1	101.8												
					302	85	6.4		77.4	106.1												
MG019	outside the landslide	c: cSocchèr formation	3	BP	20	25	6.8	5	93.5	101.8	3.2	77.76	68	60	35°	0.30	20667	17783	3.08	GOOD	55	65
					230	60	6.6	4	65.4	125.6												
					325	80	5.6	3	121.7	128.3	3.9	94.56										
MG020	outside the landslide	b: conglomerate Fonzasò formation	3	BP	86	21	6.3	8	79.0	161.8			68	57	34°	0.29	14000	14962	2.91	GOOD	52	40
					302	78	5.4	8	59.1	80.7												
					356	84	7.0	5	84.2	158.4												
MG026	deposit area	c: Socchèr formation	3	BP	17	14	5.9	3	95.5	107.3	4.2	101.52	65	52	31°	0.26	2667	11220	2.62	GOOD	47	42
					76	72	5.1	7	95.5	107.3												
					265	86	3.6	6	54.1	88.7	5.6	133.2										
MG027	deposit area	e:Socchèr formation	3	BP	16	41	4.3	8	71.9	96.5	3.3	79.68	61	53	32°	0.27	6667	11885	2.72	FAIR	48	43
					240	42	4.6	8	74.2	10.7												
					138	65	5.0	7	68.9	114.3	4.4	106.08										
MG028	deposit area	f:Socchèr formation	3		15	50	3.8	4	83.3	90.6	2.5	59.76	64	53	31°	0.26	5333	11659	2.69	GOOD	48	43
					140	62	5.9	5	69.6	96.5												
					262	84	6.8	6	58.8	83.3	5.8	138.96										
MG029	deposit area	c: Socchèr formation	3		335	75	5.6	6	77.4	131.0			73	62	36°	0.31	23000	19953	3.14	GOOD	57	50
					240	80	7.4	8	78.2	94.5	4.1	98.4										
					72	30	25				5.6	134.64										
MG030	deposit area	c: Socchèr formation	3	BP	168	20	5.0	3	135.2	151.9			72	58	34°	0.29	16667	15849	2.97	GOOD	53	50
					15	80	5.4	8	94.5	102.8												
					274	88	4.3	10	74.2	94.5												
MG031	deposit area	c: Socchèr formation	3	BP	173	30	6.8	9	96.5	129.6	6.4	153.12	63	58	34°	0.29	16000	15849	2.96	GOOD	53	55
					70	81	9.0	7	102.8	125.6	17.6	421.68										
					322	50	6.8	9	106.1	158.4												

STOP	area	Lithology	N. Joint sets	Sets	mean attitude		spacing mean [cm]	JRC	JCS mean [Mpa] natural surface	JCS mean [Mpa] polished surface	I <sub>S50</sub>	Point Load [Mpa]	SRM	RMR <sub>b</sub>	φ	c (Mpa)	E (Mpa) Bieniawski	E (Mpa) Serafim Pereira	C (Kg/cm <sup>2</sup> )	Rock mass classification based on SMR	G.S.I. (analytical)	G.S.I. (subjective)
					Dip_dir	Dip																
MG032	deposit area	d: Socchèr formation	3	BP	30	20	18.7	5	88.7	138.1			78	65	37°	0.32	29331	23714	3.30	GOOD	60	50
					180	78	5.9	7	73.4	131.0												
					244	70	49.7	8	93.5	131.0												
MG033	deposit area	c: Socchèr formation	3	BP	330	30	4.2	2	82.4	100.7			66	54	32°	0.27	7333	12589	2.74	GOOD	49	50
					220	72	5.3	7	75.0	98.6												
					130	60	3.0	9	85.1	110.7												
MG034	deposit area	c: Socchèr formation	3	BP	130	49	3.3	3	136.7	153.5			57	48	29°	0.24		8913	2.46	FAIR	43	37
					240	72	3.9	4	92.6	117.9												
					354	60	3.7	10	86.9	120.4												
MG037	deposit area	e:micriti selcifere (calcare Socchèr)	3	BP	32	22	5.2	2	62.0	81.6			73	58	34°	0.29	16666	15849	2.97	GOOD	53	50
					220	68	14.8	5	91.6	103.8												
					292	86	10.3	4	80.7	116.7												
MG038	deposit area	e:Socchèr formation	3	BP	155	60	5.4	8	119.2	131.4			74	60	35°	0.30	20667	18127	3.08	GOOD	55	50
					60	70	6.7	5	101.8	172.3												
					240	80	7.6	4	121.7	161.8												
MG039	deposit area	e:Socchèr formation	3	BP	220	56	6.4	3	87.8	98.6			70	64	37°	0.32	28667	22387	3.28	GOOD	59	50
					102	50	8.1	9	80.7	128.3												
					320	62	6.6	6	92.6	120.4												
MG041	deposit area	d: Socchèr formation	3	BP	350	40	5.0	5	81.6	119.2			65	53	32°	0.27	6000	11885	2.70	GOOD	48	45
					187	40	8.0	8	106.1	168.7												
					100	74	2.0	5	71.1	124.3												
MG042	deposit area	e:Socchèr formation	4	BP	346	18	4.9	2	96.5	148.7			79	64	37°	0.32	28000	22387	3.26	GOOD	59	47
					195	75	6.0	3	82.4	141.1												
					240	85	6.6	9	99.6	129.6												
					145	65	5.9	4	102.8	144.1												
MG043	deposit area	c: Socchèr formation	3	BP	150	10	7.3	2	89.7	163.5			68	53	31°	0.26	2000	11885	2.60	GOOD	46	40
					138	88	4.8	8	133.8	199.7												
					218	86	5.2	3	142.6	187.5												
MG044	deposit area	e:Socchèr formation	3	BP	200	15	6.2	2	172.3	179.8			69	60	35°	0.30	20000	17783	3.06	GOOD	55	37
					78	78	7.3	4	172.3	191.5												
					344	72	7.9	3	172.3	221.9												
MG045	deposit area	d: Socchèr formation	3	BP	160	15	11.3	2	115.5	133.8	4.5	107.52	39	66	38°	0.33	32667	25606	3.38	POOR	61	
					244	84	17.7	4	147.1	183.6	3.4	81.84										
					20	63	7.9	5	129.7	172.3												
MG046	deposit area	a":Fonzaso formation	3	BP	340	36	5.6	5	115.5	155.1			77	62	35°	0.31	23333	19953	3.14	GOOD	57	52
					146	70	9.3	4	98.6	125.6												
					223	76	15.0	5	113.1	165.2												

DOC. 5 (continued)

STOP	area	Lithology	N. Joint sets	Sets	mean attitude		spacing mean [cm]	JRC	JCS mean [Mpa] natural surface	JCS mean [Mpa] polished surface	I <sub>S50</sub>	Point Load [Mpa]	SRM	RMR <sub>b</sub>	φ	c (Mpa)	E (Mpa) Bieniawski	E (Mpa) Serafim Pereira	c (Kg/cm <sup>2</sup> )	Rock mass classification based on SMR	G.S.I. (analytical)	G.S.I. (subjective)
					Dip_dir	Dip																
MG047	deposit area	a":Fonzaso formation	3	BP	134	30	2.7	3	89.7	119.2			80	65	38°	0.33	30000	23714	3.31	GOOD	60	43
					270	70	2.0	7	119.2	158.4												
					338	60	9.3	4	108.4	167.0												
MG048	deposit area	e:Socchèr formation	3	BP	22	10	7.4	5	120.4	183.6	4.3	103.92	69	55	33°	0.28	10000	13335	2.80	GOOD	50	50
					182	84	2.0	3	195.6	212.8												
					254	88	9.3	4	155.1	183.6	4.2	101.52										
MG049	deposit area	c: Socchèr formation	3	BP	100	20			151.9	185.5												
					184	78			145.6	204.0												
					268	72			139.6	160.1												
MG050	deposit area	e:Socchèr formation	3	BP	160	15	6.2	2	127.0	156.7			77	63	36°	0.31	25333	20733	3.20	GOOD	58	65
					226	84	14.6	3	136.7	174.2												
					320	72	11.3	7	139.6	172.3												
MG051	deposit area	f: Socchèr formation	3	BP	174	4	6.0	3	72.6	150.3			72	58	33°	0.29	16000	15849	2.96	GOOD	53	45
					356	82	6.6	5	89.7	106.1												
					60	84	7.1	5	54.6	62.7												
MG052	deposit area	c: Socchèr formation	3	BP	30	16	3.9	3	97.6	127.0			72	57	33°	0.28	10000	14962	2.80	GOOD	52	43
					245	78	6.0	4	116.7	151.9												
					160	78	5.5	5	131.0	179.8												
MG053	deposit area	b: conglomerate Fonzaso formation	3	BP	158	28	3.8	4	81.6	148.7			70	58	34°	0.29	16667	15849	2.97	GOOD	53	55
					290	76	4.9	5	107.3	141.1												
					0	80	5.7	9	125.6	153.5												
MG054	deposit area	c: Socchèr formation	3	BP	65	20	15.2	4	87.8	127.0			64	58	34°	0	16000	15849	3	GOOD	53	60
					200	40	3.6	5	90.6	138.1												
					160	78		6	127.0	147.1												

## **5 - LABORATORY TEST**

### **5.1 Introduction**

Rock strength and elastic constants such as Young's modulus and Poisson's ratio are required for modeling triggering and propagation of landslides. Such properties can be obtained by static or dynamic methods. Static methods refer to laboratory tests where the rock material is gradually loaded in uniaxial, biaxial (conventional triaxial) or triaxial compression up to failure, axial and lateral strains being measured as function of applied stress. The static constants are representative of the in-situ stress conditions and hence are used for elastic modeling. In the case of Vajont landslide, much experimental work was performed on the mechanical properties of the Vajont clays (Ferri et al., 2011 and references therein), which represent interbedded clay-rich layers within the Fonzaso Formation which presumably played a key role in the evolution of the landslide. However, a complete mechanical characterization of the rock sequence involved in the Vajont movement is still lacking. For such reason, uniaxial and triaxial experiments were performed on samples collected from the stratigraphic units involved in the 1963 rockslide: the Socchèr Formation, the Fonzaso Formation and the Vajont Limestone.

### **5.2 Experimental Apparatus**

The uniaxial and triaxial experiments were performed at the Rock Mechanics Laboratory at the Department of Geosciences at the University of Padova which is equipped with the automatic systems ADVANTEST9 and SERCOMP7 (CONTROLS Italia, s.r.l.) (Fig. 5.1). The ADVANTEST9 system controls the vertical load applied to the sample, while the SERCOMP7 system is used to apply the confining pressure by means of an Hoek cell.

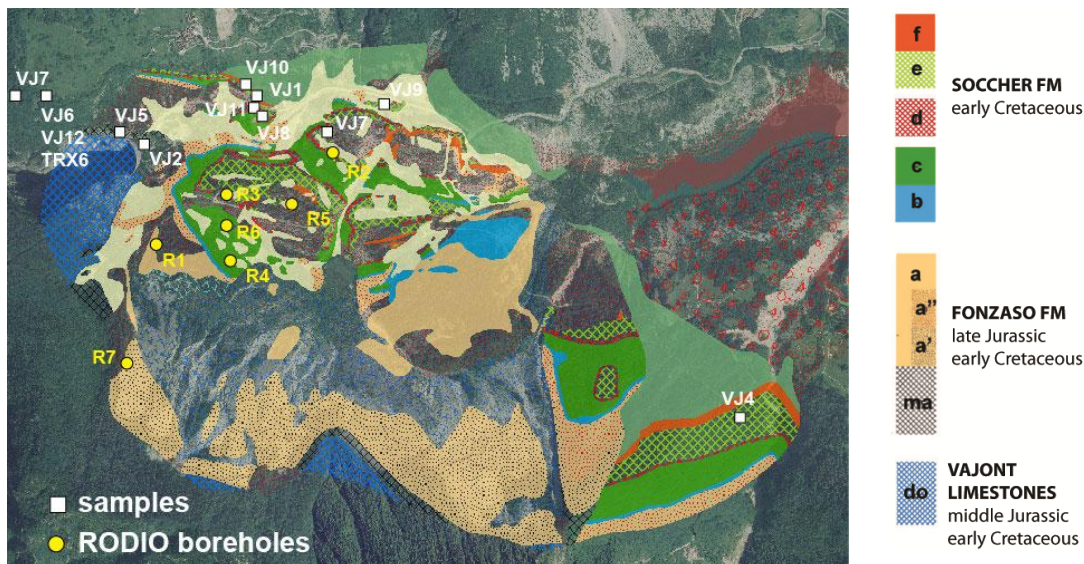


**Figure 5.1** – Uniaxial and triaxial apparatus.

The vertical load is supported by two compressive frames (3000 kN and 4000 kN maximum load, right and left in Fig. 5.1) and applied to cubic samples up to 300 mm or cylinders up to 500 mm diameter. The machine is certified according to the UNI EN 12390-4, ASTM C39 and AASHTO T22 standard procedures.

### **5.3 – Samples**

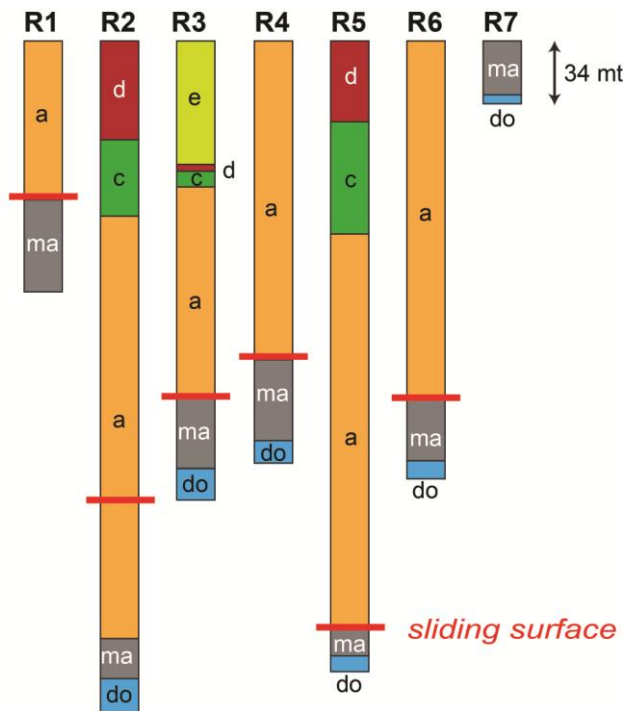
In order to evaluate the mechanical and elastic properties of the Vajont series before the collapse, samples were collected from selected outcrops outside the landslide area (Fig. 5.2). A few samples of the Fonzaso Formation Ma and of the Vajont limestone were also collected directly from the RODIO boreholes performed on the landslide deposit (see detailed description in Martinis, 1978). Samples from the boreholes R5 and R6 (Fig. 5.2) were collected at depth corresponding to the landslide surface.



**Figure 5.2** – Filed map with location of the samples used for laboratory experiments by both field outcrops and RODIO boreholes.

The boreholes were commissioned by the Court of Belluno (Italy), to the RODIO Company and the ENEL Company in order to investigate the slip surface location as well as the structural and stratigraphic features of the landslide after the 1963 disaster. Seven boreholes named R1, R2, R3, R4, R5, R6 and R7 were drilled between August 1964 and May 1965. Except for R7, all boreholes were drilled on the western portion of the landslide deposit (Fig. 5.2) to a depth ranging from 116.50 m to 325.50 m (Martinis, 1978). The stratigraphy of the boreholes is described in detail by Martinis (1978) and schematically reported in Fig. 5.3.

After 50 year, the RODIO boreholes could be directly examined thanks to the partnership and collaboration of the Fondazione Vajont Onlus and the Longarone Municipality (Italy). All the boreholes were drilled using the continuous core technique, with a diameter ranging from 330 mm to 85 mm. The recovery of material was highly variable, and sometimes not determinable due to the intense fracturing and fragmentation of the collapsed mass (Martinis, 1978). In general, very few samples were suitable for laboratory investigation and mostly from the lower portion of the holes, which is represented by the Fonzaso Formation Ma and by the Vajont limestone. Samples from the boreholes R6 and R5 were used in both uniaxial and triaxial tests (see Table 5.1 and Table 5.3).



**Figure 5.3** – Stratigraphy of the RODIO boreholes (Martinis, 1978). Note that the sliding surface is always located between the levels A and Ma of the Fonzaso Formation, with the exception R2.

## 5.4 – Uniaxial compressive test

### 5.4.1 - Test procedures

Experiments were performed on cylindrical samples. Several test parameters affect the Uniaxial Compressive Strength (UCS) of the rock materials, as the core diameter, the length to diameter ratio (L/D) and the loading velocity. According to the ASTM-D7012 (2010) and ASTM-D4543 (2008) specifications, samples were drilled with approximately 38 mm diameter and a length to diameter ratio between 2.0 and 2.5 (see Table 5.1). The shape effect in the Uniaxial Compressive Strength (UCS hereafter) is still under discussion (e.g., Tuncay and Hasancebi, 2009) and the equations suggested to correct the results for L/D (e.g. Hoek and Brown, 1980; Hawkins, 1998; Tuncay and Hasancebi, 2009) are not applicable to every rock type. However the selected diameter of ~ 38.00 mm is in agreement with Hawkins (1998) who observed that a maximum strength is obtained on samples between 38 and 54 mm in diameter, and is a good compromise to obtain intact and homogeneous representative samples. All the samples were loaded at constant rate of 0.300 MPa/s, to achieve failure in a test time between 2 and 15 min in agreement with the requirement of ASTM-D7012 (2010) standard procedure.



**Table 5.1** – Rock samples characteristics for uniaxial tests.

Rock	sample	ID	load dir.	$\Phi$ (mm)	L (mm)	A (mm <sup>2</sup> )	$\Delta L$ (mm)	L/D	Wt. (g)	Vol. (cm <sup>3</sup> )	$\rho$ (g/cm <sup>3</sup> )	
Socchèr	VJ10	F1	parall	37.71	82.99	1116.3 0	0.22	2.2	250. 0	92.69	2.70	
		F2	perp	37.98	87.71	1132.3 5	0.22	2.3	266. 9	99.37	2.69	
		F3	perp	37.99	84.47	1132.9 4	0.30	2.2	257. 5	95.75	2.69	
		F4	parall	37.64	78.74	1112.1 6	0.40	2.1	234. 4	87.62	2.68	
	VJ1	E1	perp	37.97	81.79	1131.6 3	0.17	2.2	248. 5	92.60	2.68	
		E2	perp	37.94	82.77	1129.9 6	0.18	2.2	NA	NA	NA	
		E3	parall	37.76	76.90	1119.2 7	0.20	2.0	NA	NA	NA	
	VJ4	E3	perp	37.96	93.08	1130.8 6	0.13	2.5	282. 5	105.3 1	2.68	
	VJ11	D1	perp	37.95	69.37	1130.5 6	0.24	1.8	211. 1	78.47	2.69	
		D2	perp	37.97	82.25	1131.7 5	0.10	2.2	247. 2	93.13	2.65	
		D4	parall	37.80	76.900	1121.6 4	0.17	2.0	NA	NA	NA	
		D5	parall	37.75	73.470	1118.6 7	0.23	1.9	NA	NA	NA	
		VJ9	C1	parall	37.95	79.91	1130.5 6	0.13	2.1	243. 6	90.39	2.70
	C2		parall	37.96	74.38	1131.1 5	0.11	2.0	227. 5	84.18	2.70	
	C3		perp	37.95	86.43	1130.5 6	0.10	2.3	264. 3	97.76	2.70	
	Fonzaso - A	VJ6	A1	perp	41.85	101.84 0	1374.8 7	0.70	2.4	377. 2	140.0 9	2.69
			A2	perp	41.65	100.82 0	1362.0 2	0.24	2.4	370. 6	137.3 9	2.70
			A4	perp	37.76	78.790	1119.2 7	0.90	2.1	238. 2	88.23	2.70
A5			parall	37.50	75.680	1103.9 1	0.26	2.0	221. 7	83.59	2.65	
A"1			perp	37.99	71.260	1132.9 4	0.30	1.9	NA	NA	NA	
Fonzaso - Ma	VJ5	Ma2	parall	37.65	84.64	1112.7 6	0.19	2.2	252. 7	94.23	2.68	
		Ma3	perp	37.58	83.10	1108.6 2	0.30	2.2	243. 5	92.17	2.64	
		Ma5	parall	37.56	102.00	1107.4 4	0.12	2.7	NA	NA	NA	

<b>Vajont</b>	VJ2	DO				1136.5			290.	110.4	
		2	parall	38.04	97.22	0	0.11	2.6	1	9	2.63
<b>Limestone</b>		DO				1131.1			246.		
		3	parall	37.95	82.36	3	0.39	2.2	1	93.16	2.64
		DO					1132.6			235.	
		4	perp	37.98	79.22	8	0.14	2.1	6	89.73	2.63
	R6	P1	perp	37.92	81.62	4	0.70	2.2	1	92.18	2.68
							1129.9			252.	
		P2	perp	37.93	83.44	4	0.40	2.2	3	94.28	2.68
							1126.3			246.	
	R5	N	perp	37.87	84.02	7	0.30	2.2	6	94.64	2.61
							1129.9			250.	
11A		perp	37.93	86.20	4	0.50	2.3	5	97.40	2.57	
						1130.5			264.		
	11B	perp	37.94	86.83	4	0.20	2.3	4	98.16	2.69	

ID = sample labels referring to different stratigraphic units (F, E, D, C for Socchèr Fm., A and Ma for Fonzaso Fm., as reported in Par.2.2 chapt. 2); load dir. = loading direction, perp = core perpendicular to stratification, parall = core parallel to stratification;  $\phi$  = diameter; L = length; A = base area;  $\Delta L$  = parallelism between core surfaces; L/D = Length/Diameter; NA = not available; Vol. = geometrical volume calculated as (Area x Length);  $\rho$  = rock density.

In uniaxial and triaxial tests, the Young's modulus and the Poisson's coefficient were also determined by means of strain gauges. The strain gauge consists of an electrical resistance wire which is stucked onto test specimen via electrical insulation glue. When the external load is applied, the stain gauge physically deforms together with the rock material and the electrical resistance changes proportionally. In the experiments, three strain gauges with 20 mm or 30 mm length were used (TML, Tokyo Sokki Kenkyujo Co., Ltd., codes PFL-20-11 and PFL-30-11 respectively), two in vertically opposite position to measure the axial deformation, and one horizontally to measure the radial deformation. When possible, all the strain gauges were glued in the middle portion of the samples to avoid board effects at the contact between the loading plates and the sample bases.

#### 5.4.2 - Results

The results of the uniaxial tests (UCS, Young's modulus and Poisson's ratio) are reported in Table 5.2. The Young's modulus was calculated according to the ASTM-D7012 (2010) suggested method, as tangent modulus ( $E_{tan50}$ ) and secant modulus ( $E_{sec50}$ ) at 50% maximum load.  $E_{sec100}$  is the secant modulus at rupture and  $\nu$  is the Poisson's ratio. Santi et al. (2000) proposed to correct the secant Young's modulus to eliminate the effect of microcrack closure which takes place at the beginning of the loading ramp. In our experimental apparatus, a pre-

load of about 8-10 kN is automatically applied by the system and cannot be changed. For such reason, it is possible that part or the whole of the initial crack closure cannot be observed. In general all the samples exhibit elastic and elasto-plastic behaviors (type 1 and 2 according to Deer and Miller, 1966) and no corrections to secant Young's moduli are required (Santi et al., 2000). In Fig. 5.4, the stress-strain curves for lateral, vertical and volumetric strain are reported for the Socchèr, Fonzaso Fm. A, Fonzaso Fm. Ma and Vajont Limestone. The behavior of the stress-strain curve is linear up to about 200 MPa for Vajont Limestone, and up to about 160 MPa for Socchèr and Fonzaso Formations. UCS changes from 104 MPa to 212 MPa for Socchèr, from da 106 MPa to 178 MPa for Fonzaso A, from 114 MPa to 236 MPa for Fonzaso Ma and is maximum for the Vajont Limestone with UCS up to  $\sim 290$  MPa. These data are in agreement with average UCS values of  $\sim 30$ -250 MPa reported in the literature for limestones (e.g., Hawkins, 1998) while the extremely strong resistance of Vajont Limestone is similar to the UCS of  $\sim 300$  MPa measured in Solenhofen limestone (Mogi, 2011) The volumetric deformation is maximum for Socchèr ( $\sim 1800 \mu\epsilon$ ) and minimum for Fonzaso Ma ( $\sim 1000 \mu\epsilon$ ).

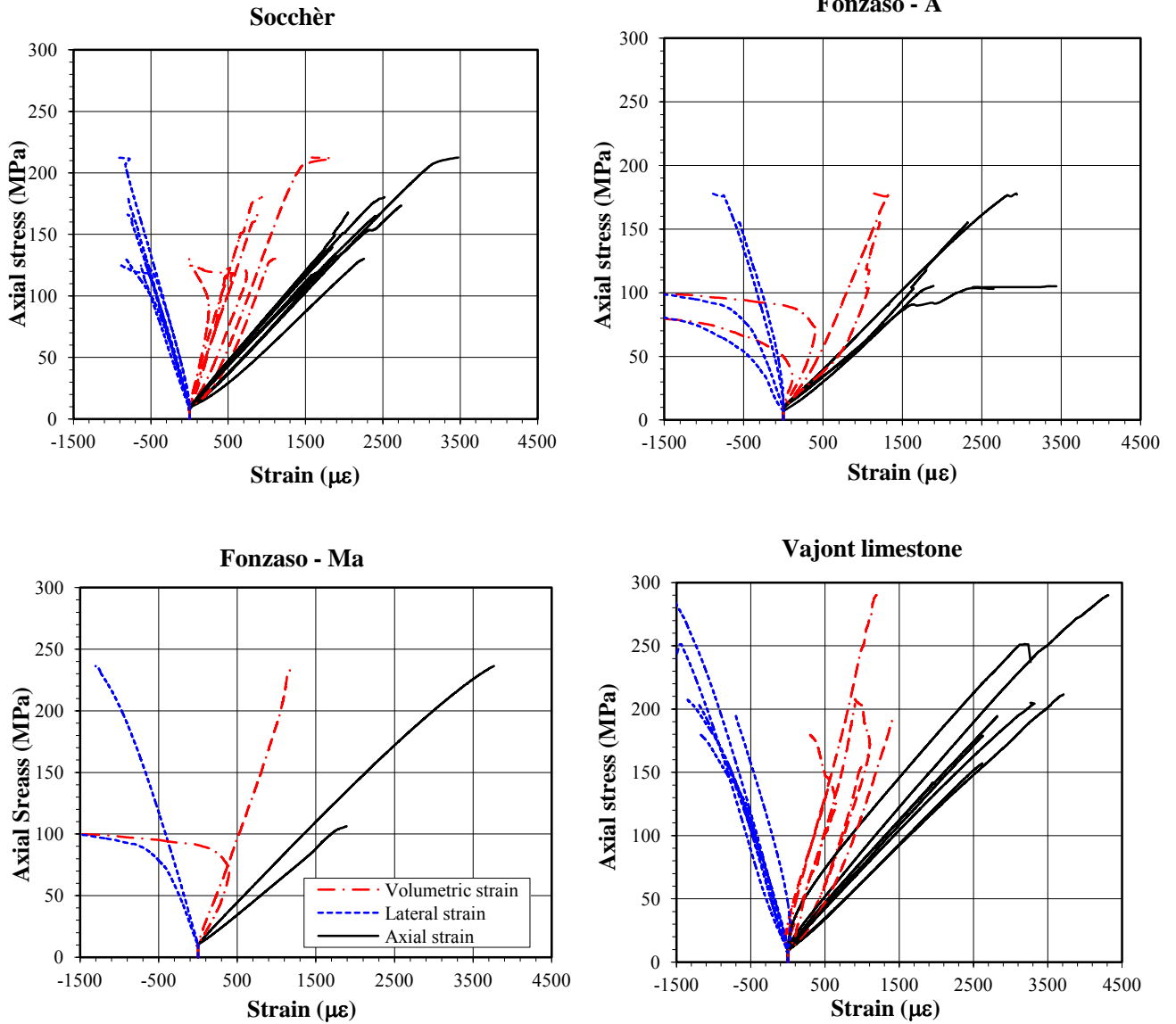
In Fig. 5.5A, the tangent Young's modulus  $E_{\tan 50}$  and the Poisson's ratio are reported as function of the UCS. The data are quite scattered and there is no systematical variation of the mechanical and elastic properties as function of the loading directions (Fig. 5.5).  $E_{\tan 50}$  changes respectively between  $\sim 49$  GPa and 71.70 GPa in the Socchèr Fm., from 55.10 GPa to 67.30 GPa in the Fonzaso Fm. A, from 55.50 a 71.35 GPa in Fonzaso Fm. Ma, and from 57.30 GPa to 67.50 GPa in Vajont Limestone. Values are consistent with those reported by Palchik (2011). The average value for  $E_{\tan 50}$  is similar for all the formations while UCS average data are different: the Socchèr is similar to Fonzaso A that is smaller than Fonzaso Ma that is in turn smaller than Vajont Limestone.

Mean Poisson's ratio are 0.31 for Socchèr and Fonzaso A, 0.35 for Fonzaso Ma and Vajont Limestone (Fig. 5.5B). Such values are consistent with average data reported for similar rocks (e.g., Gercek, 2007).

**Table 5.2** - Mechanical data from uniaxial tests.

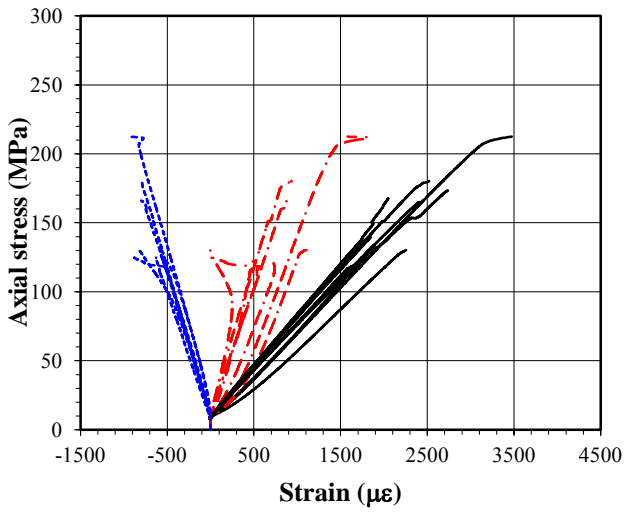
<b>Rock</b>	<b>sample</b>	<b>ID</b>	<b>load dir.</b>	<b>UCS (MPa)</b>	<b>E<sub>tan50</sub> (GPa)</b>	<b>E<sub>sec50</sub> (GPa)</b>	<b>E<sub>sec100</sub> (GPa)</b>	<b>v</b>
<b>Socchèr</b>	VJ10	F1	parall	143.99	66.50	57.55	67.06	0.33
		F2	perp	174.62	62.50	62.48	58.71	NA
		F3	perp	166.06	65.00	68.01	64.37	0.30
		F4	parall	173.23	69.80	67.83	59.84	0.31
	VJ1	E1	perp	180.93	69.10	75.28	49.43	0.32
		E2	perp	212.52	66.80	62.91	58.61	0.31
		E3	parall	124.7	65.40	60.8	65.91	0.31
	VJ4	E3	perp	104.17	56.50	49.35	NA	NA
	VJ11	D1	perp	79.65	49.00	43.32	45.93	NA
		D2	perp	172.43	61.40	61.56	51.26	0.37
		D4	parall	119.81	46.00	41.64	47.59	0.31
	VJ9	D5	parall	167.57	73.20	73.7	NA	NA
		C1	parall	125.52	66.40	66.59	65.36	0.30
		C2	parall	139.71	71.70	72.94	71.02	0.21
			C3	perp	141.38	61.80	50.22	82.38
		<b>mean</b>	<b>148.42</b>	<b>63.41</b>	<b>60.95</b>	<b>60.57</b>	<b>0.31</b>	
		<b>std</b>	<b>(34.29)</b>	<b>(7.75)</b>	<b>(10.66)</b>	<b>(10.39)</b>	<b>(0.04)</b>	
<b>Fonzaso - A</b>	VJ6	A1	perp	155.66	55.10	58.80	49.15	0.38
		A2	perp	178.09	62.80	60.83	57.05	0.28
		A5	parall	106.63	59.90	50.97	NA	NA
		A"1	perp	155.99	67.30	54.48	154.22	0.27
		<b>mean</b>	<b>149.09</b>	<b>61.28</b>	<b>56.27</b>	<b>86.81</b>	<b>0.31</b>	
	<b>std</b>	<b>(30.19)</b>	<b>(5.12)</b>	<b>(4.42)</b>	<b>(58.52)</b>	<b>(0.06)</b>		
<b>Fonzaso Ma</b>	VJ5	Ma2	parall	148.08	71.35	71.8	NA	NA
		Ma3	perp	114.00	55.50	50.45	NA	NA
		Ma5	parall	236.27	64.80	65.88	59.88	0.35
		<b>mean</b>	<b>166.12</b>	<b>63.88</b>	<b>62.71</b>	<b>59.88</b>	<b>0.35</b>	
	<b>std</b>	<b>(63.10)</b>	<b>(7.96)</b>	<b>(11.02)</b>	NA	NA		
<b>Vajont limestone</b>	VJ2	DO2	parall	147.19	66.45	72.64	72.51	0.38
		DO3	parall	194.21	65.10	67.37	63.40	0.33
		DO4	perp	194.45	65.50	70.46	66.28	0.37
	R6	P1	perp	290.75	67.50	72.74	62.98	0.34
		P2	perp	251.45	72.80	96.15	75.86	0.35
		N	perp	162.89	61.50	55.67	137.34	0.32
	R5	11°	perp	205.64	61.80	63.3	58.70	0.34
		11B	perp	211.67	57.30	55.27	54.36	0.34
			<b>mean</b>	<b>207.28</b>	<b>64.74</b>	<b>69.20</b>	<b>73.93</b>	<b>0.35</b>
			<b>std</b>	<b>(46.07)</b>	<b>(4.64)</b>	<b>(12.91)</b>	<b>(26.54)</b>	<b>(0.02)</b>

ID = sample labels referring to different stratigraphic units (F, E, D, C for Socchèr Fm., A and Ma for Fonzaso Fm., as reported in Par.2.2, chapt 2); load dir. = loading direction, perp = core perpendicular to stratification, parall = core parallel to stratification; UCS = Uniaxial Confining Strength; E<sub>tan50</sub> = Young's modulus at 50% maximum load; E<sub>sec50</sub> = secant Young's modulus at 50% maximum load; E<sub>sec100</sub> = secant Young's modulus at maximum load; v = Poisson's ratio at 50% maximum load; mean = average value; std = standard deviation.

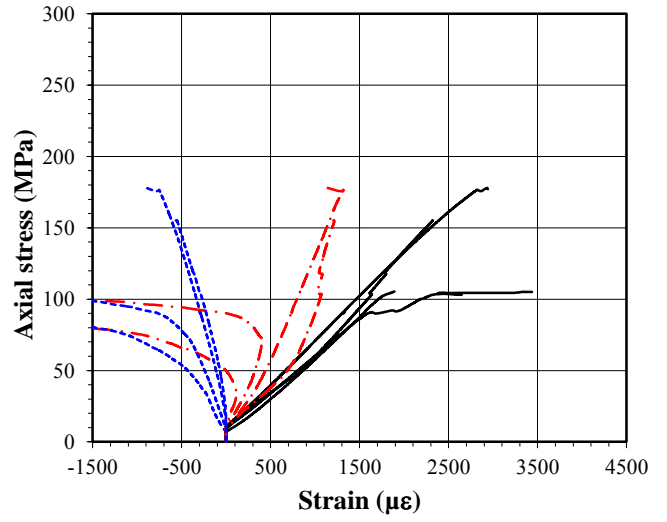


**Figure 5.4** – Stress-strain curves of experiments with lateral strain (left), vertical (right) and volumetric strain (middle).

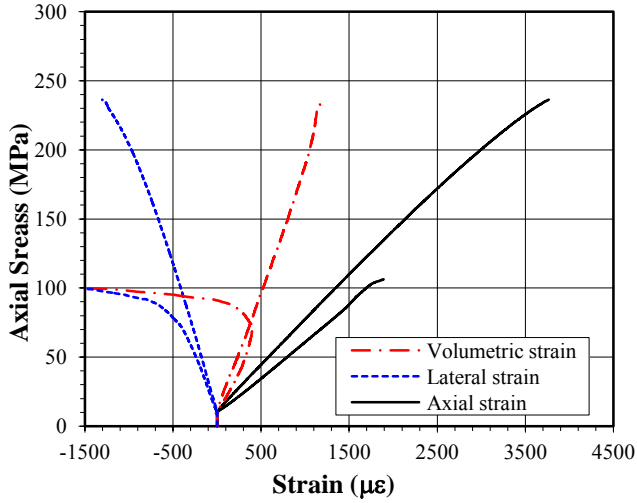
**Socchèr**



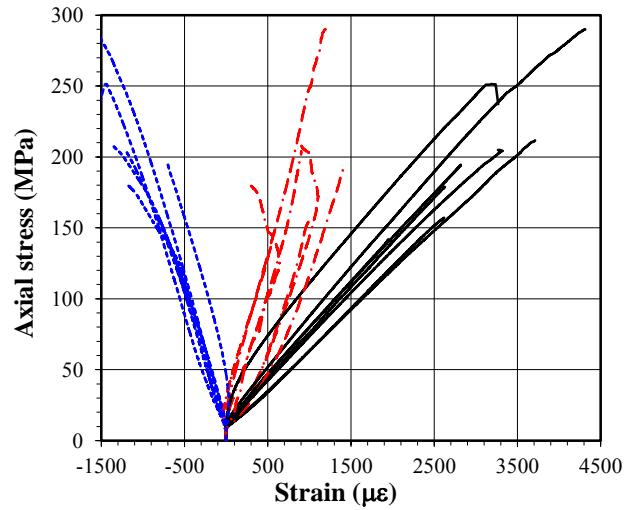
**Fonzaso - A**

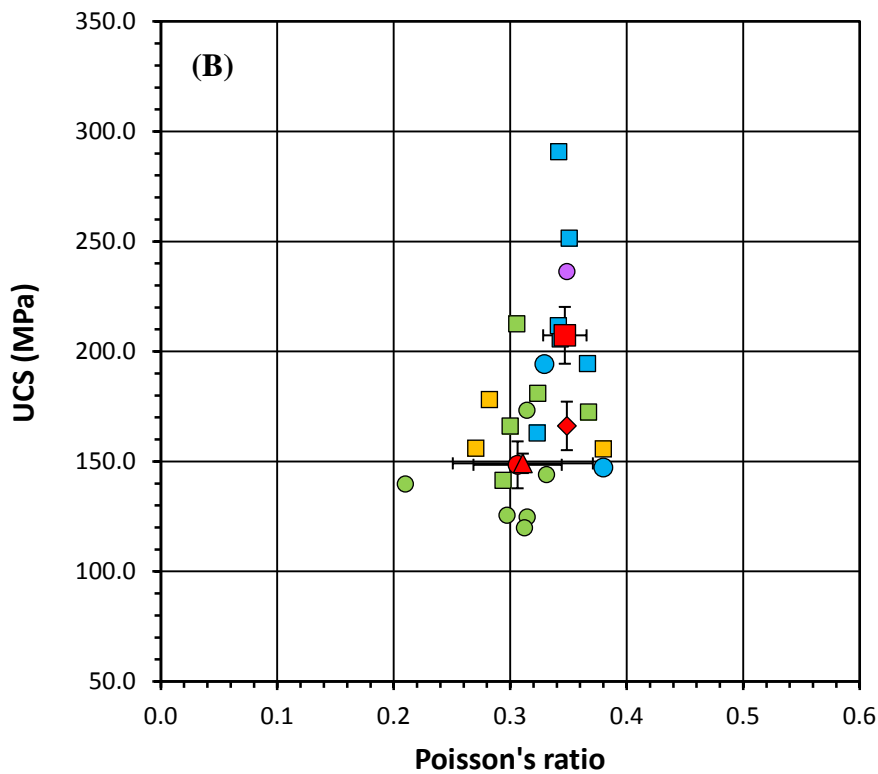
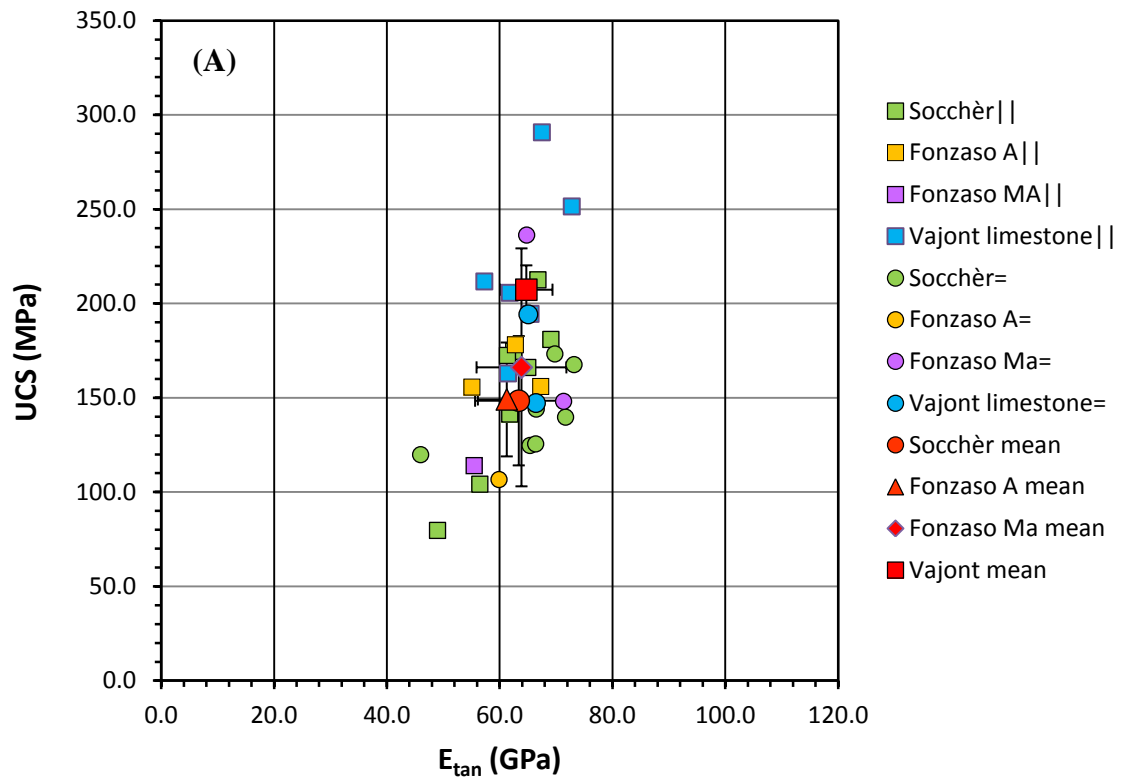


**Fonzaso - Ma**



**Vajont limestone**

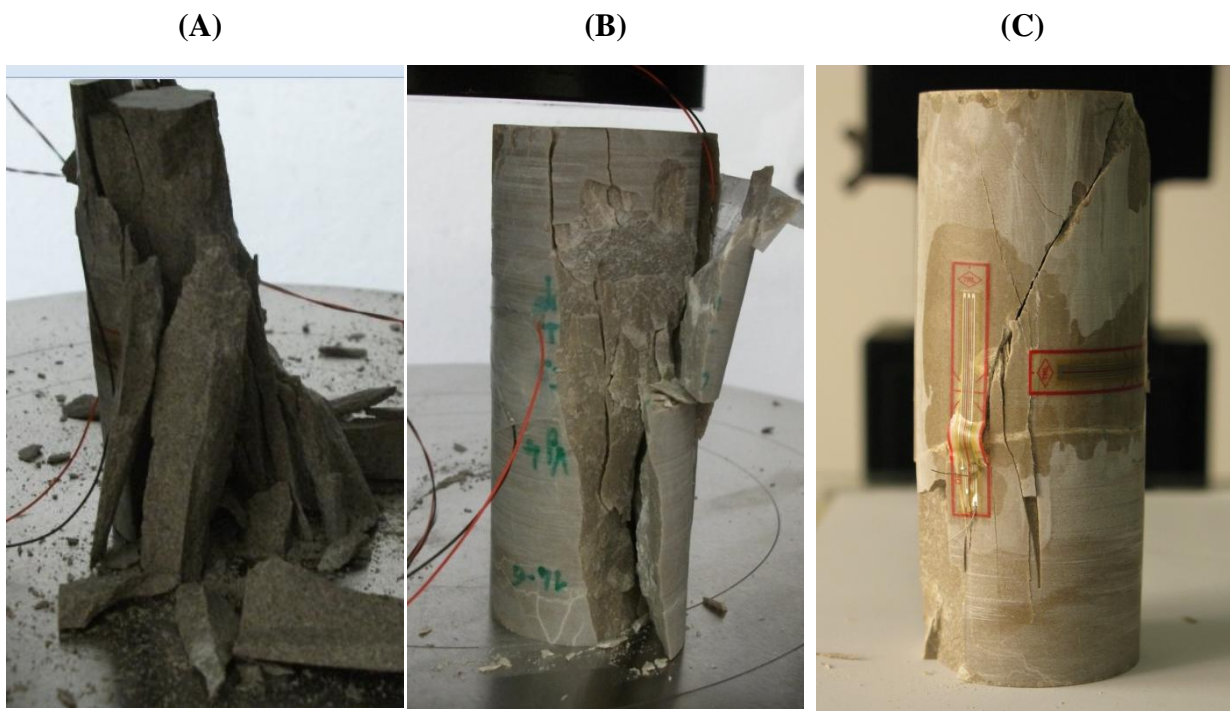




**Figure 5.5** – Variation of the A) Uniaxial Compressive Strength (UCS) vs. tangent Young's modulus, and B) Uniaxial Compressive Strength (UCS) vs. Poisson's ratio from uniaxial tests. Normal load directions as squares, parallel load directions as circles, averages in red symbols with standard deviations.

### 5.4.2.1 - Fracture characterization

From the fracture analysis, rock samples predominantly fail in shear or in extension mode in the uniaxial loading tests (Fig. 5.6). The extension mode denotes failure along planes parallel to the compression direction (Fig. 5.6A and B) and suggest that the sample was relatively free of microscopic discontinuities. The shear failure (Fig. 5.6C) is less common and involves one or more major parallel shearing planes which develop in more homogeneous materials.



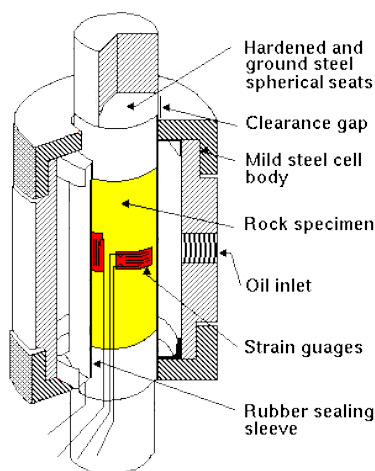
**Figure 5.6** - Failure modes of rock samples tested in uniaxial compression: A) multiple extension; B) single extension; C) shear mode.



## 5.5 - Triaxial compressive test

The Triaxial Compressive tests were performed on selected samples from the Fonzaso Formation A and Ma, which correspond to the lithologies crossed by sliding surface. From new seismic refraction profile (unpublished) and from the analysis of boreholes performed by the RODIO Company in 1965 (Martinis, 1978), the sliding surface is located at maximum 200 m depth which corresponds to about 6.0 MPa pressure (average rock density is 2.68-2.70 g/cm<sup>3</sup>, see Table 5.3). For such reason, experiments were performed at confining pressures between 1.0 MPa and 6.0 MPa.

From uniaxial experiments, rock strength does not change as function of sample drilling direction, so rock cores were all obtained perpendicular to the bedding plane. Rock cylinders about 38.0 mm diameter and length to diameter ratio up to 2.3 (Table 5.3) were obtained. The Young's modulus and the Poisson's ratio were obtained by using two linear electrical resistance strain gauges (TML), located in the central portion of the cores, and bonded along the axial direction and the horizontal direction. Tests were performed with the ADVANTEST9 and SERCOMP7 apparatus (CONTROLS s.r.l.) by means of a 3000 kN capacity oil press. The experiments were performed at constant velocity of 1.0  $\mu\text{m/s}$  controlled by means of three vertical Linear Velocity Displacement Transducers (LVDT, Solartron), having 10 mm maximum displacement. The confined compression tests were performed in accordance with the ASTM-D7012 (2010) suggested method.



**Figure 5.7** – The Hoek triaxial cell.

The confining pressure was applied through a Hoek cell (see fig. 5.7). The Hoek triaxial cell, developed by Hoek and Franklin (1968) at the Rock Mechanics Centre, Imperial College,

London, is widely used for testing cylindrical specimens of rock under triaxial compression. The cell is able to achieve 70-80 MPa pressure. The confinement hydraulic oil is retained inside the cell and sealed between a durable synthetic rubber sleeve and a steel cylinder with threaded end caps, making it possible to test and remove the specimen without breaking the seal. A cut-away view of the cell is shown in Fig. 5.7.

The complete list of experimental conditions is reported in Table 5.3. In general, one single confining pressure was selected and applied to the sample which was loaded at constant velocity until rupture. Two experiments, VJ6-A1 and VJ5-Ma4, were performed as multistep, by imposing three different pressures, 1.0 MPa, 3.0 MPa and 6.0 MPa for VJ6-A1, and at 1.0 MPa, 2.0 MPa and 4.0 MPa for VJ5-Ma4 (Gräsle, 2011). In multistep experiments, the initial confining pressure  $\sigma_{31}$  is imposed and the sample is loaded until the evidence of initial break. Afterwards, the sample is slightly decompressed while the second pressure  $\sigma_{32}$  is imposed and the sample again loaded until beginning of second break. The same procedure is applied for the third pressure  $\sigma_{33}$ , and the sample is loaded until complete rupture.

**Table 5.3** – Rock samples characteristics for triaxial tests

Rock	sample ID	$\phi$ (mm)	L (mm)	A (mm <sup>2</sup> )	$\Delta L$ (mm)	L/D	Wt. (g)	Vol. (cm <sup>3</sup> )	$\rho$ (g/cm <sup>3</sup> )		
<b>Fonzaso - A</b>	VJ6	A1	37.77	83.75	1119.86	0.20	2.2	252.2	93.84	2.69	
		A2	37.83	82.85	1123.42	0.04	2.2	250.4	93.12	2.69	
	VJ12	A2	37.93	81.31	1129.37	0.05	2.1	246.9	91.87	2.69	
		A3	37.94	78.65	1129.96	0.04	2.1	235.1	88.92	2.64	
		A4	A4	38.10	81.83	1139.27	0.05	2.1	246.5	93.27	2.64
			A1	38.05	82.45	1136.52	0.03	2.2	252.3	93.75	2.69
	TRX6	A2	38.04	79.10	1135.93	0.04	2.1	242.4	89.90	2.70	
		A3	38.05	81.08	1136.52	0.03	2.1	248.5	92.20	2.70	
		A4	38.07	85.77	1137.72	0.02	2.3	262.8	97.63	2.69	
		A5	38.07	82.14	1137.72	0.03	2.2	251.4	93.50	2.69	
<b>Fonzaso - Ma</b>	VJ5	Ma1	38.06	68.09	1137.12	0.03	1.8	204.2	77.47	2.64	
		Ma4	37.56	102.00	1107.44	0.12	2.7	NA	113.02	NA	
	R6H	Ma2	37.91	60.89	1128.18	0.02	1.6	178.6	68.73	2.60	
		Ma3	37.89	80.72	1126.99	0.02	2.1	244.6	91.02	2.69	

ID = sample labels referring to different stratigraphic units (A and Ma for Fonzaso Fm., as reported in Par.2.2, chapt 2);  $\phi$  = diameter; L = length; A = base area;  $\Delta L$  = parallelism between core surfaces; L/D = Length/Diameter; NA = not available; Vol. = geometrical volume calculated as (Area x Length);  $\rho$  = rock density.

### 5.5.1 - Set up of triaxial tests.

The loading system is made of two different units, the ADVANTEST9 (Controls, s.r.l.), which controls the oil system to apply the axial load, and the SERCOMP7 (Controls, s.r.l.), which is used to apply the oil pressure to the Hoek cell. The triaxial tests are always performed under controlled displacement to avoid explosive fracture of the sample and possible damage to the Hoek cell.

Here follows a short guide reporting the main steps for experimental setup and the suggested values for the control system parameters.

- 1) Prepare the sample and glue one vertical and one horizontal strain gauges.
- 2) To avoid electrical contacts during the pressurization of the sample chamber, wrap the gauge wires with tape at the contact with the load piston.
- 3) Put the sample into the middle portion of the chamber together with the top and bottom pistons.
- 4) Apply the pre-load to the Hoek cell. The system automatically stops at the set value of  $\sim 0.2$  MPa. During the preload, the air present between the cell and the rubber jacket must be released by pushing the spheric valve.
- 5) Put the chamber in vertical position and on of the sustaining structure above the bottom plate.
- 6) Release the confining pressure from the Hoek cell and apply the vertical pre-load ( $\sim 9$  kN). This operation is required to get contact and align the sample and the pistons.
- 7) Put the three LVDT on the bottom plate into contact with the top plate. The maximum displacement of each LVDT is 10 mm and it is preferable to start at position of about 2.0 mm displacement for each LVDT.
- 8) Apply the pressure to the Hoek cell.
- 9) Set to zero the readings of the two strain gauges (CH6 and CH7) and of the average displacement (CH5).
- 10) Set the parameters of the control systems to the following initial values: a)  $K_p = 0.5$ ; b)  $K_i = 0.04$ ; c)  $\text{Max corr}^- = 3000$ ; d)  $\text{Max corr}^+ = 3000$ .
- 11) Start the vertical load under controlled-load velocity of about 0.100 MPa/s.
- 12) At  $\sim 20$  MPa load, switch the control system to “displacement control”.
- 13) Shear until rupture.
- 14) To avoid breakage of the confining rubber jacket, release the confining oil by use of the safety button.

### 5.5.2 - Results

The results of the triaxial experiments are reported in Table 5.4. The Young's modulus was calculated according to the ASTM-D7012 (2010) suggested method as tangent modulus and secant modulus at 50% maximum load (respectively  $E_{\tan 50}$  and  $E_{\sec 50}$  in Table 5.4). In Table 5.4, the secant modulus at rupture  $E_{\sec 100}$  is also reported in.

Fig. 5.8 and 5.9 report the variations of Young's modulus and Poisson's ratio respectively, in Fonzaso A and Fonzaso Ma as function of confining pressure. The data measured in uniaxial tests (no confining pressure) are also reported for reference. The average Poisson's ratio is almost constant with increasing pressure and up to 0.37-0.4 at 6.0 MPa. The Young's modulus changes from 53.9 GPa to 72.9 GPa in Fonzaso A and from 57.7 GPa to 82.5 GPa. In Fonzaso Ma, the Poisson's ratio decreases with pressure from  $\sim 0.38$  at 1.0 MPa to a minimum of 0.24-0.29 at 6.0 MPa. The value of elastic modulus obtained are compatible with the ranges reported in the literature for limestone rocks (ref. in Al-Shayea, 2004) but some values are higher (e.g.,  $E_{\tan} > 60$  GPa and  $\nu > 0.31$ ).

**Table 5.4** - Mechanical data from triaxial tests.

<b>Rock</b>	<b>sample</b>	<b>ID</b>	<b><math>\sigma_3</math> (MPa)</b>	<b><math>\sigma_{\max}</math> (MPa)</b>	<b><math>E_{\tan 50}</math> (GPa)</b>	<b><math>E_{\sec 50}</math> (GPa)</b>	<b><math>E_{\sec 100}</math> (GPa)</b>	<b><math>\nu</math></b>	
<b>Fonzaso Fm. A</b>	VJ6	A1	1.0	175.61	72.90	73.52	72.82	0.39	
			3.0	250.00	71.10	NA	71.22	0.39	
			6.0	213.60	72.20	NA	NA	0.40	
	VJ12	A2	3.0	247.38	64.30	62.88	61.35	0.30	
			1.0	146.00	66.10	63.55	NA	0.31	
			6.0	269.60	53.90	55.06	53.05	0.24	
	TRX6	A4	2.0	164.86	56.60	55.35	56.79	NA	
			A1	1.0	182.13	71.20	74.36	72.99	0.33
			A2	6.0	302.78	69.40	76.09	63.52	0.37
			A3	2.0	250.43	65.10	66.58	62.19	0.32
			A4	3.0	260.19	65.70	64.26	57.48	0.32
	<b>Fonzaso Fm. Ma</b>	VJ5	Ma4	4.0	217.59	70.40	73.61	68.70	0.34
Ma1				6.0	290.40	70.80	73.58	68.68	0.29
1.0				130.13	77.60	76.26	78.72	0.38	
2.0				162.32	82.50	82.23	84.24	0.40	
R6H		Ma2	4.0	240.51	77.60	NA	83.49	0.39	
			3.0	208.79	63.20	67.16	NA	NA	
			6.0	148.07	57.70	55.00	56.11	0.24	

---

ID = sample labels referring to different stratigraphic units (A and Ma for Fonzaso Fm., as reported in Par.2.2, chapt.2);  $\sigma_3$  = confining pressure;  $\sigma_{\max}$  = maximum vertical load;  $E_{\tan 50}$  = Young's modulus at 50% maximum load;  $E_{\text{sec}50}$  = secant Young's modulus at 50% maximum load;  $E_{\text{sec}100}$  = secant Young's modulus at maximum load;  $\nu$  = Poisson's ratio at 50% maximum load.

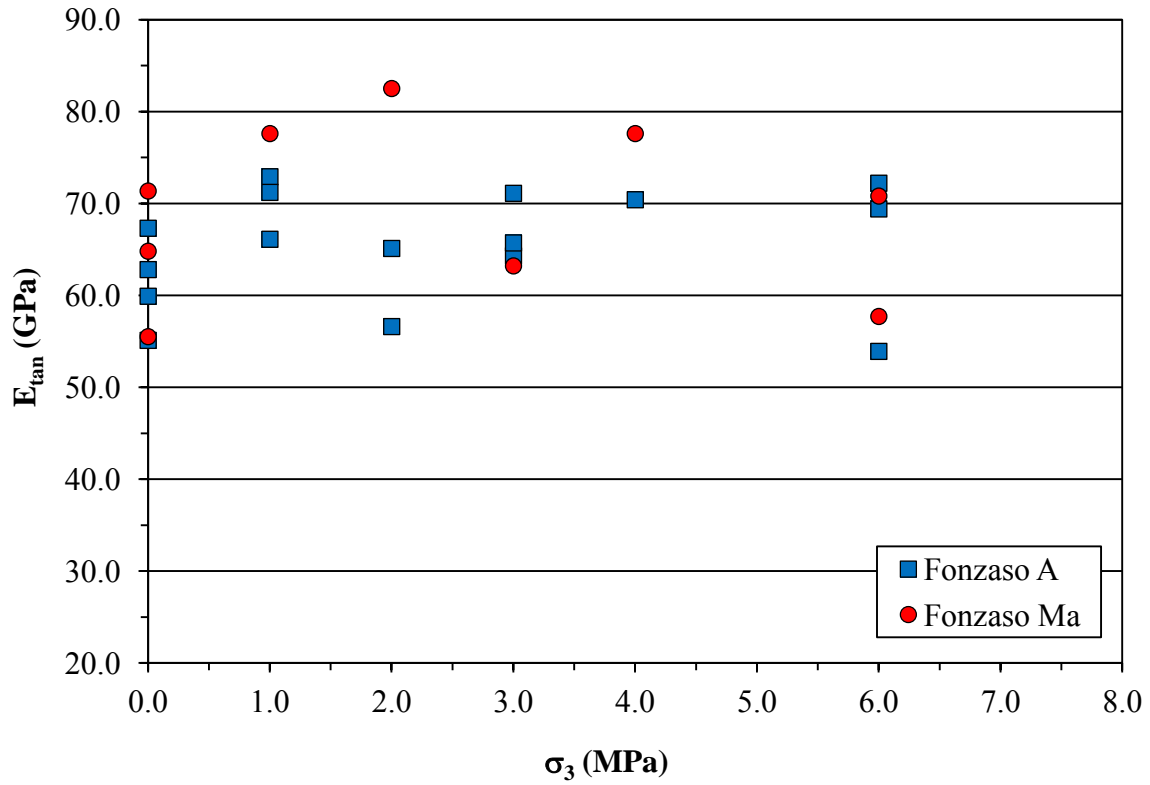


Figure 5.8 – Variation of the tangent Young's modulus  $E_{tan50}$  as function of  $\sigma_3$ .

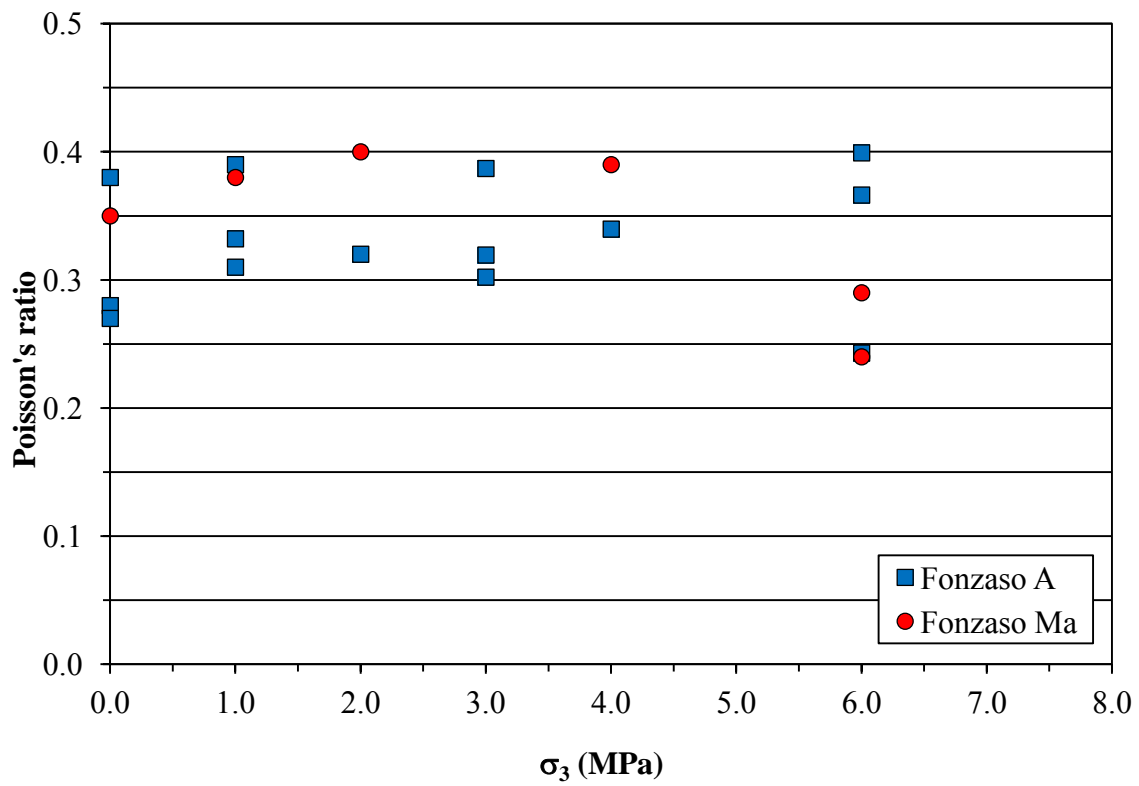


Figure 5.9 – Variation of the Poisson's ratio as function of  $\sigma_3$ .

The behavior of the rock samples from Fonzaso A and Fonzaso Ma is approximately elastic. Fig. 5.10 shows the curves of differential axial stress versus differential lateral strain  $\varepsilon_r$  (left), differential axial strain  $\varepsilon_h$  (right) and volumetric strain  $\varepsilon_v$  at 1.0, 2.0, 3.0, 4.0 and 6.0 MPa. Volumetric strain is calculated as:

$$\varepsilon_v = \varepsilon_h + 2 \varepsilon_r \quad (\text{Eq.1})$$

where  $\varepsilon_h$  is taken positive and  $\varepsilon_r$  is taken negative.

In some experiments the horizontal deformation could not be calculated due to failure of the horizontal strain gauges. In such case, only the vertical deformation is reported. Every sample display a positive volumetric deformation which means that the samples experienced development of fractures during loading. The vertical and lateral strain display a linear behaviour almost up to the failure which is in agreement with an elastic behaviour of the limestones. In some experiments the evolution of the lateral strain is not linear at load > 70% of the maximum load. In sample TRX6 and VJ6, the average volumetric deformation is  $\sim 1000 \mu\varepsilon$ , while in VJ12 the deformation is up to  $\sim 2000 \mu\varepsilon$ . In Fonzaso Ma (Fig. 5.10), the lateral and volumetric strain data are not available due to frequent failure of lateral strain gauges. In most cases, failure is ascribed to the presence of cherts nodules or levels below the strain gauges, as the deformation of the two material, limestone and cherts, is quite different.

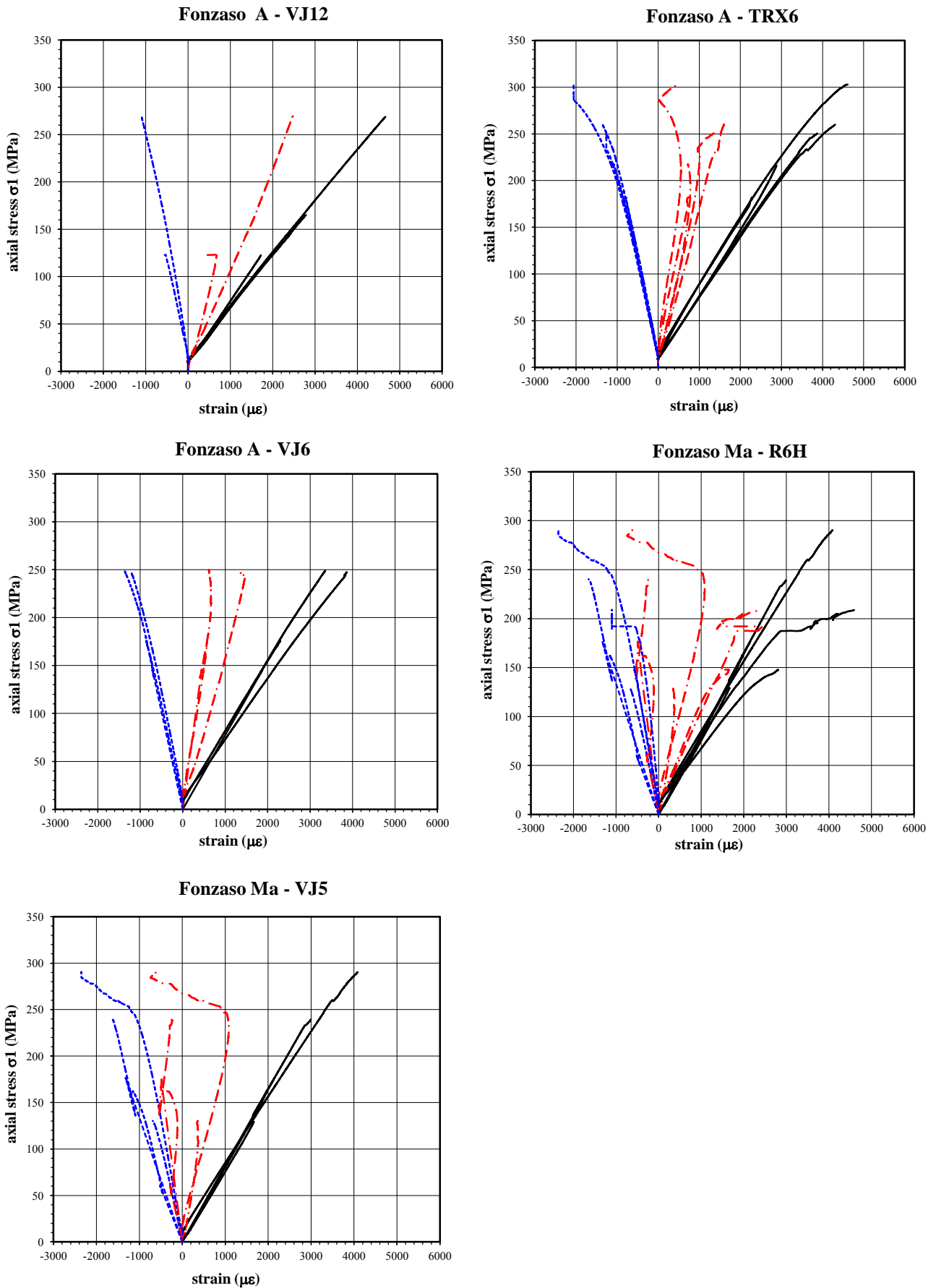


Figure 5.10 – Stress-strain curves of Fonzaso A and Fonzaso Ma triaxial tests.



### 5.5.2.1 - Estimation of material constants

The data from triaxial tests can be used as input parameters for estimating both intact rock and rock mass strength using either Mohr-Coulomb or Hoek-Brown failure criteria (Mogi, 2006; Hoek et al., 2002). In particular we need to consider that:

- 1) the Mohr-Coulomb criterion is the most suitable at high confining pressures when the material fails developing shear planes;
- 2) the Hoek-Brown criterion is suitable for rock masses.

The Mohr-Coulomb is defined by the equation:

$$\tau = \sigma \tan(\phi) + c \quad \text{Mohr-Coulomb (Eq. 2)}$$

where  $\tau$  is the shear strength,  $\sigma$  is the normal stress,  $c$  is the intercept of the failure envelope with the  $\tau$  axis, and  $\phi$  is the slope of the failure envelope. The quantity  $c$  is called the cohesion and the angle  $\phi$  is called the angle of internal friction.

The generalized Hoek-Brown criterion is defined by the equation:

$$\sigma_1 = \sigma_3 + \sigma_c \sqrt[m_b]{\frac{\sigma_3}{\sigma_c} + s} \quad \text{Hoek-Brown (Eq. 3)}$$

where  $\sigma_1$  and  $\sigma_3$  are the major and minor effective principal stresses at failure,  $\sigma_c$  is the uniaxial compressive strength of the intact rock material,  $m_b$  is a reduced value of the material constant  $m_i$  and

$s$  and  $a$  are constants give by:

$$s = \exp\left(\frac{GSI-100}{9-3D}\right) \quad (\text{Eq. 4})$$

$$a = \frac{1}{2} + \frac{1}{6} (e^{-GSI/15} - e^{20/3}) \quad (\text{Eq. 5})$$

with  $s = 1$  for intact rocks.  $D$  is a factor which depends upon the degree of disturbance to which the rock mass has been subjected by blast damage and stress relaxation. It varies from 0 for undisturbed in situ rock masses to 1 for very disturbed rock masses.

The material constants may be obtained from the analysis of the triaxial tests. In particular, the Hoek-Brown strength parameters of the rock mass ( $m$ ,  $s$  and  $a$ ) were calculated with

RocLab (RocScience) while the Mohr-Coulomb equivalent parameters  $\phi$  and  $c$  were calculated from the generalized Hoek-Brown envelope over a given stress range. In RocLab, the input data are a given set of parameters:

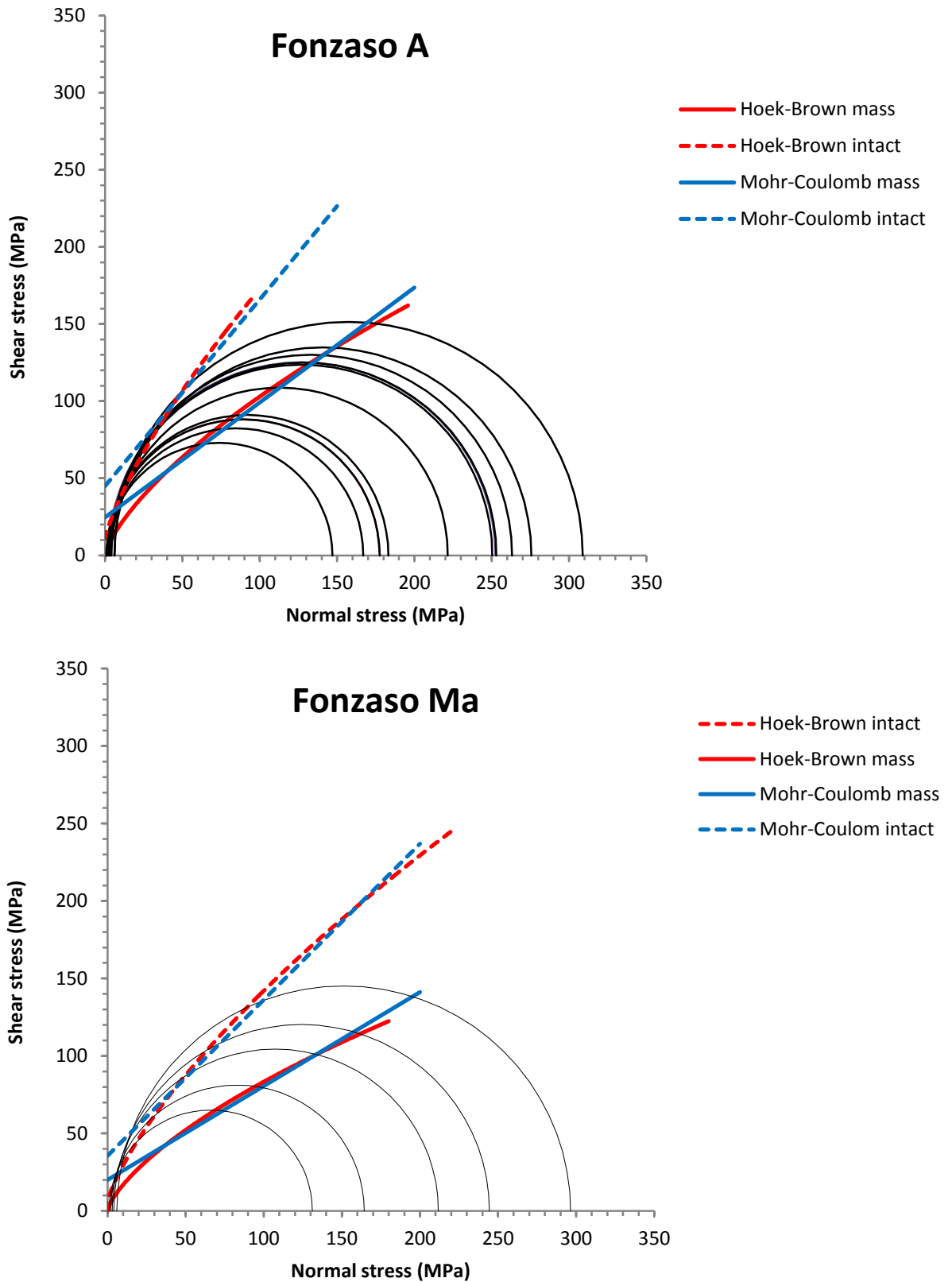
- 1)  $\sigma_c$  = unconfined compressive strength of intact rock,
- 2)  $m$  = the intact rock parameter,
- 3) GSI = the geological strength index,
- 4)  $D$  = the disturbance factor.

The input parameters  $\sigma_c$  and  $m$  can be calculated on the base of triaxial laboratory tests on intact rock using the Marquardt-Levenberg fitting technique. With such procedure, a relatively small number of data points (e.g., 6 or 7 triaxial tests) are required to obtain good results. RocLab calculates the parameters of the generalized Hoek-Brown failure criterion ( $m_b$ ,  $s$  and  $a$ ) and the equivalent Mohr-Coulomb parameters ( $\phi$  and  $c$ ) for the rock mass.

Two sets of fitting parameters were obtained: 1) for intact rock material by imposing GSI= 100 ( $s = 1.0$ ); 2) by imposing GSI = 60, i.e. the average value resulting from the measurements on field outcrops outside the slide mass. In Fig. 5.12 the failure envelopes for the rock mass (i.e. with GSI = 60) for Fonzaso A and Fonzaso Ma are plotted and values for the Hoek-Brown and Mohr-Coulomb parameters are reported in Table. 5.5.

**Table 5.5** – Data resulting from Hoek-Brown and Mohr-Coulomb failure criteria calculated with RocLab (RocScience) for intact rock and rock mass.

	<b>Fonzaso A</b>		<b>Fonzaso Ma</b>	
	rock mass	intact rock	rock mass	intact rock
<b>Hoek-Brown</b>				
$\sigma_c$ (MPa)	145.04	145.04	75.68	75.68
$m_i$	50.0	50.0	50.0	50.0
$D$	0.3	0.0	0.3	0.0
GSI	60	100	60	100
$m_b$	9.31	50.00	9.31	50.00
$s$	0.01	1.00	0.01	1.00
$a$	0.5	0.5	0.5	0.5
<b>Mohr-Coulomb</b>				
$c$ (MPa)	24.6	45.0	20.0	35.6
$\phi$ (°)	36.7	50.4	31.2	45.2



**Figure 5.11** - Failure envelopes of Fonzaso A and Fonzaso Ma with the Hoek-Brown and Mohr-Coulomb failure criteria calculated with RocLab (RocScience) for rock mass and intact rock. The input and output parameters of the fittings are listed in Table 5.5.

### 5.5.2.2 - Fracture characterization

Sample failure in triaxial tests occurs through the development of fractures as effect of stress concentration and propagation. Fractures observed in samples deformed under confining pressure  $\sigma_3$  are reported in Fig. 5.12 for Fonzaso A and Fonzaso Ma. Most of the samples failed by a combination of shear and tensile fractures. According to Holznausen and Johnson (1979) and Bahat et al. (2001), the critical angle above which the tensile fractures transform to shear ones is approximately  $10^\circ$ . In general, the shear fractures appear to be prevalent and limited to one or two major surfaces which develop along the entire sample length.

In Fonzaso A at 1.0 MPa, the samples exhibit quasi-conic shear fracture near the top and bottom surfaces of the sample and evolve as longitudinal tensile splitting to the center of the cylinder. This pattern is consistent with the Sequence 2 mode reported by Bahat et al. (2001). With increasing confining pressure (Fig. 5.12), one major shear plane dominates the rupture process (e.g., at 3.0 MPa and 6.0 MPa). At 4.0 MPa, the major shear plane is at  $\sim 20^\circ$  angle with the vertical axes (S1) and is crossed by a second higher angle shear plane (S2) approximately in the central portion of the sample. In Fonzaso A, the angle between the fracture plane and the vertical axis increases with the confining pressure from about  $12^\circ$  at 2.0 MPa, to  $19^\circ$  at 3.0 MPa, and  $24^\circ$  at 6.0 MPa. In two samples of Fonzaso A, VJ12 at 2.0 MPa and VJ6 at 6.0 MPa, the shear planes develop along preexisting veins cemented with calcite with an angle of about  $30\text{-}34^\circ$ .

In Fonzaso Ma, the rupture is more irregular. When the amount of silica is higher, fractures are irregularly oriented and abundant. At 3.0 MPa, the sample broke along the contact between the silica nodule and the carbonate rock. At 6.0 MPa, the sample R6H developed a high angle curved fracture while sample VJ5 broke along vertical planes.


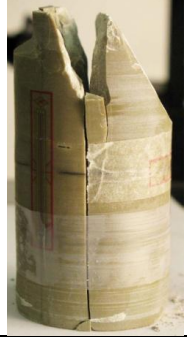



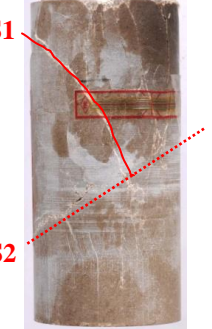


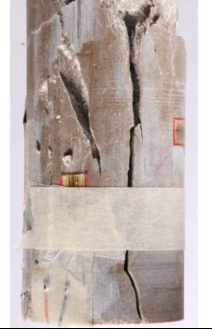



$\sigma_3$ MPa	Fonzaso A TRX6	Fonzaso A VJ12	Fonzaso A VJ6	Fonzaso Ma VJ5	Fonzaso Ma R6H
6.0					
4.0					
3.0					
2.0					
1.0					

Figure 5.12 – Fracture characterization of Fonzaso A and Fonzaso Ma from triaxial tests.

# CHAPTER 6

## VAJONT 3D GEOLOGICAL MODEL RECONSTRUCTION

### *GOCAD Software*

#### **6.1 Introduction**

The Vajont landslide has been the object of numerous studies, because of its catastrophic consequences and unexpected behavior. Several interpretations of the event have been attempted during the last 49 years, but a comprehensive explanation of both triggering and dynamics of the phenomenon still remains not completely understood.

To date, all the slope analyses on the Vajont rockslide have involved just 2D modelling. In order to better clarify the mechanics and dynamics of the 1963 landslide, the construction of a 3D geological model result to be fundamental. Indeed, it allowed to investigate slope structures, the landslide kinematics and the spatial/temporal development of the failure surface. Furthermore, the 3D implementation of the geological features represents a useful check of the geological bi-dimensional interpretation and represents the potential starting point for future 3D mechanical modelling (Sterlacchini et al., 2008).

The main advantages of the GoCAD 3D geological model consisted in the geometric reconstruction of the major geological, structural and geomechanical features discussed in the previous chapters.

## 6.2 Input Data to Gocad 3D modeling

The descriptive component associated to any Gocad geometric entity has been directly imported from implemented GIS-database and used afterwards in the phase of 3D reconstruction.

The typologies of data considered to the purpose of implementing the Vajont 3D model have different geometrical nature and contain several type of information that are consequentially organized in different informative strata geo-referenced in “Gauss Boaga Monte Mario Italy 2” system.

The data can be classified in:

- ✓ linear (contour lines) and punctual (strata orientation) topographic 2D;
- ✓ geological data (stratigraphic, and morpho-structural limits), polygonal and punctual. Each of them univocally identified through coordinates X,Y,Z. said points necessary for structuring vectors. constituting a set point in Gocad (Vset) .

In the framework of the Gocad software, stratigraphic and tectonic surfaces, as well as the volumes resulting from their intersection, structured, showed and modeled in the tridimensional space

- In particular the input data used for the 3D Vajont landslide model derived from: pre- and post-landslide geological maps scale 1:5.000 (Semenza, 1986) (Figure 6. 1), pre- and post-landslide digital elevation models, post-landslide orthophotos, field structural data, aerial Lidar data (Friuli Venezia Giulia Region), and boreholes.

The DEM highlights the relationships between geological structures and topography, and provides georeferencing quality control by overlaying topographic contour lines into the raster map.

- The seven borehole data(R1, R2, R3, R4, R5, R6, R7) (Figure 6. 2), drilled by Rodio company between August 1964 and May 1965, located on the landslide deposit, were recorded including every single well marker.

They were fundamental to a more detailed reconstruction of the sliding surface in depth.

The depth information in Gocad is stored in the properties of Z and Zm. Z is the True Vertical Depth Sub Sea (TVDSS). The TVDSS is defined as the vertical distance from a

point in the well to normal height null.  $Z_m$  is the measured depth (MD) and is the length measured along the wellbore. The depth is then converted into the rectilinear Gocad coordinate system  $(x, y, z)$  using the wellhead location and borehole orientation. Moreover, additional geologic information from Semenza' study have been acquired in order to improve the accuracy of the model. In particular, the horizontal band of cataclasite mapped by Semenza before 1963 (see chapt.2 paragraph 2.5), and marked as the northern boundary of the sliding surface, has been considered (

Figure 6. 3).

### **6.3 3D Surface construction**

Discretization is a fundamental process in 3D Gocad surface reconstruction. It is based on the following criteria:

1. the geometry of any object is defined by a finite set of nodes (points) in the 3D space
2. its topology is modeled by links bridging these nodes
3. Its physical properties are modeled as values attached to these nodes.. The location of nodes defining the objects in the 3D.

Indeed, the model describes any propriety objects as spatial coordinates and other continuous properties including structural property, such as surface' attitude, lithology, stratigraphic features etc.

All these properties in the model can be obtained by linear interpolation at any other point in the model space. The basic interpolation algorithm used from Gocad package is DSI (Discrete Smooth Interpolator; Mallet, 2002). DSI solves for the optimal location of the surface nodes to minimize a weighted sum of the surface roughness and the constraint . Constraint is a generic term to describe how data and interpretations are accounted for. Strict constraints restrict the degrees of freedom of surface nodes during the interpolation. (Cherpeau et al., 2011)

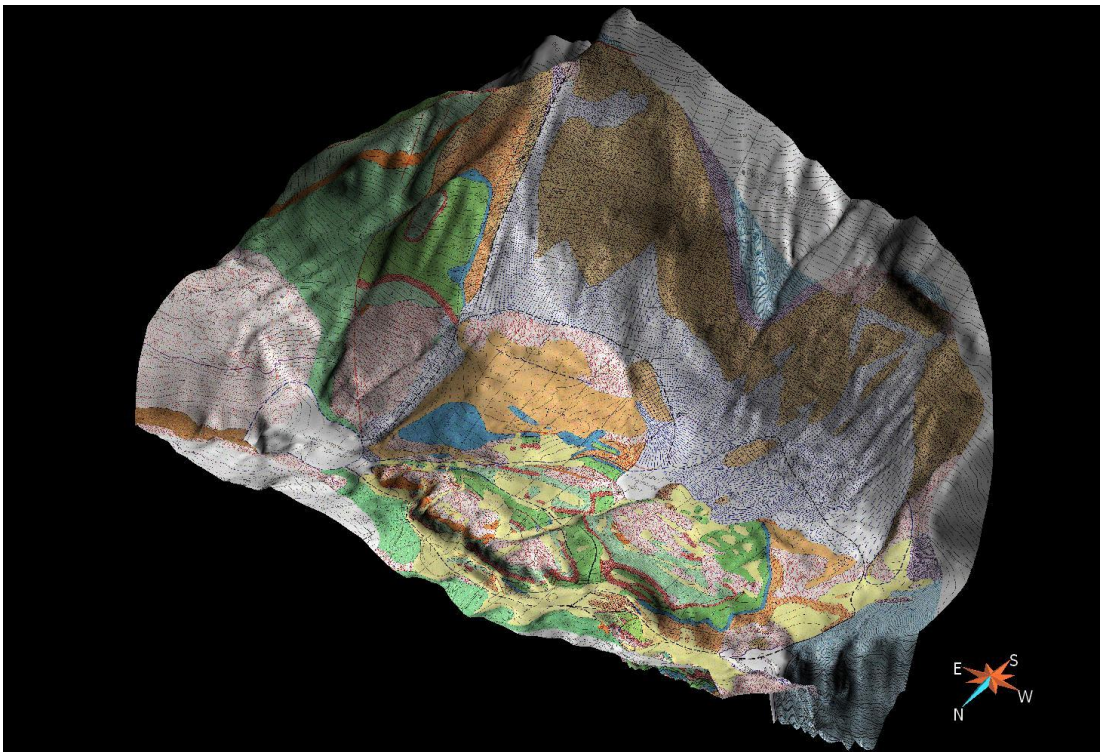
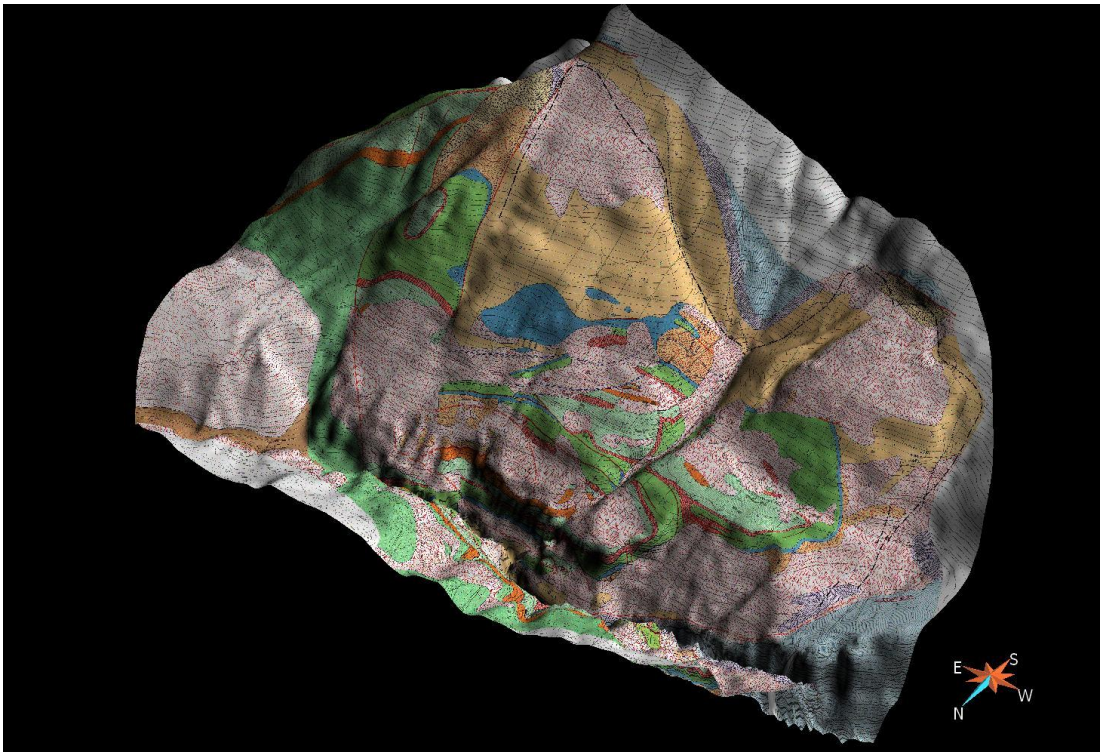


## 6.4 3D modeling of the Vajont surfaces

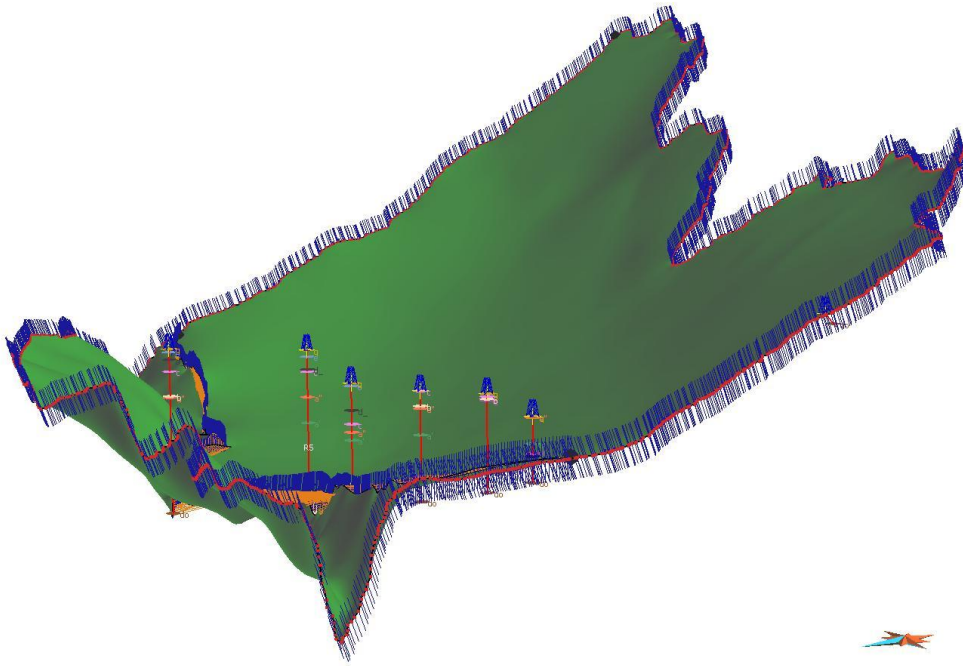
The model was reconstructed into two main steps. First the discontinuities have been interpolated with conventional "explicit" techniques. Then the stratigraphy has been modeled with an implicit approach, using the GRGPack plugin (Caumon et al., 2009; Massiot & Caumon. 2010). In explicit modeling the geological interfaces are represented as polygonal surfaces.(Lecour et al,2011)..

In the case of discontinuities, the data integrated in the model consist in: topography (either Lidar point cloud, or photogrammetry point cloud from pre-landslide aerial photos), surface geology (traces of main discontinuities from pre- and post-landslide 1:5.000 geological maps), and boreholes (constraining at depth the sliding surface, fig. 6.4). All these data have been introduced as control points in surfaces pinned to the branch lines which mark the intersections between different discontinuities. After DSI interpolation, a network of curved surfaces, which separate lens-shaped blocks, was reconstructed.

Implicit surface modeling was applied in a volume where the discontinuities have been introduced a-priori, allowing to independently model the stratigraphy within each block. The input data in this case have been traces of stratigraphic contacts (pre- and post-slide), structural data, including fold axes considered as in Massiot & Caumon. (2010), and borehole stratigraphy.



**Figure 6. 1** - Pre- and post-landslide geological maps (Semenza, 1965), draped on the pre- and post-slide topography.



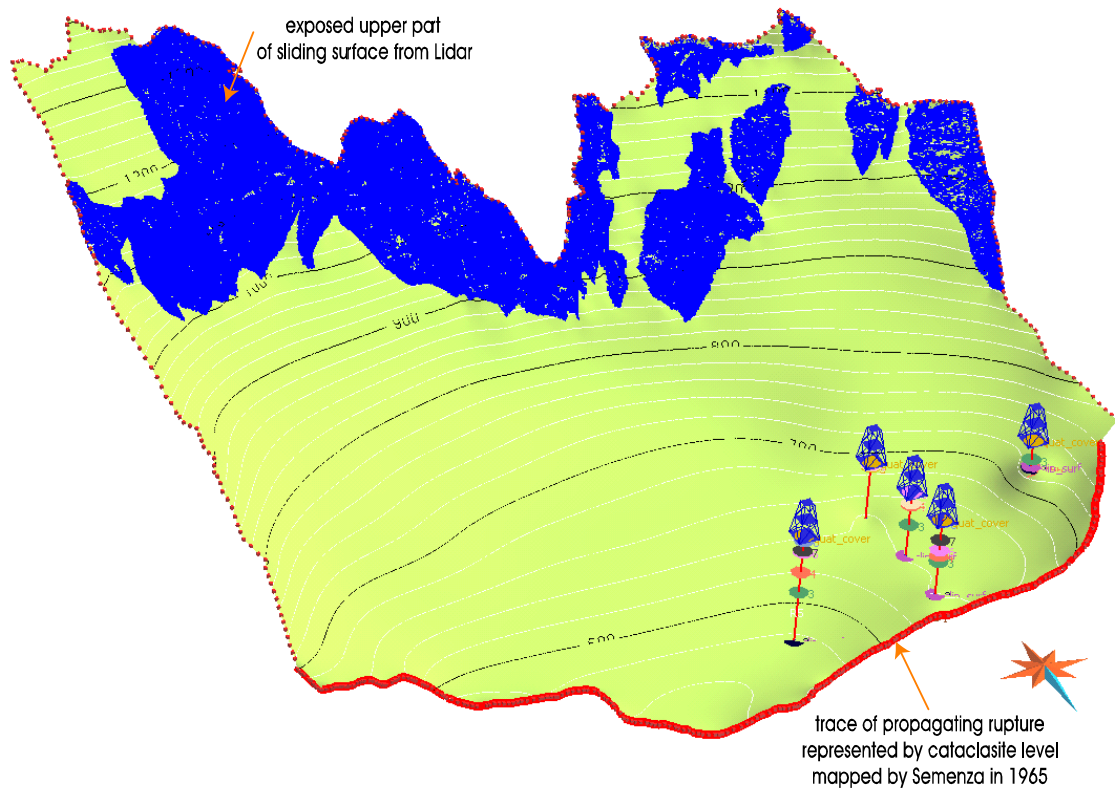
**Figure 6. 2** – Boreholes constrained of the Vajont sliding surface

## 6.5 kinematics blocks evaluation

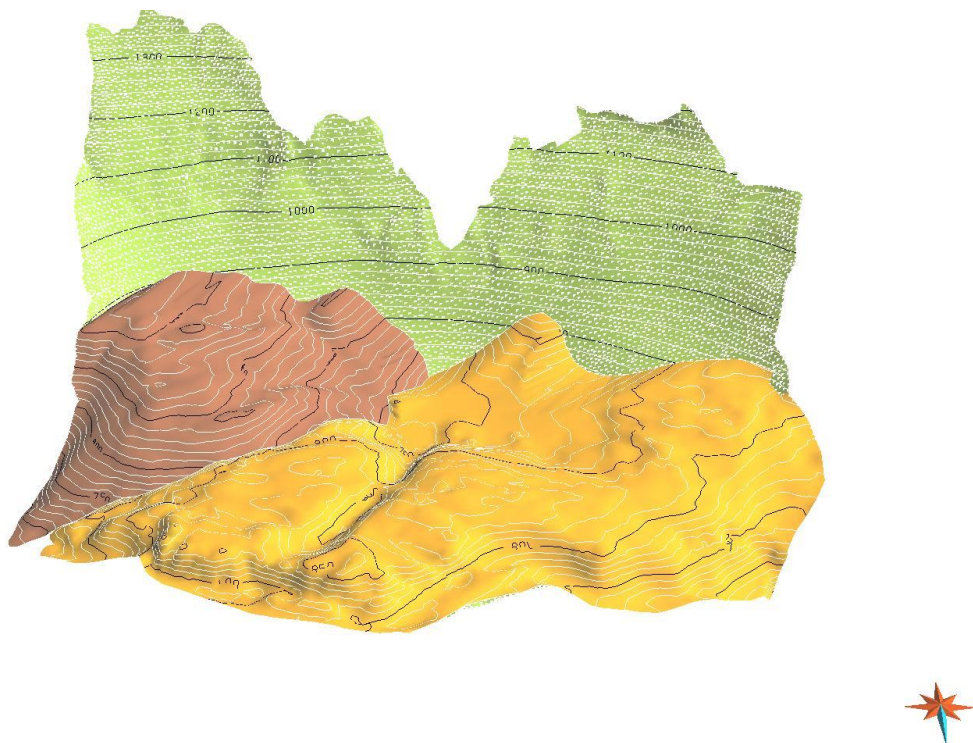
Due to the particular behavior of the landslide - a rock slide where large coherent blocks glided along a very localized basal slipping surface, the slide deposit is composed of a few large blocks where the original stratigraphy is preserved (Figure 6. 1). These blocks are separated one from each other by localized discontinuities, and from the bedrock by the main sliding surface (Figure 6. 4). This allowed us to reconstruct the stratigraphy within each block, which could be considered as a fault-bounded block in common 3D modeling terms, whilst the discontinuities are modeled as faults (sometimes they resemble low-angle faults).

In order to evaluate the rockslide kinematics, a retro-deformation study has been carried out. Having as a reference the pre-slide geological model the homologous points were detected (Figure 6. 5). Since the landslide mass is quite competent and continuous, basically composed of two main blocks The blocks were defined on the basis of stratigraphic continuity and morphological evidences acquired during the field survey and by mean remote sensing techniques.

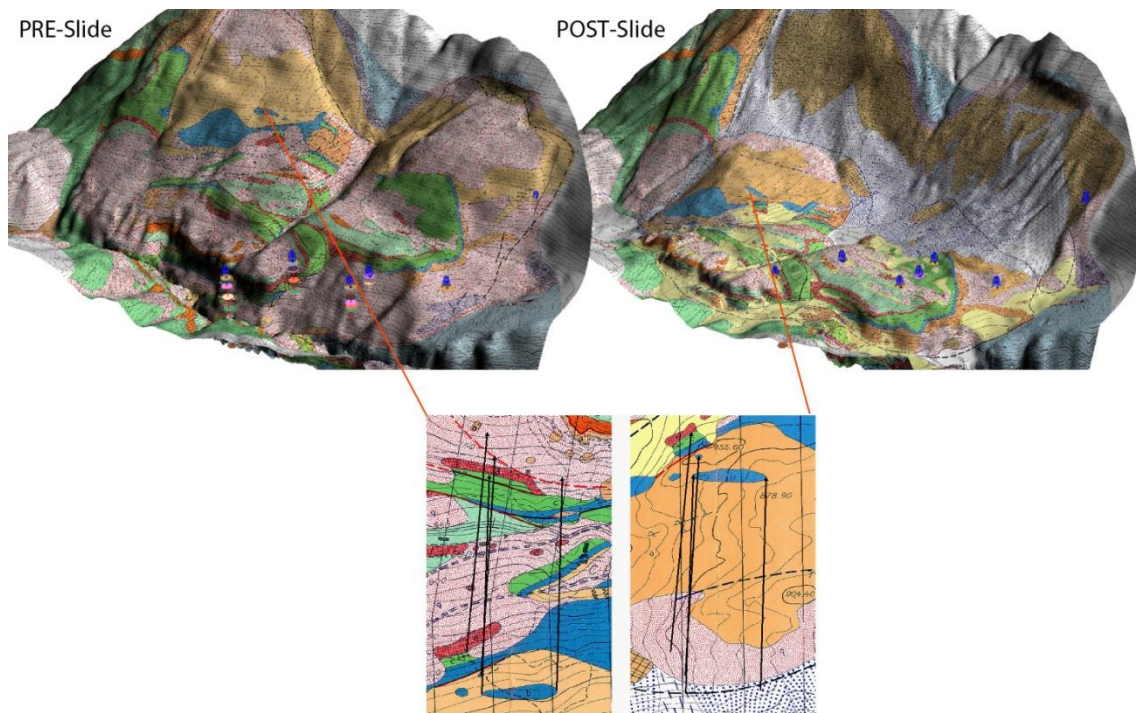
The constraints to the stratigraphy potential field are outcropping boundaries, borehole markers, orientation measurements, fold axes.



**Figure 6. 3** – Cataclasite level marked as the northern boundary of the sliding surface



**Figure 6. 4** – The two main rigid blocks glided along the sliding surface and constituting the rockslide deposit. Separate done each other by local discontinuity.



**Figure 6. 5** – Homologous points detected in pre and post geological landslide maps (Semenza,1965)

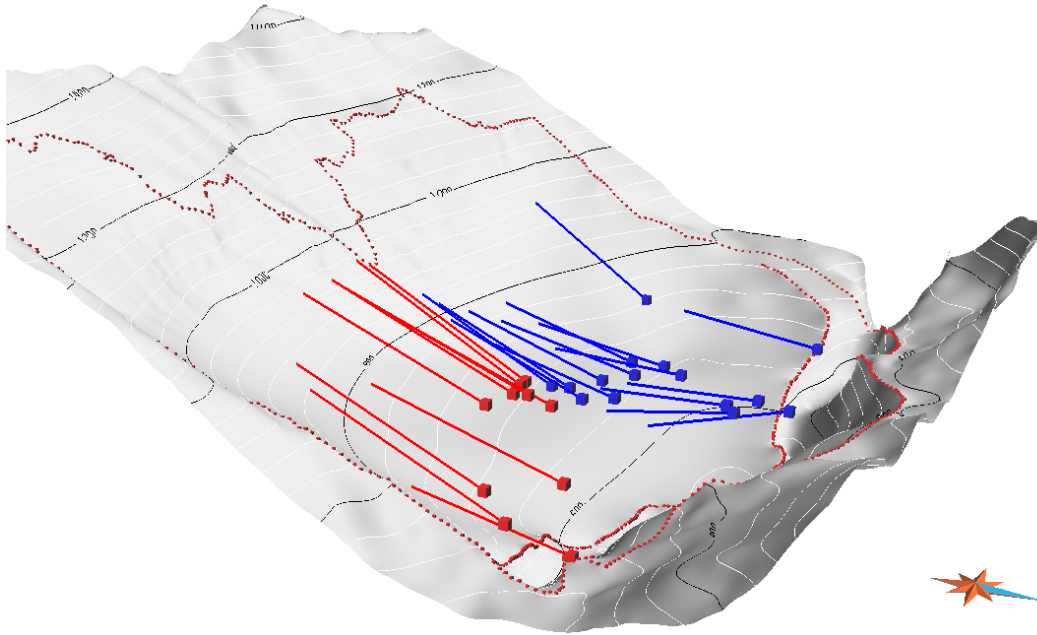
## 6.6 Results

The boreholes stratigraphy analyzed, constitute a solid constrains for the 3D model construction. Indeed they allowed to define the sliding surface depth and geometry more precisely than ever.

The geometric 3D model allowed us to straightforward constrain the rock volumes involved in the 1963 movement. Finally homologous points selected on the bases of pre and post-landslide geological maps, aerial photograph and DTMs were used to retrieve a kinematic model of the event showing two blocks with distinct slip amount and azimuth rotational component. Indeed, From the kinematics analysis of the blocks results that block B fell after on top of block A (

Figure 6. 6). As vectors direction showed block A presents a rotational component toward east and stopped in the gorge, the block B instead, not shows a relevant rotational component and stopped on block A. The table below show the distance and rotational component measured for each block.

BLOCK	Map distance	Azimuth
A	$361 \pm 12$ (m)	$8 \pm 3$ N
B	$463 \pm 12$ (m)	$3 \pm 2$ N



**Figure 6. 6** - Vector directions of two Vajont blocks . Blue vectors represent the block A and red vectors B.

## CONCLUSIONS

The Vajont rockslide represents a dramatic example of the inadequacy of investigations and poor knowledge of both methodological and technological skills necessary to understand the complex mechanics and dynamics of large rock slope instabilities.

Despite the many research investigations undertaken to date, the Vajont landslide continues to provide an engineering-geological case study of great scientific interest. Indeed, many contradictory statements and conclusions in the international literature on the Vajont landslide still remain.

To this purpose the main thesis objectives consisted of a re-evaluation of the geomorphological, structural and geomechanical features of the Vajont landslide, in order to reveal the importance of the highly three-dimensional character of the geological structures of the northern slope of Mount Toc.

Indeed the knowledge of the geometry and shape of the sliding plane, is therefore no doubt the priority aspect to be considered in any kind of approach to the Vajont, whether hydrogeological, or geomorphological and numerical modelling.

The innovative character of the re-evaluation consist of:

The creation of a GIS database collecting all existing (published and unpublished) and new acquisition data (bibliographic and spatial), making them available to the scientific community, and by the use of new methods and technologies not available in the 60's.

New techniques and technologies have been applied to investigate more in detail the mentioned features and to better understand their role in the 1963 event.

The increasing availability and precision of remote sensing techniques (DEM analyses, LIDAR technologies, photogrammetric analyses) integrated by field data surveys provided an accurate knowledge and in-depth evaluation of structural and geomechanical setting of the area.

The application of remote sensing techniques, as a powerful tool support, revealed a very useful instrument to obtain a homogenous data distribution (including inaccessible areas) in that way the morpho-structural features of the area have been better identified.

The identification of the interference fold systems of the Vajont landslide area represented by Erto (E-W) and Massalezza (N-S) syncline, marking a great part of the Vajont sliding surface

and constitutes a fundamental point to take in account for the evaluation of the rockslide kinematics.

This last aspect has been approached by different observation scales. On the one hand, the 3D geological model constructed with Gocad software allowed, on the basis of morphological and stratigraphic differences between pre and post landslide, to identify the rockslide blocks movement and their direction. On the other hand the collaborative research between Simon Fraser University (SFU) and the University of Padova aims to deep characterise the Vajont sliding surface through different point of view in order to achieve a complete overview of the geological factors affecting the slope and to improve the rockslide interpretation behaviour. The ongoing inspection of the sliding surface (it will be include in the Phd thesis of Mrs. A. Wolter), by photogrammetric models revealed both small- and large-scale roughness. The photogrammetric models allowed us to refine the domain boundaries detected by field and aerial photo analyses.

The geomechanical characterization of the rock-masses outcropping on the Vajont area (inside and outside the landslide) performed by both remote sensing analyses and traditional field surveys, allowed to identify the most significant parameters of the Vajont rock masses, that influenced the rockslide triggering and displacement, so helping in the comprehension of both the geomechanical and structural control on the slope deformations.

In particular the Coltop3D and photogrammetry were used to the joints sets identification and their possible correlation to regional tectonic structures.

The traditional geomechanical parameters such as Joint Compressive Strength, Joint Roughness Coefficient, Geological Strength Index, Point Load Test performed on 89 geomechanical stations allowed to evaluate the rock mass and the rock mass properties (geometric and mechanical) of each formation composing the stratigraphic sequence of the northern slope of Mount Toc.

The amount of data collected were applied to characterize the rock mass quality, through different classifications like: Rock Quality Designation (RQD) Rock Mass Rating System (RMR) and Slope Mass Rating (SMR). The implementation of laboratory test (Uniaxial and Triaxial) on Vajont rock samples completed the geomechanical characterization of the rock-masses.

Furthermore, the directly examination of the RODIO boreholes cores allowed to deep define the mechanical properties at a depth corresponding to the sliding surface.

The mechanical and elastic properties obtained in laboratory experiments were applied to constrain mechanical modeling of the landslide.



In order to determine the degree of correlation and variability of compressive strength of samples taken outside the landslide, the results performed between uniaxial compressive strength rock (measured uniaxial compressive strength) and corresponding results from the point load and Schmidt hammer tests (predicted uniaxial compressive strength) were compared.

Literature data showed that the ability to predict the compressive strength of rock using empirical equations is the best for low to medium strength, and becomes less reliable at higher strength (Cargill & Shakoor, 1990). The data plotted, show that considering the high values of measured uniaxial compressive strength of Vajont samples, the predicted data result less reliable.

A cross-correlation analysis was carried out to estimate linkage among rainfall and spring water discharge, conductivity and temperature. The results show clear karst behaviour within the springs, with a very short recharge circuit, since the time delay from the rainy event to the increase of the spring discharge is very short.

The knowledge of all geological features including the geometry and shape of the sliding plane, geometry and shape of minor structures, such as folds, cascades structures and steps, together with the rock mass characterization of all the lithological units involved in the movement, represent the starting point for any subsequent analyses and interpretation of the landslide.

## REFERENCES

- Alonso, E.E. and Pinyol, N.M. (2010). Criteria for rapid sliding I. A review of Vaiont case. *Engineering Geology*, **114** (3–4), 198–210.
- Alonso, E.E., Pinyol, N.M., Puzrin, A.M. (2010). Geomechanics of Failures. Advanced Topics. Berlin, Springer Verlag, 266 pp.
- Anderson, D.L. (1985). Calculation of slide velocities. In: *The Vaiont Slide, a Geo-technical analysis based on new geologic observations of the failure surface* (A.J. Hendron and F.D. Patton eds). 2, Appendix E and F, *Technical Report GL-85-5, U.S. Army Engineer Waterways Experiment Station, Vicksburg, MS*.
- ASTM (2008). Standard Practices for Preparing Rock Core as Cylindrical Test Specimens and Verifying Conformance to Dimensional and Shape Tolerances, D4543.
- ASTM (2010). Standard test method for compressive strength and elastic moduli of intact rock core specimens under varying states of stress and temperatures, D7012.
- Arthur, W., Snoke, J T. and Todd, V.R. (1998). Fault-related Photographic Atlas. Princeton University Press, 617 pp.
- Aydin, A. (2009). ISRM Suggested method for determination of the Schmidt hammer rebound hardness: Revised version. *International journal of Rock Mechanics and Mining Science*, **46** (3), 627–634.
- Bahat, D., Rabinovitch, A., and Frid, V. (2001). Fracture characterization of chalk in uniaxial and triaxial tests by rock mechanics, fractographic and electromagnetic radiation methods. *J. Structur. Geol.*, **23**, 1531-1547.
- Barton, N., Choubey, V. (1977). The shear strength of rock joints in theory and practice. *Rock Mechanics and Rock Engineering*, **54** (1), 1–54.
- Beer, A.J., Stead, D. and Coggan, J.S. (2002). A critical assessment of discontinuity roughness characterisation. *Journal of Rock Mechanics and Rock Engineering*, **35**, 65–74.
- Bellian, J.A., Kerans, C. and Jennette, D.D. (2005). Digital outcrop models: Applications of terrestrial scanning LIDAR technology in stratigraphic modeling. *Journal of Sedimentary Research*, **75** (2), 166–176.
- Belloni, L.G. and Stefani, R. (1987). The Vaiont slide: instrumentation - Past experience and the modern approach. *Engineering Geology*, **24** (1–4), 445–474.

- Bertotti, G., Picotti, V., Bernoulli, D. and Castellarin, A. (1993). From rifting to drifting: tectonic evolution of the South-Alpine upper crust from the Triassic to the Early Cretaceous. *Sedimentary Geology*, **86** 53–76.
- Bistacchi, A., Massironi, M. and Menegon, L. (2010). Three-dimensional characterization of a crustal-scale fault zone: The Pusteria and Sprechenstein fault system (Eastern Alps). *Journal of Structural Geology*, **32**, 2022–2041
- Bosa, S. and Petti, M. (2011). Shallow water numerical model of the wave generated by the Vajont landslide. *Environmental Modelling & Software*, **26** (4), 406–418.
- Bosellini, A. (1996). *Geologia delle Dolomiti*. Athesia, Bolzano, 1-192 pp.
- Bosellini, A., Masetti, D. and Sarti, M. (1981). A Jurassic “Tongue of the Ocean” infilled with oolitic sands: The Belluno Trough, Venetian Alps, Italy. *Marine Geology*, **44**, 59–95.
- Boyer, R.A. (1913). Etude géologique des environs de Longarone (Alpes Vénitiennes). *Bulletin de la Société géologique de France*, **13**, 451–485.
- Broch, E. and Franklin, J. A. (1972): The point load strength test. *International Journal of Rock Mechanics and Mining Sciences*, **9**, 669–697.
- Broili, L. (1967). New knowledge on the geomorphology of the Vaiont Slide slip surfaces. *Rock Mechanics and Rock Engineering*, **1**, 38–88.
- Caloi, P. (1966). L'evento del Vajont nei suoi aspetti geodinamici. *Annali di Geofisica*, XIX, **1**.
- Caloi, P. and Spadea, M.C. (1960). Serie di esperienze geosismiche eseguite in sponda sinistra a monte della diga del Vajont (dicembre 1959). *Unpublished technical report for S.A.D.E., Venezia, Italy*.
- Carlioni, G.C. and Mazzanti, R. (1964 a). Rilevamento geologico della frana del Vaiont. *Giornale di Geologia*, **XXXII** (1), 105–138.
- Carlioni, G.C. and Mazzanti, R. (1964 b). Aspetti geomorfologici della frana del Vaiont. *Rivista Geografica Italiana*, **71** (3), 201–231.
- Castellarin, A. and Cantelli, L. (2000). Neo-Alpine evolution of the Southern Eastern Alps. *Journal of Geodynamics*, **30**, 251–274.
- Caumon, G., Collon-Drouaillet, P., Le Carlier de Veslud, C., Viseur, S., and J. Sausse (2009). Teacher's aide: Surface-based 3D modeling of geological structures. *Math Geosciences*, **41**: 927–945
- Chowdhury, R. (1978). Analysis of the Vaiont slide - New approach. *Rock Mechanics*, **11**, 29–38.

- Ciabatti, M. (1964). La dinamica della frana del Vaiont. *Giornale di Geologia*, **XXXII** (I), 139–154.
- Cobianchi, M. and Picotti, V. (2003). The Vaiont gorge section: the Toarcian to Bajocian Igne Formation and the Unconformable base of the Vaiont Limestone. In *General Field Trip Guidebook, 6th International Symposium on the Jurassic System* (M. Santantonio ed). Palermo, Italy, pp. 310–312.
- Corbyn, J.A. (1982). Failure of a partially submerged rock slope with particular references to the Vaiont rock slide. *International Journal of Rock Mechanics and Mining Sciences & Geomechanics Abstracts*, **19**, 99 –102.
- Crosta, G.B., and Agliardi, F. (2003). Failure forecast for large rock slides by surface displacement measurements. *Canadian Geotechnical Journal*, **40** (1), 176–191.
- Dal Piaz, G. (1928). Relazione di massima su due sezioni del Vajont prese in considerazione per progetti di sbarramento idraulico. *Unpublished technical report for S.A.D.E.*, Venezia, Italy.
- Dal Piaz, G., Bistacchi, A. and Massironi, M. (2003). Geological outline of the Alps. *Episodes*, **26**, 3, 175–180.
- Deere, D .U., and Miller, R. P. (1966). Engineering classification and index properties of rock. *Technical Report n. AFNL-TR-65-116* Air Force Weapons Laboratory, New Mexico
- Derron, M.H.; Jaboyedoff, M.; Blikra, L. H. (2005). *Natural Hazards and Earth System Sciences*, **5**, 285–292.
- Doglionni, C. (1990). Thrust Tectonic examples from the Venezia Alps. *Studi Geologici Camerti*, 117–129.
- Erismann, T. H. and Abele, G. (2001). *Dynamics of Rockslides and Rockfalls*. Berlin, Springer Verlag, pp. 316.
- Ferri, F., Di Toro, G., Hirose, T. and Shimamoto, T. (2010), Evidence of thermal pressurization in high-velocity friction experiments on smectite-rich gouges. *Terra Nova*, **22**, 347–353.
- Frattini, M., Arredi, F., Boni A., Fasso, C. and Scarsella, F. (1964). Relazione sulle cause che hanno determinato la frana nel serbatoio del Vajont (9 Ottobre 1963). *Frattini Commission Report prepared for ENEL*. Roma, pp. 92.
- Fukuzono, T. (1985). A new method for predicting the failure time of a slope. In *Proceedings of the fourth international conference and field workshop on landslides*, Tokyo: Japan Landslide Society; 145–50.

- Genevois, R. and Ghirotti, M. (2005). The 1963 Vaiont Landslide. *Giornale di Geologia Applicata*, **1**, 41–52.
- Gercek, H. (2007). Poisson's ratio values for rocks. *Int. J. Rock Mech. Min. Sci.*, **44**, 1-13.
- Ghirotti, M. (1994). Modellazione numerica della frana del Vajont sulla base di nuovi dati. *Geologica Romana*, **30**, 208–216.
- Ghirotti, M. (2006). Edoardo Semenza: the importance of geological and geomorphological factors for the identification of the ancient Vaiont landslide. In *Landslide from Massive Rock Slope Failure* (S.G. Evans, G. Scarascia Mugnozza, A. Strom and R.L. Hermanns eds). NATO Science Series 2003, Dordrecht, The Netherlands, Kluwer Academic Publisher, 395–406.
- Ghirotti, M. and Genevois, R., 2007. A complex rock slope failure investigated by means of numerical modelling based on laser scanner technique. In *Proceedings: 1st Canada-US Rock Mechanics Symposium*, May 27-31, Vancouver, 917-924.
- Ghirotti, M. and Semenza, E. (2000). History of 1963 Vaiont Slide. The importance of the geological factors to recognize the ancient landslide. *Bulletin of Engineering Geology and the Environment*, **59**, 87–97.
- Giudici, F. and Semenza, E. (1960). Studio geologico del serbatoio del Vajont. *Unpublished report for S.A.D.E.*, Part A: 21 pp, text, Part B: 68 photos with discussions, 42 pp. Venezia, Italy.
- Gosh, D., K. and Srivastava. M., (1991). Point load strength: an index for classification of rock material. *International Association for Engineering Geology*, **44**, 27-33.
- Habib, P. (1967). Sur un mode de glissement des massifs rocheux. *Comptes Rendus des Seances de l'Academie des Sciences. Serie D, Sciences Naturelles*, **264**, 151–153.
- Habib, P. (1975). Production of gaseous pore pressure during rock slides. *Rock Mechanics*, **7**, 193–197.
- Hawkins, A. B. (1998). Aspects of rock strength. *Bull. Eng. Geol. Environ.*, **57**, 17-30.
- Haecker, M.A. (1992). Convergent gridding: a new approach to surface reconstruction. *Geobyte*, **7** (3), 48–53.
- Helmstetter, A., Sornette, D., Grasso, J.-R., Andersen J.V., Gluzman S., and Pisarenko, V. (2004). Slider block friction model for landslides: Application to Vaiont and La Clapière landslides. *Journal of Geophysical Research*, **109**, B02409, doi:10.1029/2002JB002160.

- Hendron, A.J. and Patton, F.D. (1985). The Vaiont Slide, a Geotechnical Analysis Based on New Geologic Observations of the Failure Surface. *Technical Report GL-85-5, U.S. Army Engineer Waterways Experiment Station, Vicksburg, MS. I, II.*
- Hoek, E. and Brown, E.T. (1980). Underground excavations in Rock. Institute of Mining and Metallurgy. *Stephen Austin and Sons Ltd., Hertford, London*, p. 527
- Hoek, E. and Bray, J.W. (1991). Rock Slope Engineering. New York, *Elsevier Science Publishing*, 358 pp.
- Hoek, E. and Brown, E.T. (1997). Practical estimates of rock mass strength. *Intl. J. Rock Mech. & Mining Sci. & Geomechanics Abstracts*. **34**(8), 1165-1186
- Hoek E., and Franklin J. A. (1968), Simple triaxial cell for field or laboratory testing of rock. *Trans. Inst. Min. Metall.* **77**, A22 (Section A).
- Hutchinson, J.N. (1987). Mechanisms producing large displacements in landslides on pre-existing shears. In *Proceedings of the 1st Sino-British Geological Conference*, Taipei, Geological Memoirs. Geological Survey of China, **9**, 175–200.
- Hutchinson, J.N. (2001). Landslide risk – to know, to foresee, to prevent. *Geologia Technica e Ambientale*, **3**, 3–22.
- Jaboyedoff, M. and Couture, R., 2003. Report on the project COLTOP3D for March 2003: stay of Michel Jaboyedoff at GSC – Ottawa. Technical report Quanterra, Lausanne.
- Jaboyedoff, M., Metzger, R., Oppikofer, T., Couture, R., Derron, M.H., Locat, J. and Turmel, D. (2007). New insight techniques to analyze rock-slope relief using DEM and 3D-imaging cloud points: COLTOP-3D software. In *Rock mechanics: Meeting Society's Challenges and demands* (E. Eberhardt, D., Stead and T., Morrison eds), Taylor & Francis, 61–68.
- Jäger, C. (1965 a). The Vaiont rockslide, Part 1. *Water Power*, **3**, 110–111.
- Jäger, C. (1965 b). The Vaiont rockslide, Part 2. *Water Power*, **4**, 142–144.
- Jäger, C. (1972). The Vaiont slide. In *Rock Mechanics and Engineering* (C. Jäger ed). Cambridge, *University Press*, pp. 340–361.
- Kenney, T.C. (1967). Stability of the Vajont valley slope, discussion of paper by L. Müller (1964) on the rock slide in the Vajont valley. *Rock Mechanics*, **5** (5), 10–16.
- Kiersch, G.A. (1964). Vaiont reservoir disaster. *Civil Engineering*, **34** (3), 32–39.
- Kiersch, G.A. (1965). Vaiont reservoir disaster. *Geotimes*, May–June, 9–12.
- Kilburn, C.R.J. and Petley, D.N. (2003). Forecasting giant, catastrophic slope collapse: lessons from Vajont, Northern Italy. *Geomorphology*, **54** (1–2), 21–32.

- Holzhausen, G. R., and Johnson, A. M. (1979). Analysis of longitudinal splitting of uniaxially compressed rock cylinders. *Int. J. Rock Mech. Min. Sci. Geomec. Abst.*, **16**, 163-177.
- Leonards, G.A. (1987). Dam failures. *Engineering Geology*, **24** (1-4), 1-577.
- Lo, K.Y., Lee, C.F. and Gelinas, P. (1972). Alternative Interpretation of the Vaiont slide. In *Stability of Rock Slopes* (E.J. Cording ed). Proceedings of the 13th Symp. on Rock Mechanics, University of Illinois, Urbana, 1971, New York; ASCE, 595-623.
- Mallet JL (2002). *Geomodeling. Applied Geostatistics*. New York, Oxford University Press, 624 pp.
- Mantovani, F. and Vita-Finzi, C. (2003). Neotectonics of the Vajont dam site. *Geomorphology*, **54** (1-2), 33-37.
- Martinis, B. (1979). Contributo alla stratigrafia dei dintorni di Erto-Casso (Pordenone) ed alla conoscenza delle caratteristiche strutturali e meccaniche della frana del Vajont. *Memorie di Scienze Geologiche*, Università di Padova, **32**, 1-33
- Masè, G., Semenza, M., Semenza, Pa., Semenza. P. and Turrini, MC. (2004). Le foto della frana del Vajont, Ferrara, ed. K-flash. 1-47, 3 maps, CD-ROM with 300 photos.
- Mencl, V. (1966). Mechanics of landslides with non-circular slip surfaces with special reference to the Vaiont slide. *Géotechnique*, **XVI** (4), 329-337.
- Mogi, K. (2006). *Experimental Rock Mechanics*. CRC Press. Print ISBN: 978-0-415-39443-7
- Müller, L. (1961). Talsperre Vaiont – 15° Baugeologischer Bericht: Die Felsgleitung im Bereich Toc. *Unpublished technical Report for S.A.D.E.*, Venezia, Italy.
- Müller, L. (1964). The Rock slide in the Vaiont valley. *Rock Mechanics and Engineering Geology*, **2**, 148-212.
- Müller, L. (1968). New considerations on the Vaiont slide. *Rock Mech. Eng. Geol.*, **6** (1-2), 1-91.
- Müller, L. (1987 a). The Vaiont catastrophe – A personal review. *Engineering Geology*, **24** (1-4), 423-444.
- Müller, L. (1987 b). The Vaiont slide. *Engineering Geology*, **24** (1-4), 513-523.
- Niedzielsk, T., Migoń, P. and Placek, A. (2009). A minimum sample size required from Schmidt hammer measurements. *Earth Surface Processes and Landforms*, **34**,13, 1713-1725.
- Nonveiller, E. (1967). Shear strength of bedded and jointed rock as determined from the Zalesina and Vaiont slides. In *On shear strength properties of natural soils and rocks*. Proceedings of the Geotechnical Conference, Oslo, 1967, 289-294.

- Nonveiller, E. (1987). The Vaiont reservoir slope failure. *Engineering Geology*, **24** (1–4), 493–512.
- Nonveiller, E. (1992). Vaiont slide – Influence of frictional heat on slip velocity. In *Proceedings of the meeting on the 1963 Vaiont landslide* (E. Semenza E. and G. Melidoro eds.). IAEG Italian Section, University of Ferrara, Ferrara 1986, **1**, 187–197.
- Oppikofer, T., Jaboyedoff, M., Blikra, L., Derron, M.-H. and Metzger, R. (2009). Characterization and monitoring of the Åknes rockslide using terrestrial laser scanning. *Natural Hazards and Earth System Sciences*, **9**, 1003-1019
- Palchik, V. (2011). On the Ratios between Elastic Modulus and Uniaxial Compressive Strength of Heterogeneous Carbonate Rocks. *Rock Mech. Rock Eng.*, **44**, 121–128
- Palmstrom, A. (2001). In-Situ Characterization of rocks. Editors: V.M. Sharma and K.R. Saxena A. Balkema Publishers Lise / Abingdon / Exton (Pa) / Tokio
- Panizzo, A., De Girolamo, P., Di Risio, M., Maistri, A., and Petaccia, A. (2005). Great landslide events in Italian artificial reservoirs. *Natural Hazards and Earth System Sciences*, **5** (5), 733–740.
- Pastor, M., Herreros, I., Fernández Merodo, J.A., Mira, P., Haddad, B., Quecedo, M., González, E., Alvarez-Cedrón, C. and Drempevic, V. (2009). Modelling of fast catastrophic landslides and impulse waves induced by them in fjords, lakes and reservoirs. *Engineering Geology*, **109** (1–2), 124–134.
- Pedrazzini, A., Jaboyedoff, M., Corey, R., Froese, C., Willem Langenberg, C. and Moreno, F. (2011). Structural analysis of the Turtle Mountain: origin and influence of fractures in development of rock slope failures. In *Slope Tectonics* (M. Jaboyedoff ed). Geological Society Special Publications, **351**, 163-183.
- Pellegrini, G.B., Surian N. and Albanese D., (2006). Landslide activity in response to alpine deglaciation: the case of the Belluno Prealps (Italy). *Geografia Fisica e Dinamica Quaternaria*, **29**, 185–196.
- Petley, D.N. and Petley, D.J. (2004). On the initiation of large rockslides; perspectives from a new analysis of the Vaiont movement record. In *Landslides from Massive Rock Slope Failures* (S.G. Evans, G. Scarascia-Mugnozza, A.L. Strom, and R.L. Hermanns eds). NATO Science Series 2003, Dordrecht, The Netherlands, Kluwer Academic Publisher, 77–84.
- Pinyol, N.M. and Alonso, E.E, (2010). Criteria for rapid sliding II. Thermo-hydro-mechanical and scale effects in Vaiont case. *Engineering Geology*, **114** (3–4), 211–227.



- Piteau D.R. (1973). Characterizing and extrapolating rock joint properties in engineering practice. *Rock Mechanics*, **2**, 5–31.
- Priest, S.D. (1993). Discontinuity analysis for rock engineering. London, Chapman and Hall, 473pp.
- Riva, M., Besio, M., Masetti, D., Roccati, F., Sapigni, M. and Semenza, E. (1990). La geologia delle valli Vaiont e Gallina (Dolomiti orientali). *Annali dell'Università di Ferrara, Sezione Scienze della Terra*, **2** (4), 55–76.
- Rose, N.D. and Hungr, O. (2007). Forecasting potential rock slope failure in open pit mines using the inverse-velocity method. *International Journal of Rock Mechanics and Mining Sciences*, **44** (2), 308–320.
- Rossi, D. and Semenza, E. (1965). Carte geologiche del versante settentrionale del M. Toc e zone limitrofe, prima e dopo il fenomeno di scivolamento del 9 ottobre 1963, Scala 1:5000. Istituto di Geologia, Università di Ferrara, 2 Maps.
- Roubtsova, V. and Kahawita, R. (2006). The SPH technique applied to free surface flows. *Computers & Fluids*, **35** (10), 1359–1371.
- Saito, M. (1965). Forecasting the time of occurrence of slope failure. In *Proceedings of the 6<sup>th</sup> International Conference on Soil Mechanics and Foundation Engineering*, Montréal, University of Toronto Press, Toronto, **2**, 537–542.
- Saito, M. (1969). Forecasting time of slope failure by tertiary creep. In *Proceedings of the 7<sup>th</sup> International Conference on Soil Mechanics and Foundation Engineering*, Mexico City. Rotterdam, Balkema, **2**, 677–683.
- Selli, R. and Trevisan, L. (1964). Caratteri e interpretazione della Frana del Vajont. *Giornale di Geologia*, serie 20, **XXXII** (I), 8–104.
- Selli, R., Trevisan, L., Carloni C.G., Mazzanti, R. and Ciabatti, M. (1964). La Frana del Vajont. *Giornale di Geologia*, serie 20, **XXXII** (I), 1–154.
- Semenza, E. (1965). Sintesi degli studi geologici sulla frana del Vaiont dal 1959 al 1964. *Memorie del Museo Tridentino di Scienz. Naturali*, **16**, 1–52.
- Semenza, E. (2000) La storia del Vaiont raccontata dal geologo che ha scoperto la frana, Tecomproject Ed., Ferrara, Italia, 280 pp.
- Semenza, E. (2010). The Story of Vaiont Told by the Geologist Who Discovered the Landslide, K-flash Ed., pp. 205. <http://www.k-flash.it>
- Semenza, E. and Ghirotti, M. (1998). Vaiont–Longarone 34 anni dopo la catastrofe. *Annali dell'Università di Ferrara (Nuova Serie), Sezione Scienze della Terra*, **7** (4), 63–94.

- Semenza, E. and Ghirotti, M. (2000). History of 1963 Vaiont Slide. The importance of the geological factors to recognise the ancient landslide. *Bulletin of Engineering Geology and the Environment*, **59**, 87–97.
- Semenza, E. and Melidoro, G. (1992). *Proceedings of the meeting on the 1963 Vaiont landslide*. IAEG Italian Section, University of Ferrara, Ferrara 1986, **1**, 218 pp.
- Sibson R.H. (1977). Fault rocks and fault mechanisms. *Journal of the Geological Society*, **133**, 191–213.
- Sitar, N. and MacLaughlin, M.M. (1997). Kinematics and discontinuous deformation analysis of landslide movement. In *Proceedings II Pan American Symposium on Landslide*, Rio de Janeiro, Brazil, 65–73.
- Sitar, N.M., MacLaughlin, M.M. and Doolin, D.M. (2005). Influence of kinematics on landslide mobility and failure mode. *Journal of Geotechnical and Geoenvironmental Engineering*. ASCE, **131** (6), 716–728.
- Skempton, A.W. (1966). Bedding-plane slip, residual strength and the Vaiont landslide. *Géotechnique*, **XVI** (1), 82–84.
- Sornette, D., Helmstetter, A., Andersen J.V., Gluzman, S., Grasso, J.R. and Pisarenko, V. (2003). Towards landslide predictions: two case studies. *Physica A*, **338** (3–4), 605–632.
- Sterlacchini, S., Salvi, F., Sironi, S. & Zanchi, A. (2008) Ricostruzioni geologiche tridimensionali: metodologie ed esempi di applicazioni. *Memorie Descrittive della Carta Geologica d'Italia*. **78**, 277-288.
- Sturzenegger, M., Sartori, M., Jaboyedoff, M. and Stead, D. (2007). Regional deterministic characterization of fracture networks and its application to GIS-based rock fall risk assessment. *Engineering Geology*, **94**, 201–214.
- Superchi, L., Floris, M., Ghirotti, M., Genevois, R., Jaboyedoff, M. and Stead, D. (2010). Implementation of a geodatabase of published and unpublished data on the catastrophic Vaiont landslide. *Natural Hazards and Earth System Sciences*, **10**, 865–873.
- Superchi, L., Wolter, A., Stead, D., Clague, J.J., Ghirotti, M. and Genevois, R. (2011). Comparison of photogrammetric and field survey data from the sliding surface of the 1963 Vajont Slide, Italy, *Geophysical Research Abstracts*, **13**, EGU2011-1632, EGU General Assembly 2011.
- Tika, Th.E. and Hutchinson, J.N. (1999). Ring shear tests on soil from the Vaiont landslide slip surface. *Geotechnique*, **49** (1), 59–74.
- Trollope, D.H. (1980). The Vaiont slope failure. *Rock Mechanics*, **13**, 71–88.

- Palchik, V. (2011). On the Ratios between Elastic Modulus and Uniaxial Compressive Strength of Heterogeneous Carbonate Rocks. *Rock Mech. Rock Eng.*, **44**: 121–128
- Van Westen, C. J. (2004). Geo-information tools for landslide risk assessment: an overview of recent developments, in: *Landslides Evaluation and stabilization* (W. A. Lacerda, M. Ehrlich, A. B. Fontoura, and A. Sayo eds). Balkema, 39–56.
- Vardoulakis, I. (2002). Dynamic thermo-poro-mechanical analysis of catastrophic landslides. *Geotechnique*, **52** (3), 157–171.
- Veveakis, E., Vardoulakis, I. and Di Toro, G. (2007). Thermoporomechanics of creeping landslides: the 1963 Vaiont slide, northern Italy. *Journal of Geophysical Research*, **112**, F03026. doi:10.1029/2006JF000702.
- Voight, B. (1988). A method for prediction of volcanic eruptions. *Nature*, **332**, 125–130.
- Voight, B. (1989). Materials science law applies to time forecasts of slope failure. *Landslide News* **3**, 8–11.
- Voight, B. and Faust, C. (1982). Frictional heat and strength loss in some rapid slides. *Geotechnique*, **32** (1), 43–54.
- Ward, S.N. and Day, S. (2011). The 1963 Landslide and Flood at Vaiont Reservoir Italy. A tsunami ball simulation. *Italian Journal of Geosciences (Bollettino della Società Geologica Italiana)*, **130** (1), 16–26.
- Wolter, A., Superchi, L., Stead, D., Clague, J., Genevois, R. and Ghirotti, M. (2011). Preliminary results of a photogrammetric characterisation of the 1963 Vajont rockslide. In *Geohazards 5th Canadian Conference on Geotechnique and Natural Hazards*, Kelowna, B.C., Canada, 9
- Superchi, L., Bistacchi, A., Massironi, M. (2011). 3D modeling of the catastrophic 1963 Vaiont landslide (N Italy) with implicit surface methods: pre- and post-slide models. 31<sup>th</sup> Gocad Meeting. 7-10 June 2011 Nancy (France)

## ***APPENDIX A***

## Technical Note: Implementation of a geodatabase of published and unpublished data on the catastrophic Vaiont landslide

L. Superchi<sup>1</sup>, M. Floris<sup>1</sup>, M. Ghirotti<sup>2</sup>, R. Genevois<sup>1</sup>, M. Jaboyedoff<sup>3</sup>, and D. Stead<sup>4</sup>

<sup>1</sup>Dept. of Geosciences, University of Padova, Italy

<sup>2</sup>Dept. of Earth and Geo-Environmental Sciences, University of Bologna, Italy

<sup>3</sup>Institute of Geomatics and Risk Analysis (IGAR), University of Lausanne, Switzerland

<sup>4</sup>Dept. of Earth Sciences, Simon Fraser University, Burnaby, Canada

Received: 9 November 2009 – Revised: 5 March 2010 – Accepted: 23 March 2010 – Published: 20 April 2010

**Abstract.** On 9 October 1963 a catastrophic landslide suddenly occurred on the southern slope of the Vaiont dam reservoir. A mass of approximately 270 million m<sup>3</sup> collapsed into the reservoir generating a wave that overtopped the dam and hit the town of Longarone and other villages nearby. Several investigations and interpretations of the slope collapse have been carried out during the last 45 years, however, a comprehensive explanation of both the triggering and the dynamics of the phenomenon has yet to be provided.

In order to re-evaluate the currently existing information on the slide, an electronic bibliographic database and an ESRI-geodatabase have been developed. The chronology of the collected documentation showed that most of the studies for re-evaluating the failure mechanisms were conducted in the last decade, as a consequence of knowledge, methods and techniques recently acquired. The current contents of the geodatabase will improve definition of the structural setting that influenced the slide and led to the propagation of the displaced rock mass.

The objectives, structure and contents of the e-bibliography and Geodatabase are indicated, together with a brief description on the possible use of the alphanumeric and spatial contents of the databases.

### 1 Introduction

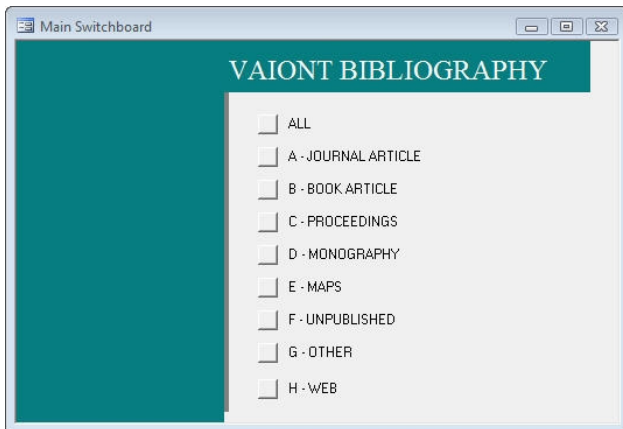
The Vaiont landslide (Fig. 1) is considered to represent a natural laboratory in which to investigate failure mechanisms and evolution in large rock masses. The catastrophic 1963 landslide demonstrated the paramount importance of detailed geologic investigations. Geological, structural, geomorphological, hydrogeological and geomechanical features at Vaiont are being re-analysed using new methods and techniques, such as photogrammetric analyses, terrestrial and aerial laser scanning data acquisition and interpretation, topographic DEM analyses, rock mass characterisation and numerical 3-D modelling. Despite that, to date, considerable research has been carried out, the Vaiont landslide continues to provide an engineering case study of both high scientific interest and significant technological challenges. The first detailed geological studies were carried out by Giudici and Semenza (1960), who emphasized the existence of a huge pre-historic landslide on the reservoir mountainside, which could be remobilized in the presence of the planned reservoir. Subsequently, following nearly 3 years of intermittent and slow slope movements, a rock mass of about 270 million m<sup>3</sup> suddenly collapsed into the reservoir, generating a huge wave that hit the town of Longarone and other villages, killing almost 2000 people. Several interpretations of this event have been proposed during the last 45 years (e.g., Müller, 1964, 1987a, b; Selli et al., 1964; Skempton, 1966; Hendron and Patton, 1985; Semenza, 2000). Some authors have attempted to explain the sudden acceleration of the mass in some cases suggesting varied mechanisms (Nonveiller, 1992; Tika and Hutchinson, 1999; Kilburn and Petley, 2003). Nevertheless, a comprehensive explanation of both the triggering and



Correspondence to: L. Superchi  
(laura.superchi@unipd.it)



**Fig. 1.** Panoramic view of the slip surface of the Vaiont landslide that occurred on 9 October 1963.



**Fig. 2.** Main switchboard of the electronic bibliographic database.

dynamics of the phenomenon still remains elusive. The most comprehensive work to date was undertaken by Hendron and Patton (1985) who concluded by emphasising the need for continued and more in depth research. A complete review of the most important papers related to the 1963 landslide is presented in Genevois and Ghirotti (2005).

In this paper, the authors describe the structure and contents of recently developed alphanumeric and spatial databases on the Vaiont landslide. The potential use of these databases in a re-evaluation of the landslide mechanics and dynamics, utilizing current knowledge on rock slides and state-of-the-art methods of data acquisition and numerical

modelling is briefly discussed. In addition, all the references to published documents, theses and unpublished technical reports on the Vaiont landslide have been organized and stored in a database and are provided as Supplementary Material (<http://www.nat-hazards-earth-syst-sci.net/10/865/2010/nhess-10-865-2010-supplement.pdf>).

## 2 The electronic-bibliographic database

The catastrophic Vaiont landslide has stimulated and generated a significant volume of research, however, most of the available documentation owing to the time at which it was produced is in a non-electronic format. Hence, the first extremely important step was to scan digitally all documentation on the landslide. All the references to published documents, theses, unpublished technical reports and maps on landslide, have subsequently been organized and stored in a database using MS Access software.

The references are contained in a main table and are divided, on the basis of document typology, into Journal article (A), Book article (B), Proceedings (C), Monography (D), Maps (E), Unpublished (F), Other (G), and Web (H), (Fig. 2). Input masks to queries that extract the relevant information for each typology, were created to help in storing and visualizing data (Fig. 3a, b). In order to facilitate data retrieval, all the masks include local (field “LOCAL LINK”) and/or internet (field “LINK”) connections to documents available in a local directory or on a web site. A further important database field is termed “NOTE” where the presence in the

**A - JOURNAL ARTICLE**

ID: A024  
 DOI: 10.1016/0013-7952(87)90080-9  
 KEYWORDS: Failure mechanics, fluid, geology, [taly, landslide, groundwat  
 AUTHOR/S: Handron A.J. & Patton F.D.  
 YEAR: 1985  
 TITLE: The Vaiont Slide, A Geotechnical Analysis Based on New Geologic Observations of the Failure Surface  
 JOURNAL: ENGINEERING GEOLOGY  
 NOTE: Contain sperimental data  
 VOLUME: 24  
 PAGES: 473-491  
 LINK: [http://www.sciencedirect.com/science?\\_ob=PublicationURL&\\_method=list&\\_tockey=%23toc%235768%231988](http://www.sciencedirect.com/science?_ob=PublicationURL&_method=list&_tockey=%23toc%235768%231988)  
 LOCAL LINK: PDF\Handron & Patton [1985]\_The Vaiont Slide, A Geotechnical Analysis Based on New Geologic

Record: 24 di 80

---

**B - BOOK ARTICLE**

ID: B002  
 DOI: 10.2495/DEB060251  
 KEYWORDS: Vaiont slide, multi-block model, residual soil strength  
 AUTHOR/S: Stamatopoulos C. & Aneroussis S.  
 YEAR: 2006  
 TITLE: Back analysis of the Vaiont slide using a multiblock sliding model  
 NOTE: Transactions of the Wessex Institute: Ecology and the Environment  
 BOOK AUTHOR/S:  
 BOOK TITLE: Monitoring, Simulation, Prevention and Remediation of Dense and Debris Flows  
 BOOK EDITOR/S: G. LORENZINI, C.A. BREBBIA, and D. EMMANOULOUDIS  
 LINK: [http://library.witpress.com/pages/listPapers.asp?q\\_bid=348](http://library.witpress.com/pages/listPapers.asp?q_bid=348)  
 LOCAL LINK: PDF/Stamatopoulos & Aneroussis [2006]\_Back analysis of the Vaiont slide using a multiblock.pdf  
 VOLUME: 90  
 PAGES:

Record: 2 di 5

---

**C - PROCEEDINGS**

ID: C003  
 CONF. NAME: II Panamerican Symposium on Landslides  
 KEYWORDS: Landslide, discontinuous deformation analysis, Vaiont landslc  
 CONF. PLACE: Rio de Janeiro  
 AUTHOR/S: Sitar N. & MacLaughin M.  
 CONF. DATE: 10-Nov-97  
 YEAR: 1997  
 TITLE: Sitar & MacLaughin [1997]\_Kinematics and Discontinuous Deformation Analysis of Landslide  
 DOI:  
 NOTE:  
 BOOK AUTHOR/S:  
 BOOK TITLE:  
 BOOK EDITOR/S:  
 LINK:  
 VOLUME:  
 LOCAL LINK: PDF\Sitar & MacLaughin [1997]\_Kinematics and Discontinuous Deformation Analysis of Landslide.pdf  
 PAGES:

Record: 4 di 30

**Fig. 3a.** Input masks created for inserting and visualizing references to journal articles (A), Book articles (B), Proceedings (C). Input mask of Monographs (D) is similar to that for Book article (B).

**Fig. 3b.** Input masks created for inserting and visualizing references to maps (E) and web site (H). Input mask of unpublished reports (F) and other (newspaper articles, conference presentations and relevant material) (G) are similar to that for maps (E).

document of data from geological and geomechanical surveys, geotechnical data from laboratory tests and scientific contents, is reported (Fig. 4).

The database currently contains references to 80 journal articles, 5 book articles, 51 monographs, 6 thematic maps, 30 conference proceedings, 5 unpublished reports, 25 web sites and 13 documents classified as “Other” (newspaper articles, conference presentations and relevant material). The chronology of the documentation shows a relatively high production immediately after the landslide (Fig. 5). After a period (1970–1979) of apparent decreasing interest, the documentation increased during 1980–1999, in a large part due to an International Conference on the Vaiont landslide, organized by E. Semenza at the University of Ferrara (Italy) on September 1986. Of note is that most of the documentation, especially journal articles and monographs, have been produced in the last 10 years, as a consequence of both new methods and techniques available for numerical analyses and

of the large increase in the electronic tools available for publishing and sharing scientific papers.

### 3 Structure and contents of the geodatabase

A geodatabase is a database designed to store, query, and manipulate geographic information and spatial data. Different types of spatial data, such as vector and raster datasets, and their attributes and location can be stored. In addition, tables and relationships between data can be included. The geodatabase forms the first step in implementing a Geographic Information System (GIS) organized to allow data collection, management and visualization of large slope instabilities and contributing factors (Chacón et al., 2006; Giardino et al., 2004). Vector datasets consist of geometrical primitives such as points, lines, curves and shapes or polygon(s), which are all based on mathematical equations and represent territorial



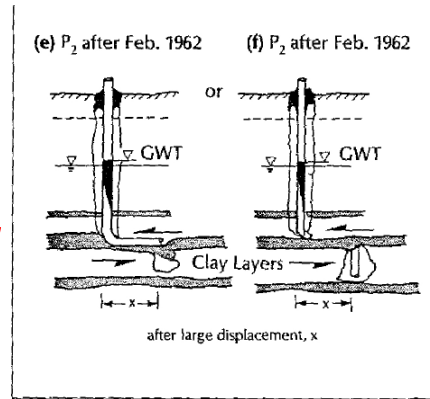
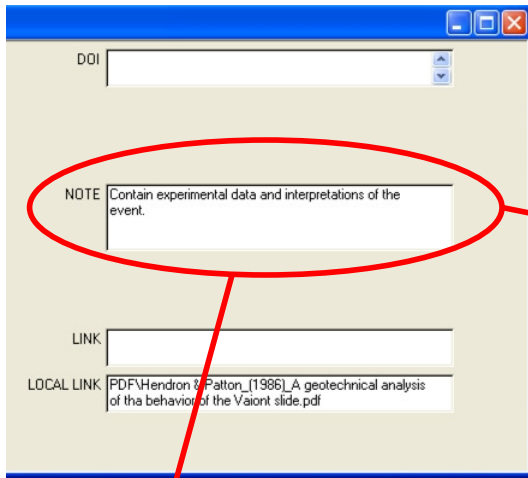


FIGURE 33. Sketches showing a possible explanation for the water levels recorded in ...

Sample No.	Liquid Limit	Plastic Limit	Plasticity Index	Descriptive Notes
12-6	72	23	49	Clay in debris about 4 m above failure plane
12-6A	35	19	16	Clay on failure plane (10 m from 12-6)
18-6	49	27	22	Clay on failure plain at scarp
18-6A	39	20	19	Clayey debris on rock surface near scarp
18-8	45	32	13	Clay in-situ forms failure plane above
18-9	37	25	12	Clay in-situ forms adjacent failure plane
18-9A	48	33	15	Clay in-situ on failure plane
18-11	38	25	13	Clay in-situ forms failure plane below

Fig. 4. Example of data and interpretations reported in the field NOTE of the e-bibliography. Sketches from Hendron and Patton (1986).

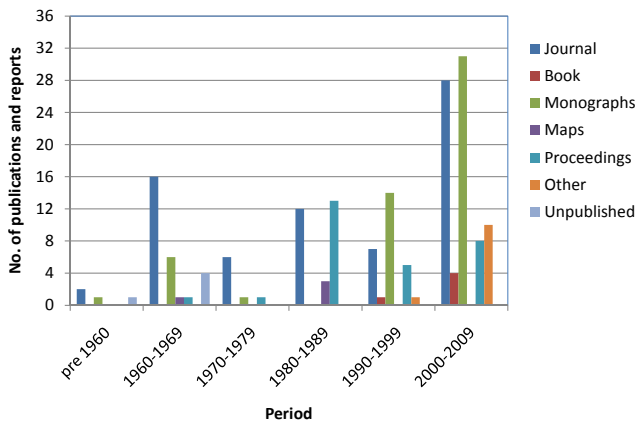


Fig. 5. Chronology of the documentation on the Vaiont landslide.

data (geomechanical stations, faults, lithology, etc.). A raster dataset is a data structure representing a generally rectangular grid of pixels, or points of colour. In the GIS, raster datasets of varying formats are usually used to represent continuous

territorial data (DEM, slope, etc.) and to perform simple to complex analyses.

The Vaiont geodatabase was implemented using ESRI ArcGIS Desktop 9.3 software and comprises:

1. *Feature classes* are homogeneous collections of common features, each having the same spatial representation, such as points, lines or polygons.
2. *Feature datasets* are objects that allow to group together related feature classes.
3. *Tables* are data collection of rows (records) and columns (attributes) used to store non-spatial data.
4. *Relationship classes* manage associations between objects in one table and objects in another. Rules to relate feature to feature (spatial relationships), row to row (non spatial relationships), and feature to row (spatial to non spatial relationships), are stored.
5. *Raster datasets* are grid-based representations of spatial data.

6. *Raster catalogues* are objects that allow efficient storage and management of multiple spatially-related raster datasets.
7. *Terrain datasets* are surfaces that represent three-dimensional space. They use measurements (stored as feature classes) and rules to generate triangular irregular network (TIN) pyramids to represent elevation. From the terrain dataset, it is possible to obtain both a vectorial-based elevation model (TIN) and a raster-based Digital Elevation Model (DEM).

Currently, the Vaiont geodatabase contains the following data.

- Vector datasets representing the attitude of strata, faults, lithology, and geological sections; digitized from pre- and post-landslide geological maps at 1:5000 scale (Rossi and Semenza, 1965).
- Vector datasets representing geognostic boreholes from Broili (1959) and geophysical investigation from Caloi (1960), and their attributes (type, depth, stratigraphy).
- Vector dataset representing geomechanical stations from past and recent surveys. Related attributes consist of rock and rock mass properties (discontinuities attributes such as orientation, size, aperture, roughness, etc., Schmidt Hammer testing, Geological Strength Index, Point Load Test, etc.) (see Table 1 for an example).
- Vector datasets representing elevation points and contour lines digitized from pre- and post-landslide topographic maps, official regional maps (CTR, Regione Friuli Venezia Giulia) and LiDAR survey.
- Raster datasets representing the Digital Elevation Model (DEM) of the area before and after the landslide. DEMs were calculated from the above mentioned topographic data.
- Raster datasets organized in a Raster Catalog, representing the aerial photos of the area before the landslide (1960).

In addition, the geodatabase contains tables of geotechnical and geomechanical properties of the rock mass inside and outside the landslide area, extracted both from the e-bibliography and from current author's field surveys and laboratory tests. From simple to complex rules, stored in the Relationships classes, join and relate records in the tables to the location of the collected samples and of the geomechanical stations.

#### 4 Using the databases

Modern techniques, such as photogrammetric analyses, ground-based and airborne LiDAR will greatly contribute

to geometric and geomechanical rock mass characterisation. DEM-based structural analysis, performed by COLTOP-3D software (Derron et al., 2005), on available data before and after the landslide, is an important tool in identifying the structural setting that led to the failure and controlled the direction of the movement. COLTOP-3D uses a colour representation merging slope aspect and slope angle in order to obtain a unique colour code for each orientation of a topographical element (Jaboyedoff et al., 2007, 2009). Simple analysis of DEMs allow rapid identification of structural features (joints, lineaments, faults) affecting the slope (Derron et al., 2005). The 3-D surface reconstruction is extremely useful as it enables easy identification of the main morpho-structural features from which joint set orientations and persistence relevant to the area of interest can be detected. Furthermore, these desktop analysis allow us to explore the area under investigation and thereby provide an aid in planning the field work and the mapping of structural data in inaccessible areas.

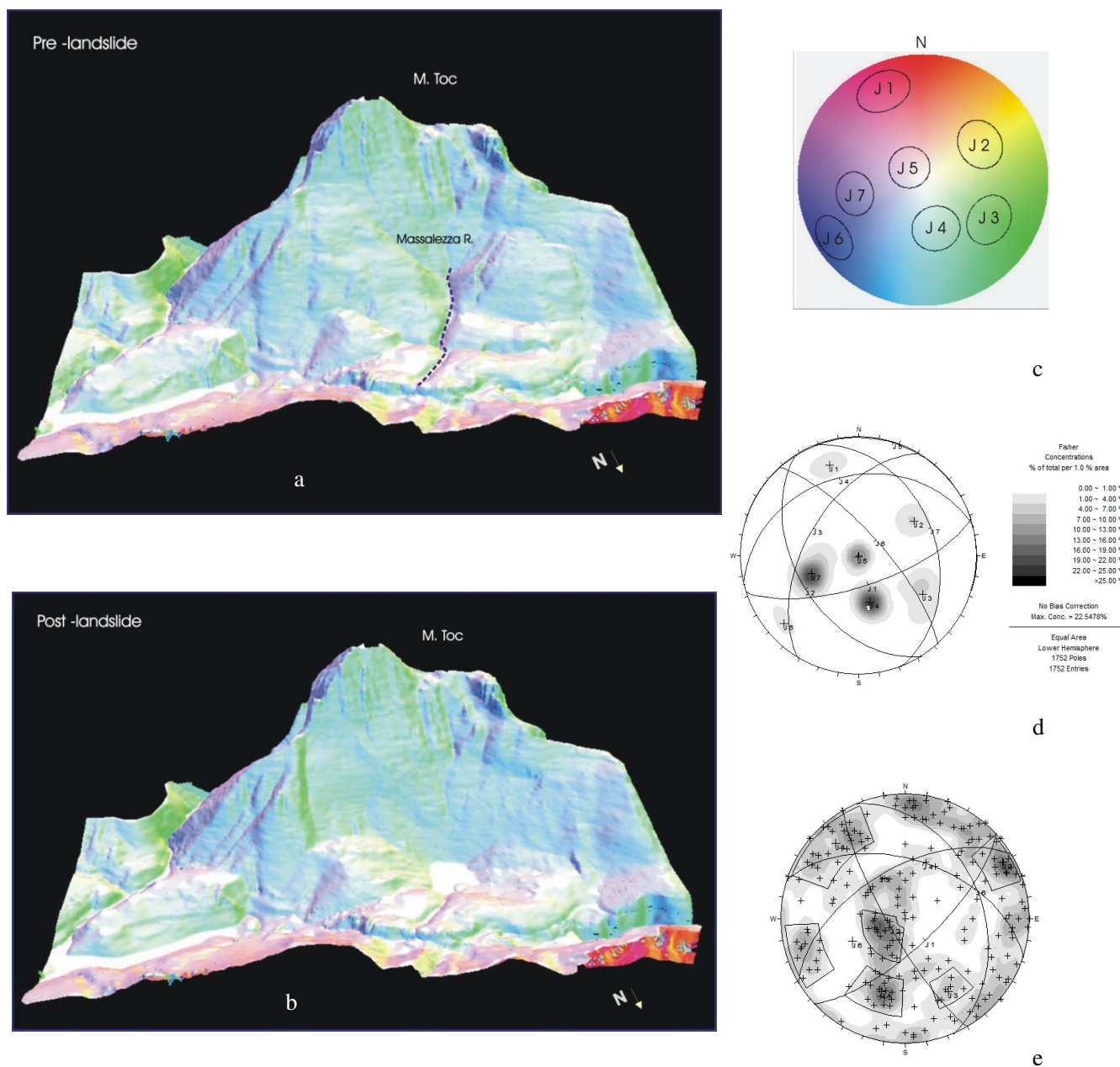
Seven main joint sets were detected in the pre- and post-Vaiont landslide slope using the colour coding of COLTOP-3D (Fig. 6). The joint surface pole orientations have been measured directly on the DEMs: J1(160°/40°), J2(238°/45°), J3(300°/50°), J4(345°/30°), J5(50°/20°), J6(50°/70°), J7(70°/45°). Figure 6a–b shows that one of the most important sets forming the morpho-structure is J4 (light-blue), dipping northward and corresponding to the orientation of the sliding plane. The data, obtained by using COLTOP-3D, agree reasonably well with the field measurements despite the present limited number of field data (Fig. 6e).

#### 5 Concluding remarks

The e-bibliography and the geodatabase represent a powerful tool to extract and select experimental data and scientific contents from the extensive documentation on the Vaiont landslide. The e-bibliography provides an important input for further scientific research not only on the Vaiont landslide but also on large rock landslides in general. Data collected in the electronic bibliographic database show that the majority of the research publications have been authored in the last decade, probably due to recent advances in both the body of knowledge on rock slides and the developments in methods and techniques for rock mass data collection and numerical analyses.

The key objective of the generated geodatabase is to store, manage, visualize and update a large number of different types of data in a central location and to make them available to the scientific community.

3-D geological, hydrogeological and geomechanical reconstruction of rock slope instabilities, such as the Vaiont 1963 event, will be more accurate and comprehensive as it will now be possible to apply new or advanced relationships



**Fig. 6.** COLTOP 3D analysis for the Vaiont area. In the pre- and post-landslide 3-D representation, different colours in the same area show different orientations of the structural features (faults and lineaments) (a–b). Seven morpho-structural sets were detected by COLTOP 3D, evaluated by means of the corresponding Schmidt-Lambert projection (c) and plotted using usual software (d). Obtained results were validated by comparison with the field data (e).

to collected data, to develop new methods of viewing the available information assets in a interrogative and discriminatory fashion; in summary, this will allow the leverage of all the collected data in order to optimize their potential for understanding rock slope failure mechanisms. Detailed examination of the geodatabase can provide important data required for numerical modelling of rock slopes i.e.: i) the geological, structural and hydrogeological characteristics prior

to the landslide; ii) the geomechanical characterisation of the involved rock masses; iii) the complete definition of the displacement field prior, during and after the landslide event.

At this stage, the Vaiont geodatabase remains largely incomplete: collected data to date relating mainly to the geological setting, whereas hydrogeological and geomechanical data are somewhat limited, scanty or absent. An example of both the potential of the geodatabase and of its current

**Table 1.** Geomechanical properties of the material involved in the slide, from past and current surveys. The slip surface has been placed at the bottom of the *Calcare di Socchér* formation (Semenza, 1965). Volumetric Joint Count (Jv), Block Size Index (Ib), Joint Roughness Coefficient (JRC), Joint Compression Strength (JCS), Geological Strength Index (GSI).

Formation	Lithology	Statistics	Jv	Ib	JRC	JCS (MPa)	GSI
Calcare di Socchér	Red and green limestones and marls with red cherts.	No. stations	7	7	7	7	7
		No. of data	3	3	4	4	2
		Minimum	35	3.9	3	44	47
		Maximum	73	11.8	6	104	52
	Fine-grained limestones with various colored cherts.	No. stations	18	18	18	18	18
		No. of data	3	3	17	17	2
		Minimum	22.8	4.3	1	29	47
		Maximum	99.3	8.8	10	180	62
	Red marly, silty limestones interbedded with conglomerate and limestones.	No. stations	8	8	8	8	8
		No. of data	1	1	8	8	1
		Minimum	58	6.4	2	30	40
		Maximum			10	150	
	Compact beds of gray limestones that alternated with a sequence of less resistant thin layers of greenish limestones and calcareous marls	No. stations	17	17	17	17	17
		No. of data	2	2	16	14	2
		Minimum	43	3.2	2	54	52
		Maximum	44.5	8	10	165	52
	conglomerate with pinkish or gray cement	No. stations	3	3	3	3	
		No. of data			3	3	
		Minimum			4	48	
		Maximum			9	130	
Micrites and e marley-micrites from light green to reddish with red cherts	No. stations	8	8	8	8	8	
	No. of data	3	3	7	5	2	
	Minimum	58.3	4.11	1	40	40	
	Maximum	66.5	9.9	8	125	62	
Amm. Rosso							
Red or nodular micrite, locally containing cherts	No. stations	1	1	1	1	1	
	No. of data	1	1	1		1	
	Minimum	46.8	7.36	5		57	
	Maximum			8			
Fonzaso	Micrites and calcarenites containing cherts, with interbeds of green clay	No. stations	3	3	3	3	3
		No. of data			2	2	
		Minimum			2	44	
		Maximum			6	96	
Calcare del Vaiont	Oolitic and crystalline limestones	No. stations	5	5	5	5	5
		No. of data	3	3	4	4	3
		Minimum	20	3.5	1	53	42
		Maximum	89	14	6	140	50

limitation in available data is given in Table 1. Values and relationships between distinctive properties, such as the Volumetric Joint Count (Jv) and Block Size Index (Ib) (Cai et al., 2004; Kalenchuk et al., 2006; Palmström, 1996, 2005), can aid in defining lithotechnical units, while the Joint Roughness Coefficient (JRC), the Joint Compressive Strength (JCS) and the Geological Strength Index (GSI) are necessary for

continuum or discontinuum modelling of the rock slope. However, the number of data available for each geological formation are insufficient to obtain spatial distributions at a statistically significant level, thus, making it currently impossible to subdivide the rock masses involved in the event into realistic geomechanical units.

A re-evaluation of the failure mechanism of the Vaiont landslide requires further research on still poorly constrained features of the area with a collection of additional spatial data. Field surveys, tests and analyses are in progress in order to improve the geodatabase. Field investigations are being extended into areas peripheral to the landslide, in order to provide a more comprehensive characterisation of the rock masses in the pre- and post-event conditions; this will form the foundation for 2-D/3-D numerical simulation using continuum and discontinuum numerical codes.

Surface based techniques, such as the comparison of pre- and post-event DEMs, and acquisition of deep level seismic tomography, to investigate the 3-D distribution of different rock masses, will allow improved definition of the displacement field of the landslide body.

Completing the geodatabase and performing the re-evaluation of the Vaiont landslide will represent an important contribution to a more comprehensive understanding of large rock slope instabilities.

*Acknowledgements.* This research was financially supported by the University of Padova, research projects CPDA085240 (Principal investigator: Mario Floris, Department of Geosciences) and GEO-RISKS (Principal investigator: Rinaldo Genevois, Department of Geosciences).

Edited by: D. Giordan

Reviewed by: F. M. Guadagno and another anonymous referee

## References

- Broili, L.: New knowledge on the geomorphology of the Vaiont Slide slip surfaces. *Rock Mechanics & Eng. Geol., J. Int. Soc. Rock Mechanics.*, V(1), 38–88, 1967.
- Cai, M., Kaiser, P. K., Uno, H., Tasaka, Y., and Minami, M.: Estimation of rock mass deformation modulus and strength of jointed hard rock masses using the GSI system. *Int. J. Rock Mech. Mining Sci.*, 41, 3–19, 2004.
- Caloi, P.: L'evento del Vajont nei suoi aspetti geodinamici, *Ist. Naz. Geofisica*, Roma, 1966.
- Chacón, J., Irigaray, C., Fernandez, T., and El Hamdouni, R.: Engineering geology maps: landslides and geographical information systems, *B. Eng. Geol. Environ.*, 65, 341–411, 2006.
- Derron, M.-H., Jaboyedoff, M., and Blikra, L. H.: Preliminary assessment of rockslide and rockfall hazards using a DEM (Oppstadhornet, Norway), *Nat. Hazards Earth Syst. Sci.*, 5, 285–292, 2005, <http://www.nat-hazards-earth-syst-sci.net/5/285/2005/>.
- Genevois, R. and Ghirotti, M.: The 1963 Vaiont Landslide – *Giornale di Geologia Applicata*, I, 41–53, 2005.
- Giardino, M., Giordan, D., and Ambrogio, S.: G.I.S. technologies for data collection, management and visualization of large slope instabilities: two applications in the Western Italian Alps, *Nat. Hazards Earth Syst. Sci.*, 4, 197–211, 2004, <http://www.nat-hazards-earth-syst-sci.net/4/197/2004/>.
- Giudici, F. and Semenza, E.: Studio geologico del serbatoio del Vajont. Unpublished report for S.A.D.E., Part A: 21 pp, text, Part B: 68 photos with discussions, 42 pp, Venezia, Italy, 1960.
- Hendron, A. J. and Patton, F. D.: The Vaiont Slide, a Geotechnical Analysis Based on New Geologic Observations of the Failure Surface. I, II, Technical Report GL-85-5, US Army Eng. Waterways Experiment Station, Vicksburg, MS, 1985.
- Hendron, A. J. and Patton, F. D.: A geotechnical analysis of the behavior of the Vaiont slide, *Civil Engineering Practice*, Fall, 65–130, 1986.
- Jaboyedoff, M., Metzger, R., Oppikofer, T., Couture, R., Derron, M.-H., Locat, J., and Turmel, D.: New insight techniques to analyze rock-slope relief using DEM and 3D-imaging cloud points: COLTOP-3D, *Rock mechanics Vol. 1: Meetings Society's Challenges and demands*, chap. 7, 61–68, edited by: Eberhardt, E., Stead, D., and Morrison, T., 2007.
- Jaboyedoff, M., Couture, R., and Locat, P.: Structural analysis of Turtle Mountain (Alberta) using digital elevation model: toward a progressive failure, *Geomorphology*, 103, 5–16, 2009.
- Kalenchuk, K. S., Diederichs, M. S., and McKinnon, S.: Characterizing block geometry in jointed rock masses, *Int. J. Rock Mech. Mining Sci.*, 43(8), 1212–1225, 2006.
- Kilburn, C. R. J. and Petley, D. N.: Forecasting giant, catastrophic slope collapse: lessons from Vajont, Northern Italy, *Geomorphology*, 54(1–2), 21–32, 2003.
- Müller, L.: The Rock Slide in the Vaiont Valley, *Rock Mech. Eng. Geol.*, 2, 148–212, 1964.
- Müller, L.: The Vaiont catastrophe - A personal review, in: *Dam Failures*, edited by: Leonards, G. A., *Eng. Geol.*, 24(1–4), 423–444, 1987a.
- Müller, L.: The Vaiont Slide, in: *Dam Failures*, edited by: Leonards, G. A., *Eng. Geol.*, 24(1–4), 513–523, 1987b.
- Nonveiller, E.: Vaiont Slide – Influence of Frictional Heat on Slip Velocity, in: *Proceedings of the meeting on the 1963 Vaiont landslide*, edited by: Semenza, E. and Melidoro, G., *IAEG Italian Section, University of Ferrara, Ferrara* 1986, 1, 187–197, 1992.
- Palmström, A.: Characterizing rock masses by the RMI for use in practical rock engineering, *Tunn. Undergr. Sp. Tech.*, 11(2), 175–188, 1996.
- Palmström, A.: Measurements of and correlations between block size and rock quality designation (RQD), *Tunn. Undergr. Sp. Tech.*, 20, 362–377, 2005.
- Rossi, D. and Semenza, E.: Carte geologiche del versante settentrionale del M. Toc e zone limitrofe, prima e dopo il fenomeno di scivolamento del 9 ottobre 1963, *Scala 1:5000, Ist. Geologia Università di Ferrara*, 2 Maps, 1965.
- Selli, R., Trevisan, L., Carloni, C. G., Mazzanti, R., and Ciabatti, M.: La Frana del Vajont, *Giornale di Geologia, serie 20, XXXII(I)*, 1–154, 1964.
- Semenza, E.: Sintesi degli studi geologici sulla frana del Vaiont dal 1959 al 1964, *Mem. Museo Tridentino Sc. Nat.*, 16, 1–52, 1965.
- Semenza, E.: La storia del Vaiont raccontata dal geologo che ha scoperto la frana. *Tecomproject Ed.*, Ferrara, Italy, 2000.
- Semenza, E. and Ghirotti, M.: History of 1963 Vaiont Slide. The importance of the geological factors to recognise the ancient landslide, *B. Eng. Geol. Environ.*, 59, 87–97, 2000.
- Skempton, A. W.: Bedding-plane slip, residual strength and the Vaiont Landslide, *Géotechnique*, XVI(1), 82–84, 1966.
- Tika, Th. E. and Hutchinson, J. N.: Ring shear tests on soil from the Vaiont landslide slip surface, *Geotechnique*, 49(1), 59–74, 1999.

# The Vaiont landslide electronic bibliographic database

## Journal articles

- Anderson D.L., 1985, Calculation of Slide Velocities, U.S. Army Eng. Waterways Experiment Station, Technical Report 85, In: HENDRON A.J. & PATTON F.D. (1985), II, Appendix E and F, GL-85-5, n, Vicksburg, MS, Contains experimental data, A054
- Atkinson B.K., 1984, Subcritical crack growth in geological materials, JOURNAL OF GEOPHYSICAL RESEARCH, 89, 4077- 4114, DOI, 10.1029/J0148-0227, <http://acnp.cib.unibo.it/cgi-ser/start/it/cnr/df-p.tcl?id=tisearch:ti-ex&id=catno:2294&catno=2294&sid=google&ft.auinit=BK&ft.aulast=Atkinson&ft.atitle=Subcritical+crack+growth+in+geologic+materials&titles=Journal+of+geophysical+research&ft.volume=89&ft.date=1984&ft.spag=4077&issn=0148-0227>, A025
- Belloni L.G. & Stefani R., 1987, The Vaiont slide: instrumentation-Past experience and the modern approach, ENGINEERING GEOLOGY, 24, 445-474, DOI, 10.1016/0013-7952(87)90079-2, Contains experimental data, [http://www.sciencedirect.com/science?\\_ob=PublicationURL&\\_cdi=5803&\\_pubType=J&\\_acct=C000031439&\\_version=1&\\_urlVersion=0&\\_userid=607988&md5=c84b8d5cb751bfb4b0f31582a31af502&jchunk=2424](http://www.sciencedirect.com/science?_ob=PublicationURL&_cdi=5803&_pubType=J&_acct=C000031439&_version=1&_urlVersion=0&_userid=607988&md5=c84b8d5cb751bfb4b0f31582a31af502&jchunk=2424), A026
- Boyer R.A., 1913, Etude géologique des environs de Longarone (Alpes Vénitiennes)., BULLETTIN DE LA SOCIETE GEOLOGIQUE DE FRANCE, 13, 451-485, A027
- Broili L., 1967, New knowledge on the geomorphology of the Vaiont Slide slip surfaces, JOURNAL INTERNATIONAL SOCIETY ROCK MECHANICS, 1, 38-88, A028
- Burland J.B., 1990, On the compressibility and shear strength of natural clays, GEOTECHNIQUE, 40, 329-378, ISSN:1751-7656, <http://acnp.cib.unibo.it/cgi-ser/start/it/cnr/df-p.tcl?catno=2394771&person=false&language=ITALIANO&libr=>, A031
- Caloi P., 1966, L'evento del Vajont nei suoi aspetti geodinamici, ISTITUTO NAZIONALE DI GEOFISICA, 21, ISSN:1590-1815, In Italian, <http://books.google.it/books?id=0ZU2AAAIAAJ&q=L'evento+del+Vajont+nei+suoi+aspetti+geodinamici&dq=L'evento+del+Vajont+nei+suoi+aspetti+geodinamici&pgis=1>, A029
- Carloni G.C. & Mazzanti R., 1964, Rilevamento geologico della frana del Vaiont, GIORNALE DI GEOLOGIA, 32, 105-138, SICI:0017-0291(1964)32:01<105:RGDFDV>2.0.ZU;2-7, Contains experimental data, [http://serials.cib.unibo.it/cgi-ser/start/it/spogli/df-s.tcl?prog\\_art=4717351&language=ITALIANO&view=articoli\\_p](http://serials.cib.unibo.it/cgi-ser/start/it/spogli/df-s.tcl?prog_art=4717351&language=ITALIANO&view=articoli_p), A032
- Carloni G.C. & Mazzanti R., 1964, Aspetti geomorfologici della frana del Vaiont, RIVISTA DI GEOGRAFIA ITALIANA, 71, 201-231, A033
- Chowdhury R., 1978, Analysis of the Vaiont Slide - New Approach, ROCK MECHANICS, 11, 29-38, DOI, 10.1007/BF00357448/78/0011/0029/, <http://www.springerlink.com/content/n861854840126v25/>, A034

- Ciabatti M., 1964, La dinamica della frana del Vaiont, *GIORNALE DI GEOLOGIA*, 32, 139-160, Contains experimental data, [http://serials.cib.unibo.it/cgi-ser/start/it/spogli/df-s.tcl?prog\\_art=4717352&language=ITALIANO&view=articoli\\_p](http://serials.cib.unibo.it/cgi-ser/start/it/spogli/df-s.tcl?prog_art=4717352&language=ITALIANO&view=articoli_p), A030
- Corbyn J.A., 1982, Failure of a partially submerged rock slope with particular references to the Vajont rock slide, *INTERNATIONAL JOURNAL ENGINEERING AND MINING SCIENCES*, 19, 99-102, DOI, 10.1016/0148-9062(82)91635-7, Contains experimental data, [http://www.sciencedirect.com/science?\\_ob=ArticleURL&\\_udi=B6V4V-4805NS1-YH&\\_user=607988&\\_coverDate=04%2F30%2F1982&\\_alid=861044321&\\_rdoc=3&\\_fmt=high&\\_orig=search&\\_cdi=5768&\\_sort=d&\\_docanchor=&view=c&\\_ct=8&\\_acct=C000031439&\\_version=1&\\_urlVersion=0&\\_userid=607988&md5=09bc9a61ab7bbf45b75125dfc966a0e1](http://www.sciencedirect.com/science?_ob=ArticleURL&_udi=B6V4V-4805NS1-YH&_user=607988&_coverDate=04%2F30%2F1982&_alid=861044321&_rdoc=3&_fmt=high&_orig=search&_cdi=5768&_sort=d&_docanchor=&view=c&_ct=8&_acct=C000031439&_version=1&_urlVersion=0&_userid=607988&md5=09bc9a61ab7bbf45b75125dfc966a0e1), A035
- Cotecchia V., 2006, The Second Hans Cloos Lecture. Experience drawn from the great Ancona landslide of 1982, *BULLETTINOF ENGINEERING GEOLOGY AND THE ENVIROMENT*, 45, 1-41, DOI, 10.1007/s10064-005-0024-z, Contains experimental data, <http://www.springerlink.com/content/985421g0081q2485/>, A004
- Crosta G.B. & Agliardi F., 2003, Failure forecast for large rock slides by surface displacement measurements, *CANADIAN GEOTECHNICAL JOURNAL*, 40, 176-191, DOI, 10.1139/T02-085, Contains experimental data, <http://pubs.nrc-cnrc.gc.ca/rp/rppdf/t02-085.pdf>, A006
- Devitt J. & Loader P., 2008, Landslides: a question of balance, *PHYSICS EDUCATION*, 43, DOI, 0031-9120/08/020151+07, Contains experimental data, [http://www.iop.org/EJ/article/0031-9120/43/2/003/pe8\\_2\\_003.pdf?request-id=e7697b60-d509-468f-ac06-520395e7ccce](http://www.iop.org/EJ/article/0031-9120/43/2/003/pe8_2_003.pdf?request-id=e7697b60-d509-468f-ac06-520395e7ccce), A057
- Fukuzono T., 1990, Recent studies on time prediction of slope failure, *LANDSLIDE NEWS*, 4, 9-12, Related to forecasting of the time of slope failure of Vaiont landslide, Contains experimental data, A061
- Genevois R. & Ghirotti M., 2005, The 1963 Vaiont Landslide, *GIORNALE DI GEOLOGIA APPLICATA*, 1, 41-53, DOI, 10.1474/GGA.2005-01.0-05.0005, [http://www.geoitalia.org/upload/home\\_page/giornale\\_di\\_geologia\\_applicata/GGA.2005-01.0-05.0005.pdf](http://www.geoitalia.org/upload/home_page/giornale_di_geologia_applicata/GGA.2005-01.0-05.0005.pdf), A021
- Ghirotti M., 1994, Nuovi dati sulla frana del Vaiont e modellazione numerica, *GEOLOGICA ROMANA*, XXX, 207-215, In italian, A079
- Goren L. & Aharonov E., 2009, On the stability of landslides: A thermo-poro-elastic approach, *EARTH AND PLANETARY SCIENCE LETTERS*, 277, 365-372, DOI, 10.1016/j.epsl.2008.11.002, Contains experimental data, <http://www.elsevier.com/locate/epsl>, A023
- Groneng G., Nilsen B., Sandven R., 2009, Shear strength estimation for Aknes sliding area in western Norway, *ROCK MECHANICS & MINING SCIENCES*, 46, 479-488, DOI, 10.1016/j.ijrmmms.2008.10.006, [http://www.sciencedirect.com/science?\\_ob=ArticleURL&\\_udi=B6V4W-4V64YTR-1&\\_user=607988&\\_rdoc=1&\\_fmt=&\\_orig=search&\\_sort=d&\\_docanchor=&view=c&\\_searchStrId=1079106792&\\_rerunOrigin=scholar.google&\\_acct=C000031439&\\_version=1&\\_urlVersion=0&\\_userid=607988&md5=ae89bbaeef14f3c770355b12aeaffe66](http://www.sciencedirect.com/science?_ob=ArticleURL&_udi=B6V4W-4V64YTR-1&_user=607988&_rdoc=1&_fmt=&_orig=search&_sort=d&_docanchor=&view=c&_searchStrId=1079106792&_rerunOrigin=scholar.google&_acct=C000031439&_version=1&_urlVersion=0&_userid=607988&md5=ae89bbaeef14f3c770355b12aeaffe66), A077

- Habib P., 1975, Production of Gaseous Pore Pressure During Rock Slides, *ROCK MECHANICS*, 7, 193-197, <http://www.springerlink.com/content/101578/?sortorder=asc&sw=production>, A053
- Handron A.J. & Patton F.D., 1985, The Vaiont Slide, A Geotechnical Analysis Based on New Geologic Observations of the Failure Surface, *ENGINEERING GEOLOGY*, 24, 479-491, DOI, 10.1016/0013-7952(87)90080-9, Contains experimental data, [http://www.sciencedirect.com/science?\\_ob=PublicationURL&\\_method=list&\\_tokey=%23toc%235768%231988%23999749993%23393942%23FLP%23&\\_auth=y&\\_version=1&refSource=toc&\\_pubType=J&PDF\\_DDM\\_MAX=20&\\_cdi=5768&md5=2b568fafcfb70d50c0759428c8944363&chunk=2&view=c&go=nex](http://www.sciencedirect.com/science?_ob=PublicationURL&_method=list&_tokey=%23toc%235768%231988%23999749993%23393942%23FLP%23&_auth=y&_version=1&refSource=toc&_pubType=J&PDF_DDM_MAX=20&_cdi=5768&md5=2b568fafcfb70d50c0759428c8944363&chunk=2&view=c&go=nex), A024
- Helmstetter A., Sornette D., Grasso J.R., Andersen J. V., Gluzman S. and V. Pisarenko, 2004, Slider block friction model for landslides: Application to Vaiont and La Clapière landslides, *JOURNAL OF GEOPHYSICAL RESEARCH*, 109, 1-15, DOI, 10.1029/2002JB002160, Contains experimental data, <http://www.agu.org/pubs/crossref/2004/2002JB002160.shtml>, A016
- Hendron A. J. & Patton F.D, 1986, A geotechnical analysis of the behavior of the Vaiont slide, *CIVIL ENGINEERING PRACTICE FALL*, 65-130, Contains experimental data, A070
- Hendron A.J & Patton F.D, 1986, A geotechnical analysis of the Behavior of the Vaiont slide, *CIVIL ENGINEERING PRACTICE FALL*, 65-130, Contains experimental data, A059
- Hewitt K. , Clague J.J., Orwin J. F., 2008, Legacies of catastrophic rock slope failures in mountain landscapes, *EARTH SCIENCE*, 87, 1-38, DOI, 10.1016/j.earscirev.2007.10.002, [http://www.sciencedirect.com/science?\\_ob=PublicationURL&\\_tokey=%23TOC%235802%232008%2399129998%23678699%23FLA%23&\\_cdi=5802&\\_pubType=J&\\_auth=y&\\_acct=C000031439&\\_version=1&\\_urlVersion=0&\\_userid=607988&md5=45254c0195af2206b06b0999167cc8c1](http://www.sciencedirect.com/science?_ob=PublicationURL&_tokey=%23TOC%235802%232008%2399129998%23678699%23FLA%23&_cdi=5802&_pubType=J&_auth=y&_acct=C000031439&_version=1&_urlVersion=0&_userid=607988&md5=45254c0195af2206b06b0999167cc8c1), A012
- Jaeger C., 1965, The Vaiont Rockslide, *WATER POWER*, 3, 110-111, Part 1, A036
- Jaeger C., 1965, The Vaiont Rockslide, *WATER POWER*, 4, 142-144, Part 2, A037
- Jaeger C., 1972, The Vaiont slide, *ROCK MECHANICS AND ROCK ENGINEERING*, 14, 340-361, Univ. Press, Cambridge, <http://www.springerlink.com/content/n861854840126v25/>, A038
- Jager C., 1968, L.Muller-Salzburg- New consideration on the Vaiont Slide. The Dynamics of the Slide, *FELSMCHANIK U. INGENIEURGEOL.*, 6, 243-247, Contains experimental data, A069
- Kenney T.C., 1967, Stability of the Vajont Valley slope, discussion of paper by L. Müller (1964) on the rock slide in the Vajont Valley, *INTERNATIONAL JOURNAL OF ROCK MECHANICS AND MINING SCIENCES*, 5, 10-16, Contains experimental data, A039
- Kiersch G., 1964, Vaiont Reservoir Disaster, *CIVIL ENGINEERING*, 34, 32-39, <http://books.google.it/books?q=Vajont+Reservoir+Disaster.+Civil+Engineering&btnG=Cerca+nei+libri>, A040
- Kiersch G.A., 1965, Vaiont Reservoir Disaster, *GEOTIMES*, MAY-JUNE, 9-12, A078
- Kilburn C.R.J & Pasuto A., 2003, Major risk from rapid, large-volume landslides in Europe (EU Project RUNOUT), *GEOMORPHOLOGY*, 54, 1-7, DOI, 10.1016/S0169-555X(03)00050-3,



[http://www.sciencedirect.com/science?\\_ob=ArticleURL&\\_udi=B6V93-47VS6JK-1&\\_user=607988&\\_rdoc=1&\\_fmt=&\\_orig=search&\\_sort=d&view=c&\\_acct=C000031439&\\_version=1&\\_urlVersion=0&\\_userid=607988&md5=cae0e54af545d94acdc14f1b3e21a4d1](http://www.sciencedirect.com/science?_ob=ArticleURL&_udi=B6V93-47VS6JK-1&_user=607988&_rdoc=1&_fmt=&_orig=search&_sort=d&view=c&_acct=C000031439&_version=1&_urlVersion=0&_userid=607988&md5=cae0e54af545d94acdc14f1b3e21a4d1), A013

Kilburn C.R.J. & Petley D. N., 2003, Forecasting giant, catastrophic slope collapse: lessons from Vajont, Northern Italy, *GEOMORPHOLOGY*, 54, 21-32, DOI, 10.1016/S0169-555X(03)00052-7, Contains experimental data, [http://www.sciencedirect.com/science?\\_ob=ArticleURL&\\_udi=B6V93-47XWM91-1&\\_user=607988&\\_rdoc=1&\\_fmt=&\\_orig=search&\\_sort=d&view=c&\\_acct=C000031439&\\_version=1&\\_urlVersion=0&\\_userid=607988&md5=3a77b61dccf49c434de728ab68590cc6](http://www.sciencedirect.com/science?_ob=ArticleURL&_udi=B6V93-47XWM91-1&_user=607988&_rdoc=1&_fmt=&_orig=search&_sort=d&view=c&_acct=C000031439&_version=1&_urlVersion=0&_userid=607988&md5=3a77b61dccf49c434de728ab68590cc6), A008

Kilburn C.R.J. & Voight B, 1998, Rock fracture as eruption precursor at Soufriere Hills volcano. Montserrat, *GEOPHYSICAL RESEARCH LETTERS*, 25, 3665-3668, DOI, 10.1029/1998-10-01, <http://www.agu.org/pubs/crossref/1998/98GL01609.shtml>, A052

Kilburn C.R.J., & Sorensen S.A., 1998, Runout lengths of sturzstroms: the control of initial conditions and of fragment dynamics, *GEOPHYSICAL RESEARCH SOLID EARTH*, 103, 17877-17884, DOI, 10.1029/1998JB01074, Contains experimental data, <http://www.agu.org/pubs/crossref/1998/98JB01074.shtml>, A076

Main I.G, 2000, A damage mechanics model for power-law creep and earthquake, *GEOPHYSICAL JOURNAL INTERNATIONAL*, 142, 151-161, DOI, 10.1046/j.1365-246x.2000.00136.x, Related to creep and time-dependent crack growth, <http://www3.interscience.wiley.com/search/allsearch?mode=quicksearch&products=journal&WISsearch2=1365-246X&WISindexid2=issn&contentTitle=Geophysical+Journal+International&contextLink=blah&contentOID=118543048&WISsearch1=10.1046%2Fj.1365-246x.2000.00136.x&WISindexid1=WISall>, A063

Mantovani F. & Vita-Finzi C., 2003, Neotectonics of the Vajont dam site, *GEOMORPHOLOGY*, 54, 33-37, DOI, 10.1016/S0169-555X(03)00053-9, <http://www.elsevier.com/locate/geomorph>, A005

Martinis B., 1979, Contributo alla stratigrafia dei dintorni di Erto-Casso (Pordenone) ed alla conoscenza delle caratteristiche strutturali e meccaniche della frana del Vajont, *MEMORIE DELLE SCIENZE GEOLOGICHE*, 32, 1-33, Contains experimental data, A041

Menci V., 1966, Mechanics of landslides with non-circular slip surfaces with special reference to the Vajont slide., *GEOTECHNIQUE*, 16, 329-337, <http://acnp.cib.unibo.it/cgi-ser/start/it/cnr/df-p.tcl?catno=2394771&person=false&language=ITALIANO&libr=>, A042

Muller L., 1964, The Rock Slide in the Vajont Valley, *ROCK MECHANISM AND ENGINEERING GEOLOGY*, 2, 148-212, [http://acnp.cib.unibo.it/cgi-ser/start/it/cnr/dc-p2.tcl?catno=42196&language=ITALIANO&libr=&person=false&year\\_poss\\_from=&year\\_poss\\_to=](http://acnp.cib.unibo.it/cgi-ser/start/it/cnr/dc-p2.tcl?catno=42196&language=ITALIANO&libr=&person=false&year_poss_from=&year_poss_to=), A043

Muller L., 1987, The Vajont catastrophe - A personal review, *ENGINEERING GEOLOGY*, 24, 423-444, DOI, 10.1016/0013-7952(87)90078-0, In :LEONARDS G.A (ed) - Dam failures, <http://www.sciencedirect.com/science/journal/00137952>, A049

- Muller L., 1987, The Vaiont slide, *ENGINEERING GEOLOGY*, 24, 513-523, DOI, 10.1016/0013-7952(87)90082-2, In : LEONARDS G.A (ed) - Dam failures, <http://www.sciencedirect.com/science/journal/00137952>, A050
- Muller L., 1968, New Considerations on the Vaiont Slide, *ROCK MECHANISM AND ENGINEERING GEOLOGY*, 6, 1-91, Contains experimental data, A044
- Nonveiller E., 1987, The Vajont reservoir slope failure, *ENGINEERING GEOLOGY*, 24, 493-512, DOI, 10.1016/0013-7952(87)90081-0, In : LEONARDS G.A (ed) - Dam failures  
Contains experimental data, [http://www.sciencedirect.com/science?\\_ob=PublicationURL&\\_cdi=5803&\\_pubType=J&\\_acct=C000031439&\\_version=1&\\_urlVersion=0&\\_userid=607988&md5=c84b8d5cb751bfb4b0f31582a31af502&jchunk=2424](http://www.sciencedirect.com/science?_ob=PublicationURL&_cdi=5803&_pubType=J&_acct=C000031439&_version=1&_urlVersion=0&_userid=607988&md5=c84b8d5cb751bfb4b0f31582a31af502&jchunk=2424), A051
- Nonveiller E., 1978, Untersuchungen zur Stabilität von Böschungen., *FREIBERG FORSCHUNGSH*, 617, 57-71, A075
- Pastor M. , Herreros I. , Fernández Merodo J.A., Mira P., Haddad B., Quecedo M.
- E. González, C. Alvarez-Cedrón, V. Drempevic, 2008, Modelling of fast catastrophic landslides and impulse waves induced by them in fjords, lakes and reservoirs, *ENGINEERING GEOLOGY*, DOI, 10.1016/j.enggeo.2008.10.006, Contains experimental data, <http://www.elsevier.com/locate/enggeo>, A022
- Petley D.N. & Allison R.J., 1997, The mechanics of deep-seated landslides, *EARTH SURFACE PROCESSES AND LANDFORMS*, 22, 747-758, DOI, CCC 0197-9337/97/080747-12, Contains experimental data, <http://www3.interscience.wiley.com/journal/8515/abstract?CRETRY=1&SRETRY=0>, A018
- Petley D.N., 2006, The Vajont (Vaiont) landslide, *Geo-Strata*, March/April 2006, 27-28, <http://cedb.asce.org/cgi/WWWdisplay.cgi?0601777>, A074
- Petley D.N, Bulmer N.H, Murphy W, 2002, Patterns of movement in rotational and translational landslides, *GEOLOGY*, 30, 719-722, 10.1130/0091-7613(2002)030, <http://geology.geoscienceworld.org/cgi/content/abstract/30/8/719>, A046
- Petley D.N., 2004, The evolution of slope failures: mechanisms of rupture propagation, *Natural Hazards and Earth System Sciences*, 4, 147-152, DOI, SRef-ID: 1684-9981/nhess/2004-4-147, Contains experimental data, <http://dro.dur.ac.uk/1282/>, A017
- Rose N.D. & Hungr O., 2006, Forecasting potential rock slope failure in open pit mines using the inverse-velocity method, *INTERNATIONAL JOURNAL OF ROCK MECHANICS AND MINING SCIENCES*, 44, 308-320, DOI, 10.1016/j.ijrmms.2006.07.014, Contains experimental data, <http://www.elsevier.com/locate/ijrmms>, A009
- Roubtsova V. & Kahawita R., 2006, The SPH technique applied to free surface flows, *COMPUTERS & FLUID*, 35, 1359-1371, DOI, 10.1016/j.compfluid.2005.08.012, Contains experimental data, [http://www.sciencedirect.com/science?\\_ob=ArticleURL&\\_udi=B6V26-4JCCJK1-1&\\_user=607988&\\_rdoc=1&\\_fmt=&\\_orig=search&\\_sort=d&view=c&\\_acct=C000031439&\\_version=1&\\_urlVersion=0&\\_userid=607988&md5=b8a7de7df1f77f74bcc98590cdc24c93](http://www.sciencedirect.com/science?_ob=ArticleURL&_udi=B6V26-4JCCJK1-1&_user=607988&_rdoc=1&_fmt=&_orig=search&_sort=d&view=c&_acct=C000031439&_version=1&_urlVersion=0&_userid=607988&md5=b8a7de7df1f77f74bcc98590cdc24c93), A019

- Rutqvist J. & Stephansson O., 2003, The role of hydromechanical coupling in fractured rock engineering, *HYDROGEOLOGY JOURNAL*, 11, 7-40, DOI, 10.1007/s10040-002-0241-5, Contains experimental data, PDF\Rutqvist\_Stephansson (2003)-The role of hydromechanical coupling in fractured rock engineering.pdf, A068
- Scheidegger A.E, 1973, On the Prediction of the Reach and Velocity of Catastrophic Landslides, *ROCK MECHANICS*, 5, 231-236, Contains experimental data, A014
- Selli R. & Trevisan L., 1964, Caratteri e interpretazione della Frana del Vajont, *GIORNALE DI GEOLOGIA*, 32, 1-154, SICI: 0017-0291(1964)32:01<7:CEIDFD>2.0.ZU;2-6, In Italian, [http://serials.cib.unibo.it/cgi-ser/start/it/spogli/df-s.tcl?prog\\_art=4717350&language=ITALIANO&view=articoli\\_p](http://serials.cib.unibo.it/cgi-ser/start/it/spogli/df-s.tcl?prog_art=4717350&language=ITALIANO&view=articoli_p), A048
- Semenza C., 1950, Le utilizzazioni idroelettriche ed irrigue nel bacino del Piave, *TOURING CLUB ITALIANO*, 1, A072
- Semenza E. & Ghirotti M., 2000, History of the 1963 Vaiont slide: the importance of geological factors, *BULLETIN ENGINEERING GEOLOGICAL ENVIROMENT*, 59, 87-97, DOI, 10.1007/s100640000067, <http://www.springerlink.com/content/t2tcy7u335kha2jb/>, A011
- Semenza E. & Ghirotti M., 2000, History of the Vaiont slide: the importance of geological factors, *BULLETIN OF ENGINEERING GEOLOGY AND THE ENVIROMENT*, 59, 87-97, ISSN:1435-9529, <http://www.springerlink.com/content/102026/>, A073
- Shengwen Qi, Fuzhang Yan , Sijing Wang , Ruichun Xu, 2006, Characteristics, mechanism and development tendency of deformation of Maoping landslide after commission of Geheyan reservoir on the Qingjiang River, Hubei Province, China, *ENGINEERING GEOLOGY*, 86, 37-51, DOI, 10.1016/j.enggeo.2006.04.004, Contains experimental data, [http://www.sciencedirect.com/science?\\_ob=ArticleURL&\\_udi=B6V63-4K5JVVH-1&\\_user=7728870&\\_rdoc=1&\\_fmt=&\\_orig=search&\\_sort=d&view=c&\\_acct=C000031439&\\_version=1&\\_urlVersion=0&\\_userid=7728870&md5=6aeee46bf2275be4762aa8d319f66571](http://www.sciencedirect.com/science?_ob=ArticleURL&_udi=B6V63-4K5JVVH-1&_user=7728870&_rdoc=1&_fmt=&_orig=search&_sort=d&view=c&_acct=C000031439&_version=1&_urlVersion=0&_userid=7728870&md5=6aeee46bf2275be4762aa8d319f66571), A002
- Sitar N., MacLaughlin M., Dolin D.M., 2005, Influence of Kinematics on Landslide Mobility and Failure Mode, *JOURNAL OF GEOTECHNICAL AND GEOENVIROMENTAL ENGINEERING*, 131, 716-728, DOI, 10.1061/(ASCE)1090-0241(2005)131:6(716), 2D Analisis, Contains experimental data, <http://scitation.aip.org/getabs/servlet/GetabsServlet?prog=normal&id=JGGEFK00013100000600071600001&idtype=cvips&gifs=yes>, A071
- Skempton A.W, 1966, Bedding-plane slip, residual strenght and the Vaiont landslide., *GEOTECHNIQUE*, 16, 82-84, A047
- Sornette D., Helmstetter A., Andersen J.V., Gluzmanc S., Grassoc J.R., Pisarenko V., 2004, Towards landslide predictions: two case studies, *PHISICAA*, 338, 605-632, DOI, 10.1016/j.physa.2004.02.065, Contains experimental data, [http://www.sciencedirect.com/science?\\_ob=ArticleURL&\\_udi=B6TVG-4BYP1SJ-2&\\_user=607988&\\_rdoc=1&\\_fmt=&\\_orig=search&\\_sort=d&view=c&\\_acct=C000031439&\\_version=1&\\_urlVersion=0&\\_userid=607988&md5=9d6bb795f61e9f26e40cd7f0f8fde4d2](http://www.sciencedirect.com/science?_ob=ArticleURL&_udi=B6TVG-4BYP1SJ-2&_user=607988&_rdoc=1&_fmt=&_orig=search&_sort=d&view=c&_acct=C000031439&_version=1&_urlVersion=0&_userid=607988&md5=9d6bb795f61e9f26e40cd7f0f8fde4d2), A020

- Tagliavini F., Reichenbach P., Maragna D., Guzzetti F. & Pasuto A., 2008, Comparison of 2-D and 3-D computer models for the M. Salta rock fall, Vajont Valley, northern Italy, *GEOINFORMATICA*, DOI, 10.1007/s10707-008-0071-2, Contains experimental data, <http://www.springerlink.com/content/?k=vajont+valley>, A045
- Tika T.H.E. & Hutchinson N., 1999, Ring shear tests on soil from the Vaiont landslide slip surface, *GEOTECNIQUE*, 49, 59-74, Contains experimental data, A015
- Tika T.E., Vaughan P. R. & Lemos L. J.L. J., 1996, Fast shearing of pre-existing shear zones in soil, *GEOTECNIQUE*, 46, 197-233, DOI, ISSN 0016-8505, Contains experimental data, <http://cat.inist.fr/?aModele=afficheN&cpsidt=3109992>, A007
- Trollope D.H., 1980, The Vaiont Slope Failure, *ROCK MECHANICS*, 13, 71-88, DOI, 0035-7448/80/0013/0071, <http://www.springerlink.com/content/k585706265877265/>, A056
- Vai G.B., 2004, La tragedia del Vaiont tra Paolini e Semenza: Mito o storia?, *NATURA & MONTAGNA*, 1, 58-62, In Italian, [http://www.patroneditore.com/Riviste/Natura/NaturaRic\\_fs.htm](http://www.patroneditore.com/Riviste/Natura/NaturaRic_fs.htm), A066
- Vardoulakis I., 2002, Dynamic thermo-poro-mechanical Analysis of Catastrophic Landslides, *GEOTECNIQUE*, 52, 157-171, DOI, 10.1680/geot.52.3.157.41012, Contains experimental data, <http://www.atypon-link.com/TELF/doi/pdf/10.1680/geot.52.3.157.41012>, A003
- Veveakis E., Vardoulakis I., Di Toro G., 2007, Thermoporo mechanics of creeping landslides: The 1963 Vaiont slide, northern Italy, *JOURNAL OF GEOPHYSICAL RESEARCH*, 112, 1-21, DOI, 10.1029/2006JF000702, Contains experimental data, <http://www.agu.org/pubs/crossref/2007/2006JF000702.shtml>, A001
- Voight B., 1978, Rockslides and avalanches, *NATURAL PHENOMENA - ELSEVIER*, A055
- Voight B., 1989, A relation to Describe Rate-Dependent Material Failure., *SCIENCE*, 243, 200-203, Contains experimental data, <http://www.jstor.org/stable/1702921?&Search=yes&term=voight&list=hide&searchUri=%2Faction%2FdoBasicSearch%3FQuery%3Dvoight%26wc%3Don&item=2&ttl=603&returnArticleService=showArticle>, A060
- Voight B., 1988, A Method for Prediction of Volcanic Eruptions, *NATURE*, 332, 125-130, DOI, 10.1038/332125a0, Related to the failure mechanism, Contains experimental data, <http://adsabs.harvard.edu/abs/1988Natur.332..125V>, A065
- Voight B., 1989, Materials science law applies to time forecasts of slope failure, *JAPAN LANDSLIDE SOCIETY, LANDSLIDE NEWS*, 3, 8-10, Related to methods to forecast the time of occurrence of slope failure., A067
- Voight B. & Faust C., 1982, Frictional heat and strength loss in some rapid landslides, *GEOTECNIQUE*, 32, 43-54, ISSN:0016-8505, Contains experimental data, <http://acnp.cib.unibo.it/cgi-ser/start/it/cnr/df-p.tcl?id=tisearch:ti-ex&id=catno:5995&catno=5995&sid=google&rft.auinit=B&rft.aulast=Voight&rft.atitle=Frictional+heat+and+strength+loss+in+some+rapid+landslides&titles=Geotechnique&rft.volume=32&rft.date=1982&rft.page=43&issn=0016-8505>, A058

Voight B. & Faust C., 1992, Frictional heat and strength loss in some rapid landslides: error correction and affirmation of mechanism for the Vaiont landslide, *GEOTECHNIQUE*, 42, 641-643, Contains experimental data, A062

Wang H. B. Xu W. Y. Xu R. C. Jiang Q. H. Liu J. H., 2007, Hazard assessment by 3D stability analysis of landslides due to reservoir impounding, *LANDSLIDE*, 4, 381-388, DOI, 10.1007/s10346-007-0095-y, Contains experimental data, <http://www.springerlink.com/content/ul97244r20542043/>, A064

## Book articles

Erismann T.H. & Abele G., 2001, Vaiont, 60-79, DOI, ISBN 3540671986, 9783540671985, [http://books.google.it/books?id=yBwksYMK\\_DkC&printsec=frontcover&dq=Dynamics+of+Rockslides+and+RockfallPPP1,M1](http://books.google.it/books?id=yBwksYMK_DkC&printsec=frontcover&dq=Dynamics+of+Rockslides+and+RockfallPPP1,M1), In: Erismann T.H & Abele G. eds., *Dynamics of Rockslides and Rockfall*, B005

Ghirotti M., 2003 Edoardo Semenza: The important of geological and geomorphological factors in the identification of ancient Vaiont landslide, 4, 395-406, DOI, 10.1007/978-1-4020-4037-5\_5, [http://www.amazon.com/Landslides-Massive-Slope-Failure-Science/dp/1402040350/ref=sr\\_1\\_1?ie=UTF8&s=books&qid=1233911253&sr=8-1](http://www.amazon.com/Landslides-Massive-Slope-Failure-Science/dp/1402040350/ref=sr_1_1?ie=UTF8&s=books&qid=1233911253&sr=8-1), In: Evans S.G., Scarascia Mugnozza G. & Storm A. eds., *Landslides from Massive Rock Slope Failure*, B001

Hinokidani O. & Michiue M., 1997, Simulation of waves generated by landslides in Vaiont Dam, 263-268, DOI, ISBN 0-7844-0281-7, <http://cedb.asce.org/cgi/WWWdisplay.cgi?9703768>, In: John S. Gulliver eds., *Energy and Water: Sustainable Development*, B006

Petley D.N., 1996, The mechanics and landforms of deep-seated landslides, 21, 823-835, DOI, ISBN 0471967742, 9780471967743, <http://books.google.it/books?id=BD8MAAAACAAJ&dq=Advances+in+Hillslope+Processes>, In: Di Malcolm G. Anderson, Sue M. Brooks eds., *Advances in Hillslope Processes*, B004

Santantonio M., 2002, General field trip guidebook, 320, <http://books.google.it/books?id=LQCwKQAACAAJ&dq=General+Field+Trip+Guidebook>, In: Santantonio M. ed., *General field trip guidebook*, B003

Stamatopoulos C. & Aneroussis S., 2006, Back analysis of the Vaiont slide using a multiblock sliding model, 90, DOI, 10.2495/DEB060251, [http://library.witpress.com/pages/listPapers.asp?q\\_bid=348](http://library.witpress.com/pages/listPapers.asp?q_bid=348), In: G. LORENZINI, C.A. BREBBIA, and D. EMMANOULOU DIS eds., *Monitoring, Simulation, Prevention and Remediation of Dense and Debris Flows*, B002

## Proceedings

Belloni L. G. & Stefani R., 1987, Vajont slide: Instrumentation past experience and the modern approach, *Engineering Geology EGGOAO*, International Workshop on Dam Failures, 24, 445-474, Purdue University, Indiana, December 1987, <http://mdl.csa.com/partners/viewrecord.php?requester=gs&collection=ENV&recid=8808704&q+=Vajont+>

slide%3A+instrumentation++past+experience+and+the+modern+approach&uid=1467277&setcookie=yes,  
C009

Belloni L.G. & Stefani R.F., 1986, Natural and induced seismicity at the Vajont slide, Semenza E. & Melidoro G. eds., Proceedings of the meeting on the 1963 Vaiont landslide, Convegno sulla frana del Vaiont, 115-132, Università di Ferrara, Italy, 17-19 September 1986, C020

Besio M., 1963, Hydrogeological notes regarding mount Toc and vicinity, Semenza E. & Melidoro G eds., Proceedings of the meeting on the 1963 Vaiont landslide, Convegno sulla frana del Vaiont, 133-155, Ferrara, Italy, 17-19- September-1986, C015

Bollettinari G. & Mantovani F., 1986, Morphotectonic aspects of Vaiont valley, Semenza E. & Melidoro G. eds., Proceedings of the meeting on the 1966 Vaiont landslide, Convegno sulla frana del Vaiont, 216, Università di Ferrara, Italy, 17-19 September 1986, C025

Bonini M., Casagli N., Corti G., Del Ventisette C., Gigli G., Sani F., Santoro S., 2008, The Vaiont landslide from analogue and numerical experiments, BOLLETTINO DI GEOFISICA TEORICA ED APPLICATA, Third International Geomodelling Conference, 49, 435-438, Florence, Italy, 22-24 september 2008, C028

Casagrande G., 2003, Lo scienziato e la valle del diavolo, Masè C & Turrini M.C eds., Commemorazione di Edoardo Semenza, , 113-120, Università di Ferrara, Italy, 20-May-2003, C017

Chowdhury R. & Flentje P., 2008, Strategic approaches for management of risk in geomechanics, The 12 th International Conference of International Association for Computer Methods and Advances in Geomechanics (IACMAG), 3031-3042, Goa - India, 1-6 october 2008, C029

Chowdury R., 1985, Aspects of the Vajont slide, International Conference on Dam Failures, 24, 533-544, Purdue University, Lafayette, Indiana, U.S.A, 5-8-August-1985, [http://www.sciencedirect.com/science?\\_ob=PublicationURL&\\_cdi=5803&\\_pubType=J&\\_acct=C000031439&\\_version=1&\\_urlVersion=0&\\_userid=607988&md5=c84b8d5cb751bfb4b0f31582a31af502&jchunk=24](http://www.sciencedirect.com/science?_ob=PublicationURL&_cdi=5803&_pubType=J&_acct=C000031439&_version=1&_urlVersion=0&_userid=607988&md5=c84b8d5cb751bfb4b0f31582a31af502&jchunk=24), C005

CNR-IIRPI, 2005, International design workshop Longarone, Erto, Casso, Ferrara, Italy, 4-11-July-2005, <http://unife.it/>, C014

Cobianchi M. & Picotti V., 2003, The Vaiont gorge section: the Toarcian to Bajocian Igne Formatio and the Unconformable base of the Vaiont Limestone, Santantonio M. ed., General Field Trip Guidebook, 6th International Symposium on the Jurassic System, 310-312, Palermo- Italy, 12-Sep-02, [http://meteor.bibvb.ac.at/F?func=find-b&find\\_code=IDN&local\\_base=acc01&request=AC03549198](http://meteor.bibvb.ac.at/F?func=find-b&find_code=IDN&local_base=acc01&request=AC03549198), C002

Garavello A. & Luciani V., 1986, Biostratigraphy of upper cretaceous and Paleocene of Vaiont valley (preliminary note), Semenza E. & Melidoro G. eds., Proceedings of the meeting on the 1966 Vaiont landslide, Convegno sulla frana del Vaiont, 217, Università di Ferrara, Italy, 17-19 September 1986, C026

Garbin C. & Vanin V., 1986, Tunnel excavation into the Vajont slide, Semenza E. & Melidoro G. eds., Proceedings of the meeting on the 1966 Vaiont landslide, Convegno sulla frana del Vaiont, 145-155, Università di Ferrara, Italy, 17-19 September 1986, C021

- Ghirotti M., 2003 Edoardo Semenza: L'importanza della geologia e della geomorfologia per l'identificazione dell'antica frana del Vaiont, Masè C & Turrini M.C eds., Commemorazione di Edoardo Semenza, , 161-171, Università di Ferrara, Italy, 20-May-2003, C018
- Guerricchio A. & Melidoro G., 1986, Geomorphological analysis of the Vaiont valley prior to the huge 1963 landslide, Semenza E. & Melidoro G. eds., Proceedings of the meeting on the 1966 Vaiont landslide, Convegno sulla frana del Vaiont, 157-168, Università di Ferrara, Italy, 17-19 September 1986, C022
- Hutchinson J.N., 1987, Mechanisms producing large displacements in landslides on pre-existing shears, 1st Sino-British Geological Conference, 9, 175-200, Taipei - Cina, <http://www.afs.enea.it/protprev/www/lineeguida2/bibliografia.htm>, C011
- Hutchinson J.N. & Kwan P.C.K., 1986, A re-assessment of some aspects of the stability of the Vaiont slide, Semenza E. & Melidoro G. eds., Proceedings of the meeting on the 1966 Vaiont landslide, Convegno sulla frana del Vaiont, 218, Università di Ferrara, Italy, 17-19 September 1986, C027
- Lo K.Y, Lee C.F. & Gelinas P., 1972, Alternative interpretation of the Vaiont slide edwards J Cording ed., Stability of Rock Slopes, Thirteenth Symposium on Rock Mechanics, 595-623, University of Illinois, Urbana, 30-Aug-1971, <http://cedb.asce.org/cgi/WWWdisplaybn.cgi?0872620476>, C004
- Mantovani F., Bollettinari G., Ghirelli C., 1991, The Vaiont rock landslide, Panizza M., Soldati M. & Coltellacci M.M. eds., European Experimental Course on Applied Geomorphology, 2, 65-76, Istituto di Geologia Università di Modena, Italy, 1991, C016
- Masetti D., 1986, Stratigraphy of the prequaternary formations outcropping in the Vaiont valley and in the neighbouring mountains groups, Semenza E. & Melidoro G. eds., Proceedings of the meeting on the 1966 Vaiont landslide, Convegno sulla frana del Vaiont, 179-186, Università di Ferrara, Italy, 17-19 September 1986, C023
- Nonveiller E., 1992, Vaiont slide Influence of frictional heat on slip velocity, SEMENZA E. & MELIDORO G eds., Proceedings of the meeting on the 1963 Vaiont landslide, 1, 187-197, Ferrara, Italy, 1986, C007
- Paronuzzi P., 2009, Un nuovo modello geologico-tecnico per l'interpretazione della catastrofica frana del Vajont, Atti del 3° Congresso Nazionale AIGA, , 358-359, Sangiovanni Valdarno (AR), 25-27-February-2009, C012
- Pasuto M. & Soldati A., 1991, Some cases of deep-seated gravitational deformations in the area of Cortina D'Ampezzo (Dolomiti). Panizza, M., Soldati, M., Coltellacci, M.M. eds., Proceedings of European Short Course on Applied Geomorphology, European experimental course on applied geomorphology, 91-104, Cortina d Ampezzo /Modena- Italy, 20-26- June -1990, <http://www.irpi.cnr.it/padova/pubblicazioni.htm>, C006
- Sadrekarami A. & Olson M., 2007, Review of the October 9, 1963 Failure of the Vaiont Reservoir Slope, Computer Applications in Geotechnical Engineering, Geo -Denver, Denver-Colorado-USA, 01-October 2007, <http://scitation.aip.org/getabs/servlet/GetabsServlet?prog=normal&id=ASCECP000220040901000010000001&idtype=cvips&gifs=yes>, C010

- Sembenelli P., 1986, Reflections on the methodology in engineering geology. The Vaiont case, Semenza E. & Melidoro G. eds., Proceedings of the meeting on the 1963 Vaiont landslide, Convegno sulla frana del Vaiont, 87-100, Università di Ferrara, Italy, 17-19 September 1986, C019
- Semenza E., 1986, New geological studies on the Vaiont Area, Semenza E. & Melidoro G. eds., Proceedings of the meeting on the 1966 Vaiont landslide, Convegno sulla frana del Vaiont, 199-213, Università di Ferrara, Italy, 17-19 September 1986, C024
- Semenza E. & Melidoro G., 1992, Proceedings of the meeting on the 1963 Vaiont landslide, SEMENZA E. & MELIDORO G. eds., Proceedings of the meeting on the 1963 Vaiont landslide, 1, 1-218, Ferrara, Italy, 1986, C008
- Sitar N. & MacLaughlin M., 1997, Sitar & MacLaughlin (1997)\_Kinematics and Discontinuous Deformation Analysis of Landslide Movement, II Panamerican Symposium on Landslides, Rio de Janeiro, 10-Nov-97, C003
- Vardoulakis I., 2001, Thermo-poro-mechanical analysis of rapid fault deformation, POWDERS & GRAINS, The 4th International Conference on Micromechanics of Granular Media, Sendai-Japan, 21-may-2001, C001
- Various Authors, 1992, Proceedings of the meeting on the 1963 Vaiont landslide., Semenza E., & Melidoro G. eds., Proceedings of the meeting on the 1963 Vaiont landslide., IAEG - Italian section, 1, 1-218, Ferrara, Italy, C030

## Monography

- Berlato P., Vajont. Una diga un'amore una tragedia, 2001, D025
- Bondesan A., Il Piave, 2000, 497, ISBN:8883140788 9788883140785, In Italian, , <http://books.google.it/books?id=9WmPuQF5JVgC>, D015
- Broglio Loriga C & Mantovani M. G, Microbiostratigrafia della serie affiorante nella massa scivolata dal M. toc (Vaiont) il 9 ottobre 1963 ed alcune ossevazioni su Foraminiferi, Radiolari, Calcisfere e Nannoconus, 1970, OCLC: 66258287, In Italian, <http://books.google.it/books?id=Lg0aGwAACAAJ&dq=vaiont>, D010
- Broglio Loriga C., Le biofacies del Cretacico della valle del Vaiont (Belluno), 1960, 1225, In Italian, , <http://books.google.it/books?id=J2ouAAAIAAJ&dq=vaiont&lr=&pgis=1>, D011
- Canestrini S., Vajont: genocidio dei poveri, 2003, 122, ISBN :97888831420938, In italian, <http://www.campedel.it/schede/158012.HTM>, D047
- Capraro V., Vajont. Itinerari nel cuore e nella storia, 1998, 12, In Italian, D030
- Carloni G. C., Il Vaiont trent'anni dopo: Esperienza di un geologo, 1995, 109, ISBN 8880911368, 9788880911364, In Italian, <http://books.google.it/books?id=uPzNAAAACAAJ&dq=Vaiont>, D002
- Casagrande G., Il disastro del Vajont. Brevi note storico-tecniche, 2004, 44, ISBN:8890125012, 9788890125010, In Italian, [http://books.google.it/books?id=yTC\\_HgAACAAJ&dq=IL+DISASTRO+DEL+VAIONT&lr=,](http://books.google.it/books?id=yTC_HgAACAAJ&dq=IL+DISASTRO+DEL+VAIONT&lr=,) D016



- Casagrande G., Storia di un lago e di una montagna, 2001, 357, ISSN: 8887274711, [http://www.unilibro.it/find\\_buy/Scheda/libreria/autore-casagrande\\_gianluca/sku-1870056/storia\\_di\\_un\\_lago\\_e\\_una\\_montagna\\_un\\_racconto\\_del\\_vajont\\_.htm](http://www.unilibro.it/find_buy/Scheda/libreria/autore-casagrande_gianluca/sku-1870056/storia_di_un_lago_e_una_montagna_un_racconto_del_vajont_.htm), D026
- Corona M., Il volo della Martora, 1998, 212, In Italian, [http://www.infolibro.it/mauro\\_corona.htm](http://www.infolibro.it/mauro_corona.htm), D032
- Corona M., Vajont: quelli del dopo, 2006, 73, ISBN: 97888045581702, In Italian, <http://www.campedel.it/schede/187606.HTM>, D039
- Dal Cin & Papin, La fiaba del Vajont, 2004, 32, ISBN :97888822211025, In Italian, <http://www.campedel.it/schede/161318.HTM>, D043
- Datei C., Vajont. La storia idraulica, 2005, 137, ISBN :97888778425349, In Italian, <http://www.campedel.it/schede/182010.HTM>, D040
- Galli A., Dopo Vajont (1963-1968). E' giusto che se ne parli, 2008, 109, In Italian, <http://www.campedel.it/schede/211499.HTM>, D035
- Galli A. & Bez M., L'ultima valigia, 2003, 165, In Italian, <http://www.campedel.it/schede/166667.HTM>, D044
- Luciani V., Biostratigrafia al limite cretaceo/terziario nella Valle del Vaiont (Alpi Bellunesi), 1998, OCLC: 65407328, In Italian, <http://books.google.it/books?id=jel4HAAACAAJ&dq=Vaiont>, D006
- Luciani V., Biostratigrafia al limite cretaceo/terziario nella Valle del Vaiont (Alpi Bellunesi), 1998, OCLC:65407328, In Italian, <http://books.google.it/books?id=jel4HAAACAAJ>, D007
- Mantovani F., Il grande movimento franoso del Vaiont, 2004, 127-129, ISBN: 88-523-8913-X, In Italian, [http://www.igmi.org/pubblicazioni/atlante\\_tipi\\_geografici/index.php](http://www.igmi.org/pubblicazioni/atlante_tipi_geografici/index.php), D024
- Masè G, Semenza M, Semenza Pa, Semenza P & Turrini MC, Le foto della frana del Vajont, 2004, ISBN:88892880090, In Italian, <http://www.k-flash.it/>, D009
- Merlin T, Sulla pelle viva. Come si costruisce una catastrofe. Il caso Vajont, 2001, 196, ISBN: 8883141210, In Italian, [http://www.unilibro.it/find\\_buy/Scheda/libreria/autore-merlin\\_tina/sku-972252/sulla\\_pelle\\_viva\\_come\\_si\\_costruisce\\_una\\_catastrofe\\_il\\_caso\\_vajont\\_.htm](http://www.unilibro.it/find_buy/Scheda/libreria/autore-merlin_tina/sku-972252/sulla_pelle_viva_come_si_costruisce_una_catastrofe_il_caso_vajont_.htm), D023
- Merlin T., La rabbia e la speranza, 2004, 264, ISBN 8883142330, 9788883142338, In Italian, <http://books.google.it/books?id=Kr5oAAAAMAAJ&q=tina+merlin&dq=tina+merlin&pgis=1>, D021
- Merlin T., Vajont 1963. La costruzione di una catastrofe, 1996, 136, ISBN: 8880790935, In Italian, [http://www.unilibro.it/find\\_buy/Scheda/libreria/autore-merlin\\_tina/sku-194032/vajont\\_1963\\_la\\_costruzione\\_di\\_una\\_catastrofe\\_.htm](http://www.unilibro.it/find_buy/Scheda/libreria/autore-merlin_tina/sku-194032/vajont_1963_la_costruzione_di_una_catastrofe_.htm), D022
- Palmieri N., Vajont, Stava, Agent Orange. Il costo di scelte irresponsabili, 1997, ISBN: 8813202423, In Italian, <http://www.deastore.com/libro/vajont-stava-agent-orange-il-nicola-w-palmieri-cedam/9788813202422.html>, D033
- Paolini M & Ponte di Pino, Quaderno del Vajont, 2005, In Italian, [http://books.google.it/books?id=j6yOOgAACAAJ&dq=VAIONT+paolini&lr=&source=gbs\\_book\\_other\\_versions\\_r&cad=0\\_1](http://books.google.it/books?id=j6yOOgAACAAJ&dq=VAIONT+paolini&lr=&source=gbs_book_other_versions_r&cad=0_1), D020

- Paolini M & Vacis G., Il racconto del Vajont, 1997, 142, ISBN 8811620309, 9788811620303, <http://books.google.it/books?id=mZUfAAAACAAJ&dq=VAIONT+paolini&lr=,> D018
- Parlamento, Commissione Parlamentare d'inchiesta, Commissione parlamentare d'inchiesta sul disastro del Vajont, 2003, 84, ISBN 8849806558, 9788849806557, In Italian, <http://books.google.it/books?id=O-4BBxt7RyEC,> D014
- Passi M., Vajont senza fine, 2003, 174, ISBN :97888849044230, In Italian, <http://www.campedel.it/schede/160450.HTM,> D045
- Pittarello B., Vajont ottobre 1963, 2008, 85, ISBN 97888831427418, In Italian, <http://www.campedel.it/schede/171323.HTM,> D037
- Pittarello B., Le pietre del Vajont, 2006, 114, ISBN 97888831437620, In Italian, <http://www.campedel.it/schede/194644.HTM,> D038
- Pro loco di Longarone, Vajont Longarone l'histoire, 2003, 47, In Italian, <http://www.campedel.it/schede/157670.HTM,> D048
- Ragogna G., Vajont. Un grande romanzo dimenticato, 2001, 229, ISBN: 9788887881578x, In Italian, <http://www.campedel.it/schede/145149.HTM,> D027
- Reberschak M., Grande Vajont, 2003, 487, ISBN :97888831419358, In Italian, <http://www.campedel.it/schede/159245.HTM,> D046
- Riva M.et ali, Geologia delle Valli Vaiont e Gallina (Dolomiti Orientali), Geologia delle Valli Vaiont e Gallina (Dolomiti Orientali), 1990, 2, 55-76, OCLC: 65535161, In Italian, OCLC: 65535161<http://OCLC:65535161,> D005
- Sacchet A., Vajont la diga, 2008, 158, In Italian, <http://www.campedel.it/schede/160979.HTM,> D034
- Semenza E & Ghirotti M., Vaiont-Longarone: 34 anni dopo la catastrofe, 1997, 7, 63-94, In Italian, <http://books.google.it/books?id=h09vHAAACAAJ&dq=vaiont,> D013
- Semenza E., Sintesi degli studi geologici sulla frana del Vaiont dal 1959 al 1964, Sintesi degli studi geologici sulla frana del Vaiont dal 1959 al 1964, 1966, 16, 3-51, In Italian, D004
- Semenza E., La storia del Vaiont raccontata dal geologo che ha scoperto la frana, 2001, 280, ISBN 8886245912, 9788886245913, In Italian, <http://books.google.it/books?id=jFN4AAAACAAJ&dq=Vaiont,> D008
- Toffolo M., Vajont: monumento e spazi espositivi. La monumentalizzazione della memoria, 1998, VII-48, # ISBN: 8888028005, In Italian, <http://www.libreriauniversitaria.it/vajont-monumento-spazi-espositivi-monumentalizzazione/libro/9788888028002,> D031
- Trevisan L., Selli R, Selli E., Carloni GC., La frana del Vaiont, 1964, OCLC: 66256116, In Italian, <http://books.google.it/books?id=4s7JHAAACAAJ&dq=Vaiont,> D003
- Vacis G. et al, Vajont 9 ottobre '63, orazione civile, 1999, 120, ISBN: 880615320X, 9788806153205, In Italian, with DVD, <http://books.google.it/books?id=X9aZAAAACAAJ&dq=VAIONT+paolini&lr=,> D019
- Various Authors, Rivista italiana di paleontologia e stratigrafia, 1969, 75, 324, In Italian, Digitalizzato il 19 apr 2006, <http://books.google.it/books?id=d2Oxirk6efUC&q=Vaiont&dq=Vaiont&pgis=1,> D001

- Various Authors, Rivista Geografica Italiana, Aspetti geomorfologici della frana del Vaiont, 1964, 71, <http://books.google.it/books?id=eFAsAAAAMAAJ&q=vaiont&dq=vaiont&lr=&pgis=1>, D012
- Various Authors, Rivista Italiana di Paleontologia e Stratigrafia, 1965, 71, In Italian, , <http://books.google.it/books?id=R-YBPTZ3MSIC&q=VAIONT&dq=VAIONT&lr=&pgis=1>, D017
- Various Authors, La notte del Vajont. Storie di solidarietà, 1998, In Italian, <http://www.libreriauniversitaria.it/notte-vajont-storie-solidarieta-cadore/libro/9788823003309>, D029
- Various Authors, Disastro del Vajont, 2004, 84, ISBN: 97888498065578, In Italian, (cd-rom), <http://www.campedel.it/schede/164905.HTM>, D042
- Various Authors, Le dighe e le centrali idroelettriche del bacino del Piave, 2001, 63, In Italian, <http://www.campedel.it/schede/143513.HTM>, D050
- Various Authors, Longarone - the history, 2001, 47, <http://www.campedel.it/schede/157669.HTM>, D051
- Vastana L., Vajont l'onda lunga, 2008, 270, ISBN 97888792897022, In Italian, <http://www.campedel.it/schede/211451.HTM>, D036
- Vendramini F., Governo locale amministratori, società a Longarone 1866-1963, 2002, 255, In Italian, <http://www.campedel.it/schede/153729.HTM>, D049
- Venturini O., Vajont. Il giorno dopo, 2005, 109, ISBN: 97888889390941, In Italian, <http://www.campedel.it/schede/181135.HTM>, D041
- Zanfron B., Vajont - 9 ottobre 1963 - Cronaca di una catastrofe, 2000, In Italian, <http://www.campedel.it/schede/117885.HTM>, D028

## Maps

- Carloni G.C & Mazzanti R., 1964, Rilevamento geologico della frana del Vaiont, GIORNALE DI GEOLOGIA, 32, In, "Selli R., Trevisan L., Carloni G.C., Mazzanti R., Ciabatti M.", La frana del Vaiont, E004
- Riva M., Besio M., Masetti D., Roccati F. Sapigni M., Semenza E., 1990, Carta geologica delle Valli Vaiont e Gallina, ANNALI DELL'UNIVERSITA' DI FERRARA, 2, 76, E005
- Riva M., Besio M., Masetti D., Roccati F. Sapigni M., Semenza E., 1990, Profili geologici delle valli Vaiont e Gallina, ANNALI DELL'UNIVERSITA' DI FERRARA, 2, 76, E006
- Rossi D. & semenza E., 1986, Carta geologica del versante settentrionale del Monte Toc e zone limitrofe, "- Vaiont slide before October 9, 1963 - Scale 1:5.000", [http://www.k-flash.it/editoria\\_en.html](http://www.k-flash.it/editoria_en.html), In, "Masè G., Semenza M., Semenza P., Semenza P.,Turrini M.C.", Le foto della frana del Vajont, E001
- Rossi D. & semenza E., 1986, Carta geologica del versante settentrionale del Monte Toc e zone limitrofe, " - Vaiont slide after October 9, 1963 - Scale 1:5.000", [http://www.k-flash.it/editoria\\_en.html](http://www.k-flash.it/editoria_en.html), In, "Masè G., Semenza M.,Semenza P., Semenza P.,Turrini M.C.", Le foto della frana del Vajont, E002
- Sapigni M. et al, 1986, Carta geologica schematica della valle del Vaiont e zone limitrofe, Scale 1:25.000, E003

## Unpublished reports

- Dal Piaz. G., 1928, Relazione di massima su due sezioni del Vajont prese in considerazione per progetti di sbarramento idraulico, Unpublished report for S.A.D.E- In Italian, Venezia, F001
- Fratini M., Arredi F., Boni A., Fasso C. , Scarsella F., 1964, Relazione sulle cause che hanno determinato la frana nel serbatoio del Vajont (9 Ottobre 1963), 92pp, Report prepared for ENEL. Roma. In Italian, Roma, F002
- Giudici F. & Semenza E., 1960, Studio geologico del serbatoio del Vajont, Report for S.A.D.E., Part A: 21 pp, text, Part B: 68 photos with discussions, 42pp. In Italian, Venezia, F003
- Muller L., 1961, Talsperre Vaiont, Report for SADE - In German, Venezia, F004
- Muller M., 1961, La frana nella zona del Toc, In Italian, Diga Vaiont: 7° rapporto geologico preparato per conto della società Adriatica di elettricità- Venezia, F005

## Other

- Agliardi F., 2006, Tecniche di monitoraggio applicate alla stabilità dei versanti, Divulgement, Geological Engineering, G001
- Bocca G., Rumiz P. & Bianchin R., 2003, Il 9 ottobre di quarant'anni fa. I 1910 morti di Longarone, La Repubblica, Divulgement, Geosciences 211, 30-March-2005, G002
- Cecinato F. & Zervos A., 2003, Thermo-mechanical modelling of catastrophic landslides, 39-41, In Italian, [www.larepubblica.it](http://www.larepubblica.it), 8-october-2003, G003
- Comitato per i sopravvissuti del Vaiont, 2007, Course Outline and Introduction, Divulgement, G004
- E.Eberhart, 2004, The Vaiont dam, Divulgement, University of Southampton, G005
- Federal Energy Regulatory Commission Division of Dam Safety and Inspections, 1999, ARCH DAMS, In Italian, Relazione sulla tragedia del Vaiont, Le roccaforti del mondo, Locarno, 26-27-April-2007, G006
- Helmstetter, 2002, Ruptures et instabilités: sismicité et mouvements gravitaires, En française, These de Doctorat del Université Joseph Fourier - Grenoble I Spécialité : Géophysique, Grenoble, 13-september-2002, G007
- Kinakin D., Introduction to Soil and Rock Engineering, In Spanish, Divulgement, G008
- Martinelli R., 2002, Vajont, In Italian - FILM, DNC, G009
- Parker R.L., 2005, Mass Movements, Earlham Physical Geology, In Italian, Video, <http://www.campedel.it/schede/122793.HTM>, STUDIO 2000Hertz, G010
- Petley D., 2008, Mechanisms of failure in large landslides, 179, Related to evaluate the safety and structural integrity of existing arch dams., Federal Energy Regulatory Commission Division of Dam Safety and Inspections, Engineering Guidelines For The Evaluation Of Hydropower Projects, Washington, October-1999, G011

Pro loco di Longarone, 2001, Longarone Vajont: la storia, In Italian, Divulgement, Course post-Laurea, Lugano, 23- february-2006, G012

Las roturas de Malpasset y Vaiont, Divulgments, G013

## Web

Animazione digitale della frana del Vajont, - In Italian (video) - Not includes scientific content, <http://www.youtube.com/watch?v=uqkFXm2HtMA>, H019

Associazione culturale TINA MERLIN, - In Italian - Not includes scientific content, <http://www.tinamerlin.it/>, H008

Associazione superstiti VAJONT, - In Italian - Not includes scientific content, [http://www.longarone.net/associazioni/superstiti\\_vajont.html](http://www.longarone.net/associazioni/superstiti_vajont.html), H004

Business Vaiont - Le Iene, - In Italian (video) - Not includes scientific content, <http://www.youtube.com/watch?v=mWaJIDcO6jM>, H020

Comitato Sopravvisuti Vajont, - In Italian - Not includes scientific content, <http://www.sopravvissutivajont.org/>, H007

COMUNE DI ERTO E CASSO, - In Italian - Not includes scientific content, <http://www.comune.ertoecasso.pn.it/>, H003

Dave's landslide blog, - Includes scientific content, <http://daveslandslideblog.blogspot.com/2008/12/vaiont-vajont-landslide-of-1963.html>, H011

DISASTRO DEL VAJONT, DIGA DEL VAJONT, - In Italian - Includes scientific content, <http://www.vajont.net/>, H001

Documentario Vajont - da rete Veneta, - In Italian (video) - Not includes scientific content, <http://www.youtube.com/watch?v=478ZQhr3ees>, H021

Fondazione Vajont, - In Italian - Not includes scientific content, <http://www.fondazionevajont.org/modules.php?name=Content&pa=showpage&pid=33&Itemid=93>, H013

I luoghi del Vajont, - In Italian - Not includes scientific content, <http://www.erto.it/>, H005

Il disastro del Vajont, - In Italian - Includes scientific content, [http://it.wikipedia.org/wiki/Disastro\\_del\\_Vajont](http://it.wikipedia.org/wiki/Disastro_del_Vajont), H009

Il racconto del Vajont, - In Italian - Not includes scientific content, [http://www.marcopaolini.it/files/index.cfm?id\\_rst=19&id\\_elm=153](http://www.marcopaolini.it/files/index.cfm?id_rst=19&id_elm=153), H006

La frana del Vaiont, - In Italian - Not includes scientific content, <http://digilander.libero.it/mlcoco/Frana%20Vajont.htm>, H017

La storia del Vaiont, In Italian Not includes scientific content, <http://www.mattolinimusic.com/vajont/uno.htm>, H0025

La strage del Vaiont - (1963), - In Italian (video) - Not includes scientific content,  
<http://www.youtube.com/watch?v=AgE2IJc7lrs>, H022

LONGARONE provincia di Belluno, - In Italian - Not includes scientific content, <http://www.longarone.net/>,  
H002

Magico Vaneto Montagna Veneta, - In Italian - Not includes scientific content,  
<http://www.magicoveneto.it/Friuli/Vajont/DigaF01.htm>, H018

Marco Paolini - Vajont 0/19, - In Italian (video) - Not includes scientific content,  
<http://www.youtube.com/watch?v=OUe2-APrVds>, H024

Museo di scienze naturali, - In Italian - Not includes scientific content,  
[http://www.regione.piemonte.it/museoscienze/mostre/temporanee/3diga\\_vajont1.htm](http://www.regione.piemonte.it/museoscienze/mostre/temporanee/3diga_vajont1.htm), H016

Museologando, - In Italian - Not includes scientific content,  
<http://www.museologando.com/museologia/navigazione/ecoVajont.php>, H015

Vaiont dam (Italy), - Includes scientific content, <http://www.geocities.com/geogsoc2000/Vaiont1.htm>, H010

Vaiont dam (Italy), - Not includes scientific content,  
<http://www.uwsp.edu/geo/projects/geoweb/participants/Dutch/VTrips/Vaiont.HTM>, H012

VAIONT: 40 anni dopo, - In Italian - Not includes scientific content,  
<http://quotidianiespresso.repubblica.it/corrierealpi/speciali/vajont2/museo.html>, H014

Vajont - documentario completo, - In Portuguese (video) - Not includes scientific content,  
<http://www.youtube.com/watch?v=WoE6uzAFoOU>, H023

# Preliminary results of a photogrammetric characterisation of the 1963 Vajont rockslide

Andrea Wolter, Doug Stead, & John J. Clague

*Department of Earth Sciences – Simon Fraser University, Burnaby, BC, CANADA*

Laura Superchi & Rinaldo Genevois

*Department of Geosciences – University of Padova, Padova, ITALY*

Monica Ghirotti

*Department of Earth and Geoenvironmental Sciences – University of Bologna, Bologna, ITALY*

## ABSTRACT

The 1963 Vajont Slide was an unparalleled natural disaster; it produced a displacement wave that overtopped the Vajont Dam and destroyed several villages, with the loss of over 2000 lives. In the aftermath of this catastrophe, numerous researchers have attempted to understand the mechanisms and behaviour of the landslide. This paper presents the results of the first detailed digital photogrammetric survey of the Vajont failure surface. Discontinuity orientations were detected and eight discontinuity sets were characterised. Surface morphology profiles reveal several scales of roughness and folding, from a regional-scale syncline to small-scale roughness, all of which played a significant role in failure behaviour.

## RÉSUMÉ

Le glissement du Vajont, en 1963, fut un désastre naturel et humain qui a détruit plusieurs villages et tué plus de 2000 personnes. De nombreux chercheurs ont tenté de comprendre les mécanismes et le comportement du glissement. Cet article présente les résultats d'une première analyse photogrammétrique détaillée de la surface de rupture. Des mesures de l'orientation des discontinuités ont été effectuées, et regroupées en huit familles. Des profils suggèrent plusieurs échelles de rugosité et de plis, de la dimension du synclinal régional à celle de la rugosité primaire, qui ont joué un rôle important dans le comportement du glissement.

## 1 INTRODUCTION

On October 9, 1963, about 270 million m<sup>3</sup> of rock slid into the newly created Vajont Reservoir. The landslide generated a displacement wave that overtopped the Vajont Dam and flooded settlements below, killing over 2000 people.

Although the landslide has been intensively studied over the past 50 years, its dynamic and kinematic behaviour remains poorly understood. Early workers, including Semenza (1965), Mencl (1966), Skempton (1966), Broili (1967), and Müller (1968) reported on the geology, geomorphology, engineering geology, and hydrogeology of the landslide and surrounding area. Hendron and Patton (1985) described the importance of clay layers in a seminal report on the landslide. In the 1970s and 1980s, the focus of study began to shift to landslide mechanisms. Most researchers agree that the 1963 failure occurred at the site of a larger prehistoric landslide (Müller 1968, Trollope 1980, Hendron and Patton 1985, Tika and Hutchinson 1999, Semenza and Ghirotti 2000). Mantovani and Vita-Finzi (2003), however, hypothesise that the failure surface is a normal fault plane, marked by fault gouge, cataclasite, and mylonite. Petley and Petley (2006) also argue against the idea that the landslide was reinitiated from a paleo-landslide; they cite brittle-ductile deformation of the clay layers as an alternative mechanism. Heat-induced vaporisation (Habib 1975, Goguel 1978, Nonveiller 1987), fluid pressure (Voight and Faust 1982), thermo-poro-mechanical

softening (Vardoulakis 2002), and rock-cracking (Kilburn and Petley 2003) are other proposed mechanisms. Ghirotti (1992) investigated the significance of in-situ stresses and reservoir level on the failure using the two-dimensional distinct element code UDEC. Sitar and MacLaughlin (1997) employed Discontinuous Deformation Analysis (DDA) to analyse the importance of block size on friction.

Researchers at Simon Fraser University (SFU) and the Universities of Padova and Bologna are currently conducting research on the structural controls of the Vajont Slide. Superchi et al. (2010) created bibliographic and GIS databases summarising research on the landslide. We use discontinuity surveys and remote sensing to characterise the geomechanics and structural geology.

This paper summarises the results of preliminary analyses of the first digital photogrammetric models of the Vajont failure surface. Remote sensing of the failure surface allows us to characterise of previously inaccessible areas, and thus is important in the analysis of the slide. Lenses with focal lengths ranging from  $f=20$  mm to  $f=400$  mm allowed for different resolutions and scales of the failure surface to be investigated. These results are compared with field data collected by researchers at the University of Padova.

## 2 STUDY AREA

The 1400-m-deep Vajont Valley is located in the Dolomites of northeastern Italy (Figure 1). Its morphology is controlled by the Erto syncline, which plunges to the east, and the erosional effects of Pleistocene glaciations. Glaciers broadened and deepened a valley that had been eroded by a proto-Vajont river prior to the Pleistocene. When glaciers last receded, they left a broad valley with oversteepened sides. Several large landslides occurred on the oversteepened slopes during the Holocene; the Vajont Slide is the most recent of these. The Vajont River incised sediments on the valley floor and created an epigenetic gorge at the mouth of the valley.

Rocks involved in the landslide include Late Jurassic and Cretaceous carbonate rocks interlayered with clay and marl laminae. Permeable limestones of the Dogger Formation underlie the failure surface (Figure 1c; Semenza and Ghirotti 2000). Although clay is not exposed on the failure plane, it is thought to have played an important role in the movement of the rock mass (Skempton 1966, Hendron and Patton 1985, Genevois and Ghirotti 2005).

The failure surface is chair-shaped: the back dips approximately 35°, whereas the seat is subhorizontal. The sliding surface follows bedding and the Erto syncline along the steeper back slope and cuts across bedding in the seat area. The profile of the sliding surface becomes more circular to the east (Rossi and Semenza 1981).

## 3 METHODOLOGY

Camera stations were located in the Vajont Valley between 1 and 2.5 km from the sliding surface (Figure 2). We used a Canon 50D digital camera and lenses with focal lengths of  $f=20$ , 50, 100, 200, and 400 mm to capture features of different scales. The results reported in this paper are based on one model built using an  $f=20$  mm lens and five models produced using an  $f=400$  mm lens (Table 1). Ground point spacing is the product of the ground pixel size and step size (Sturzenegger et al. 2009). Our analysis focused on discontinuity orientation and failure surface morphology. We mapped and analysed discontinuities on the photogrammetric models using Adam Technology and InnovMetric software. Surface morphology was characterised using surface residuals and selected topographic profiles. The  $f=20$  mm profiles followed the strike and dip of the bedrock, whereas those on the  $f=400$  mm models followed the highest amplitude of surface features. These profiles were chosen to illustrate the variability in morphology. The length of the profiles ranged from 40 to 480 metres. Four of the five  $f=400$  mm models were used in the discontinuity analysis; two of these models were used for preliminary morphology analysis. The two models chosen for morphology analysis were the smoothest and roughest models.

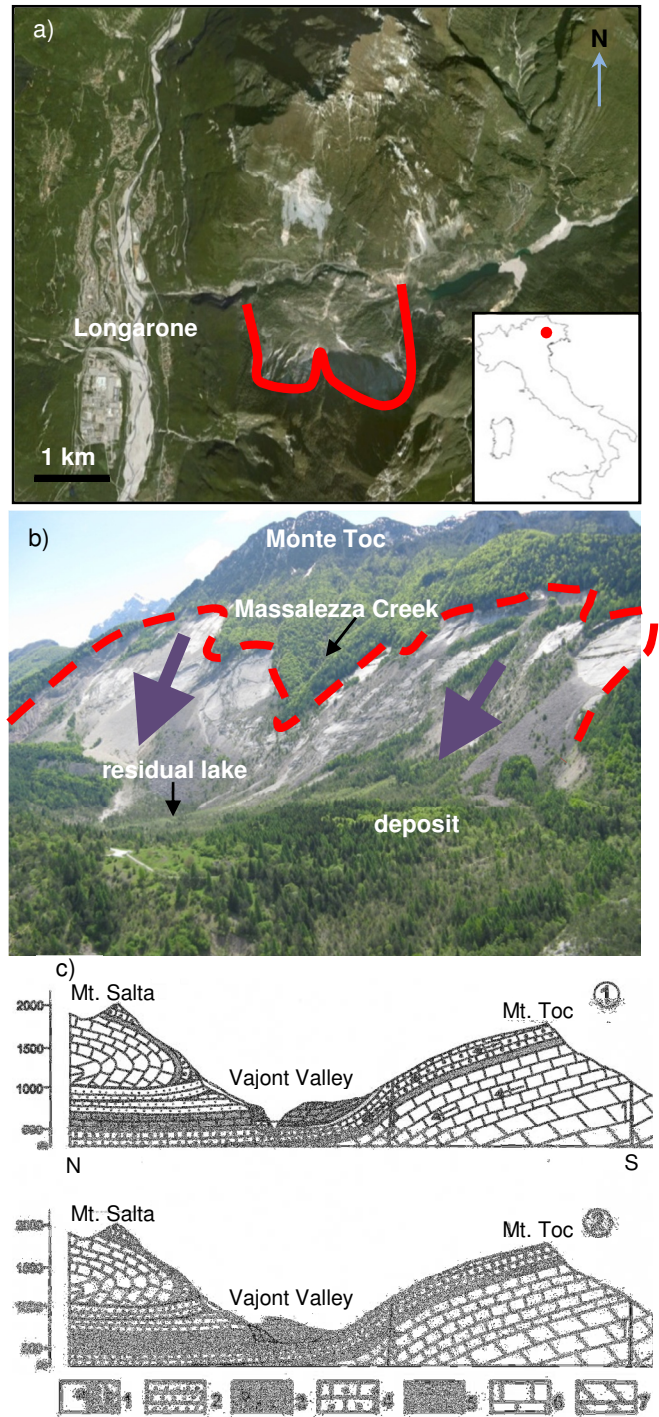


Figure 1. a) Location of the Vajont Slide. The red line delineates the landslide margin. b) Photograph of the landslide; red line marks the failure limit and purple arrows show the direction of movement. c) Cross-sections of the slide (1) before and (2) after the landslide. Legend: 1a) Quaternary, 1b) stratified alluvial gravels; 2) Cretaceous Scaglia Rossa; 3) Cretaceous-Jurassic formations, b) Soccher Formation, c) Fonzaso Formation; 4) Dogger Calcare del Vajont; 5) Jurassic Igne Formation; 6) Jurassic Soverzene Formation; 7) Triassic Dolomia Principale (Semenza and Ghirotti 2000).



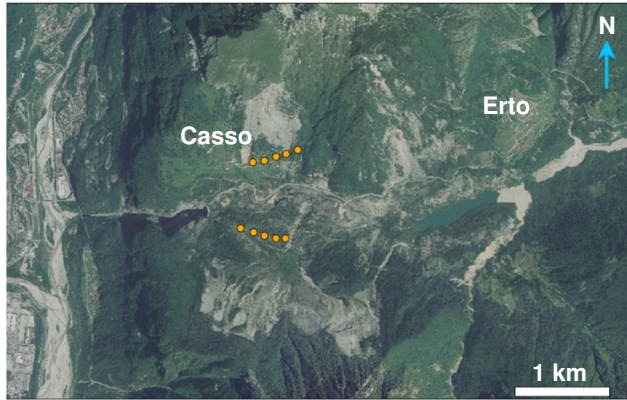


Figure 2. Locations of camera stations where photographs were taken for the f=20 mm and f=400 mm models, denoted by solid gold circles.

Table 1. Focal lengths and ground point resolutions of the models used for analysis. Model numbers correspond to those in Figure 4.

Model	Focal Length (mm)	Distance (m)	Ground point spacing (cm)	Description
1	20	2000	375	whole area
2	400	1000	10	west corner
3	400	1000	10	west headscarp
4	400	1000	10	east fold
5	400	1000	10	central area
6	400	2500	24	central area

## 4 RESULTS

### 4.1 Discontinuity Sets

The field-mapped geomechanical data and photogrammetric results correspond well. Field surveys indicate the existence of five domains within the landslide area, three of which incorporate the sliding surface (Figure 3). Domains 1 and 3 are the east and west halves of the failure surface; they are separated by Domain 2, which is an area of complex folding. Seven discontinuity sets (DS) occur within these domains. The photogrammetric analysis yielded eight discontinuity sets, one of which was not recognised in the field or in COLTOP analyses conducted by Superchi et al. (2010) (Table 2, Figures 4 and 6). The f=20 mm model shows the failure surface orientation, as well as DS6 and DS8 as identified in the field mapping. The f=400 mm models exhibit all eight discontinuity sets and the change in the orientation of the sliding surface from east to west. DS6 and DS8, as well as two discrete discontinuities not mapped previously, were recorded in Model 2. These isolated discontinuities require further field investigation to determine if they are random discontinuities or representations of a distinct joint set. Model 3 included DS1, DS3, DS7, DS8, and a new set (DS9). DS3, DS8,

and a discontinuity with the same orientation as DS9 were also identified in Models 4 and 5.

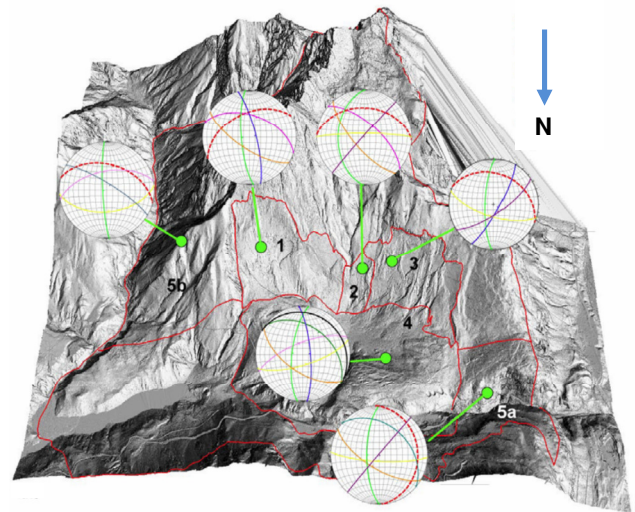


Figure 3. Domains (outlined in red) and discontinuity sets determined from field surveys. See Table 2 for legend.

Table 2. Discontinuity sets (DS) recognised in the field and photogrammetric models. See Figures 3 to 6.

DS	Symbol	Dip (°)	Dip Direction (°)
1		30	060
2 <sup>1</sup>		30	005
3		60	270
5 <sup>2</sup>		75	100
6		50	200
7		70	220
8		80	300
9		50	310

<sup>1</sup>bedding plane

<sup>2</sup>DS4 has been used in field domains 4 and 5 (see Figure 3).

The orientations and locations of steps in the failure surface were noted while mapping the discontinuity sets. Most of the steps are in the central and western parts of the sliding surface and coincide with the orientation of DS 8 (Figures 3 and 4). Other steps have more variable orientations.

### 4.2 Surface Morphology

Preliminary analysis of the undulations on the sliding surface indicates a complex folding history. The bedding and most of the failure surface follow the Erto syncline. Two main sets of mesoscale folds, identified both in the field and the photogrammetric models, trend approximately NNE and E. Parasitic folds and small-scale roughness are present in each of these fold sets.

Surface morphology was analysed qualitatively using residuals and surface profiles. Residuals were derived from a plane fit to a selected area of the two f=400 mm point clouds (Figure 7). Plots of the residuals are useful for visualising the three-dimensional morphology of the failure surface. They highlight undulations related to the interference patterns of the two mesoscale folding events.

The western area (Figure 7a) is concave and much smoother than the central folded area (Figure 7b). It is marked by one large and several smaller steps, as well as conjugate discontinuities. The central area includes a large fold with smaller parasitic folds along its limbs. The upper fold limb has a step that is visible on the f=20 mm model.

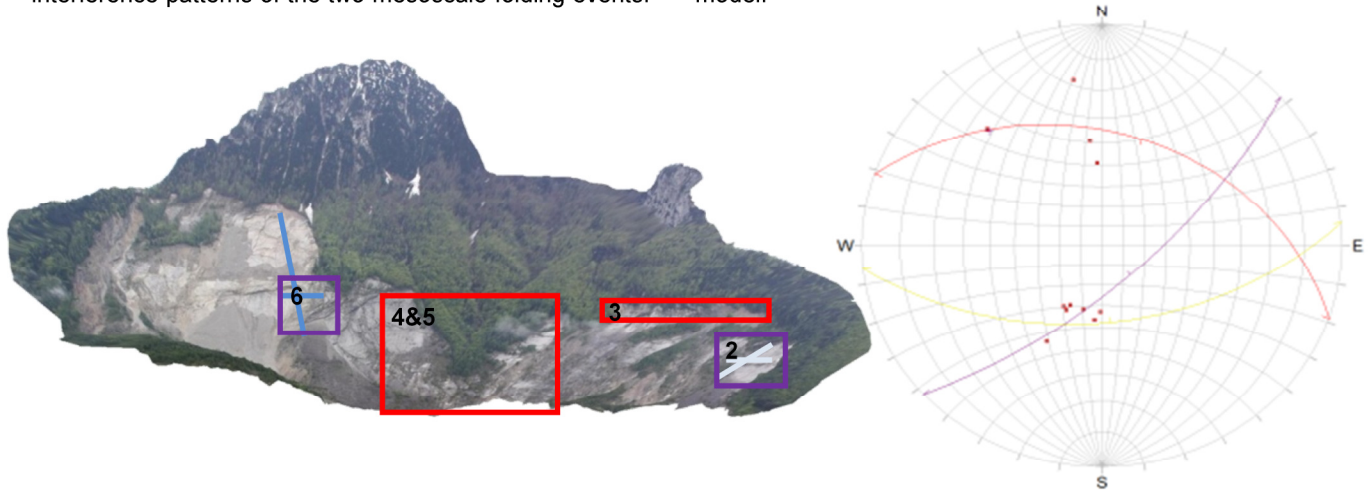


Figure 4. Preliminary f=20 mm photogrammetry model and stereonet of the Vajont Slide. Purple outlines indicate models used for surface morphology analysis (Figure 5), and red outlines indicate those used for discontinuity analysis (two are included in the lower central outline; Figure 6). The model outlined in purple on the right was used for both discontinuity and morphology analyses. Numbers refer to models in Table 1. Thick blue lines are approximate locations of the f=20 mm cross-sections in Figure 8.

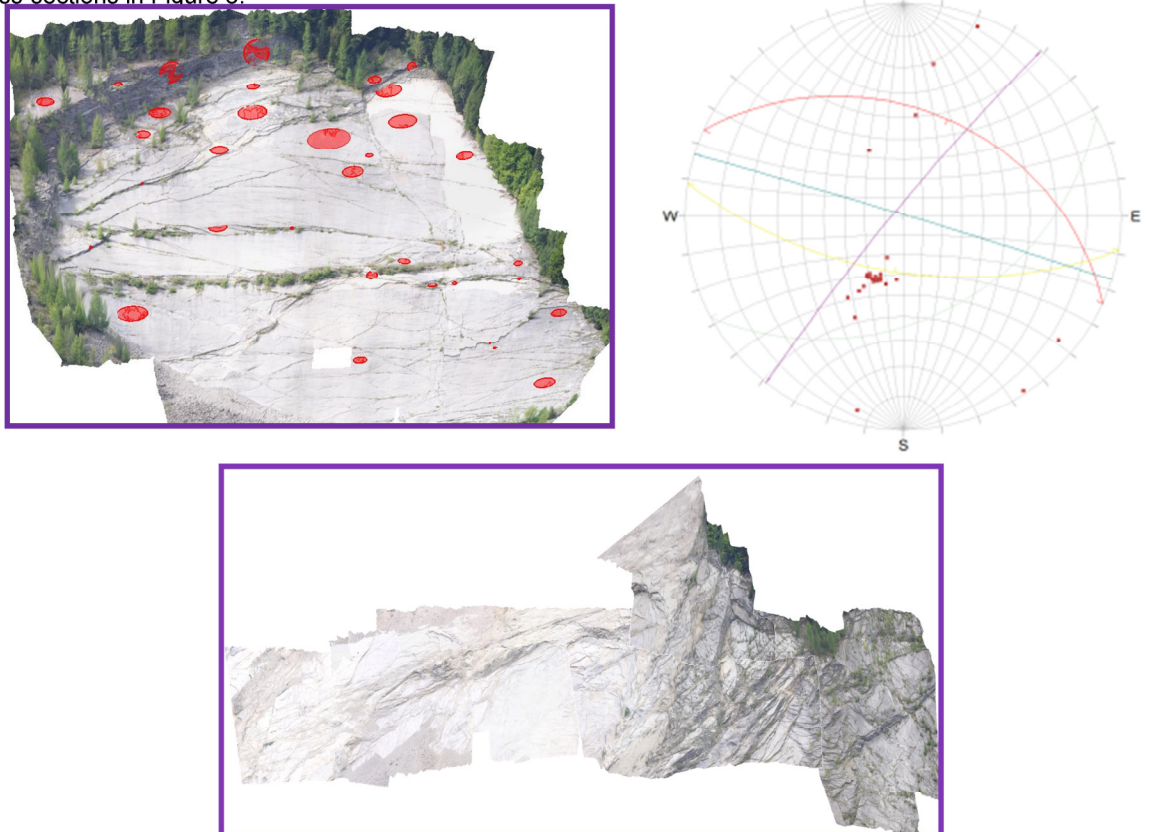
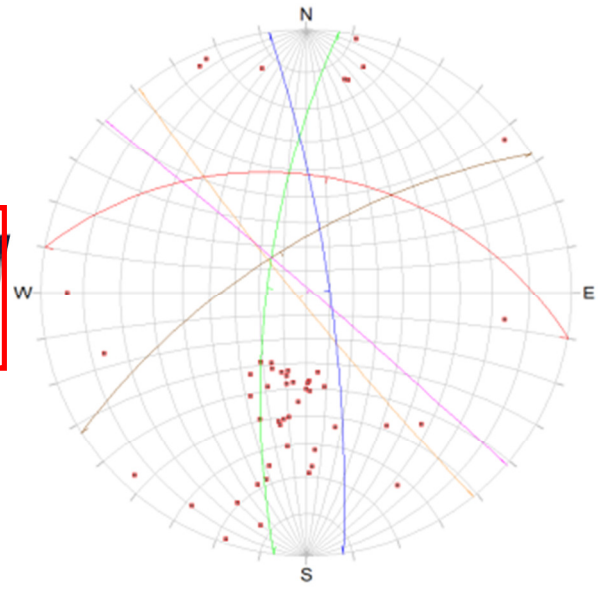


Figure 5. Model 2 and its stereonet (above), and Model 6 (below) used for morphology analysis. Red circles are planes mapped on the models. See Figure 4.

a) Model 3



b) Models 4 & 5

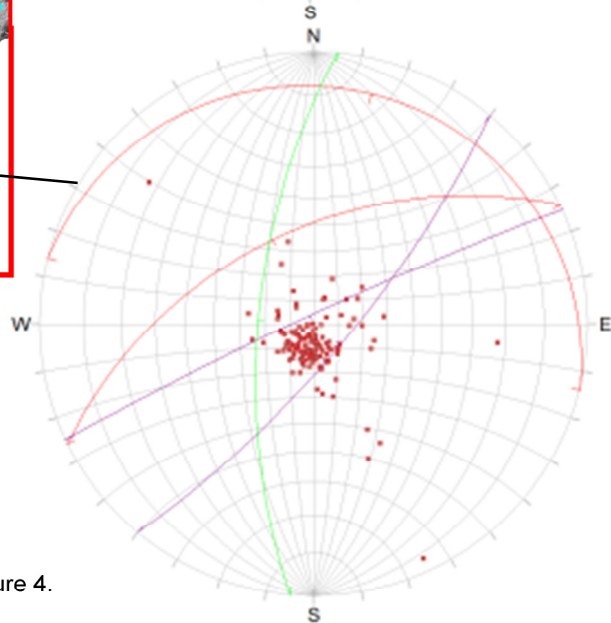
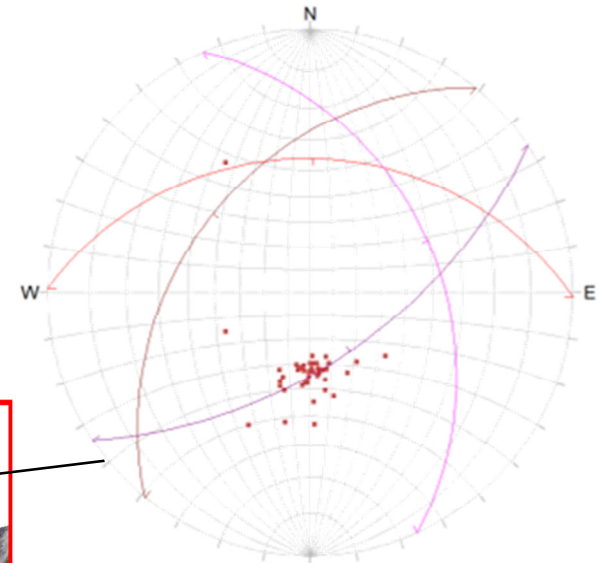
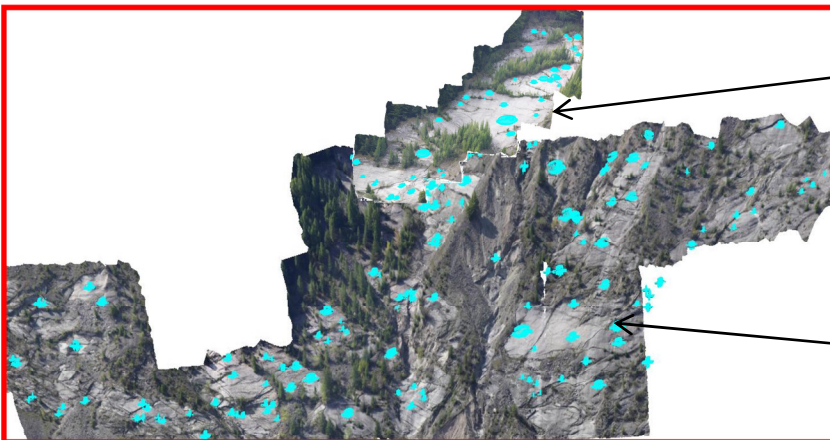


Figure 6. a) Model 3 and b) Models 4 and 5 with stereonets. See Figure 4.

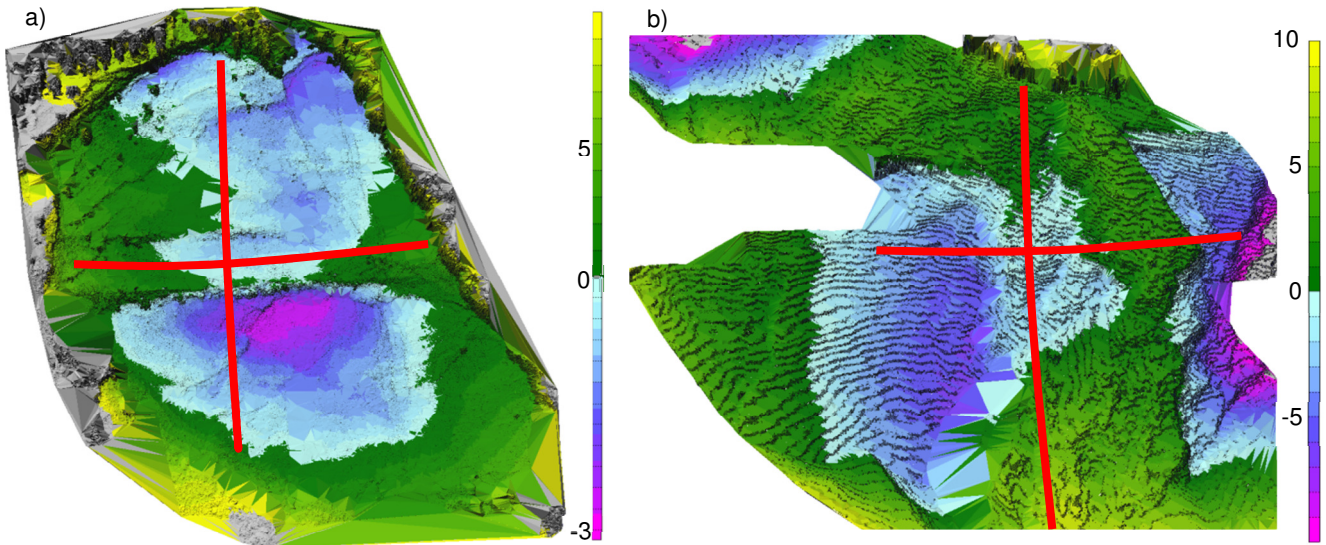


Figure 7. Residual plots of a) the western corner and b) the east-central area of the Vajont failure surface. Distances are in metres above or below a best-fit plane. The red lines indicate the locations of the  $f=400$  mm cross-sections shown in Figure 8.

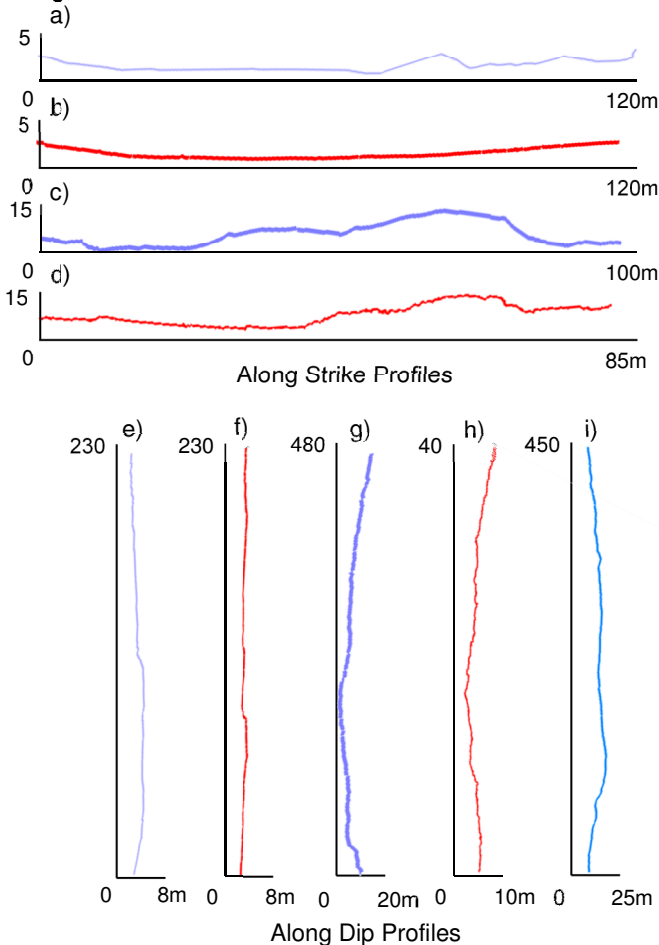


Figure 8: Profiles of the failure surface at a), b), e), and f) the western corner, and c), d), g), h), and i) the central zone. The blue profiles are derived from the  $f=20$  mm model and the red profiles are derived from the  $f=400$  mm models.

Preliminary profiles were created on the  $f=20$  mm and  $f=400$  mm models to compare roughness as a function of scale (Figure 8). The along-dip profiles created from the  $f=20$  mm model show E trending, asymmetrically cascading folds (Figures 8e, g, and i). A less conspicuous feature in these profiles is the three-dimensional undulation of the failure surface. Along dip, the surface ranges from convex (Figure 8e-f) to concave (Figure 8g-i). Along strike, the undulations are more gradual, with a longer wavelength (Figure 8c-d). An exception is the anomalous fold in the east-central zone (Figure 8a-b). The hinge and limbs of this fold are conspicuous features of the western failure surface, and illustrate the complexity of Domain 2. A profile east of Figure 8g shows the variability of the failure surface over a distance of a few metres and thus the potential bias of two-dimensional profiles and the importance of three-dimensional characterisation (Figure 8i). It also suggests that asperities may be important in the slide movement (see Discussion). Together, the along-dip and along-strike profiles indicate that the orientation of the failure surface is a product of several episodes of folding.

The  $f=400$  mm profiles reveal smaller-scale roughness features superimposed on the large scale morphology. Although possibly noise (Poropat 2008), detection of these features shows that higher focal-length models provide more detail than low focal-length models and that this smaller scale roughness requires further investigation to assess its influence on the shear strength of the discontinuities. The difference in detail is highlighted in Figures 8c and d of the same profile.

## 5 DISCUSSION

The results of the preliminary discontinuity and morphology analyses derived from the photogrammetric models have important implications for sliding behaviour and mechanisms. Discontinuities acted as release surfaces in the headscarp and lateral margins of the

Vajont Slide. Steps observed on the failure surface are of two types: one follows DS8 and other discontinuity sets; the other is the result of fracturing of intact rock bridges. The first type plays an important role in the central and western areas of the failure surface where several steps have the same orientation. This consistent orientation indicates that DS8 was an important control on slide behaviour. Steps aligned with other discontinuity sets are less common but nonetheless are important. The second step type includes steps oriented in several directions. They are less obvious than the prominent discontinuity set, and may provide a possible explanation for the slow creep of the rock mass prior to catastrophic failure in 1963; each rock bridge or asperity had to be destroyed before movement could occur. The discontinuity and rock-bridge steps illustrate the complexity of the sliding surface. Other factors such as clay mineralogy infill thickness, clay properties, pore water pressure, dilation of the material moving, material softening, and overconsolidation need to be considered in studies of the slide mechanisms.

The Erto syncline created a biplanar to circular failure surface. Active and passive zones of the sliding mass likely developed due to the biplanarity of most of the failure surface. The passive lower seat impeded movement from the active upper back of the chair-like surface, and a transition zone developed between the two areas. This transition zone was first analysed by Mencl (1966), who applied the concept of a Prandtl wedge to the zone. Simple two-dimensional Phase2 finite element and UDEC distinct element modelling of the wedge using Ghirotti's (1992) parameters and geometry supports the Prandtl wedge theory (Figure 9). It also shows the bulging in the transition zone that may have occurred. The stresses that develop as the active and passive blocks interact focus within a Prandtl wedge or transition zone, causing more internal deformation. This concentration of stress contributed to the complex deformation of the central zone of the Vajont Slide, which was also affected by easterly directed tectonic compression. This highly folded and faulted zone is another possible barrier to motion. It may have acted not only as the transition zone in the active-passive cross-section, but also to prevent interaction between the east and west sides of the sliding mass. For example, the west limb of the large fold in the east-central zone was a metre-scale obstruction to east-west movement. Previous studies (Hendron and Patton 1985) support the existence of this barrier, and survivor accounts suggest that the western part of the slide mass moved before the eastern part.

Hendron and Patton (1985) hypothesise that the cascading E-trending folds may have increased normal stress slightly, but their orientation and amplitude indicate that their role in preventing motion was small. However, the morphology profiles, particularly Figures 6g and i, show that the folds could have influenced motion: this will be investigated in more detail in future numerical modelling using 3DEC.

Small-scale roughness has been recognised as significant in landslide and fracture behaviour (Nasseri et al. 2010, Tatone and Grasselli in press). The  $f=400$  mm profiles may indicate this scale of roughness. Due to the

distance of the photogrammetric stations from the sliding surface, however, it is not clear that these small-scale features are statistically significant. It may be necessary to complete closer-range photogrammetry.

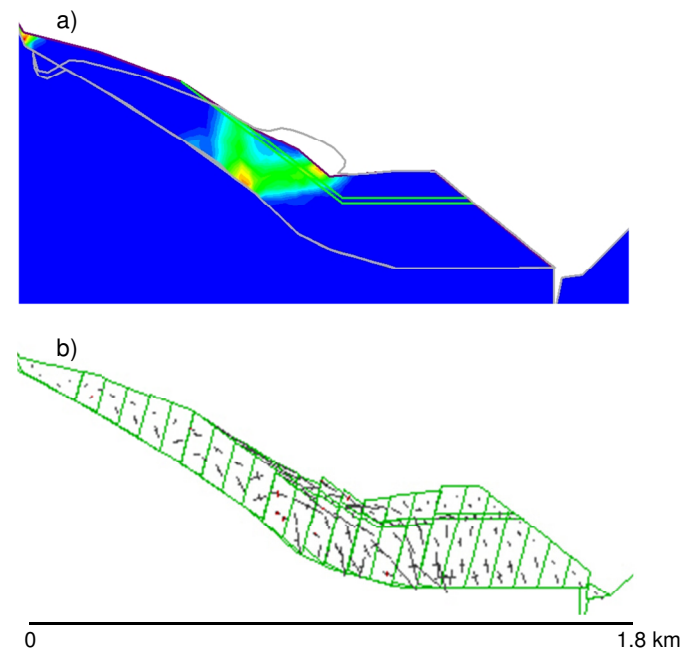


Figure 9. Preliminary models of the Prandtl wedge zone based on Ghirotti's (1992) parameters and geometry. a) Area of interest in a Phase2 model of the maximum shear strains in the sliding mass. Grey outlines indicate magnified displacement. b) UDEC model showing stress trajectories within the sliding mass.

### 5.1 Error and Uncertainty in Photogrammetric Analysis

The surface observed today is not the original failure surface. Erosion and weathering have removed material, especially clay. However, our results based on the modern surface, especially tectonic features, are important in characterising the failure.

Field and photogrammetric discontinuity mapping has involved inherent structural, sampling, and measurement errors. Rock masses are highly complex, and any quantification of a rock mass involves an estimation of actual characteristics, with associated accuracy and sampling limitations (Lyman et al. 2008). For example, due to resolution and orientation, a discontinuity surface mapped on a photogrammetry model may be the only representation of a particular discontinuity set, or it may be a random discontinuity. In addition, because of the direction the photographs were taken from, the sliding surface is over-represented relative to other discontinuities in the photogrammetric mapping. Therefore, photogrammetric results must be compared with field data to validate results.

Error in the morphology analysis depends largely on the resolution of the point clouds, which depends in turn on the distance from the outcrop and the focal length of

the lens used. All photographs were taken at distances of 1 to 2.5 km, with a relative ground resolution of 10 cm possible. The meshes generated from the point clouds are limited by the point cloud resolution. Vegetation and orientation bias affect the meshing process. For example, the spike in the  $f=20$  mm, along-strike profile (Figure 8a) is due to orientation bias and shadowing, and does not represent the actual failure surface. Fortunately, these anomalous spikes in the mesh surface are easy to recognise. The residual surfaces also depend on the adequacy of the best-fit method used to create the plane. As mentioned above, apparent centimetre-scale roughness is most likely roughness noise associated with the distance from the outcrop and point cloud processing (Poropat 2008). Any analysis at this scale should be completed with caution and be subject to ground truthing by field mapping.

## 5.2 Current Work

Quantitative analysis of the photogrammetry data and comparison with field data are continuing. This work includes statistical and kinematic analyses of the mapped discontinuities. More data will be collected in the field to characterise the three-dimensional character of the failure surface and its roughness. Undulation amplitude and wavelength will be measured and recorded to decipher the folding events. If possible, small-scale roughness will be analysed using techniques similar to the 3D roughness method correlated with the roughness coefficient  $R_s$  (Tatone and Grasselli 2009), or 2D roughness anisotropy method by Nasser et al. (2010). A quantitative approach will allow further characterisation of the failure surface and failure mechanisms, and determination of the role of the different scales of roughness in preventing or facilitating movement. The photogrammetric data will also be used to model the landslide with two- and three-dimensional codes such as UDEC, 3DEC, and ELFEN.

## 6 CONCLUSIONS

Application of photogrammetric techniques to the study of the Vajont Slide illustrates the importance of geologic structure on the failure. Some of the eight discontinuity sets that we identified in the photogrammetric may have acted as release surfaces. We also identified fold-controlled steps that may have controlled motion along the failure surface. Different scales of roughness represent discrete episodes of folding. The Erto syncline provided the characteristic chair shape of the failure surface, and cascading NNE trending mesoscale folds, undulating E-trending folds, and smaller-scale roughness elements also influenced movement.

## ACKNOWLEDGEMENTS

Funding for the project was provided by NSERC, through a scholarship to A. Wolter and NSERC Discovery Grants to D. Stead and J. Clague. Funding for L. Superchi, R. Genevois, and M. Ghirotti was provided by the University of Padova's Strategic Project Geo-Risks coordinated by

R. Genevois. The LiDAR for the analysis was provided by the Region of Friuli Venezia Giulia.

## REFERENCES

- Broili, L. 1967. New knowledges on the geomorphology of the Vaiont Slide slip surfaces. *Felsmechanik und Ingenieurgeologie*, 5(1): 38 – 88.
- Genevois, R. and Ghirotti, M. 2005. The 1963 Vaiont Landslide. *Giornale di Geologia Applicata*, 1: 41 – 52.
- Ghirotti, M. 1992. Aspetti geomeccanici e modellazione numerica della frana del Vajont. PhD thesis. Universita di Parma, Ferrara, Firenze e Pavia, Italy.
- Goguel, J. 1978. Scale-dependent rockslide mechanisms, with emphasis on the role of pore fluid vapourization. Chapter 20. *In Rockslides and Avalanches: Natural Phenomena. Edited by B. Voight.* Elsevier, New York. pp. 693 – 705.
- Habib, P. 1975. Production of gaseous pore pressure during rock slides. *Rock Mechanics and Rock Engineering*, 7(4): 193 – 197.
- Hendron, A.J. and Patton, F.D. 1985. *The Vaiont Slide, a geotechnical analysis based on new geologic observations of the failure surface.* Available from the US Army Corps of Engineers, Washington, DC. Technical Report GL-85-5.
- Kilburn, C.R.J. and Petley, D.N. 2003. Forecasting giant, catastrophic slope collapse: lessons from Vajont, Northern Italy. *Geomorphology*, 54: 21 – 32.
- Lyman, G., Poropat, G.V., and Elmoultie, M. 2008. Uncertainty in rock mass jointing characterisation. *SHIRMS 2008*. Perth. 419 – 432.
- Mantovani, F. and Vita-Finzi, C. 2003. Neotectonics of the Vajont dam site. *Geomorphology*, 54 (1-2): 33 – 37.
- Menci, V. 1966. Mechanics of landslides with non-circular slip surfaces with special reference to the Vaiont slide. *Geotechnique*, 16 (4): 329 – 337.
- Müller, L. 1968. New considerations on the Vaiont Slide. *Felsmechanik und Ingenieurgeologie*, 6: 1 – 91.
- Nasser, M.H.B., Grasselli, G., and Mohanty, B. 2010. Fracture toughness and fracture roughness in anisotropic granitic rocks. *Rock Mechanics and Rock Engineering*, 43: 403 – 415.
- Nonveiller, E. 1987. The Vajont Reservoir slope failure. *Engineering Geology*, 24(1-4): 493-512.
- Poropat, G.V. 2008. Remote characterisation of surface roughness of rock discontinuities. *SHIRMS 2008*, Perth. 447 – 458.
- Petley, D.N. and Petley, D.J. 2006. On the initiation of large rockslides; perspectives from a new analysis of the Vaiont movement record. *In Landslides from massive rock slope failures. Edited by S.G. Evans, G. Scarascia-Mugnozza, A.L. Strom, and R.L. Hermanns.* NATO Science Series, Celano, Italy. pp. 77 – 84.
- Rossi, D. and Semenza, E. 1981. Carte geologiche del versante settentrionale del Monte Toc e zone limitrofe, primo e dopo il fenomeno di scivolamento del 9 Ottobre, scala 1:5000. *Ist. Geologia*, Universite Ferrara.

- Semenza, E. 1965. Sintesi degli studi geologici sulla frana del Vaiont dal 1959 al 1964. *Memorie del Museo Tridentino di Scienze Naturali*, 16: 3-51.
- Semenza, E. and Ghirotti, M. 2000. History of the 1963 Vaiont slide: the importance of geological factors. *Bulletin of Engineering Geology and the Environment*, 59: 87 – 97.
- Sitar, N. and MacLaughlin, M.M. 1997. Kinematics and Discontinuous Deformation Analysis of landslide movement, *II Panamerican Symposium on Landslides*, Rio de Janeiro, Brazil.
- Skempton, A.W. 1966. Bedding-plane slip, residual strength and the Vaiont Landslide. *Geotechnique*, 16(1): 82 – 84.
- Sturzenegger, M., Stead, D., Beveridge, A., Lee, S., van As, A. 2009. Long-range terrestrial digital photogrammetry for discontinuity characterization at Palabora open-pit mine. In Proceedings of the 3<sup>rd</sup> CANUS Rock Mechanics Symposium, Toronto, May 2009. Edited by M. Diederichs and G. Grasselli. Paper 3984.
- Superchi, L., Floris, M., Ghirotti, M., Genevois, R., Jaboyedoff, M., and Stead, D. 2010. Implementation of a geodatabase of published and unpublished data on the catastrophic Vaiont landslide. *Natural Hazards and Earth System Sciences*, 10: 865 – 873.
- Tatone, B.S.A. and Grasselli, G. 2009. A method to evaluate the three-dimensional roughness of fracture surfaces in brittle geomaterials. *Review of Scientific Instruments*, 80: 125110.
- Tatone, B.S.A. and Grasselli, G. in press. A new 2D discontinuity roughness parameter and its correlation with JRC. *International Journal of Rock Mechanics and Mining Sciences*.
- Tika, T.H.E. and Hutchinson, N. 1999. Ring shear tests on the soil from the Vaiont landslide slip surface. *Geotechnique*, 49: 59 – 74.
- Trollope, D.H. 1980. The Vaiont slope failure. *Rock Mechanics*, 13: 71 – 88.
- Vardoulakis, I. 2002. Dynamic thermo-poro-mechanical analysis of catastrophic landslides. *Geotechnique*, 52: 157 – 171.
- Voight, B. and Faust, C. 1982. Frictional heat and strength loss in some rapid landslides. *Geotechnique*, 32: 43 – 54.